KU Leuven
Biomedical Sciences Group
Faculty of Medicine
Department of Cellular and Molecular Medicine
Laboratory of Cellular Transport Systems

Purification of the Secretory Pathway Ca^{2+}/Mn^{2+}-ATPases for Functional Analysis and Drug Discovery

Jialin CHEN

Jury:

Promoter:	Prof. Dr. Peter Vangheluwe
Co-promoter:	Prof. Dr. Jan Eggermont
Chair:	Prof. Dr. Patrizia Agostinis
Jury members:	Prof. Dr. Rajini Rao
	Prof. Dr. Maria del Rosario Sepúlveda Justo
	Prof. Dr. Sergei Strelkov
	Prof. Dr. Ludwig Missiaen

Dissertation presented in partial fulfilment of the requirements for the degree of Doctor in Biomedical Sciences

June 2019

Acknowledgements

Getting a PhD on the other side of the Eurasia continent is a journey of adventure, I am only one of many parts that made this thesis possible.

First, I am deeply grateful to my promotor Peter. Thank you for giving me the opportunity to be a master student in this lab and later on offering me a position as a PhD student, which result in this thesis. Thank you for the continuous support and invaluable guidance, for always ready to discuss about results and problems of the experiments and open to give advices. Moreover, thank you for spending a lot of time on correcting my writings and giving suggestions for presentations. I also would like to thank my co-promotor Jan. Thank you for so many feedbacks and encouragement that helped me during my PhD, and for your patience and efficiency in correcting my thesis. Frank, thank you very much for the interesting discussions during the lab meetings. You always come up with good ideas from a different perspective. And Luc, I liked your lectures a lot and thank you for introducing me to the exciting P-type ATPases world during my Master.

I would further like to thank Prof. Rao, Prof. Sepúlveda, Prof. Strelkov and Prof. Missiaen for accepting to be my thesis advisory committee, and for spending time on reading this thesis and provide insightful comments. Many thanks to Prof. Strelkov and Prof. Missiaen who followed up the progress of my PhD training over the years, and gave helpful feedbacks after each milestone.

I am also grateful to all the excellent members in LCTS. Susanne, thank you for working on the same subject with me. I really appreciate all the discussions we had, scientific and non-scientific. I'm really grateful that you started the PhD a while before me so that I always have an example to follow and suggestions to take from, even now ☺. Ilse, thank you for your supervision and training during my master thesis. You taught me many techniques that you initiated in the lab. I am very grateful that you are still around nowadays and are still willing to discuss about my work and give suggestions. Vero, it is always so nice to discuss with you about the projects and to brainstorm solutions to many problems in my work. Also thank you so much for sharing a lot of useful tips and experiences on other important things. Norin, thank you for always being supportive and encouraging, and for your accompany when experiments / deadlines went late in the evenings. Marleen, big thank you to all the trivial questions I bothered you over the years, and thank you for always concern about people and willing to offer help. Stephanie, Sarah, Rongjie, Muj and Manuel, thank you for being my neighbors in the office and in the lab. I enjoyed all the small chats between experiments and thank you for all the helps that you provided during my pregnancy. Shaun and Alya, thank you for all the discussions and suggestions during lab meetings and being a nice colleague at work. Igor, Tugce and Tine, I really liked to work with you and thank you for being supportive even after you left the lab. And Jo, thank you for the encouragement

when I was frustrated about SPCA purification when I was still a master student. Diane and Els, thank you for a lot of technical helps in the work, especially in the beginning of my PhD.

Many thanks go to the collaborators. Joren and Prof. De Maeyer, thank you for the help on Tg docking. Prof. Lescrinier and Charles-Alexandre, thank you for your help and patience in explaining me my questions regarding NMR.

I would also like to thank Anja and Marina, Raf and Luc for helping with the cell culture and fixing many broken devices, and also Vivianne, Ingrid and Jeaninne, for your help in ordering and administration related matters.

Furthermore, I need to express my gratitude to many Chinese friends that I met here: Ying Ting, Song Huiying, Mao Dun, Shang Min, Zhao Xiaocheng, Li Zhiling, Yan Bing, Jia Xu, Chan Ya-Chien, Gao Bo, Bai Yang, Huang Zengjin, Shi Chenyan, Li Chen, Cai Yanyan, Liang Sayuan, Wu Guiqin, Si Jianmin, Wang Xiangdong. Many thanks to all of you for having a great time in Leuven. Your friendship shall always be remembered.

More importantly, I need to thank my mother for the unconditional love, care and support throughout my life and during this study. You always believe in me and want the best for me. Also, thank you for understanding of me being far way for over ten years and for me not being around when help is needed in the family. And, Han Xu, it was very lucky to meet you here. Thank you for understanding me so well and enlightening my life with your presence. I am grateful that you are always there for me during my ups and downs. I would also like to thank all my other family members for the support. Finally, I also need to thank my father, who was always so enthusiastic to know what I was doing, and had faith in me that things will work out. He would be very excited to see the completion of this PhD.

Leuven

May 2019

Table of Contents

List of abbreviations

I. Introduction* 1

1. The role of calcium in cellular processes 1

1.1 The intracellular Ca^{2+} transporters 1

1.2 Intracellular Ca^{2+} stores 2

1.3 Ca^{2+} as a second messenger 3

2. Intracellular manganese 4

3. The organellar Ca^{2+}-ATPases 5

3.1 Transporting mechanism of Ca^{2+}-ATPases 5

3.2 SERCA 8

3.3 SPCA 10

4. Regulation of intracellular Ca^{2+}-ATPases 11

4.1 Regulation by small regulatory proteins 11

4.2 Regulation by N- and C-termini 14

4.3 Regulation by post-translational modifications 16

5. Small molecule modulators of SERCA and SPCA 17

5.1 Inhibitors of SERCA 17

5.2 Inhibitors of SPCA 19

6. Ca^{2+}-ATPases as drug targets 19

6.1 SERCA and prostate cancer 19

6.2 SERCA and energy expenditure 20

6.3 SERCA2a and heart failure 21

6.4 SPCA and breast cancer 21

6.5 SPCA and neurodegeneration 22

7. Reconstitution of Ca^{2+}-ATPases 22

7.1 Criteria of reconstitution 23

7.2 Reconstitution into proteoliposomes 24

7.3 The “Step-by-step” reconstitution strategy 24

7.4 Detergent removal 26

7.5 Other reconstitution methods 27

II. Aims of the study 31

III. Results 33

1. Structure/activity relationship of thapsigargin inhibition on the purified Golgi/secretory pathway Ca^{2+}/Mn^{2+}-transport ATPase (SPCA1a) 33

2. An N-terminal Ca^{2+} binding motif regulates the secretory pathway Ca^{2+}/Mn^{2+}-transport ATPase SPCA1 58

IV. General discussion and future perspectives 77

1. The proteoliposome system as an improved method to study SPCA1/2 77

2. Stimulation of SPCA1 activity by lipids 78

3. A deep narrow groove for Tg in SPCA1 78

4. Future design of SPCA1 specific inhibitors based on Tg analogues 79

5. The discrepancy between the phosphorylation and the ATPase assay in relation to the active state distribution 80

6. Possible mechanisms of N-terminal regulation of SPCA1 81

7. Different physiological roles of SPCA1 and SPCA2 83

8. Extending the functional characterization to Ca^{2+} transport assays 84

V. Summary 85

VI. Samenvatting 87

References 89

Curriculum Vitae 101

Acknowledgement, Personal Contribution and Conflict of Interest statement 104

List of abbreviations

ADP	adenosine 5’-diphosphate
ALN	another-regulin
ATP	adenosine 5’-triphosphate
BAT	brown adipose tissue
BHQ	2,5-di-(t-butyl)-dihydroxybenzene
BP	bis(2-hydroxy-3-tert-butyl-5-methylphenyl)methane
BSA	bovine serum albumin
$[Ca^{2+}]_{cyt}$	free cytosolic Ca^{2+} concentration
C12E8	octaethylene glycol monododecyl ether
CMC	critical micelle concentrations
CPA	cyclopiazonic acid
CRAC	Ca^{2+} release-activated Ca^{2+} channel
DDM	dodecylmaltoside
DTT	dithiothreitol
DWORF	DWARF open reading frame
ECL	enhanced chemi-luminescence
EDTA	ethylene diamine tetra-acetic acid
ELN	endoregulin
ER	endoplasmic reticulum
GST	glutathione S transferase
HF	heart failure
HHD	Hailey-Hailey disease
IC_{50}	half maximal inhibitory concentration
IGF1R	Insulin-like growth factor 1 receptor
IP_3	inositol 1,4,5-trisphosphate
IP_3R	inositol 1,4,5-trisphosphate receptor
K_d	dissociation constant
kDa	kilo Dalton
K_m	concentration giving half-maximal effect
LE	luminal extension
MLN	myoregulin
MOPS	3-(N-morpholino)propanesulfonic acid
MSP	membrane scaffolding protein

NCX	Na^+/Ca^{2+}-exchanger
NMR	nuclear magnetic resonance
Orai1	Ca^{2+} release-activated Ca^{2+} channel protein 1
PLN	phospholamban
PMCA	plasma membrane Ca^{2+}-ATPase
PMR1	plasma membrane-related Ca^{2+}-ATPase
PTM	post-translational modification
PVDF	polyvenylidene difluoride
r	rabbit
R_{sat}	the ratio of detergent : lipid when the detergent concentration just reaches saturation on the lipid vesicles
R_{sol}	the ratio of detergent : lipid when the detergent concentration just reaches the total vesicle solubilization
RyR	ryanodine receptor
SAR	structure-activity relationship
SDS	sodium dodecylsulphate
SEM	standard error of the mean
SERCA	sarco(endo)plasmic reticulum Ca^{2+}-ATPase
SICE	store-independent Ca^{2+} entry
SLN	sarcolipin
SMA	styrene maleic acid
SMALP	styrene maleic acid lipid particle
SOCE	store-operated Ca^{2+} entry
SPCA	secretory pathway Ca^{2+}/Mn^{2+}-ATPase
SR	sarcoplasmic reticulum
STIM	stromal interaction molecule
SUMO1	small ubiquitin-related modifier 1
TBBPA	tetrabromobisphenol A
Tg	thapsigargin
TGN	*trans*-Golgi network
TM	transmembrane
UCP1	uncoupling protein 1
VGCC	voltage-gated calcium channel
V_{max}	maximal turnover rate

WB	Western blotting
WT	wild-type

I. Introduction*

1. The role of calcium in cellular processes

Calcium (Ca) is the 5th most abundant element inside the human body and present as an ion (Ca^{2+}). Around 99% of the Ca^{2+} can be found in mineralized forms mainly as hydroxyapatite ($Ca_{10}(PO_4)_6(OH)_2$) in bones, where it not only provides the compressive strength to the skeleton, but also serves as a mineral storage site for the rest of the body. The remaining Ca^{2+} is present mainly in the extracellular fluid and to a lesser extent intracellularly, in either protein bound or free form, where it plays many important roles in human physiology, such as neurotransmission, muscle contraction, fertilization and cell death. Extra- and intracellular Ca^{2+} concentrations are tightly regulated: the free Ca^{2+} concentration is around 1.2 mM in the extracellular fluid. It is below 100 nM in the cytosol under resting conditions and reaches micromolar levels in the lumen of organelles (1). In this thesis, we focus on the intracellular Ca^{2+} transport ATPases that are vital for regulating the intracellular Ca^{2+} homeostasis.

1.1 The intracellular Ca^{2+} transporters

The free cytosolic Ca^{2+} concentration ($[Ca^{2+}]_{cyt}$) is tightly controlled by a versatile set of Ca^{2+} buffer proteins and Ca^{2+} transporters, which operate in either of two modes of Ca^{2+} transport: passive or active transport. Passive transport follows the electrochemical gradient and occurs through Ca^{2+} channels. Pumps and carriers transport Ca^{2+} actively, *i.e.* against the electrochemical gradient, and they are powered by the energy respectively from ATP hydrolysis (primary active) or from the passive transport of a coupled substrate (secondary active) (2). Extracellular Ca^{2+} enters the cell passively via, amongst other, receptor-operated Ca^{2+} channels, store-operated Ca^{2+} channels or voltage-gated calcium channels (VGCCs) that are all located in the plasma membrane. The inositol 1,4,5-trisphosphate receptor (IP_3R) and ryanodine receptor (RyR, expressed in excitable tissues) release Ca^{2+} passively into the cytosol from intracellular Ca^{2+} stores (ER/SR and *cis*-Golgi). Meanwhile, active transporters remove Ca^{2+} from the cytosol into the lumen of organelles or into the extracellular compartment. The plasma membrane located Na^+/Ca^{2+}-exchanger (NCX) is a secondary active transporter that when the cytosolic Ca^{2+} concentration is elevated uses the energy stored in the Na^+ gradient to export 1 Ca^{2+} whilst importing 3 Na^+ ions (3). For maintaining a sub-µM cytosolic Ca^{2+} concentration, mammalian cells further critically depend on three primary active Ca^{2+}-ATPase transport systems that power Ca^{2+} transport by ATP hydrolysis: the sarco(endo)plasmic reticulum Ca^{2+}-

** Introduction is based on the book chapters Primary active Ca^{2+} transport systems in health and disease. Chen et al, 2019 and Regulation of Ca^{2+} transport ATPases by amino- and carboxy-terminal extensions: Mechanisms and (patho)physiological implications. Chen et al, 2016.*

transport systems that power Ca^{2+} transport by ATP hydrolysis: the sarco(endo)plasmic reticulum Ca^{2+}-ATPases (SERCA), secretory pathway Ca^{2+}-ATPase (SPCA) and the plasma membrane Ca^{2+}-ATPase (PMCA) (2).

1.2 Intracellular Ca^{2+} stores

Within a cell, Ca^{2+} is mainly stored in the intracellular organelles, *i.e*., the endoplasmic reticulum (ER) (free Ca^{2+} concentration of 100-500 µM (1)), the Golgi network (free Ca^{2+} concentration of 130 - 300 µM (4)) and to a lower extent the mitochondria and lysosomes. These organelles employ Ca^{2+} transporters to accumulate Ca^{2+} inside, either for subsequent cytosolic Ca^{2+} release, or to use the luminal Ca^{2+} for protein folding, processing, sorting, vesicular transport and energy production.

For example, the ER, or the sarcoplasmic reticulum (SR) in skeletal, heart and smooth muscle, is filled with Ca^{2+} by SERCA ATPases that pump Ca^{2+} against a 1,000 to 10,000-fold concentration gradient. Ca^{2+} can be released via activated IP_3R and RyR into the cytosol. The resulting rise in $[Ca^{2+}]_{cyt}$ is part of a signal transduction cascade that leads to specific cellular responses such as contraction, secretion or neurotransmission.

The Ca^{2+} concentration in the Golgi follows a gradient from high (around 250 µM) in the *cis*- to low in the *trans*-Golgi network (around 80 µM), accompanied by the presence of heterogeneous Ca^{2+} transporters. The *cis*-Golgi contains mainly SERCA pumps that fill the lumen with Ca^{2+} and IP_3Rs for Ca^{2+} release into cytosol (4). The *trans*-Golgi compartment, *trans*-Golgi network (TGN) and secretory vesicles are devoid of IP_3Rs and SERCAs, but are enriched with SPCA proteins that pump Ca^{2+} and Mn^{2+} into the lumen (4). The RyR is ubiquitous throughout the Golgi in excitable cells such as muscle and neurons (4). Similar to SR/ER, the Golgi also participates in Ca^{2+} signaling (5,6). The Ca^{2+} in the Golgi network allows the luminal Ca^{2+}-dependent enzymes to perform proteolytic processing and regulates trafficking of the newly synthesized proteins. Interestingly, an insufficient Ca^{2+} load in the TGN also compromises the cleavage of glycoproteins, including the maturation of various viral particles, rendering them less infectious for spreading (7).

1.2.1 Store-operated and store-independent Ca^{2+} entry

Store-operated Ca^{2+} entry (SOCE) is an important route for Ca^{2+} entry in non-excitable cells. Prolonged activation of the IP_3R leads to the depletion of Ca^{2+} in the ER, which is sensed by stromal interaction molecule (STIM), an integral ER membrane protein (8). The decrease in ER Ca^{2+} content causes STIM to oligomerize and relocalize into punctae in ER–plasma membrane junctions, which allows STIM to

interact directly with the Ca^{2+} release-activated Ca^{2+} channel protein 1 (Orai1), a plasma membrane protein that constitutes the pore part of the Ca^{2+} release-activated Ca^{2+} channel (CRAC). This interaction opens CRAC and leads to Ca^{2+} influx into the cytosol following its electrochemical gradient across the plasma membrane. This generates a local Ca^{2+} signal that is crucial for controlling long-term cellular events, for example gene expression and cell motility (9). In addition, the elevated $[Ca^{2+}]_{cyt}$ is used to refill the ER via SERCA ATPases.

More recently, a related process termed store-independent Ca^{2+}-entry (SICE) was identified, which involves activation of Orai1 by SPCA isoforms (10,11). Unlike SOCE, the activation of SICE does not depend on a lower luminal Ca^{2+} concentration in intracellular Ca^{2+} stores or the relocalization of STIM1/2. In SICE, SPCA binds to the plasma membrane Orai1 channel, leading to the activation of the Orai1 channel and consequently Ca^{2+} influx into the cytosol (10). The locally elevated $[Ca^{2+}]_{cyt}$ is partially used by SPCA pumps to increase the Golgi Ca^{2+} content, which can be transported along the secretory pathway (12). Since increased expression levels of SPCA isoforms are observed during lactation, SICE may promote an increased cellular Ca^{2+} influx into mammary epithelial cells for subsequent secretion in the milk (13).

1.3 Ca^{2+} as a second messenger

To achieve versatile functions from fertilization to cell death by Ca^{2+} signaling, the cytosolic Ca^{2+} concentration is precisely regulated both spatially and temporally. For example, exocytosis is induced by short Ca^{2+} spikes in milliseconds, while gene transcription and cell proliferation are regulated by elevated Ca^{2+} signals over minutes to hours (2). Besides the previously mentioned Ca^{2+} transporters, the extremely low resting $[Ca^{2+}]_{cyt}$ is maintained by many intracellular Ca^{2+} buffering proteins, which are located in the cytosol or organelles. For example, calreticulin and calsequestrin are Ca^{2+} binding proteins in the ER/SR. By complexing Ca^{2+}, they reduce the free luminal Ca^{2+} level while increasing the Ca^{2+} storage capacity of the ER/SR (14). Another example of a Ca^{2+} binding protein is the cytosolic calmodulin.

Many Ca^{2+} binding proteins including the above mentioned calmodulin and calreticulin, contain structural features that are known as Ca^{2+} binding motifs. The EF-hand is the prototype, of which the structure was first solved in 1973 in parvalbumin, and later identified in many other proteins **(Figure 1)** (16). This motif contains two α-helices resembling the spread thumb and forefinger, connected by a flexible loop that contains residues for Ca^{2+} coordination in the pentagonal bipyramidal configuration. The loop of a canonical EF-hand contains 12 residues, and Ca^{2+} is coordinated by residues at position 1, 3, 5, 12 with their sidechains and also the backbone from the 12th residue, which is a Glu or Asp. The

pseudo EF-hand contains a 14 amino acid loop, and coordinates Ca^{2+} mainly via backbone oxygens of the 1, 4, 6, 9 residues. EF-hand motifs typically function in pairs. By binding Ca^{2+}, EF-hand proteins undergo conformational changes, and either induce Ca^{2+} signaling, or function as Ca^{2+} buffers. Proteins containing an odd number of EF-hands often undergo homo- or heterodimerizations, serving as docking proteins (14).

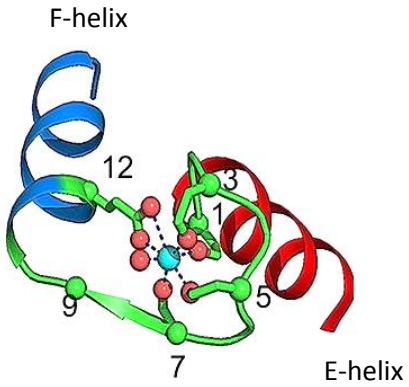

Figure 1: Cartoon representation of the EF-hand motif. The two α-helices are indicated in red and blue, which are connected by a flexible loop (green). The Ca^{2+} ion (cyan) in the center is coordinated by seven oxygen atoms (red) from the loop in the pentagonal bipyramidal configuration (figure is adapted from (15)).

2. Intracellular manganese

Manganese (Mn^{2+}) is an essential trace element for living organisms in development, metabolism, and the antioxidant system. It enters the body via dietary intake or through the respiratory system, and can enter the cells via various divalent ion channels and carriers. Many enzymes use Mn^{2+} as a cofactor, such as the mitochondrial superoxide dismutase, which protects against lipid peroxidation by superoxide radicals, and is found in nearly all aerobic organisms. Free Mn^{2+} in the cytoplasm can also act as a scavenger of reactive oxygen species in bacteria and yeast cells lacking superoxide dismutase (17). Manganese in the Golgi is important for the synthesis of the milk sugar lactose, since one of the enzymatic steps involves beta-1,4-galactosyltransferase that binds Mn^{2+} (18). Golgi-residing glycosyltransferases and sulfotransferase also require Mn^{2+} for activity (19).

Mn^{2+} is able to cross the blood-brain barrier and blood-cerebrospinal fluid barriers (20). In the brain, Mn^{2+} is mainly deposited in the *basal ganglia* and *globus pallidus*. Excessive exposure to Mn^{2+} may lead to a neurological disorder called manganism that presents symptoms similar to Parkinson's disease (21). Its exact neurotoxic mechanism is not yet known, but it may involve the inhibition of the tyrosine hydroxylation step of dopamine synthesis, interfering with Mg^{2+}-binding, or disturbing iron metabolism associated with neural oxidative damage. In mouse primary cell cultures of neurons and glia cells, high levels of Mn^{2+} induce Golgi fragmentation, a hallmark of neuronal degeneration (22). Since SPCA is the

only high affinity Mn^{2+} pump in animals, the removal of Mn^{2+} via the secretory pathway may represent a major route for cytosolic Mn^{2+} detoxification (23). The Mn^{2+} sequestering role of SPCA1 has been demonstrated in rat liver and liver-derived cells (24) as well as in mouse brain where $MnCl_2$ has been delivered continuously with a mini-osmotic pump (25).

3. The organellar Ca^{2+}-ATPases

The Ca^{2+} transport ATPases belong to the family of P-type ATPases that undergo cyclic auto-(de)phosphorylation on a conserved aspartic acid, a feature that connects the Ca^{2+} binding, occlusion and transport processes (26,27).

The P-type ATPases comprise five subfamilies (P1-5) categorized by their sequence homology and substrate specificity. The P1-type ATPases include the K^+-ATPase and heavy-metal pumps that play a role in metal homeostasis. The P2-type ATPases are a group of cation pumps to which the Ca^{2+}-ATPases belong. Other substrates transported by P2-type ATPases include Na^+, K^+ and H^+. The P3-type ATPases are mainly the plasma membrane H^+ pumps that maintain the intracellular pH and membrane potential in plants and fungi. The P4-type ATPases are lipid flippases that build up lipid asymmetry, whereas the substrate of the P5-type ATPases remains unknown (26). In this thesis, we focus on the P2-type ATPases, particularly on the SERCA and SPCA pumps that belong to the P2A subfamily.

3.1 Transporting mechanism of Ca^{2+}-ATPases

Currently, the structures of SERCA1a, SERCA2a (28) and PMCA1 (29) have been resolved (30). Due to the overall high degree of sequence similarity and domain organization, predicted homology models of several other Ca^{2+}-ATPases were generated. The topology follows the classical P-type ATPase architecture, with typically 10 transmembrane (TM) helices that form the TM-domain, which holds the Ca^{2+}-binding sites and ion entrance/exit pathways. The cytosolic loops form three distinct functional domains: a nucleotide-binding domain (N), a phosphorylation domain (P) and an actuator domain (A), which make up the core of the ATPase function and couple ATP hydrolysis to Ca^{2+} transport **(Figure 2)** (30).

The transport process of P-type ATPases follows the Post-Albers cycle, as shown in **Figure 3**. It cycles between four major conformational states E1, E1P, E2P, and E2. In the following description, we use SERCA1a, one of the best studied P-type ATPases, as an example.

In the high Ca^{2+} affinity E1 state, the cytosolic gate of SERCA1a is open, allowing 2-3 H^+ to be displaced by two Ca^{2+} ions from the cytosol. The two Ca^{2+} ions bind sequentially and cooperatively at the TM ion binding sites, and the signal of this induced fit process at the TM region is transmitted to the cytoplasmic domain, for ATP binding and subsequent hydrolysis to take place. The adenosine of ATP interacts with Phe487 at the N-domain and the γ phosphate is bridged to Asp351 at the P-domain for phosphorylation to take place. At the same time, TM1 is lifted toward the cytosolic side of the membrane and forms a kink that closes the cytosolic entry gate, creating an occluded state (E1~P). Once ATP is hydrolyzed and the ADP is released, the tension created by the ATP as a bridge between the N- and P-domain is relieved, which causes the N-domain to move. This in turn creates tension between TM3 and the A-domain, which allows the A-domain to rotate massively. This rotation is transmitted to the TM region, which not only distorts the high affinity Ca^{2+} binding sites, but also creates a luminal gate through which Ca^{2+} can exit, forming the low Ca^{2+} affinity E2-P state. Here, the TM ion binding sites are stabilized by several protons followed by closure of the luminal pathway. The rotation of the A-domain positions its TGE motif to capture a H_2O molecule for catalyzing the dephosphorylation reaction toward the phosphorylated Asp351, which is followed by phosphate release, and transiting to the E2 state. The A-domain then rotates away from the P-domain. The movement at the cytosolic part induces the TM helices to reposition and recreate the high affinity Ca^{2+} binding sites, thereby returning the pump to the E1 state with cytosolic release of H^+ and binding of Ca^{2+} (26,27).

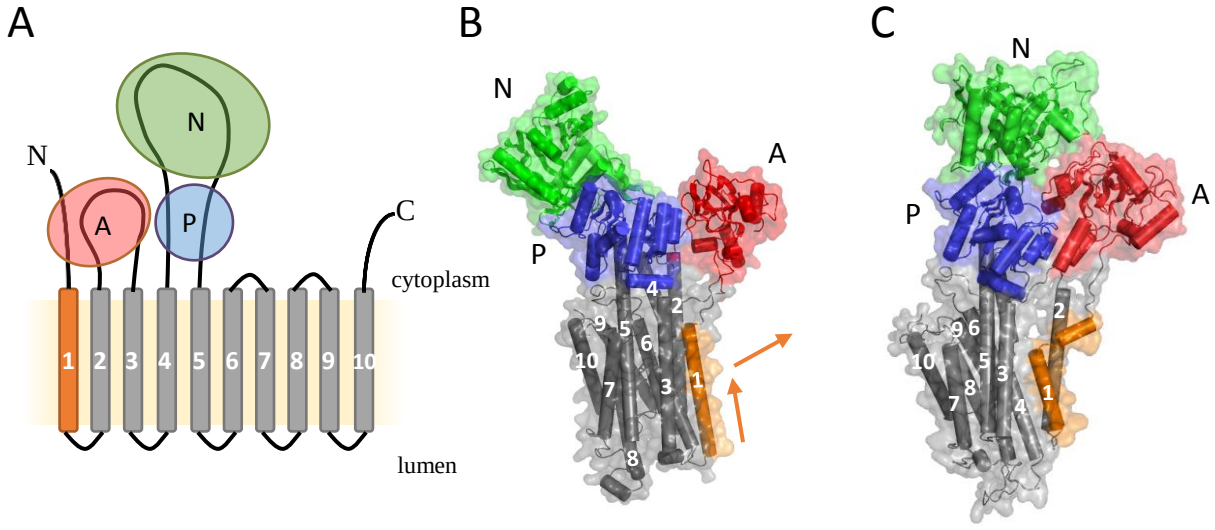

Figure 2: Topology and architecture of the P-type ATPases, represented by rabbit (r) SERCA1a. A) The topology of P-type ATPases comprising 10 transmembrane (TM) helices that are numbered and the three cytosolic domains. A: actuator domain (red), N: nucleotide binding domain (green), P: phosphorylation domain (blue). B-C) Crystal structures of the rSERCA1a in the E1 conformation (B), (PDB:1SU4) and E2 conformation (C), (PDB:1IWO). The M1 helix (highlighted in orange) is lifted up and forms a kink during E1 to E2 conformation transition.

In the high Ca^{2+} affinity E1 state, the cytosolic gate of SERCA1a is open, allowing 2-3 H^+ to be displaced by two Ca^{2+} ions from the cytosol. The two Ca^{2+} ions bind sequentially and cooperatively at the TM ion binding sites, and the signal of this induced fit process at the TM region is transmitted to the cytoplasmic domain, for ATP binding and subsequent hydrolysis to take place. The adenosine of ATP interacts with Phe487 at the N-domain and the γ phosphate is bridged to Asp351 at the P-domain for phosphorylation to take place. At the same time, TM1 is lifted toward the cytosolic side of the membrane and forms a kink that closes the cytosolic entry gate, creating an occluded state (E1~P). Once ATP is hydrolyzed and the ADP is released, the tension created by the ATP as a bridge between the N- and P-domain is relieved, which causes the N-domain to move. This in turn creates tension between TM3 and the A-domain, which allows the A-domain to rotate massively. This rotation is transmitted to the TM region, which not only distorts the high affinity Ca^{2+} binding sites, but also creates a luminal gate through which Ca^{2+} can exit, forming the low Ca^{2+} affinity E2-P state. Here, the TM ion binding sites are stabilized by several protons followed by closure of the luminal pathway. The rotation of the A-domain positions its TGE motif to capture a H_2O molecule for catalyzing the dephosphorylation reaction toward the phosphorylated Asp351, which is followed by phosphate release, and transiting to the E2 state. The A-domain then rotates away from the P-domain. The movement at the cytosolic part induces the TM helices to reposition and recreate the high affinity Ca^{2+} binding sites, thereby returning the pump to the E1 state with cytosolic release of H^+ and binding of Ca^{2+} (26,27).

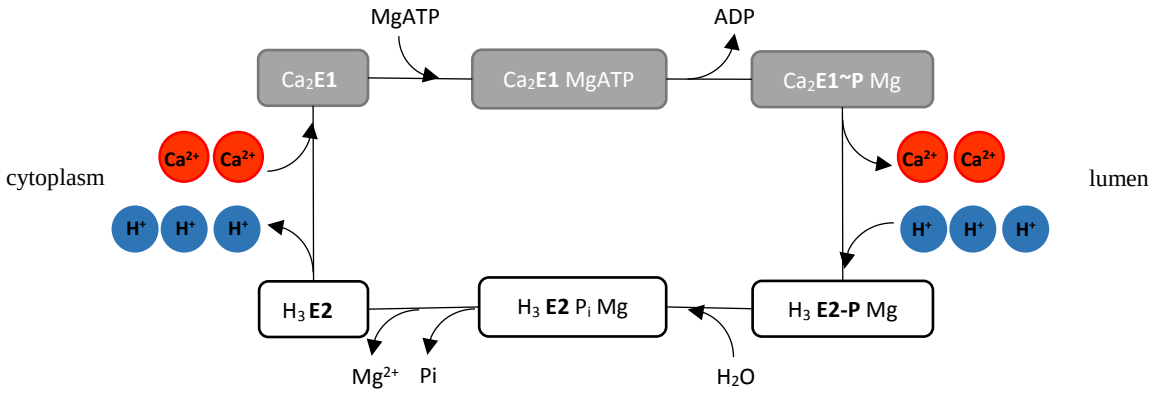

Figure 3: The Post-Albers cycle during the Ca^{2+} transport of SERCA. SERCA is alternating between the E1 (gray) and E2 (white) conformations. It transports two Ca^{2+} ions to the lumen in exchange to three protons to the cytoplasm. During the transport, ATP is hydrolyzed into ADP and Pi. (The scheme is modified from (31)).

3.2 SERCA

In humans, three different genes (*ATP2A1-3*) generate multiple SERCA isoforms and splice variants (SERCA1a-b, SERCA2a-d and SERCA3a-f) as a result of developmental or tissue-specific gene expression and alternative splicing (27,32). The splice variants of each SERCA gene only differ at their C-termini (33).

3.2.1 SERCA1

The *ATP2A1* gene encodes two splice variants of 110 kDa: SERCA1a/b. SERCA1a is highly expressed in adult fast- and slow-twitch skeletal muscle cells, whereas SERCA1b is only expressed in neonatal fibers (34), myoblasts, developing myotubes and regenerating muscle (35). These two isoforms share the same 993 amino acids starting from the N-terminus. SERCA1a ends with only one Gly residue, whereas the SERCA1b splice variant holds a slightly longer and highly charged C-terminus (-DPEDERRK). SERCA1a is by far the best characterized SERCA isoform. This protein was the first member of the P-type ATPase family to be cloned (36) and it has been extensively studied by site-directed mutagenesis and crystallography, leading to detailed insights in its structure-function relationship **(Figure 2)**. Mutations in *ATP2A1* are associated with Brody disease (OMIM 601003), an autosomal recessive muscle disorder characterized by painless muscle cramping and exercise-induced impairment of muscle relaxation (37,38).

3.2.2 SERCA2

The products of the housekeeping *ATP2A2* gene are found in both muscle and non-muscle tissues (39,40). SERCA2 predominantly exists as two splice variants that contain a common 993 amino acid stretch and a variable C-terminus. SERCA2a ends with a four residue-tail (-AILE), while SERCA2b contains a longer tail (41). Through intra-molecular interactions with a distal site in the transmembrane region near TM10 and the luminal loop L7-8, the SERCA2b C-terminus imposes a two-fold higher Ca^{2+} affinity and two-fold lower turnover rate in comparison to the shorter splice variant SERCA2a (42,43).

In contrast to the developmentally regulated splicing of SERCA1, the splicing of SERCA2 is regulated in a tissue-specific manner. SERCA2a is the main isoform found in the SR of cardiac, slow-twitch skeletal and smooth muscle cells (44,45). SERCA2b is ubiquitously expressed in the ER of most cell types and is considered as the house-keeping ER Ca^{2+} pump. The mRNA of SERCA2c was detected in differentiating monocytes and cardiac cells, and the SERCA2c protein was confirmed in the heart, although at minor amount compared to SERCA2a or SERCA2b (46,47).

SERCA2 and Darier Disease

Heterozygous mutations in *ATP2A2* are implicated in Darier disease (OMIM 124200), an autosomal dominant skin disorder characterized by distinctive nail abnormalities, warty papules and plaques mainly on the chest, neck, back, ears, forehead and groin (48). It is characterized by a disruption of cell-cell contacts (acantholysis) in the suprabasal layers of keratinocytes in the epidermis. So far, over 250 mutations in the *ATP2A2* gene are identified that lead to Darier disease, many of which result in a loss of the Ca^{2+} transport activity (49,50), indicating that haplo-insufficiency of SERCA2 underlies the disease onset. Interestingly, a gain-of-function mutant was also identified, resulting in a temperature sensitive leaky Ca^{2+} pump that dissipates the ER Ca^{2+} gradient, which may explain the dominant phenotype of the disease (51).

SERCA2a and heart relaxation

SERCA2a is the major cardiac isoform. In mouse, the cardiac SERCA2 pool mainly consists of SERCA2a (95%), while SERCA2b (5%) expression is very modest (52). The SERCA2c is also expressed in the human heart (33).

In the cardiac excitation-relaxation cycle, depolarization of the sarcolemma causes opening of the VGCCs, leading to Ca^{2+} influx. This Ca^{2+} then binds to the RyR in the SR which causes Ca^{2+}-induced Ca^{2+} release from the SR and an increase in the $[Ca^{2+}]_{cyt}$ (53). The Ca^{2+} ions then bind to troponin C in the myofilament causing muscle contraction (54). To end contraction, the majority of Ca^{2+} is pumped back into SR by SERCA2a for the next Ca^{2+} release. In another route, a smaller amount of Ca^{2+} (~30%) is extruded to the extracellular space via the NCX (55). The reduced cytosolic Ca^{2+} level induces muscle relaxation (55,56). Since the majority of the activating Ca^{2+} is recycled across the SR, the SERCA2a pump represents a key determinant of cardiomyocyte contractility and Ca^{2+} loading of the SR.

3.2.3 SERCA3

At least six different splice variants of SERCA3 are recognized (SERCA3a-f) in humans (39). SERCA3 is expressed in hematopoietic cell lineages, endothelial cells (57), monocytes, colon, pancreatic β-cells (58) and cardiomyocytes (33). SERCA3 differs from the other SERCA isoforms by a remarkably low affinity for cytosolic and luminal Ca^{2+} (59) and a higher pH optimum (59,60). It is also insensitive to the cardiac regulator phospholamban (PLN; see further in 4.1.1) and displays a higher resistance to oxidative damage (61,62).

3.3 SPCA

The secretory pathway Ca^{2+}-ATPase was first described in *Saccharomyces cerevisiae* and was named plasma membrane-related Ca^{2+}-ATPase (PMR1) (63). Later, the mammalian SPCA isoforms were cloned and characterized (64,65). In higher order animals, including amphibians, reptiles and mammals, two isoforms are recognized, SPCA1 and SPCA2 (encoded by *ATP2C1* and *ATP2C2*). SPCA1 is the housekeeping Golgi Ca^{2+} pump present in most cell types, whereas the expression of SPCA2 is mainly restricted to brain and secretory cells, in the gastrointestinal tract, trachea, thyroid, salivary gland, mammary gland, and prostate (66,67), suggesting a more specialized physiological function for SPCA2.

Human SPCA1 displays a 29% sequence identity and 43% similarity with SERCA1a. However, SPCA presents distinct enzymatic properties compared to SERCA. i) SPCA lacks the Ca^{2+} binding site I and transports only one Ca^{2+} ion per cycle. The Ca^{2+} binding site corresponds to the conserved site II in the SERCA pump (27). ii) In addition to Ca^{2+}, SPCA is able to transport Mn^{2+}, which is competing with Ca^{2+} transport. Mutations at the TM region affect transport of both Ca^{2+} and Mn^{2+} further suggesting that both ions are transported via the same TM binding site (68-70). SPCA pumps ensure uptake of Mn^{2+} into the lumen of the Golgi compartment, where several Mn^{2+}-depending enzymes reside, such as the glycosyltransferases and sulfotransferases (27). iii) SPCA transports Ca^{2+} ions at a higher affinity than SERCA (71). The high apparent Ca^{2+} affinity indicates that the Ca^{2+} uptake into the Golgi/secretory pathway is permanently activated and is independent of a transient elevation of the cytosolic Ca^{2+} concentration. The maximal turnover rates of the SPCA isoforms and splice variants are 2-6 fold lower as compared to SERCA1a (71). iv) SPCA is more compact than SERCA with shorter cytosolic and luminal loops (27). At least some of the longer loops in SERCA, which contain regulatory sites for protein interactions (72), are absent in SPCA isoforms. For instance, HCLS1-associated protein X-1 interacts with the unique part of a cytosolic loop in the SERCA2 N-domain (73), whereas ERp57 interacts with the larger luminal L7-8 loop in SERCA (74).

3.3.1 SPCA1 and Hailey-Hailey disease

ATP2A2 and *ATP2C1* are two housekeeping genes that are both implicated in related skin disorders in humans. Homozygous mutations on either of the two genes lead to embryonic lethality in mice (75,76). In humans, heterozygous mutations in SERCA2 result in Darier disease (see above in 3.1.2.1), whereas those in SPCA1 cause Hailey-Hailey disease (HHD), a related benign chronic skin disease with similar symptoms, showing blisters and itchy erosions mainly at the sites of sweating and friction, such as the groin and the axillar regions (77). So far, 168 different mutations in *ATP2C1* have been identified in HHD patients (78). In contrast to human patients, both *Atp2a2*$^{+/-}$ (79) and *Atp2c1*$^{+/-}$ (76) heterozygous

mice have an increased incidence of squamous tumors. However, the underlying reason for this phenotype difference between human and mice is unknown.

3.3.2 SPCA proteins in lactation

The activity and expression of multiple Ca^{2+} transporters in the mammary gland is tightly coordinated during pregnancy, lactation after parturition and the process of involution. These remarkable changes are required to support the release of large amounts of Ca^{2+} in the milk (8-60 mM, depending on the species) (80). SPCA1/2 and Orai1 levels are highly upregulated in the mammary gland during lactation, resulting in a 150-fold increase in SPCA2 and a 15-fold increase in SPCA1 protein levels (13,81). SPCA2 activates Orai1 at the basolateral side of the mammary gland epithelial cells via its N- and C-terminal extensions, leading to an increased Ca^{2+} influx (13). An increased level of SPCA1 is also able to cause Ca^{2+} influx via Orai1 (11). Ca^{2+} is subsequently transferred into the milk at the apical side via two main Ca^{2+} transport routes: via the ER/secretory pathway through SERCA/SPCA and across the apical plasma membrane via PMCA2 (13,82,83). PMCA2 knock-out mice exhibit 60% lower Ca^{2+} levels in the milk suggesting the remaining 40% may be released via the ER/secretory pathway (82).

4. Regulation of intracellular Ca^{2+}-ATPases

Due to their central position in maintaining the Ca^{2+} homeostasis, the intracellular Ca^{2+} pumps are tightly regulated via various mechanisms. For example, by interacting with regulatory proteins, via post-translational modifications (PTM) on Ca^{2+} pumps, or by *cis*-regulation through the flexible and variable N- and/or C-termini **(Figure 4)**. In this section, we limit the introduction to new regulatory concepts that have emerged in recent years, by focusing on the micropeptides and PTMs that regulate SERCA proteins, and the N- and C-terminal regulations of SPCA that are currently under exploration.

4.1 Regulation by small regulatory proteins

4.1.1 Regulation of SERCA isoforms by small TM regulators

PLN (**Figure 5**) is a membrane protein of 52 amino acids, comprised of a cytosolic helical domain connected by a loop to a TM helix. PLN follows the expression pattern of SERCA2a and is expressed in the SR of cardiac muscle, slow-twitch skeletal muscle and smooth muscle (27). It binds as a monomer to SERCA and reduces the apparent affinities of SERCA1a, SERCA2a/b, but not SERCA3 (53,85). The inhibition is relieved by 1) an elevated Ca^{2+} concentration or 2) phosphorylation of PLB at Ser16 by cAMP-dependent protein kinase or at Thr17 by Ca^{2+}/calmodulin-dependent protein kinase II.

Phosphorylation of PLN promotes its dissociation from SERCA and the formation of inactive PLN pentamers (27).

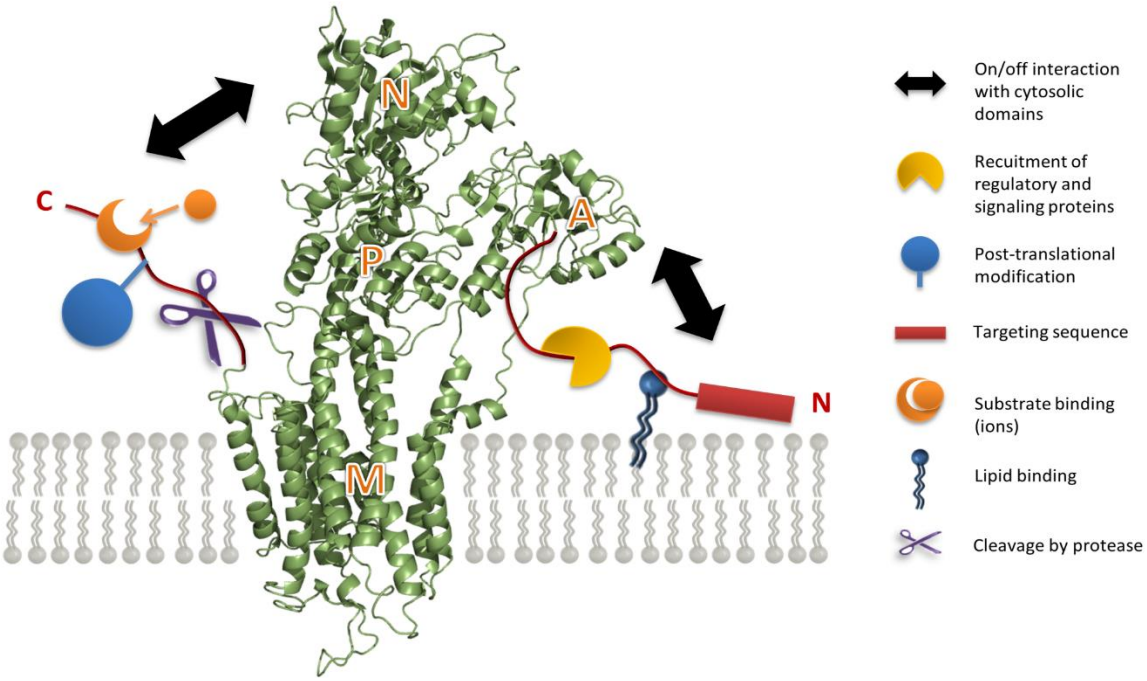

Figure 4. Overview of the N- and C- terminal regulations of the P-type ATPases. A model of the P-type ATPase is colored in green with their extended N- and C-termini highlighted in red. A-, N-, P- and TM-domains as well as the N- and C-termini are indicated. The extended N- and C-termini are possibly functioning as the on/off switches for the pumping activity by reversibly interacting with the main body of the pump. Activity regulation may also occur via binding of regulatory proteins, lipids, substrates, by post-translational modifications, and by protease cleavages, which often take place on the N- and C-termini. Besides, N- and C-termini may contain sequences that are important for subcellular targeting, or domains for recruiting signaling proteins. Figure is adapted from (84).

According to the structure of SERCA1a-PLN4 (a mutated form of PLN with a higher affinity for SERCA), the TM region of the monomeric PLN binds to SERCA in a groove formed by TM2, 4, 6 and 9 (86). This interaction distorts the two SERCA TM Ca^{2+} binding sites that are formed between TM4, 5, 6, 8 and thereby lowers the apparent affinity of the Ca^{2+} pump (86). In the PLN-bound state SERCA partially resembles the E1 conformation adopting an open arrangement of the cytosolic domains, however with a lower positioned M1 helix forming a kink and an open Ca^{2+}-access channel, which is an indication of the E2 conformation (86). When SERCA shifts to the E1 conformation, the movement of TM2 makes the TM groove narrower, which disrupts the PLN interaction (87).

Sarcolipin (SLN. **Figure 5**) is a smaller homologue protein of PLN (31 amino acids). It has a shorter cytosolic part, a single membrane span helix, which has very high sequence identity with PLN, and a highly conserved luminal extension, which plays a role in ER membrane retention and SERCA inhibition

(55,90). In humans, SLN has the highest expression in fast-twitch skeletal muscles, and a lower expression in heart atria and slow-twitch skeletal muscles (27).

SLN binds in the same TM groove on SERCA as PLN, and lowers the apparent Ca^{2+} affinity and maximal turnover rate (V_{max}) of SERCA1a and SERCA2 (91-93). SLN is also modulated by phosphorylation at Thr5 (94,95), thereby playing a role during β-adrenergic stimulation in contraction of the atria. Phosphorylation of SLN destabilizes the hydrogen bonding between SLN and SERCA, hence relieving SERCA inhibition (92). Moreover, SLN can coexist and synergize with PLN *in vitro*, leading to formation of the superinhibitory ternary PLN-SLN-SERCA complex. Modelling shows that the SLN-PLN heterodimer fits into the same groove in SERCA, but tighter, which increases the binding affinity (53,96).

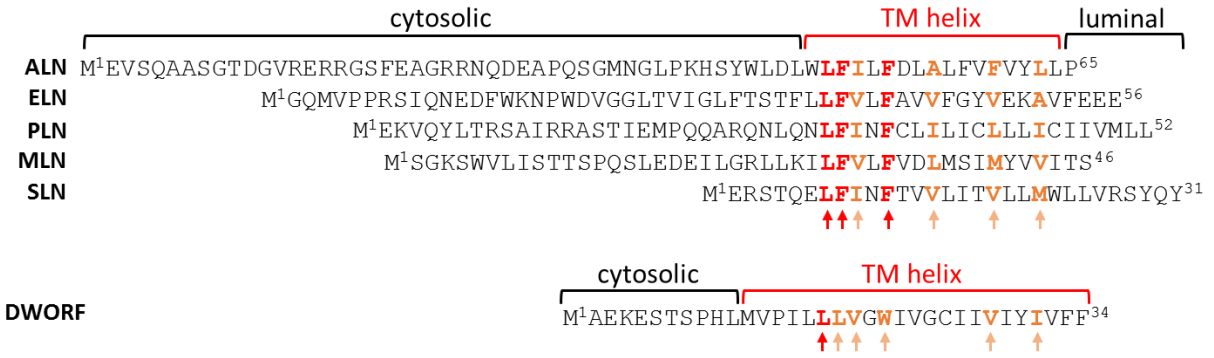

Figure 5. Sequence alignment of the transmembrane regulators of SERCA. The amino acid sequences of another-regulin (ALN), endoregulin (ELN), phospholamban (PLN), myoregulin (MLN), sarcolipin (SLN) and DWARF open reading frame (DWORF) in mouse are aligned for the transmembrane (TM) helix region. Numbering of the first and last residue of each regulator is shown as superscript. The identical amino acids were highlighted in red and indicated with a red arrow. The conserved amino acids are highlighted in orange and indicated with an orange arrow. Figure is adapted from (88,89)

Recently, a few other small peptides were identified that regulate SERCA activity and that are encoded by annotated long noncoding RNAs. These small TM proteins are the muscle specific peptide myoregulin (MLN) (97), DWARF open reading frame (DWORF) (89), as well as the non-muscle regulators endoregulin (ELN) and another-regulin (ALN. **Figure 5**) (88). The MLN, ELN, ALN and previously described PLN and SLN are structurally related, as they all contain a membrane embedded C-terminal helix with a conserved LFxxF motif. They also bind at the same site on SERCA and exert inhibition directly. In mice, the expression pattern of MLN overlaps with SERCA1a in skeletal muscles, PLN overlaps with SERCA2a, ALN with SERCA2b, and ELN with SERCA3 (88). SLN is expressed in the atria of heart, and DWORF in soleus muscle, heart ventricle and diaphragm in mice. Although DWORF binds

at the same pocket as other regulators, it does not in itself change SERCA activity, but by displacing other regulators, it activates SERCA (89). The interplay of co-expressed regulators remains unclear (88).

4.1.2 Regulation of SPCA isoforms by protein interactions

As was mentioned in (3.3.2), SPCA2 directly interacts with and activates the plasma membrane Ca^{2+} channel Orai1 via its N- and C-terminal extensions, which leads to an increased Ca^{2+} influx (10). Once activated, SPCA2 transfers the incoming Ca^{2+} into the Golgi/secretory pathway (12). Later on, SPCA1 was also found to induce SICE through Orai1, which controls the luminal Ca^{2+} content of the Golgi/secretory pathway (11). Together with PMCA2, the SPCA-Orai1 coupling contributes to enrich the milk with Ca^{2+} during lactation.

SPCA1 plays an important role in filling the TGN store with Ca^{2+}, which is essential for protein sorting and secretion (98). It was shown that the actin filament severing protein cofilin-1 interacts with SPCA1 through the P-domain, and activates SPCA1 in filling the TGN with Ca^{2+} (99). The transient increase of local Ca^{2+} concentration in the lumen induces the polymerization of the TGN luminal 45 kDa calcium-binding protein Cab45 (100), which directly binds to a variety of secretory proteins such as cartilage oligomeric protein and lysozyme C in its oligomer state for secretion (100,101).

4.2 Regulation by N- and C-termini

Members of all P-type ATPase sub-families are closely regulated by their N- and/or C-termini. For instance, the N-terminus of the P1-type copper-transport ATPase holds a membrane associated platform that recruits copper chaperones for subsequent substrate delivery to the copper binding sites in the N-terminus or to the copper transport sites in the TM-domain (102). The C-terminus of the P2-type Na^+/K^+-ATPase docks into the C-terminal TM-domain and regulates the access to a non-canonical Na^+-entrance pathway (103) impacting on the Na^+ affinity (104). In the P3-type plant H^+-ATPases, the C-terminus includes an auto-inhibitory domain that upon removal leads to the release of the auto-inhibitory restraints and a strong activation of proton pumping (105,106). The P4-type lipid flippases are also controlled by the N- and C-terminal ends. The auto-inhibition of the yeast Drs2p lipid flippase by the C-terminal tail (107) can be relieved by lipid interaction (108). Similarly, the poorly characterized P5-type ATPases also display unique N-terminal stretches that contain unusual membrane associated segments resembling the N-terminal stretches of the P1-type ATPases (109), which regulate its auto-phosphorylation activity (110). Below we focus on the N- and C-termini regulation of the SERCA and SPCA pumps, which belong to the P2A-type Ca^{2+}-ATPases.

4.2.1 Regulation of SERCA pumps by alternative C-termini

As mentioned earlier, each of the three SERCA genes was translated to multiple isoforms that differ in the C-termini. For SERCA1, there are no differences between the two SERCA1 isoforms in Ca^{2+}-binding affinity, ATPase activity or Ca^{2+}-transporting capacity (111). However, they are likely to be functionally different *in vivo*, due to 1) their strictly regulated translation and 2) the heavily charged C-terminus of SERCA1b which might play an unknown signaling role (112).

Compared to the cardiac isoform SERCA2a, which ends with four residues after a common 993 amino acid stretch, the housekeeping SERCA2b displays a 49 amino acid tail that forms the 11th transmembrane helix with its C-terminus ending at the luminal side of the ER/SR, which is named as the luminal extension (LE) (41). SERCA2b is therefore the only Ca^{2+} transporter with 11 membrane segments. The 2b-tail grants SERCA2b unique biochemical properties compared to SERCA1a or SERCA2a as mentioned previously in 3.2.2. Interestingly, fusion of the 2b-tail to SERCA1a or supplying synthetic peptides corresponding to the 2b-tail to SERCA2a or SERCA1a impose SERCA2b-like properties to these pumps (43,113). This indicates that both the TM11 and LE can be regarded as a transferable, functional peptide that modulates the Ca^{2+} affinity of the pump by direct interaction. According to the model constructed from SERCA1a crystal structures, combined with the NMR structure of TM11 and mutagenesis results, TM11 may interact in the region close to TM10 of the SERCA pump, which is a relatively immobile part, resembling the binding site of the β subunit on the Na^+/K^+-ATPase (43,113). TM11 affects the Ca^{2+} free E2 state via slowing down the E2P to E2 and E2 to E1 transitions (113,114). In contrast, LE affects SERCA2b by interaction between the C-terminal portion of the LE (1039-MFWS) and the luminal loop L7/8, which stabilizes the pump in the Ca^{2+} bound E1 conformation. It reduces the rate of Ca^{2+} dissociation into the cytosol and the E1P to E2P conversion (43,114).

4.2.2 Regulation of yeast PMR1 by N-terminal EF-like domain

The N-terminus of the *S. cerevisiae* PMR1 holds an unpaired EF-hand-like motif that has been demonstrated to bind Ca^{2+} (69). Of interest, the Ca^{2+} binding in the PMR1 motif can be reduced by molar excess of Mn^{2+}, but not Mg^{2+}, suggesting possible competition between Ca^{2+} and Mn^{2+} binding (69). Disruption of the EF-hand in PMR1 by D51A and D53A single point substitutions in this motif leads to a lower Ca^{2+} transport activity and reduced Ca^{2+} affinity, whereas the D51A/D53A double mutant is retained in the ER. These results highlight the importance of the N-terminal EF-hand motif in PMR1 activity and subcellular targeting (69). Remarkably, the PMR1 N-terminus, which is distal from the membrane regions that shape the Ca^{2+}/Mn^{2+} pathway, also regulates substrate preference.

Overexpression of the D51A mutant fails to rescue the Mn^{2+} hypersensitivity in the Δpmr1 yeast strain, in line with impaired Mn^{2+} transport. However, the D53A single or D51A/D53A double mutants are only impaired in Ca^{2+} transport (69). Moreover, the EF-hand like motif also influences proteolytic stability of the downstream part of the protein, including the ATP binding region, suggesting a possible regulatory role in the intra-molecular interaction between the N-terminus and the rest of the protein (69).

4.2.3 Regulation of human SPCA1 via C-terminal splicing

In contrast to orthologues that are named PMR1 in other species, the human housekeeping SPCA1 gene undergoes alternative splicing, giving rise to 4 splice variants (SPCA1a-d) that differ at the C-termini. The SPCA1a, b, and d isoforms are functional, while SPCA1c is not (115). Although neither the tissue specific localization nor the functional differences have been compared among the splice variants, it is likely that these variants may play distinct physiological roles. It has been proposed that, due to the overlap of the 3' end of the *ATP2C1* gene with the 3' end of the *ASTE1* gene (which codes for Asteroid1, with unknown function) on the complimentary strand, the translation of the *ASTE1* gene could influence the translation of *ATP2C1* variants (116). The peculiar gene overlap and the alternative splice variants are only observed in humans.

4.3 Regulation by post-translational modifications

Multiple possible PTMs were documented for SERCA and SPCA proteins (documented in PhosphoSitePlus, a repository of experimentally observed post-translational modifications; www.phosphosite.org) (117). The functional effects of PTMs in SPCA have not been studied, although double bands of SPCA proteins were often detected in immunoblotting, which may indicate that a sub-population of SPCA proteins may be modified by PTMs (13,118).

PTMs in SERCA have been investigated into more detail. For example, in SERCA1a there is a disulfide bond between the Cys876 and Cys888 on the luminal loop L7-8 and its disruption abolishes the Ca^{2+} transport activity (119). Besides, both SERCA1 (120) and SERCA2 (see further) undergo age-related oxidative modifications. Upon low level oxidative stress, the SERCA2a activity can be stimulated by nitric oxide derived peroxynitrite via formation of a disulfide bridge between Cys674 and glutathione, in a process called S-glutathiolation (121). On the other hand, prolonged elevated reactive oxygen/nitrogen species levels such as during atherosclerosis lead to permanent oxidization of the Cys674 to sulfonylation, as observed in 21-months aged mice (122), which partially explains the impaired cardiomyocyte relaxation during aging. In addition, SERCA2 accumulates nitro-tyrosine with

age on residues Tyr294 and Tyr295, accompanied by a loss of activity (123,124). This modification contributes to oxidative stress in a hyperglycemic condition, as nitro-tyrosine levels were significantly increased in rat hearts perfused with high glucose (125). SERCA2a is also modulated by the small ubiquitin-related modifier 1 (SUMO1) via SUMOylation. It is linked to Lys480 and Lys585 at the N-domain, and improves the stability and activity of SERCA2a (72). In murine (72) models of heart failure induced by pressure overload, the expression level of SERCA2a, SUMO1 as well as the SUMOylated SERCA2a is reduced, and the restoration of SUMOylation by SUMO1 gene delivery improves the SERCA2a stability and heart contractility. Reversal of heart failure was also observed in a porcine model (126). Acetylation and glycosylation have also been observed on SERCA2a, both reducing the SERCA2a activity (127,128). Acetylation on Lys492 of SERCA2a significantly reduces the activity, presumably via interfering of ATP binding. This acetylation is associated with a reduced level of SIRT1, a class III histone deacetylase, and mediated by p300, a histone acetyltransferase (129). The striated muscle preferentially expressed protein kinase was found to directly associate to SERCA2. It phosphorylates SERCA2a on Thr484 and enhances SERCA2a activity via promoting oligomerization (130).

5. Small molecule modulators of SERCA and SPCA

5.1 Inhibitors of SERCA

Thapsigargin (Tg), cyclopiazonic acid (CPA), and 2,5-di-(t-butyl)-dihydroxybenzene (BHQ) are three extensively studied SERCA inhibitors. Co-structures of SERCA1a with these compounds have been solved via X-ray crystallography (131-134) **(Figure 6)**.

Tg is a sesquiterpene lactone derived from plant *Thapsia garganica*. Although the plant has been used in Arabian medicine for centuries, it was until the early 1980s before people started to understand the pharmacology. In general Tg has an extremely high affinity for SERCA, but varies between different SERCA isoforms: the concentration that reaches half maximal inhibition (IC_{50}) of Tg for SERCA1 is at sub-nM, for SERCA2 at 1.3 nM, and for SERCA3 at 12 nM (135). Tg binds to SERCA at the M-domain in a groove close to the cytoplasmic leaflet of the membrane. Within this binding pocket, TM3 and TM7 flank the tricyclic guaianolide ring core of Tg, while TM5 forms the back of the pocket (136). Mutagenesis studies in SERCA1a revealed residues that are critical for the coordination of Tg, which include Phe256 (TM3), Ile765 (TM5) and Tyr837 (TM7) (137). Alternatively, by functional evaluation of a series of Tg analogues that differ in each of the sidechains or backbone, information was collected on the contributions of Tg structural elements to SERCA1a inhibition (summarized in (138)). By stacking the Tg lactone ring to the Phe256 side group in the binding pocket, the sidechains of Tg are accurately

positioned. This allows hydrophobic interactions between the Tg sidechains with the SERCA pocket, which accounts for ~80% of total Tg binding energy (136). Among the sidechains, O3, O10 and O8 contribute most to the interaction with SERCA1, while the O2 octanoyl group is positioned in the SERCA1-lipid interface, and provides the least binding energy among the four Tg sidechains (136). These strong hydrophobic interactions prevent the required TM movements during E2 to E1 transition, hence fixing the pump at the Ca^{2+}-free E2 state. The Tg binding pocket is also proposed to bind steroids, such as alisol B (IC_{50} 27 µM) (139), an autophagy enhancer that is extracted from the plant *Alisma orientale*.

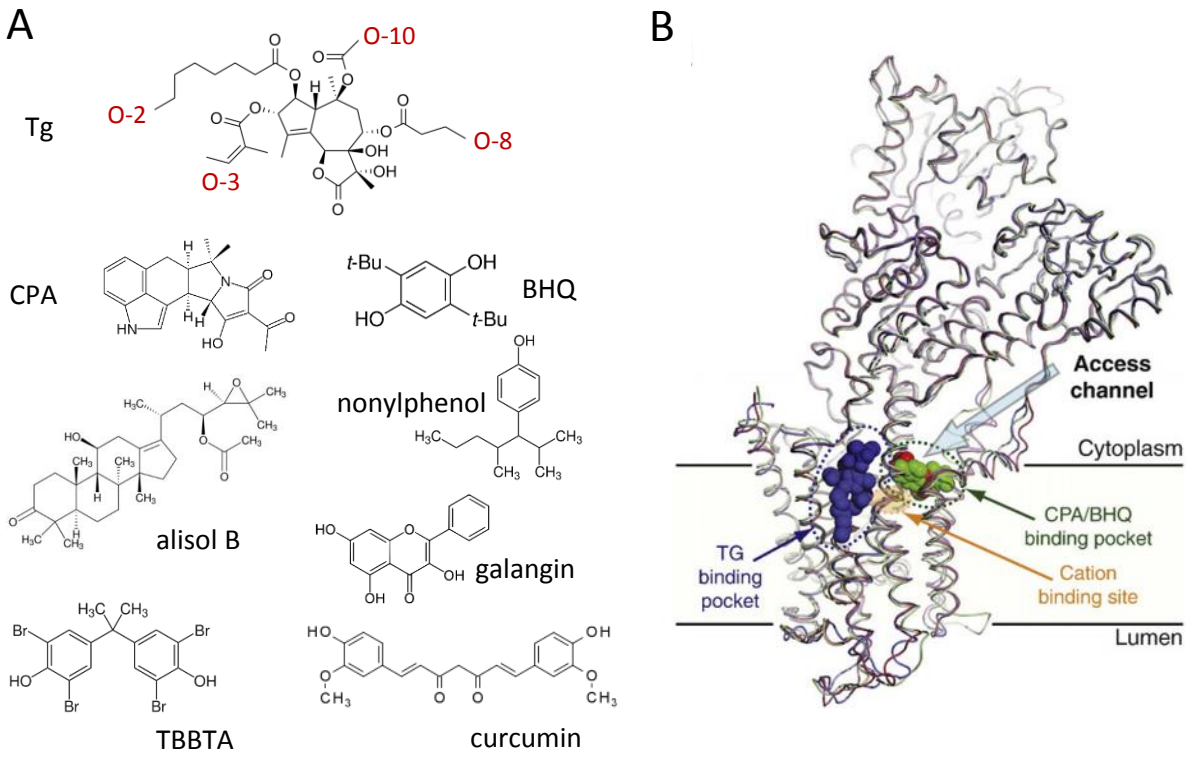

Figure 6. The structures of SERCA inhibitors and binding sites of thapsigargin (Tg), cyclopiazonic acid (CPA), and 2,5-di-(t-butyl)-dihydroxybenzene (BHQ) in SERCA inhibition. A) The chemical structures of SERCA inhibitors. B) A general presentation of the binding pockets of Tg, CPA, BHQ in SERCA1a TM region in the E2 conformation. Tg is colored in blue, CPA in green, BHQ in red. Figure 6B is adapted from (140).

CPA (IC_{50} 0.09-2.5 µM) is a toxic fungal metabolite from *Penicillium* and *Aspergillus* species, and BHQ (IC_{50} 2-7 µM) is synthetically made as an antioxidant (140). The two molecules inhibit SERCA by a similar mechanism: they stabilize SERCA in the E2 conformation, by binding at a partially overlapping pocket within the Ca^{2+} entry pathway formed between TM1-4. This pocket is created due to the kink conformation adopted by TM1 (141). The binding of CPA and / or BHQ hinders the Glu309, which is the gating residue for Ca^{2+} binding (140). In addition, some other small hydroxylated hydrophobic

inhibitors such as tetrabromobisphenol A (TBBPA, IC_{50} 1.5-2.3 µM) and nonylphenol (IC_{50} 6 µM) that lock the enzyme in the E2 conformation were proposed to work in a similar way (141). There are also inhibitors known to stabilize SERCA in the E1 conformation, such as curcumin (IC_{50} 15 µM) and flavonoids (*e.g.* dihydroxyflavone, IC_{50} 5.4 µM, galangin, IC_{50} 10.3 µM, and quercetin, IC_{50} 8.7 µM) that inhibit SERCA1 by preventing ATP binding (142,143) **(Figure 6)**.

5.2 Inhibitors of SPCA

Although SPCA shows a high degree of similarity with SERCA, only a few reports about SPCA specific inhibitors have been published so far. Bis(2-hydroxy-3-tert-butyl-5-methylphenyl)methane (bis-phenol or BP) and 2-aminoethoxydiphenylborate are suggested to be more specific for SPCA1 than for SERCA2 (144), whereas oleamide, linoleamide are more specific for SPCA2 than SERCA1 (145).

6. Ca^{2+}-ATPases as drug targets

To date, several P-type ATPases are therapeutic targets in the clinic. For example, omeprazole inhibits gastric H^+/K^+-ATPase, which is widely used to treat gastroesophageal reflux disease and peptic ulcer disease. Cardiac glycosides such as digoxin and digitoxin inhibit Na^+/K^+-ATPase, and were used as positive inotropic agents to increase heart contraction, although they are not widely used now due to the side effects (146). Also Ca^{2+}-ATPases are considered as drug targets, which will be discussed below.

6.1 SERCA and prostate cancer

The selective and targeted inhibition of SERCA by Tg was proposed for the treatment of cancer. By blocking SERCA, ER Ca^{2+} uptake is prevented, leading to a gradual depletion of Ca^{2+} from the ER. The decrease in ER Ca^{2+} levels induces Ca^{2+} entry via SOCE. Due to the inability to refill the ER store, a prolonged high $[Ca^{2+}]_{cyt}$ eventually leads to apoptosis (147), which may potentially be useful for cancer therapy.

As SERCA2b is ubiquitously expressed and functionally required in all cell types, selective targeting of SERCA2b only in the cancer tissue is needed. As a strategy, an inactive prodrug was developed for prostate cancer treatment, which consists of Tg conjugated to a small peptide carrier (148). The proteolytic removal of the conjugated peptides by prostate specific antigen or prostate specific membrane antigen for subsequent activation of Tg molecules is specifically executed by the target cancer cells. This strategy may be advantageous in slow-growing prostate cancer cells that are difficult

to target by conventional chemotherapy (149). The prodrug mipsagargin (G202) has passed phase I clinical trials and met the safety and tolerance requirements. It is now being tested in a phase II clinical trial (148,150).

6.2 SERCA and energy expenditure

Endotherms including human keep their body at a stable and metabolically favorable temperature by using the heat produced during routine metabolism. When experiencing cold stress, other mechanisms such as shivering of the skeletal muscle or non-shivering within brown adipose tissue (BAT) are applied. The latter is working primarily via the protein thermogenin (also called uncoupling protein 1 (UCP1)), a mitochondrial protein that uncouples the respiratory electron chain from mitochondrial ATP synthesis, while dissipating energy in the form of heat (151). Some species of deep sea fish, which lack BAT, evolved heater organs. The heater organ is derived from non-contractile extraocular muscle, which continuously cycles Ca^{2+} via the SERCA pump and a leaky RyR as a mechanism of non-shivering thermogenesis (152).

In skeletal muscle, SERCA1a is regulated by small endogenous regulators (see section 4.1). Among them, SLN is an uncoupler, *i.e.* SLN uncouples the ATPase activity from Ca^{2+} transport. SLN increases the rate of slippage of the ATPase and the rate of passive Ca^{2+} leak through the pump (153), which leads to increased heat production (154), a mechanism different from the futile Ca^{2+} cycling mentioned above. An *in vivo* study shows that thermogenesis is fully restored by reintroducing SLN in $SLN^{-/-}$ mice with surgically removed intrascapular BAT (155). Interestingly, during a high fat diet, $SLN^{-/-}$ mice gained more weight and gained more fat accumulation than WT, while WT had upregulated SLN expression (3 to 5-fold in the soleus) and were less obese. Mice with ablated intrascapular BAT consume more energy to adapt to cold temperature. Since the SLN-SERCA coupling is able to increase energy expenditure and reduces adiposity, this complex is considered as a potential target for obesity treatment.

The inducible brown-like white adipocytes (or the beige adipocytes) express UCP1 at a lower level compared to BAT. They play a marginal role in whole-body energy metabolism, but are important in glucose tolerance. Recently Ikeda *et al.* reported that the UCP1-independent thermogenic mechanism in beige fat involves ATP-dependent Ca^{2+} cycling through the SERCA2b-RyR2 pathway (156). Both the SERCA2 and RyR2 mRNA levels were increased in mice with promoted beige adipocyte biogenesis. Depletion or inhibition of SERCA2b or RyR2 significantly reduced oxygen consumption rates in $UCP1^{-/-}$ beige adipocytes. These mice also displayed an increased glucose tolerance and insulin sensitivity during a 24-week high fat diet (156). These results suggested that beige fat plays anti-obesity and anti-

diabetic roles that were independent of UCP1, but required a Ca^{2+} transporting cycle mediated by SERCA2b.

It was also found that the SERCA2b levels are reduced in liver of obese mice, leading to ER stress (157). Restoration of the SERCA2b level in the liver of these mice lowered ER stress, improved glucose tolerance and reduced the blood glucose levels (157). Moreover, enhancing SERCA2b levels in the liver of obese mice significantly reduced the lipogenic gene expression and triglyceride content in liver (157). Together, the activation of SERCA2b may be a promising approach for the treatment of diabetes and steatohepatitis.

6.3 SERCA2a and heart failure

Heart failure is a syndrome characterized by the inability of the heart to maintain the circulation of blood to meet the body's needs. Reduced SERCA2a levels are often observed in end stage failing hearts (56,158-160), and heart failure progression may be reversed by enhancing SERCA2a expression or activity, which has already been demonstrated in small and preclinical animal models (161-163). Although gene delivery of SERCA2a restores the contractility of human cardiomyocytes (164), the phase II clinical trial of cardiac specific SERCA2a viral gene delivery in end stage heart failure patients named CUPID failed. Most likely, the low transduction efficiency into patients explains the poor outcome (165).

An alternative approach to improve SERCA2a function is interfering with the SERCA-PLN complex via shRNA-mediated knockdown of PLN expression, gene delivery of dominant negative PLN mutants (K3E/R14E) (166), a PLN mutant that is pseudo-phosphorylated at Ser16 (Ser16Glu) (167), or of a SERCA2a mutant that is not sensitive to PLN inhibition (168). In addition, enhancing SERCA2a stability and activity by increasing SUMOylation level though SUMO1 gene delivery is also explored in murine and swine models (126). Finally, small peptide/molecule modulators that improve SERCA2a functionality are of therapeutic interest (43).

6.4 SPCA and breast cancer

The store-independent mechanism of Ca^{2+} influx through the SPCA2-Orai1 interaction contributes to the disturbed Ca^{2+} homeostasis in some breast cancer sub-types. SPCA2 is upregulated and involved in luminal and HER2 (estrogen-receptor and progesterone-receptor negative, HER2 positive) sub-types of breast cancer (10,169). Also, Orai1 expression is dramatically increased in several mammary tumor cell lines like MCF-7 and MDA-MB-231 (81). The Orai1 channel in MCF-7 breast cancer cells remains

constitutively activated by SPCA2 leading to constitutive Ca^{2+} influx, activation of MAP kinase pathways, high rates of proliferation and tumorigenesis (10). Knockdown of SPCA2 in MCF-7 cells attenuated cell proliferation, colony formation in soft agar and MCF-7-induced tumor formation in mice (10). In contrast to SPCA2, a high SPCA1 expression is observed in the highly metastatic basal-type cell line MDA-MB-231 (169,170), which may also lead to Orai1 channel activation (11). Interestingly, SPCA1 knockdown in MDA-MB-231 cells impairs the post-translational modification of Insulin-like growth factor 1 receptor (IGF1R), a protein important in tumor progression, and reduces cell proliferation (170).

Thus, SPCA1/2 isoforms play a prominent role in the Ca^{2+} dyshomeostasis of breast cancer cells (10,170-172). Furthermore, SPCA1/2 pumps might be potential therapeutic targets for breast cancer therapy. The use of SPCA1/2 inhibitors could be helpful since knockdown of SPCA1/2 showed impaired IGF1R processing (170) and reduced microcalcification level (169). Besides, interfering with the N-/C-terminal dependent activation of Orai1 may be a valuable approach, since a 40-amino acid fragment corresponding to the SPCA2 N-terminus interferes with the SPCA2-Orai1 interaction, which may prevent the pathological activation of Ca^{2+} influx (10).

6.5 SPCA and neurodegeneration

Yeast is a commonly used model organism to study human disease, since nearly 1000 yeast genes are members of orthologous gene families associated with human disease (173), but it has the advantage of a lower complexity. α-synuclein is a presynaptic protein that through formation of aberrant fibrils deposits in Lewy bodies, exerting toxic effects, which contribute to Parkinson's disease (174). Buttner *et al.* found that the yeast PMR1 mediates Ca^{2+} dyshomeostasis and oxidative stress as a consequence of heterologous expression of human α-synuclein, eventually leading to cell death (175). The high basal $[Ca^{2+}]_{cyt}$ and cell death caused by heterologous α-synuclein expression can be reversed by deletion of *pmr1*, but not of other genes coding Ca^{2+} transporters. Similarly, in *C. elegans* and in *D. melanogaster*, deletion of the pmr1 or SPoCk (orthologue of human SPCA1 in *D. melanogaster*) protects against loss of dopaminergic neurons as well as the compromised locomotion (175). Together, SPCA could be a conserved mediator of α-synuclein cytotoxicity.

7. Reconstitution of Ca^{2+}-ATPases

According to The Human Protein Atlas, 5,480 (*i.e.* about 28%) out of 19,613 human protein-coding genes are predicted to encode membrane protein products. However, due to their amphipathic nature,

membrane proteins are prone to aggregation in aqueous solutions, which makes them difficult to handle for biochemical studies that traditionally use water-based buffers. In addition, the numerous components present in a typical biological membrane add to the complexity for the characterization of a specific protein of interest.

To solve this problem, the protein of interest is often purified from the biological membranes, traditionally with the end products solubilized by detergents in aqueous solutions. However, as strong dissociation agents, detergents very often exert a negative impact on protein stability and activity (176,177). Furthermore, detergents form micelles above the critical micelle concentrations (CMC), above which monomers and micelles of the detergent coexist **(Figure 7A)**. To ensure proper membrane protein solubilization, the detergent concentration is usually kept above 2 CMC. The excess in detergent micelles may interfere with many biochemical/biophysical assays (178). Therefore, it is valuable to remove the detergent by reincorporating the purified membrane proteins into a controlled lipid bilayer membrane, a process called reconstitution, which is a very useful, but complex method that needs to be optimized for each protein/detergent system.

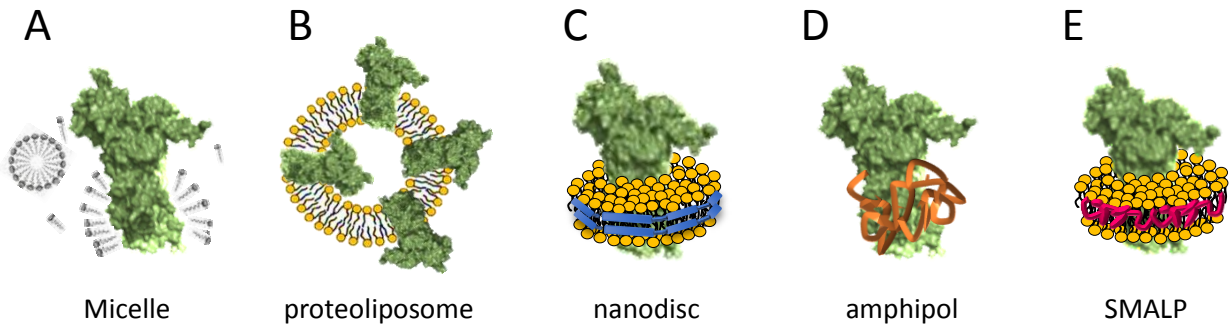

Figure 7: Scheme of various membrane protein systems. A) Detergent (grey) solubilized membrane protein (green) in detergent micelle, which co-exists with excess detergent micelles, and detergent monomers. B) Proteoliposome: a closed lipid (yellow headgroup with black tails) vesicle with inserted membrane proteins. The orientation of the inserted proteins is difficult to control. C) Nanodisc: a small lipid bilayer system with a membrane protein inserted. The hydrophobic edge of the lipid is shielded by membrane scaffolding proteins (blue). D) Amphipol (orange) polymer stabilized membrane proteins. E) 7.5.3 Styrene maleic acid lipid particles (SMALPS, pink) solubilized and stabilized membrane protein.

7.1 Criteria of reconstitution

A successful reconstitution depends on many criteria (179). The activity of the reconstituted membrane protein should remain high, which not only confirms successful protein insertion into the lipid membrane, but also the proper folding of the protein. Biological activity can be evaluated using specific biochemical assays depending on the nature of the protein. A high protein incorporation efficiency ensures a more effective reconstitution. Depending on the purpose of downstream

applications, homogeneous size distribution of the produced proteoliposomes, unidirection and/or low density of the inserted proteins in the lipid vesicles, low/high membrane permeability for ions/small molecules, unilamellar vesicular structure and large vesicular volume may be required.

7.2 Reconstitution into proteoliposomes

A proteoliposome **(Figure 7B)** is a lipid vesicle (liposome) system in which proteins are embedded. This system enables compartmentalization of cytosolic and exoplasmic domains at each side of the bilayer, which may be important for studying the vectorial transport function of ion pumps and channels. It also allows ordered packing of membrane protein in the membrane to form 2D crystals for structural study (179,180), which remains a challenge for membrane proteins.

In 1988, Lasic *et al.* proposed a mechanism by which vesicles are formed by detergent depletion (181). During the gradual removal of detergent from a detergent-phospholipid micelle solution, the interaction and coalescence between micelles could lead to growth in size and formation of large disc-like phospholipid structures, where the edge of the disc is shielded by detergent. As the detergent continues to be depleted, it can no longer shield the edge of the phospholipid discs, thus the discs start to bend in order to minimize the energy and will finally close to form bilayer vesicles (181). This standard principle can be applied to all detergent-mediated reconstitutions (179). Co-micellization of the purified protein with the excess lipids and detergent leads to formation of a mixture of protein-detergent-lipid micelles and detergent-lipid micelles. After detergent removal, proteoliposomes are formed. However, due to the different nature of the detergents, lipids and proteins of choice, as well as due to alternative approaches to remove the detergent, each membrane protein responds differently to the reconstitution procedures, which therefore needs to be optimized for each protein. Moreover, due to the short live times of the reconstitution intermediate states and to the lack of characterization methods, the knowledge about the mechanism of reconstitution remains limiting, which hampers the optimization of protocols to make reproducible proteoliposomes.

7.3 The “Step-by-step” reconstitution strategy

Proteoliposomes can be prepared by mixing detergent solubilized biological membrane fractions with liposomes followed by dilution until the detergent concentration falls below the CMC, at which point the membrane proteins start to partition into liposomes. It is important to use detergent types with a high CMC in this method, and an extra step is required for concentrating the samples (179). In the late 90’s, Rigaud *et al.* developed a new reconstitution method, which he named the “step-by-step” strategy **(Figure 8)** (179). This strategy not only allows efficient reconstitution of many membrane

proteins, but also revealed the mechanism and optimal detergent conditions for the proteins to associate with lipids.

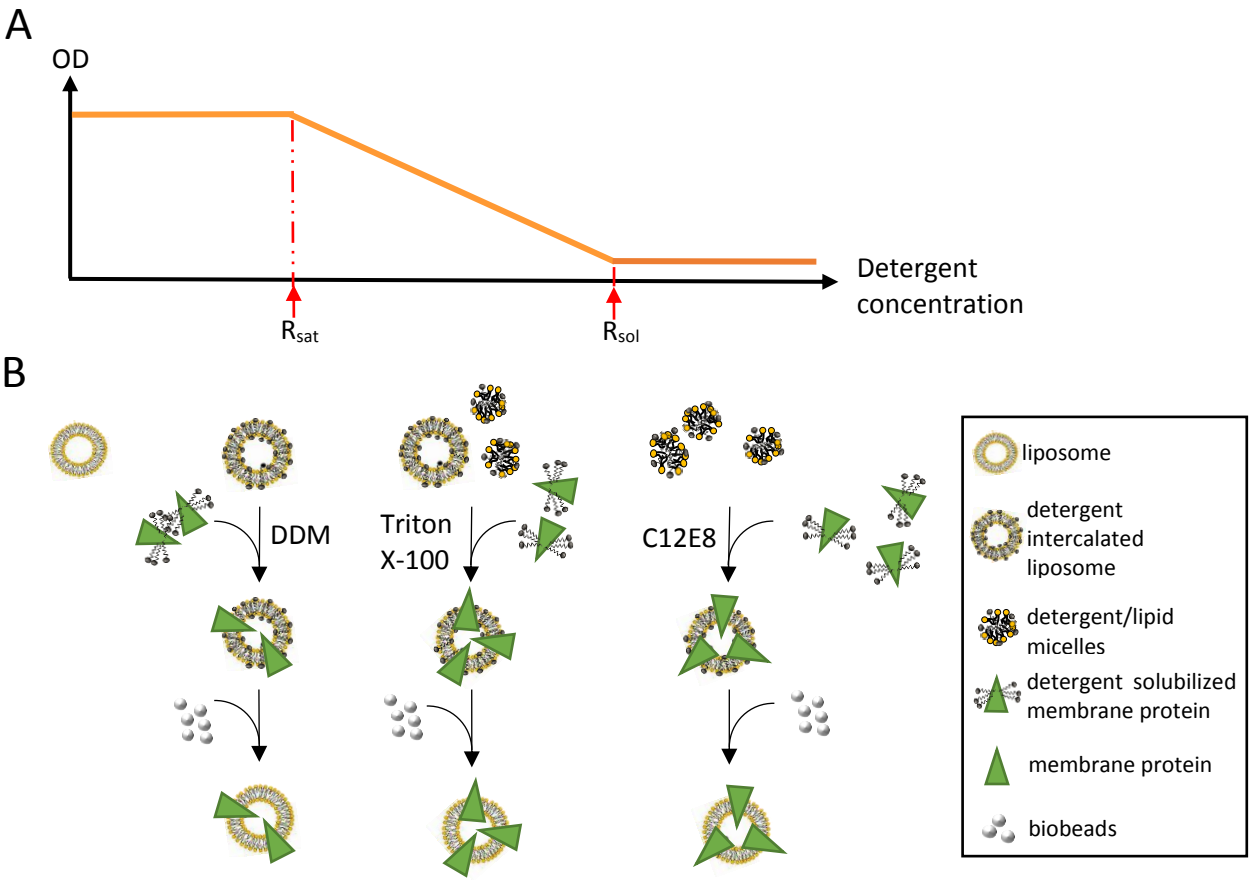

Figure 8. A scheme of the "step-by-step" reconstitution protocol. A) Change of the optical density (OD) of the preformed liposomes according to increased concentration of detergent. At each stage, the status of the lipid/detergent mixture is depicted below the x-axis: intact preformed liposomes before adding detergent, liposomes with intercalated detergent monomers until the detergent is saturated on the liposomes (R_{sat}, the ratio of detergent : lipid when the detergent concentration just reaches saturation on the lipid vesicles), afterwards the liposomes start to be dissolved, forming mixed micelles of detergent/lipids, and the OD starts to decrease. Once the R_{sol} (the ratio of detergent : lipid when the detergent concentration just reaches the total vesicle solubilization) point is reached, the OD becomes stable again with complete solubilization of liposomes. B) Reconstitution schemes start from each stage of solubilized liposomes. According to Rigaud *et al.*, the detergent DDM, Triton X-100, and C12E8 work most efficiently from the three different stages of detergent/lipid mix (figure adapted from (179)).

In this method, it is assumed that the lipid vesicle formation during detergent extraction is a reverse process of lipid vesicle solubilization by the detergent. After preparation of liposomes, they are subjected to various amounts of detergent for equilibration. The detergent monomers intercalate into lipid vesicles when the concentration is low, and gradually saturate the lipid vesicles. When the detergent concentration just reaches saturation on the lipid vesicles, we refer the ratio of detergent :

lipid at this point as R_{sat}. At above-saturation concentration, the detergent starts to solubilize the lipid vesicles (lamellar-to-micellar transition). When the detergent concentration just reaches the total vesicle solubilization, we refer the ratio of detergent : lipid at this point as R_{sol}. Above this concentration no lipid vesicles but only detergent-lipid micelles exist. Next, purified protein is added to the mixture and carefully equilibrated. The last step is detergent extraction, during which process the proteoliposomes form (179).

With this method, Rigaud *et al.* identified three categories of detergents that preferably mediate protein–lipid association via different mechanisms: 1) detergents that mediate membrane protein incorporation directly into the detergent partitioned lipid vesicles; *e.g*. dodecylmaltoside (DDM). 2) detergents that mediate membrane protein incorporation during transfer from mixed micelles to detergent saturated liposomes; *e.g.* Triton X-100. 3) detergents that mediate membrane protein incorporation during coalescence of micelles; *e.g*. octaethylene glycol monododecyl ether (C12E8) (179). According to these alternative methods of actions, DDM and Triton X-100 are more likely to promote unidirectional insertion of protein on the liposomes than C12E8.

7.4 Detergent removal

Detergent removal is a final step in detergent-mediated reconstitution, and it is a critical step to optimize if the proteoliposomes form by coalescence of mixed protein-lipid-detergent micelles. The lipid-detergent vesicles are very dynamic and can change in size when they just form and the detergent concentration is high. Thus, slow detergent removal results in more homogeneous liposomes. However, fast detergent removal is beneficial for proteins that are prone to aggregate or to be unstable when exposed to the detergents.

Detergent removal can be achieved by several methods, such as dialysis, gel filtration, dilution and adsorption by hydrophobic polystyrene beads (biobeads) (179). Among them, dialysis and biobeads adsorption are the most widely used methods.

Dialysis is often chosen because of its low cost and simplicity. During dialysis, detergent monomers from the protein-lipid-detergent mixture diffuse through the membrane of the dialysis bag to the bulk detergent-free solution. The speed of diffusion is dependent on the detergent monomer concentration gradient across the dialysis bag, and detergents of high CMC are more prone to dissociate from micelles to monomers upon dilution from the same concentration, therefore it is more suitable for removal of detergents with high CMC. For detergents with low CMCs, it may take weeks for complete

removal (182), which may be detrimental for many membrane proteins. In addition, it is difficult to control the rate of detergent removal, and hence the reproducibility of proteoliposome formation.

Biobeads are hydrophobic polystyrene beads to which the hydrophobic part of the detergent adsorbs. Biobeads appear to be superior due to several advantages: 1) the method is suitable for low CMC detergents, such as DDM, Triton X-100 and C12E8, which are mild detergents commonly used for handling membrane proteins; 2) the rate of detergent removal can be controlled by varying the amount of biobeads added and the time interval of biobead addition, which has been extensively characterized using radioactive detergents; 3) fast and complete detergent removal can be achieved, usually within a couple of hours (179).

7.5 Other reconstitution methods

Besides proteoliposomes, alternative reconstitution methods have been widely applied for detergent solubilized membrane proteins, such as the nanodiscs and the amphipols (see further in 7.5.1 and 7.5.2). However, even mild detergents can disrupt intramolecular interactions between protein subunits or domains, causing protein precipitation (176), or may affect intermolecular ligand or protein interactions. Therefore, alternative surfactants that serve the same purpose of solubilization, but that are less disruptive for protein complexes were developed. Reconsitution with the new classes of polymers, styrene maleic acid lipid particles (SMALPs), will also be discussed into more detail (in 7.5.3). Each of these systems has their unique advantages and disadvantages, which are summarized in **Table 1**.

7.5.1 Nanodiscs

A nanodisc **(Figure 7C)** is a small disc-shaped lipid bilayer system with a typical diameter of 8-16 nm (183). The hydrophobic edge of each leaflet is protected by an amphiphatic helical protein named membrane scaffolding protein (MSP). Besides preparation of detergent solubilized membrane protein, construction of nanodiscs also requires the purification of MSP separately. Typically, human serum apoliporotein A1 and its derivatives are chosen as the MSP. Mixing lipids, MSP and membrane protein followed by detergent extraction leads to the formation of nanodics with the membrane protein integrated in the lipid bilayer (184). Interestingly, proteins in nanodiscs can be accessed from both sides of the membrane, and are therefore ideal to study ligand binding at both sides of the membrane. The size of a nanodisc is controlled by the length of MSP that wraps around it, thus this system is more easy to achieve monodispersity (184,185), which could be important for spectroscopic studies.

However, the presence of MSP may interfere with techniques such as electron paramagnetic resonance and nuclear magnetic resonance (NMR) based assays (184).

7.5.2 Amphipols

Amphipols **(Figure 7D)** are short amphiphatic polymers that keep membrane proteins soluble by wrapping around the TM surface. Most amphipols contain densely spaced monomers with short alkyl chains (C8-C12) that are separated by a few hydrophilic monomers. All types of amphipols self-assemble into compact micelle-like particles with well-defined size, depending on their chemical structure. The best characterized type of amphipols is A8-35, a polyacrylic acid based polymer bearing around 35% free carboxylate groups, and assembles into particles averaging in size around 40 kDa, with an extremely low critical aggregation concentration (~0.002 g/L) (186). A8-35 is highly water soluble (>200 g/L) due to the anionic charges provided by the protonated carboxylate groups in aqueous solutions with a pH ≥ 7.

Typically, amphipols are used to replace detergent after membrane proteins are solubilized, which involves incubation of detergent solubilized protein with amphipols, followed by extraction of detergent with biobeads. The membrane proteins are then kept in detergent-free solutions, which often dramatically improve the stability of membrane protein. For example, bacteriorhodopsin completely denatures at room temperature within six days in a solution containing ~20 mM octylthioglucoside. However, once the detergent is replaced with amphipols, bacteriorhodopsin retains ~90% activity after one week, even at 40°C (187). In many cases, the use of amphipols does not alter the protein binding of ligands or the functions, nor interferes with most purification techniques and can even be used to refold denatured proteins. However, exceptions are found. For example, in the case of purified SERCA1a, the replacement of detergent by amphipols reduces SERCA1a turnover rate (188). This might be due to relative large movements in the SERCA1a TM region during the conformational changes that require adaptive reorganization of the amphipols, which increases free-energy demand compared to the situation in detergent micelles and slows down the turnover of the amphipols - trapped SERCA1a. In the case of poly-His tag-fused protein, the small tag might be shielded by the amphipols if it is close to the TM region. As a consequence, the His-tag may not bind to the nickel or cobalt column as efficiently as when it is in detergent micelles during affinity purification. Due to high dependence of the amphipols solubility on the degree of protonation, experimental conditions at a pH below 7 or in the presence of multivalent ions, especially Ca^{2+}, are not well tolerated. Therefore, care has to be taken in the assays for investigating P-type ATPases, in particular for Ca^{2+}-transporting ATPases, where Mg^{2+} is present in millimolar concentrations as an ATP-binding cofactor and where Ca^{2+} is often used in a high concentration for protein stabilization at E1 conformation (187).

Table 1. Advantages and disadvantages of different reconstitution system

system	advantages	disadvantages
Detergent micelle	-Keeps membrane proteins soluble in aqueous solution	-Poor mimetic system for native membrane; -May inactivate the protein -May dissociate protein-protein / protein-ligand interaction -Interference with biochemical assays
Proteoliposome	-No detergent present in the final state -Vectorial transport possible	-Limited control over the direction of protein insertion -Polydispersity of the vesicles (size, number of layers)
Nanodisc	-No detergent present in the final state -Controllable size of the disc -Access to both sides of the membrane proteins	-Not suitable to study vectorial transport activity -Not compatible with electron paramagnetic resonance / NMR based assays
Amphipol	-No detergent present in the final state -Access to both sides of the membrane proteins	-Not compatible with a high concentration of divalent ions -Not compatible when large conformational changes of the inserted protein are important -Not compatible at pH < 7
SMALP	-No detergent needed throughout purification	-Not compatible with high concentration of divalent ions -Not compatible if large conformational change is required -Not compatible at pH < 7

7.5.3 Styrene maleic acid lipid particles

SMALPs **(Figure 7E)** are made by using styrene maleic acid (SMA), an amphipathic polymer that is composed of a hydrophobic styrene part and a hydrophilic maleic acid part that contains carboxylates. Therefore, the solubility depends on the composition of the monomers as well as the pH that determines the protonation states of the SMA. In contrast to amphipols, SMAs are not only able to

stabilize membrane proteins by forming a belt surrounding the TM region of the protein with a layer of lipids in between, they also possess a solubilizing ability which enables them to extract membrane proteins from their native membranes, leading to the formation of “native nanodiscs” (189). Therefore, it allows for complete detergent-free handling of a membrane protein throughout the extraction till purification, even in small protein complexes.

Similar to amphipols, SMALPs precipitate at acidic pH and millimolar concentration of divalent ions, thus this method is incompatible with many biochemical assays. Furthermore, the stronger lateral pressure it provides as compared to a biological membrane can also hinder conformational changes in kinetic studies (178). The heterogeneity in the polymer size makes it unsuitable for some structural studies such as NMR.

Due to the combined solubilizing and stabilizing properties of SMA, several alternatives were developed to overcome the drawbacks, such as lower polydispersity, lower UV absorbance, and divalent cation tolerance (184).

II. Aims of the study

SPCA shares 43% sequence similarities with the related SERCA and is implicated in human diseases such as HHD and breast cancer. SPCA may also mediate α-synuclein induced toxicity, and may be important for viral particle maturation. In contrast to SERCA pumps, which have been studied in great detail, the experimental approach to investigate the housekeeping SPCA1 pumps is hampered by their moderate to low expression levels, the lack of specific high affinity inhibitors and their coexistence with (more active) SERCA pumps. All these factors complicate the characterization of SPCA pumps, both *in vivo* and *in vitro*.

The aim of this work was to study the housekeeping SPCA1 in purified and reconstituted systems, which allowed 1) the rational design of small molecule inhibitors of SPCA, and 2) a detailed biochemical characterization of SPCA1 in comparison to SPCA2.

To achieve the above mentioned aims, we proposed the following objectives:

1. **Purification of His-tagged hSPCA1a and hSPCA2 overexpressed in yeast, followed by reconstitution into proteoliposomes.**

   Yeast is a simple eukaryote microorganism that has been proven to be a suitable system for human SPCA protein expression. Here, we planned to heterologously express C-terminal His-tagged hSPCA1a/2 in yeast, isolate the membrane fractions and purify the SPCA proteins via Ni-NTA affinity chromatography. We also developed a protocol for reconstitution of SPCA1a and SPCA2 into proteoliposomes.

2. **Using the reconstituted SPCA1a to develop specific inhibitors of SPCA, based on the SERCA specific inhibitor Tg.**

   A specific inhibitor of SPCA potentially holds therapeutic value for *e.g.* breast cancer, but would also be useful for the biochemical and cellular characterization of these pumps. As Tg showed differential inhibitory potency towards SERCA1a and SPCA1a, we planned to use Tg as the starting lead compound to develop an SPCA specific inhibitor. To achieve this objective, the structure-activity relationship (SAR) information of Tg binding to SPCA1a was collected in detail via assessing a collection of Tg analogues. The conservation and differences in Tg binding mechanisms for the two related Ca^{2+}-ATPases could guide us to design a specific SPCA inhibitor.

3. Detailed biochemical characterizations and comparisons will be performed on reconstituted SPCA1a and SPCA2.

The SPCA1a and SPCA2 isoforms share 64% sequence identity, but differ in tissue and subcellular distribution as well as in function. Here we performed detailed biochemical characterizations of SPCA1a and SPCA2 via Ca^{2+}- and Mn^{2+}-dependent ATPase and phosphorylation assays. In yeast PMR1, the N-terminal unpaired EF-hand-like motif is critical for the pumping activity, substrate affinity and selectivity. This region is conserved in SPCA1a, but not in SPCA2, suggesting a similar regulatory role of the N-terminus in PMR1 and SPCA1a. The overlapping region in SPCA2 contains critical residues involved in the unconventional store-independent Ca^{2+} entry. Therefore, in this part we focused in particular on the N-terminus of SPCA1a. We explored its potential regulatory role in SPCA1, and whether it may contribute to the differences in biochemical properties between the two isoforms.

III. Results

1. Structure/activity relationship of thapsigargin inhibition on the purified Golgi/secretory pathway Ca^{2+}/Mn^{2+}-transport ATPase (SPCA1a)

Chen J., De Raeymaecker J., Hovgaard JB., Smaardijk S., Vandecaetsbeek I., Wuytack F., Møller JV., Eggermont J., De Maeyer M., Christensen SB., Vangheluwe P.

Abstract:

The Golgi/secretory pathway Ca^{2+}/Mn^{2+}-transport ATPase (SPCA1a) is implicated in breast cancer and Hailey-Hailey disease. Here, we purified recombinant human SPCA1a from *Saccharomyces cerevisiae* and measured Ca^{2+}-dependent ATPase activity following reconstitution in proteoliposomes. The purified SPCA1a displays a higher apparent Ca^{2+} affinity and a lower maximal turnover rate than the purified sarco(endo)plasmic reticulum Ca^{2+}-ATPase (SERCA1a). The lipids cholesteryl hemisuccinate, linoleamide/oleamide, and phosphatidylethanolamine inhibit and phosphatidic acid and sphingomyelin enhance SPCA1a activity. Moreover, SPCA1a is blocked by micromolar concentrations of the commonly used SERCA1a inhibitors thapsigargin (Tg), cyclopiazonic acid, and 2,5-di-tert-butylhydroquinone. Because tissue-specific targeting of SERCA2b by Tg analogues is considered for prostate cancer therapy, the inhibition of SPCA1a by Tg might represent an off-target risk. We assessed the structure-activity relationship (SAR) of Tg for SPCA1a by in silico modeling, site-directed mutagenesis, and measuring the potency of a series of Tg analogues. These indicate that Tg and the analogues are bound via the Tg scaffold but with lower affinity to the same homologous cavity as on the membrane surface of SERCA1a. The lower Tg affinity may depend on a more flexible binding cavity in SPCA1a, with low contributions of the Tg O-3, O-8, and O-10 chains to the binding energy. Conversely, the protein interaction of the Tg O-2 side chain with SPCA1a appears comparable with that of SERCA1a. These differences define a SAR of Tg for SPCA1a distinct from that of SERCA1a, indicating that Tg analogues with a higher specificity for SPCA1a can probably be developed.

Author contributions:

P. V. conceived the idea for the project and coordinated the study. J. C. conducted most of the experiments and analyzed the data. J. D. R., M. D. M., J. B. H., S. S., and I. V. conducted experiments on *in silico* modeling, Tg analogue synthesis, and SPCA1a purification. J. V. M., J. E., S. B. C., P. V., and F. W. analyzed the data and critically reviewed the manuscript. P. V. and J. C. wrote the manuscript. All authors reviewed the results and approved the final version of the manuscript.

JBC ARTICLE

Structure/activity relationship of thapsigargin inhibition on the purified Golgi/secretory pathway Ca^{2+}/Mn^{2+}-transport ATPase (SPCA1a)

Received for publication, January 26, 2017, and in revised form, March 2, 2017 Published, Papers in Press, March 6, 2017, DOI 10.1074/jbc.M117.778431

Jialin Chen[‡], Joren De Raeymaecker[§], Jannik Brøndsted Hovgaard[¶], Susanne Smaardijk[‡], Ilse Vandecaetsbeek[‡], Frank Wuytack[‡], Jesper Vuust Møller[‖], Jan Eggermont[‡], Marc De Maeyer[§], Søren Brøgger Christensen[¶], and Peter Vangheluwe[‡1]

From the [‡]Laboratory of Cellular Transport Systems, Department of Cellular and Molecular Medicine, and [§]Biochemistry, Molecular and Structural Biology Section, Department of Chemistry, KU Leuven, 3000 Leuven, Belgium, the [¶]Department of Drug Design and Pharmacology, University of Copenhagen, DK-2100 Copenhagen, Denmark, and the [‖]Department of Biomedicine, University of Aarhus, 8000 Aarhus, Denmark

Edited by F. Anne Stephenson

The Golgi/secretory pathway Ca^{2+}/Mn^{2+}-transport ATPase (SPCA1a) is implicated in breast cancer and Hailey-Hailey disease. Here, we purified recombinant human SPCA1a from *Saccharomyces cerevisiae* and measured Ca^{2+}-dependent ATPase activity following reconstitution in proteoliposomes. The purified SPCA1a displays a higher apparent Ca^{2+} affinity and a lower maximal turnover rate than the purified sarco(endo)plasmic reticulum Ca^{2+}-ATPase (SERCA1a). The lipids cholesteryl hemisuccinate, linoleamide/oleamide, and phosphatidylethanolamine inhibit and phosphatidic acid and sphingomyelin enhance SPCA1a activity. Moreover, SPCA1a is blocked by micromolar concentrations of the commonly used SERCA1a inhibitors thapsigargin (Tg), cyclopiazonic acid, and 2,5-di-*tert*-butylhydroquinone. Because tissue-specific targeting of SERCA2b by Tg analogues is considered for prostate cancer therapy, the inhibition of SPCA1a by Tg might represent an off-target risk. We assessed the structure-activity relationship (SAR) of Tg for SPCA1a by *in silico* modeling, site-directed mutagenesis, and measuring the potency of a series of Tg analogues. These indicate that Tg and the analogues are bound via the Tg scaffold but with lower affinity to the same homologous cavity as on the membrane surface of SERCA1a. The lower Tg affinity may depend on a more flexible binding cavity in SPCA1a, with low contributions of the Tg O-3, O-8, and O-10 chains to the binding energy. Conversely, the protein interaction of the Tg O-2 side chain with SPCA1a appears comparable with that of SERCA1a. These differences define a SAR of Tg for SPCA1a distinct from that of SERCA1a, indicating that Tg analogues with a higher specificity for SPCA1a can probably be developed.

As an important secondary messenger, the partitioning of intracellular Ca^{2+} controls a wide range of cellular responses, including contraction, secretion, cell growth, differentiation, proliferation, and cell death (1, 2). A sub-micromolar basal cytosolic Ca^{2+} concentration range is strictly maintained by intracellular Ca^{2+} pumps, whereas Ca^{2+} channel activity produces confined spatial and temporal cytosolic Ca^{2+} signals up to 10–100 μM that control various cellular activities. Ca^{2+} transporters belonging to the P2-type Ca^{2+} transport ATPases maintain the low housekeeping cytosolic Ca^{2+} levels and reduce the cytosolic Ca^{2+} concentration when a Ca^{2+}-signaling event ceases. The P2-type ATPases encompass the plasma membrane Ca^{2+}-ATPase, SERCA,[2] and SPCA Ca^{2+} pumps that perform active Ca^{2+} transport across the plasma membrane, the intracellular membranes of the sarco(endo)plasmic reticulum, and the Golgi/secretory pathway, respectively (3). SERCA and SPCA belong to the subfamily P2A and share around 30% sequence identity and over 40% similarity (4).

In humans, the SPCA proteins are encoded by two genes (*ATP2C1* and *ATP2C2*) (4–7). SPCA1 is the housekeeping isoform, which by transporting Ca^{2+} and Mn^{2+} into the Golgi lumen supports essential Golgi/secretory pathway functions. Ca^{2+}/Mn^{2+} transport is required for proper protein folding, enzymatic activities (*e.g.* glycosylation), sorting, and/or trafficking of proteins (8). In conjunction with SERCA, this ATPase also provides Ca^{2+}-storage pools for subsequent Ca^{2+}-release events (4, 9, 10). A total of four SPCA1 splice variants exist, SPCA1a–d, differing only at the C terminus. Although SPCA1a is considered to be the housekeeping variant, the differential tissue/subcellular distributions of the SPCA1 isoforms remain

This work was supported by Flanders Research Foundation FWO Grants G044212N and G0B1115N, the Inter-University Attraction Poles Program P7/13, and by the Danish Council for Strategic Research. The authors declare that they have no conflicts of interest with the contents of this article.

This article contains supplemental Materials and methods and additional references.

[1] To whom correspondence should be addressed: Laboratory of Cellular Transport Systems, Dept. of Cellular and Molecular Medicine, ON1 Campus Gasthuisberg, KU Leuven, Herestraat 49/Box 802, B3000 Leuven, Belgium. Tel.: 32-16-330720; E-mail: peter.vangheluwe@kuleuven.be.

[2] The abbreviations used are: SERCA, sarco(endo)plasmic reticulum Ca^{2+}-ATPase; Tg, thapsigargin; PSA, prostate-specific antigen; SAR, structure-activity relationship; CPA, cyclopiazonic acid; BHQ, 2,5-di-*tert*-butyl-hydroquinone; BP (bisphenol), 2,2′-methylenebis(6-*tert*-butyl-4-methylphenol); ANOVA, analysis of variance; MOE, molecular operating environment; PDB, Protein Data Bank; BisTris, 2-[bis(2-hydroxyethyl)amino]-2-(hydroxymethyl)propane-1,3-diol; 2-ME, 2-mercaptoethanol; DDM, *n*-dodecyl β-D-maltoside; Ni-NTA, nickel-nitrilotriacetic acid; PC, phosphatidylcholine; CL, cholesterol; SM, sphingomyelin; PA, phosphatidic acid; PE, phosphatidylethanolamine; CHEMS, cholesteryl hemisuccinate; CV, column volume; PS, phosphatidylserine; SPCA, Golgi/secretory pathway Ca^{2-}-ATPase.

© 2017 by The American Society for Biochemistry and Molecular Biology, Inc. Published in the U.S.A.

largely unexplored (11). The more restricted expression pattern of SPCA2 in cultured hippocampal neurons, colon, secretory acini, and luminal epithelial cells of mouse mammary tissue suggests that the second isoform may play a more specialized function, for instance in secretion (6, 12–14).

In humans, SPCA1 haploinsufficiency, due to heterozygous loss-of-function mutations, causes Hailey-Hailey disease (OMIM169600), a heritable autosomal-dominant skin disorder characterized by recurrent skin vesicles and erosions that typically arise in adulthood (15, 16). In addition, SPCA1a and/or SPCA2 proteins are up-regulated in mammary gland during lactation and in various breast cancer sub-types thereby contributing to a pathological Ca^{2+} dyshomeostasis (17, 18). Independent of its transport activity, SPCA2 interacts with and activates the plasma membrane Ca^{2+} channel Orai1 via the N and C termini (18), leading to store-independent Ca^{2+} entry (18) and subsequent Ca^{2+} transfer into the secretory pathway (19). During lactation, this system contributes to the cellular uptake of Ca^{2+} in mammary gland epithelial cells for the subsequent release of Ca^{2+} into the milk (20).

In general, SPCA1 isoforms display a higher Ca^{2+} affinity but a lower maximal turnover rate than SERCA isoforms (21), but so far, a detailed functional analysis of SPCA isoforms has remained difficult due to the confounding presence of other abundant housekeeping Ca^{2+}-ATPases in cellular membrane fractions. In addition, although several potent SERCA inhibitors (thapsigargin (Tg), cyclopiazonic acid (CPA), and 2,5-di-*tert*-butylhydroquinone (BHQ)) are widely used to selectively inhibit endoplasmic reticulum Ca^{2+} transport (4, 22), selective pharmacological tools for SPCA inhibition are lacking. Because of the close sequence homology between SERCA and SPCA isoforms, several of the so-called highly selective SERCA inhibitors are also reported to inhibit SPCA in isolated membrane fractions of various organisms, albeit at much higher concentrations (4, 23–25).

The inhibition of SPCA1a by Tg may give rise to some concerns in connection with the clinical use of Tg analogues that target SERCA for prostate cancer therapy. In this therapeutic approach, a non-toxic, cell-impermeable pro-drug is administered that consists of a Tg analogue, which is coupled to a peptide that is specifically cleaved by the prostate-specific antigen (PSA) protease (26, 27). Extracellular cleavage of the peptide by local PSA in or near the prostate cancer releases the toxic Tg analogue Leu-8ADT, which is taken up by neighboring PSA-excreting cancer cells inducing targeted cell death (27). The estimated 3 orders of magnitude difference in the binding affinity of Tg for SERCA and SPCA may be considered sufficiently discriminatory to enable the use of Tg analogues for selective SERCA inhibition *in vitro* and *in vivo*. However, it remains unclear whether this is also true for other Tg analogues.

Toward the design of Tg analogues for clinical therapy related to SPCA dysfunction (see "Discussion"), we wanted to understand the off-target effect of Tg on SPCA1a, the closest relative of SERCA, by determining the structure-activation relationship (SAR) of Tg for SPCA1a. Moreover, due to the reported micromolar affinity of Tg to SPCA1 (24), one might consider Tg as a possible lead compound for the development of an SPCA1a inhibitor. Insights in the SAR of Tg for SPCA1a may aid the design of specific SPCA1a inhibitors as powerful pharmacological tools.

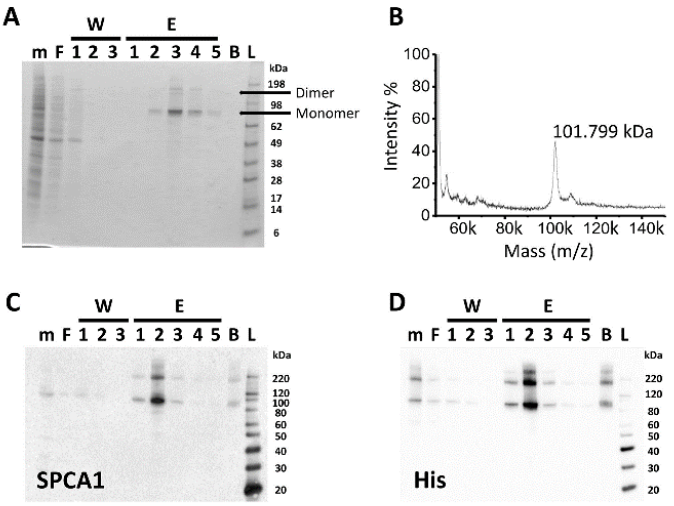

Figure 1. Purification of the human SPCA1a isoform by affinity chromatography. Gel stained for an SDS-PAGE (*A*), mass spectrometry analysis (*B*), and immunoblotting (*C* and *D*) of hSPCA1a fractions collected during affinity purification. The yeast membrane fractions (*m*), the flow-through after binding to Ni-NTA beads (*F*), the flow-through of each washing step (*W1–3*), each elution fraction (*E1–5*), and the beads (*B*) after elution were collected. Equal volumes of each fraction were separated via SDS-PAGE. Immunoblotting was performed with antibodies against SPCA1a (*C*) or the C-terminal His tag (*D*). Images are representative for a minimum of $n = 3$ experiments. *L*, ladder.

In this study, we purified the human SPCA1a isoform from a yeast recombinant expression system and reconstituted it into lipid vesicles. This purified system eliminates the influence of other membrane-bound contaminants or Ca^{2+}-ATPases, allowing the biochemical characterization of SPCA1a relative to purified and reconstituted SERCA1a. In particular, we demonstrate that SPCA1a activity is sensitive to the lipid environment, and we show that Tg and cholesteric compound sensitivity of SPCA1a may depend on the same or the overlapping binding pocket formed by transmembrane helices M3, M5, and M7. Finally, we have established the SAR of Tg for SPCA1a to facilitate the design of more selective SPCA inhibitors.

Results

Affinity purification of recombinant human SPCA1a from Saccharomyces cerevisiae

The relatively low expression level of SPCA1a in native tissues, typically in a background of high SERCA expression, hampers biochemical analysis of SPCA1a. As an alternative approach, we purified His_8-tagged human SPCA1a via Ni-NTA affinity chromatography from *S. cerevisiae*, which serves as an excellent model system to produce and purify P-type transport ATPases (8). SDS-PAGE analysis reveals that SPCA1a monomer and dimer bands were highly enriched in the elution fractions (Fig. 1*A*). Using mass spectrometry, we observed a molecular mass of 101.8 kDa, close to the predicted molecular mass of 101.7 kDa and high purity (>95%) of the human SPCA1a (Fig. 1*B*). The concentrated His-tagged SPCA1a in the elution fraction was further demonstrated by immunoblotting with SPCA1 (Fig. 1*C*) and His tag (Fig. 1*D*)-specific antibodies.

Inhibition of SPCA1a by thapsigargin

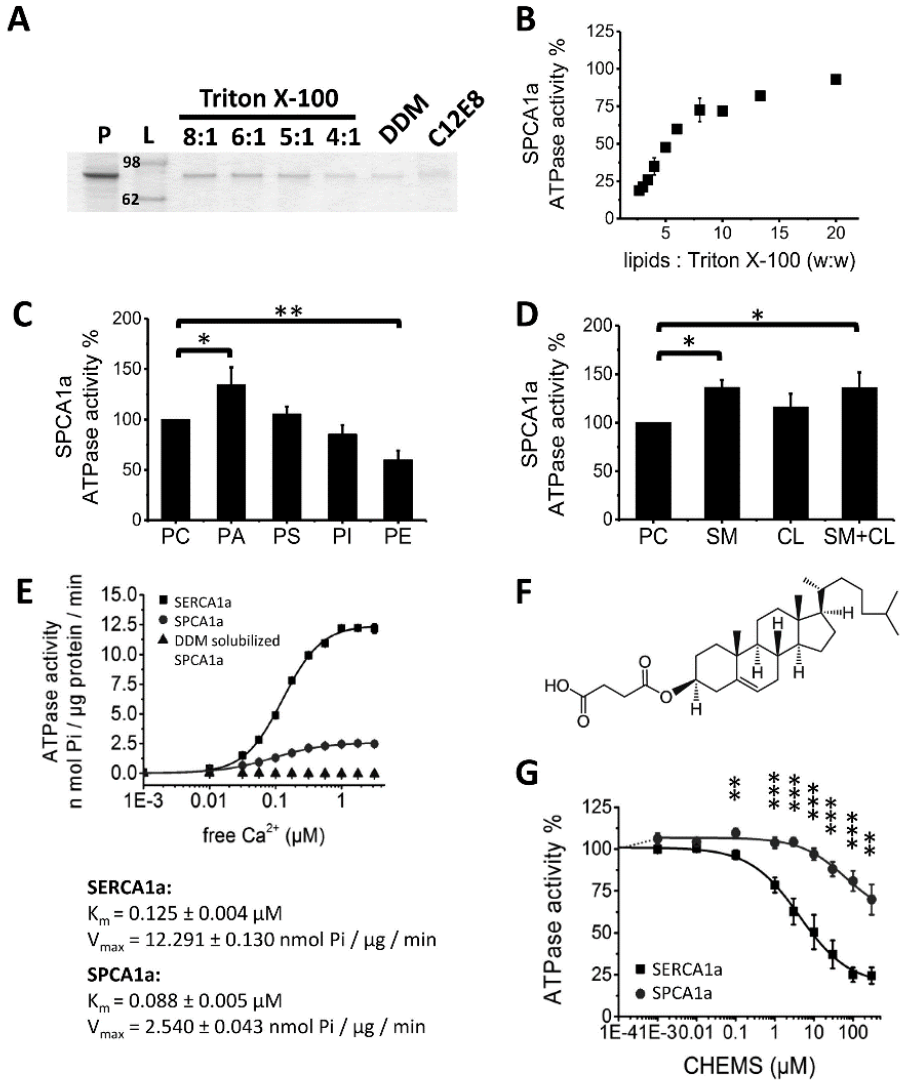

Figure 2. Optimization of SPCA1a reconstitution into proteoliposomes. *A*, SDS-polyacrylamide gel stained with SPCA1a proteoliposomes generated with the detergents Triton X-100, DDM, or C12E8. Same volume of samples was loaded on the gel after reconstitution. The lipid/Triton X-100 ratios (w/w) are indicated *above* the lanes. *B*, comparison of the SPCA1a ATPase activity following reconstitution with a different (w/w) ratio of lipids/Triton X-100. *C* and *D*, 20% weight percent of the indicated lipid(s) were supplemented to PC for SPCA1a reconstitution, and the maximal Ca^{2+}-dependent ATPase activity was determined at 1 μM free Ca^{2+} concentration ($n \geq 3$). The ATPase activities were normalized to the activity when only PC was used. Comparison of the specific SPCA1a ATPase activities in the presence of indicated phospholipids (*C*), CL, SM, or the combination of CL and SM (1:1 molar ratio) (*D*). *E*, comparison of the specific ATPase activities between SERCA1a and SPCA1a in proteoliposomes, and SPCA1a in lipid-free, DDM-solubilized state ($n = 3$). The DDM-solubilized SPCA1a was purified without supplement of PC in the buffers. *F*, structure of CHEMS. *G*, dose-responses of CHEMS on reconstituted SERCA1a and SPCA1a ATPase activities. *P*, purified SPCA1a; *L*, ladder; *PA*, phosphatidic acid; *PE*, phosphatidylethanolamine; *PS*, phosphatidylserine; *PI*, phosphatidylinositol; *CL*, cholesterol; *SM*, sphingomyelin; *CHEMS*, cholesteryl hemisuccinate. *, $p < 0.05$; **, $p < 0.01$; ***, $p < 0.001$.

SPCA1a reconstitution into proteoliposomes restores Ca^{2+}-dependent ATPase activity

We found that purified and lipid-free SPCA1a became reversibly inactivated in detergent solution (Fig. 2*E*). This we considered to be a result of either a removal of specific lipid component(s) essential for activity or loss of physical membrane constraints originally imposed by the membrane lipids. To restore a functional lipid environment, we reconstituted as described under "Experimental procedures" the proteoliposomes from detergent-solubilized SPCA1a by addition of defined lipid components, followed by removal of detergent with Bio-beads. For this, 600 μg of phosphatidylcholine (PC) was first mixed with 200 μg of purified and detergent-solubilized SPCA1a (*i.e.* the protein was solubilized with detergent at a lipid/protein ratio of 3:1, w/w). The efficiency of SPCA1a incorporation into liposomes was compared for three types of detergents, *i.e.* Triton X-100 (PC/Triton X-100 = 8:1, 6:1, 5:1, 4:1 (w/w)), *n*-dodecyl β-D-maltoside (DDM) (PC/DDM = 1:1 (mol/mol)), and octaethylene glycol monododecyl ether (C12E8) (PC/C12E8 = 1:2 (w/w)), in line with already established protocols for SERCA1a (28, 29). Reconstitution with Triton X-100 rendered the most efficient incorporation of SPCA1a into proteoliposomes, especially at a high lipid to detergent ratio (Fig. 2*A*). Importantly, we were able to recover the Ca^{2+}-dependent ATPase activity of the purified SPCA1a reconstituted with Triton X-100 or DDM but not with C12E8. Moreover, we determined that a lipid/detergent ratio of 20:1 generated the most active SPCA1a in proteoliposomes (Fig.

2*B*). Therefore, all further reconstitutions were carried out with a lipid/protein/detergent weight ratio of 60:20:3.

Lipids phosphatidic acid, sphingomyelin, cholesterol, and linoleamide/oleamide modulate SPCA1a activity

Membrane proteins are functionally adapted to the local lipid environment of their cellular membranes. We therefore analyzed the impact of different lipid types on the Ca^{2+}-dependent ATPase activity of SPCA1a, which in human colon adenocarcinoma cells is sensitive to cholesterol (CL) and is preferentially associated with lipid rafts (30). For reconstitution, various phospholipids (Fig. 2*C*), CL, sphingomyelin (SM), or a combination of the latter two (SM + CL) (Fig. 2*D*) were supplied together with PC, and SPCA1a ATPase activity was assessed. Compared with PC alone, the presence of phosphatidic acid (PA), SM, or SM/CL slightly but significantly enhanced activity, whereas phosphatidylethanolamine (PE) lowered the SPCA1a ATPase activity. In further experiments, PA was routinely added during SPCA1a reconstitution, as has been done previously for SERCA1a reconstitution (29), although we cannot exclude that PA may be a low-abundance lipid in the native Golgi membrane (31, 32).

Next, we directly compared the biochemical properties of purified and reconstituted SPCA1a (4:1 PC/PA ratio) and SERCA1a, the skeletal muscle Ca^{2+}-transport ATPase, which was purified and reconstituted according to a well established protocol (29) (with a 9:1 PC/PA ratio as in Ref. 33) (Fig. 2*E*). Compared with SERCA1a, SPCA1a displays a higher apparent Ca^{2+} affinity (K_m of 0.125 ± 0.004 and 0.088 ± 0.005 μM, respectively) and a 5-fold lower turnover rate (V_{max} of 12.29 ± 0.13 and 2.54 ± 0.04 nmol of P_i/μg/min), in line with previous reports (21).

Although we previously reported that SPCA1a and SERCA1a respond differently to CL (30), we observed here little functional effects of incorporating 20% CL upon reconstitution. However, by replacing CL with cholesteryl hemisuccinate (CHEMS), a more soluble cholesterol derivative (Fig. 2*F*), we found that it affected both the reconstituted SPCA1a or SERCA1a activities (Fig. 2*G*). SERCA1a displayed a concentration-dependent inhibition by CHEMS with an IC_{50} (defined as the concentration that leads to 50% inhibition of activity) of 8.8 ± 0.66 μM and a maximal inhibition of 80% at around 100 μM. For SPCA1a, a slight and not significant activation up to 106% was observed at lower concentrations, whereas higher concentrations above 6 μM impaired SPCA1a to a maximal inhibition of 47% at 300 μM, in line with the previous observation that SPCA1a and SERCA1a respond differently to CL (30).

Because two endogenous lipids oleamide and linoleamide have recently been reported to be inhibitors of SPCA2 (34), we tested here whether these lipids also modify SPCA1a or SERCA1a activity (Fig. 3, *A* and *B*). Up to 1 mM, oleamide only partially inhibited SPCA1a and SERCA1a (Fig. 3*A*), whereas complete inhibition was previously reported for SPCA2 (34). In contrast to SERCA1a, linoleamide fully inhibited SPCA1a with an IC_{50} of 30 μM (Fig. 3*B*), which is 8-fold higher than the value that has been reported for SPCA2 (34), although a side by side SPCA1a/2 comparison could not be performed.

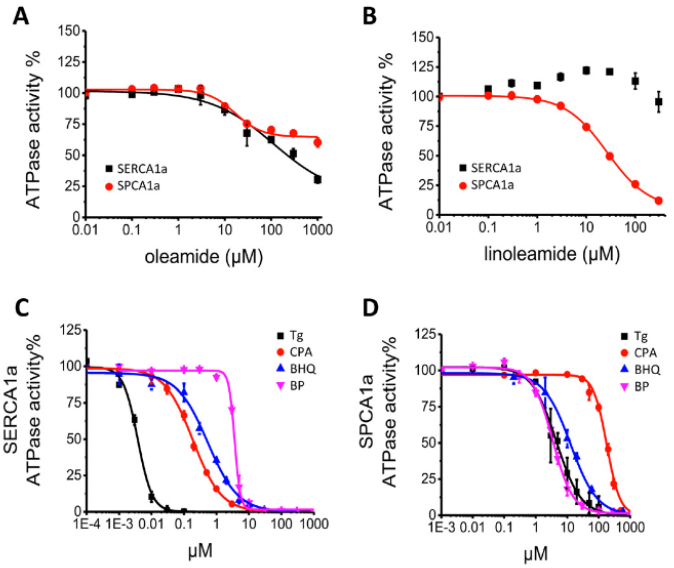

Figure 3. Dose-response effects of SPCA1a and SERCA1a inhibitors. Dose-response curves of oleamide (*A*) and linoleamide (*B*) on SERCA1a and SPCA1a. Dose-response curves for the inhibition of SERCA1a (*C*) and SPCA1a (*D*) by Tg, CPA, BHQ, and BP. $n = 3$ for all experiments.

Several SERCA inhibitors block SPCA1a activity at micromolar concentration

To further validate the reconstituted SPCA1a system, we verified whether bisphenol (35, 36) and the SERCA inhibitors Tg, CPA, and BHQ also inhibit SPCA1a (24, 25). We confirmed that all compounds completely inhibit SERCA1a and SPCA1a, but we show that the compounds are effective in different concentration ranges for SERCA1a and SPCA1a (Table 1 and Fig. 3, *C* and *D*). For SERCA1a, the IC_{50} value of Tg falls below 10 nM, whereas higher (sub-μM) IC_{50} values are observed for CPA and BHQ. 2,2′-Methylenebis(6-*tert*-butyl-4-methylphenol) (bisphenol, BP) displays the lowest potency with an IC_{50} above 1 μM. For SPCA1a, the IC_{50} values of Tg and CPA are at least 3 orders of magnitude higher than for SERCA1a, whereas the IC_{50} value of BHQ is only 20 times higher. The IC_{50} value of BP is comparable for the two pumps, indicating that unlike what was suggested by a previous study (35), BP cannot be considered as a more selective inhibitor of SPCA1a than of SERCA1a. Remarkably, the slopes of the dose-response curves for BP (SERCA1a) and CPA (SPCA1a) are higher than 2 (2.9 ± 0.1 and 2.3 ± 0.1, respectively). This was also observed in earlier studies (25, 35) and may reflect differences in the cooperativity (37). In conclusion, the SERCA inhibitors Tg, CPA, and BHQ also inhibit SPCA1a, although at much higher concentrations.

Tg scaffold together with the O-2 moiety are mainly responsible for the inhibition of SPCA1a

Of the so-called specific SERCA inhibitors, Tg has the highest affinity for SPCA1a. Insights into the SAR of Tg on SPCA1a might be helpful to aid the development of Tg analogues with either low or high SPCA1a affinity. We therefore explored the SAR of Tg for SPCA1a and compared it with the well established SAR of Tg for SERCA1a (38).

First, we compared the Tg-binding pocket in the SERCA1a-Tg structure and in an SPCA1a homology model in the same E2

Inhibition of SPCA1a by thapsigargin

Table 1
IC_{50} values for SPCA1a and SERCA1a measured for Tg, CPA, BHQ, and BP

Tg is thapsigargin; CPA is cyclopiazonic acid; BHQ is 2,5-di-*tert*-butylhydroquinone; BP is bisphenol.

	SPCA1a IC_{50}	SERCA1a IC_{50}
	μM	μM
Tg	7.7 ± 1.5	< 0.01
CPA	182 ± 10	0.19 ± 0.01
BHQ	13 ± 2	0.54 ± 0.06
BP	3.5 ± 0.2	3.63 ± 0.09

conformation. In SERCA1a, the non-flexible tricyclic guaianolide nucleus of Tg provides a scaffold for the optimal position of side chains within the Tg-binding pocket formed by transmembrane helices M3, M5, and M7 (Fig. 4*B*). The lipophilic groups at O-3, C-4, O-8, and O-10 of Tg (Fig. 4*A*) critically determine the hydrophobic interaction and provide complementarity to the binding cavity in SERCA1a (39, 40). In the SERCA1a-Tg structure (41), the O-8 moiety of Tg orients to the interior of M3 and M5, whereas the O-2 chain is located in the interface between the transmembrane region and the membrane (42). By comparing the residues in the Tg-binding pocket of SERCA1a (Fig. 4*B*) and the homology model of SPCA1a (Fig. 4*C*), we anticipate that the Tg-binding affinity, mechanism of inhibition, and/or positioning of Tg are affected by several amino acid substitutions, including the homologous SERCA1a/SPCA1a substitutions labeled in Fig. 4, *B* and *C* (Phe-256/Leu-265, Val-263/Tyr-272, Ile-765/Leu-707, Ile-829/Leu-771, and Phe-834/Ile-776), which might result in an altered SAR of Tg for SPCA1a as compared with SERCA1a.

To establish the SAR of Tg for SPCA1a, we measured the IC_{50} values of a series of Tg analogues with various side chain substitutions. First, the acyl groups O-2, O-3, O-8, and O-10 (Fig. 4*A*) were one by one replaced by –OH or –H, which significantly increases the IC_{50} of Tg in SERCA1a (39, 40, 43). Remarkably, only the removal of the Tg O-2 chain led to a significantly higher IC_{50} value in SPCA1a, suggesting that of all tested side groups O-2 contributes the most to the inhibitory effect of Tg in SPCA1a (Table 2). Based on the calculation of the free energy change for binding caused by the removal of a side chain, the O-2 contribution is comparable in SPCA1a and SERCA1a, whereas O-3, O-8, and O-10 contribute much less in SPCA1a (Table 2). The absence of O-3, O-8, and O-10 contributions at least partially explains the lower Tg affinity in SPCA1a than in SERCA1a.

Besides the side-chain contribution by O-2, the Tg scaffold might be mainly responsible for the inhibitory effect of Tg in SPCA1a. Indeed, like in SERCA1a, the conversion of the 7,11-gem diol in Tg into an epoxide led to a dramatic reduction of the inhibitory effect in SPCA1a (Table 2), presumably by the loss of hydrogen donors in the molecule or by the changed conformation of the tricyclic nucleus due to the conversion of the stereochemistry at C-11. Of note, some Tg analogues require a longer pre-incubation time with SERCA1a to obtain the full inhibitory potential, which can be explained by a time-dependent induced fit of Tg into the SERCA1a pocket (44). However, the weaker inhibitory potential of the Tg analogues in which the octanoyloxy group has been substituted with a hydrogen atom (ΔO-2), and Tg-epoxide did not significantly increase after a longer pre-incubation time with SPCA1a (Table 2).

Only the O-2 moiety of Tg binds to a spatially restricted pocket in SPCA1a

In the further exploration of the poor contribution of the side chains at O-3, O-8, and O-10 to the affinity of Tg to SPCA1a, we considered the possibility that it might arise from a more spacious Tg-binding cavity than in SERCA, which in a more flexible way would accommodate these Tg side groups. This hypothesis was tested by replacing the O-2, O-3, O-8, and O-10 moieties with more bulky groups (Table 3). Replacing O-3 and O-10 with a slightly bulkier chain (HzL09012012 and HzL12012012, respectively) is well tolerated, whereas a more bulky biphenyl group on O-3 (HzL170809) or O-10 (HzL271009) led to a 7- and 49-fold higher IC_{50}, respectively (Table 3). However, the higher IC_{50} was significantly reduced after a longer pre-incubation time, indicating that a sufficiently large three-dimensional space is potentially available in the Tg pocket near O-3 and O-10 to allow accommodation of biphenyl groups (Table 3). The large but flexible Leu-8ADT substitution on O-8 led to a 19-fold reduction of the potency in SPCA1a most likely as a result of steric hindrance. However, overnight incubation of Leu-8ADT led to a lower IC_{50}, indicative of an induced fit effect and sufficient space to accommodate a larger O-8 chain (Table 3).

Of all tested Tg side groups, O-2 contributes most to the inhibition of SPCA1a. To determine the SAR of Tg in SPCA1a, we therefore focused on the role of O-2 by testing the functional impact of various substitutions of the O-2 group (Table 4). The IC_{50} remains unaffected when the O-2 octanoyl group was substituted with a benzoyl (HzL20072015) or naphthalenecarboxyl group (HzL18072015). Thus, the difference between HzL20072015, HzL18072015, and the −H substitution of nortrilobolide (ΔO-2) indicates that the O-2 chain facilitates a hydrophobic interaction in the SPCA1a-binding pocket. However, a substitution of the O-2 moiety with a phenylbenzoyl group (HzL17072015) led to a significantly higher IC_{50} than with smaller substituents (HzL20072015 and HzL18072015), which was independent of the pre-incubation time. This reveals that the local three-dimensional space to accommodate a bulky O-2 group is restricted in SPCA1a, although the O-2 acyl group is larger in one dimension.

Therefore, we explored the replacement of the O-2 chain with several longer but flexible acyl groups (Table 4). We observed little effect on the IC_{50} by elongating the O-2 chain with two carbons (JBH04012016), whereas addition of four carbons (JBH09022016) increased the IC_{50} 3.4-fold (Table 4). Of interest, the inhibition of SPCA1a was completely abolished by introducing a more bulky end group (HzL24042015). The inhibitory effect of this compound is unaffected by the pre-incubation time.

Thus, strict spatial restrictions around O-2 are likely present, because only thin flexible O-2 chains are allowed, whereas more voluminous groups lower or prohibit the affinity for SPCA1a.

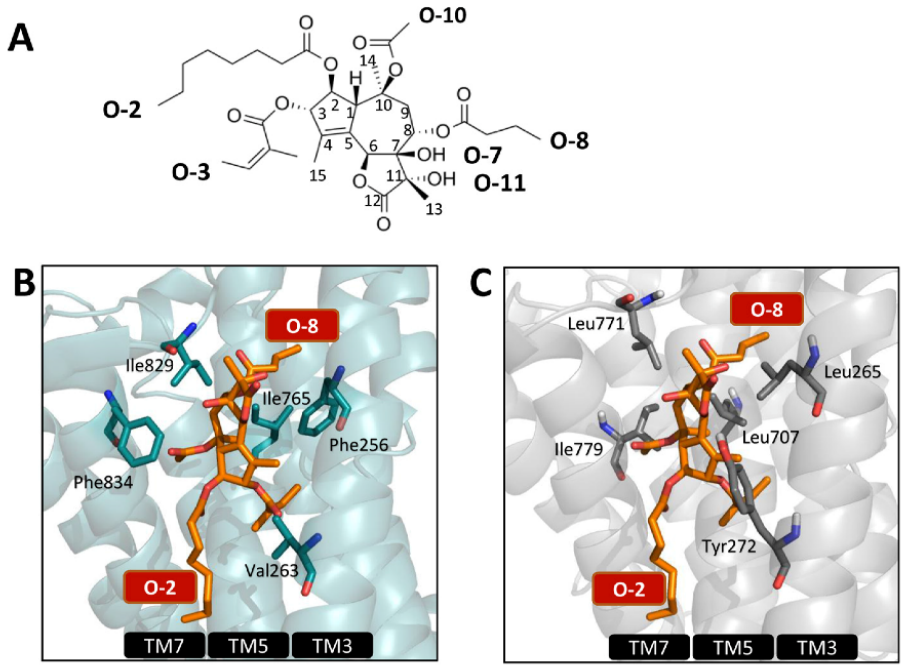

Figure 4. Establishing the structure-activity relationship of Tg in SPCA1a. *A*, structure of Tg with the numbering of the carbon atoms and side chains indicated. *B*, Tg pocket in SERCA1a in the E2 conformation with bound Tg (1IWO (41)) with important residues shown as *blue sticks*. The same view of the SPCA1a homology model is shown in *C*, and the residues that are different between SPCA1a and SERCA1a are labeled.

Table 2

Contributions of the Tg side chain and scaffold modalities in SPCA1a inhibition

IC_{50} values of Tg analogues with indicated modifications were measured for SPCA1a and compared with the IC_{50} of Tg by Student's *t* test (***, $P < 0.001$ *versus* Tg). Changes in free energy of SPCA1a and SERCA1a were calculated from $\Delta\Delta G^\circ - RT\ln K_{d,\,Tg} - RT\ln K_{d\ compound}$. The K_d is based on the concentration of compound required for 50% inhibition of SPCA1a or SERCA1a.

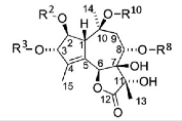

Compound	$IC_{50\ SPCA1a}$ (μM)	$\Delta\Delta G^\circ_{SPCA1a}$ (kJ/mol)	$\Delta\Delta G^\circ_{SERCA1a}$ (kJ/mol)
Tg	7.7 ± 1.5	0	0
ΔO-2	51 ± 1*** 56 ± 7***(ON)	-4.9	-4.7
ΔO-3	11 ± 5	-1.0	-11.4
ΔO-8	7 ± 3	0.3	-7.9
ΔO-10	7 ± 3	0.4	-7.8
Tg-epoxide [a]	256 ± 33*** 205 ± 46*** (ON)	-9.0	-7.7

[a] Tg-epoxide has a β-epoxide group formed between C7 and C11; ON is overnight incubation with compound. ΔO-3, −8, and −10 indicate that the acyl group at O-*X* has been replaced with a proton, and ΔO-2 means that the octanoyloxy group has been replaced with a proton to give nortrilobolide.

SPCA1a inhibition by Tg and cholesteric compounds involves the same or overlapping binding pocket

To explore the functional role of amino acid replacements in SPCA1a on Tg binding and confirm that Tg binds to the same pocket in SPCA1a and SERCA1a, we generated and purified three SPCA1a mutants in the Tg-binding pocket in which we substituted one or more of the SPCA1a-specific residues into the corresponding SERCA1a amino acids (L265F, Y272V, and L265F/Y272V/L776F) (Fig. 5*A*). Phe-256 is a critical residue for Tg central scaffold binding in SERCA1a (45) and is replaced in SPCA1a by Leu-265. The replacement of Val-263 in SERCA1a by Tyr-272 in SPCA1a introduces a bulky aromatic side chain in the Tg pocket possibly hindering Tg binding to SPCA1a. The Leu-776 in SPCA1a corresponds to Phe-834 in SERCA1a, which exerts unfavorable interaction with the O-10 group of Tg.

Compared with wild-type SPCA1a (WT), the more SERCA-like L265F and L265F/Y272V/L776F mutants are more sensitive to Tg, whereas Y272V behaves similarly as WT (Fig. 5*B*). This is consistent with the view that as in SERCA1a, Tg binds to a conserved pocket in the transmembrane region formed by M3, M5, and M7. Furthermore, the L265F substitution in SPCA1a significantly enhanced the binding affinity of Tg, possibly by promoting a direct interaction between Phe-265 and the Tg scaffold as is the case for SERCA1a (39). This result is also consistent with the view that binding of the Tg scaffold in SPCA1a may closely resemble the interaction in SERCA1a. Finally, the three SPCA1a mutants also displayed a more potent and stronger inhibition by CHEMS, a cholesterol analogue (Fig. 5*C*), suggesting that cholesteric compounds may bind at the same or overlapping site as Tg.

Modeling confirms the importance of the Tg scaffold in the binding to SPCA1a

To further explore how Tg might be accommodated in SPCA1a, we generated a homology model of SPCA1a and performed an *in silico* docking of Tg into the M3, M5, and M7 pocket, while allowing flexibility of 10 amino acid side chains in the pocket. To validate our modeling approach, we first docked Tg into an E2 crystal structure of SERCA1a without Tg (PDB code 3W5C (46)) and compared the results with the 1IWO crystal structure of SERCA1a with bound Tg (Fig. 5*D*) (41). Among the best 10 docking poses (Chemscore scoring function of GOLD), two major populations were recognized (Fig. 5, *E* and *F*, and Table 5). Model 1 (Fig. 5*E*) corresponds to a Tg

Inhibition of SPCA1a by thapsigargin

Table 3

IC_{50} values of Tg analogues with modified O-3, O-8, or O-10 side chains on SPCA1a

Columns provide information on compound name, the structure of the side-chain modification, and the IC_{50} value on SPCA1a. Student's *t* test were performed to compare between IC_{50} of each analogue and $IC_{50\ Tg}$, and before/after overnight (ON) incubation. * $P < 0.05$, *** $P < 0.001$.

Compound	Structure	$IC_{50\ SPCA}$ (μM)
Tg	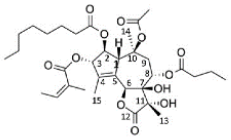	7.7 ± 1.5
O-3 substitutions	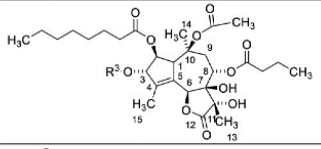	
HzL09012012		6.7 ± 1.4
HzL170809	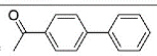	56 ± 10*** 28 ± 9* (ON)
O-8 substitutions	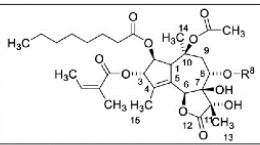	
Leu8ADT	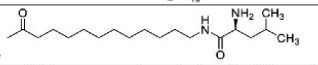	143 ± 28*** 7 ± 3 (ON)
O-10 substitutions	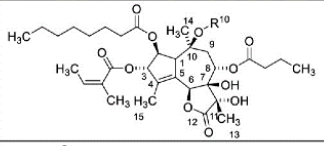	
HzL12012012	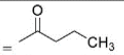	10 ± 1
HzL271009	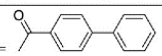	400 ± 100*** 47 ± 16* (ON)

Table 4

IC_{50} values of Tg analogues with modified O-2 side chain on SPCA1a

Columns provide information on compound name, the structure of the side-chain modification and the IC_{50} value on SPCA1a. Student's *t* test were performed to compare between IC_{50} of each analogue and $IC_{50\ Tg}$, and before/after overnight (ON) incubation. * $P < 0.05$, *** $P < 0.001$.

Compound	Structure	$IC_{50\ SPCA}$ (μM)
O-2 substitutions	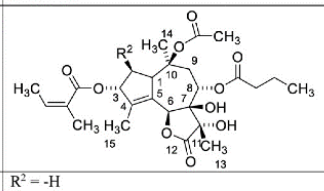	
Nortrilobolide	R^2 = -H	51 ± 1*** 57 ± 6***(ON)
HzL20072015		12.5 ± 0.6
HzL18072015	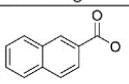	13 ± 2
HzL17072015	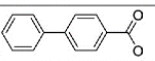	37 ± 7***
JBH04012016	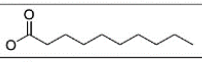	12 ± 1
JBH09022016	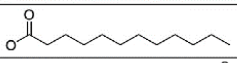	26 ± 2*
HzL24042015	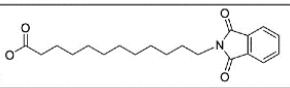	No inhibition

position that is highly similar to the Tg position in the 1IWO crystal structure (Fig. 5*D*), with the O-8 group that is oriented toward the space flanked by M3 and M5 helices. Of the 10 highest ranked scores, six docking poses, including the five best belong to model 1 (Fig. 5*E*), validating the docking approach. The other four solutions belong to model 2 (Fig. 5*F*), which contains docking poses displaying a remarkable flipped orientation of Tg into the pocket, *i.e.* with the O-2 group of Tg facing M3 and M5.

Next, we docked Tg onto the SPCA1a homology model, and again two major populations were recognized with opposite orientations of O-2 and O-8 (Fig. 5, *G–I*). Model 1 (Fig. 5*G*) displays a similar Tg orientation as in the SERCA1a crystal structure, except that the O-2 chain extends to the outside of the pump. Model 2 (Fig. 5, *H* and *I*) corresponds to docking poses with O-8 pointing away from the protein, whereas O-2 is directed toward the interior of the pump with two main variations in the path of the O-2 chain as displayed in Fig. 5, *H* and *I*). Our experimental results highlighted that the inhibition of SPCA1a by Tg is mainly explained by the Tg scaffold and the O-2 moiety, whereas the O-3, O-8, and O-10 side chains contribute little. Of interest, the position of the Tg scaffold in the 10 best docking results is always aligned into the same plane flanked by M3 and M7, irrespective of the opposite O-2/O-8 directions in models 1 (Fig. 5*J*) or 2 (Fig. 5*K*). The strict positioning of the Tg scaffold in SPCA1a may indicate the presence of spatial restrictions and/or critical interactions between the scaffold and the protein. The scaffold is in close proximity of Leu-265 on M3, which might explain the affinity-enhancing effect of the L265F substitution (Fig. 5*B*).

Thus, our docking analysis confirms the contribution of the Tg scaffold to the SPCA1a, and it points to two possible but opposite orientations of Tg inside the pocket formed by M3, M5, and M7.

Discussion

In this study, we purified for the first time the human Golgi/secretory pathway Ca^{2+}/Mn^{2+}-ATPase SPCA1a from a yeast overexpression model. The one-step affinity purification protocol generates hSPCA1a with over 95% purity offering opportunities for structure/function analysis and inhibitor screening. We demonstrate that SPCA1a is highly sensitive to the lipid environment and that several SERCA inhibitors, including Tg, also block SPCA1a activity, although at higher concentrations only. Because of the wide use of Tg in cellular studies and prospects for the use of Tg analogues in prostate cancer therapy, we focused on deciphering the SAR of Tg for SPCA1a. We observed differences in the relative contribution of Tg side chains in the inhibition of SERCA1a *versus* SPCA1a, which might be exploited for the future design of more selective SPCA1a or SERCA1a inhibitors.

Activity of SPCA1a depends on the membrane environment

Ca^{2+} transporters are tightly regulated by their lipid environment. For instance, the plasma membrane Ca^{2+}-ATPase con-

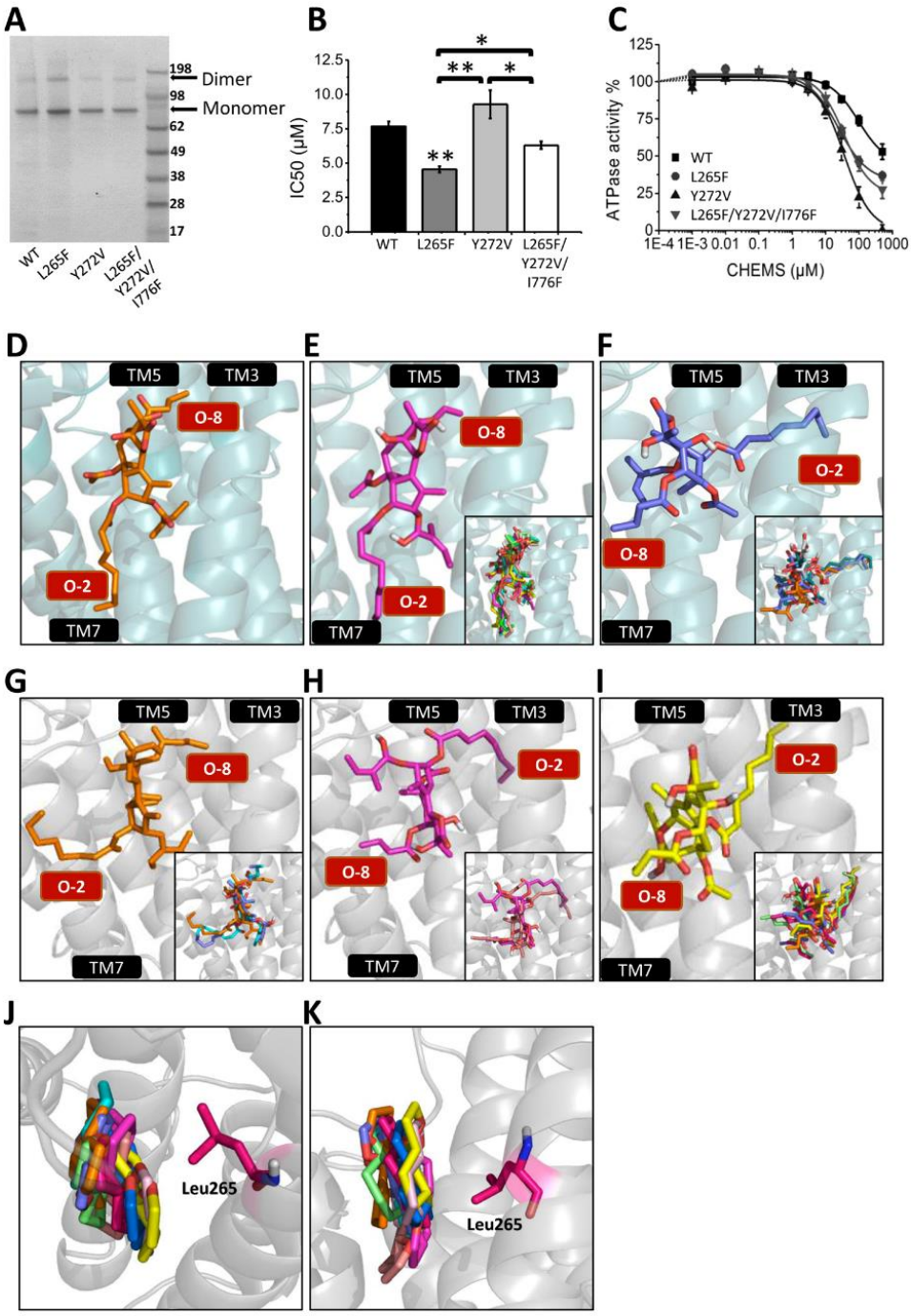

Figure 5. Modeling Tg into the binding pocket of SPCA1a. SDS-polyacrylamide gel staining (*A*), IC_{50} values of Tg (*B*), and CHEMS dose-response curves (*C*) of the reconstituted SPCA1a WT and L265F, Y272V, and L265F/Y272V/I776F mutants. *D*, crystal structure of SERCA1a-Tg complex (1IWO (41)). *E* and *F*, Tg docking simulation performed on the SERCA1a E2 crystal structure without Tg (3W5C (46)) (side-chain torsion rotations were assigned to Glu-255, Phe-256, Gln-259, Leu-260, Val-263, Ile-765, Val-769, Ile-829, Phe-834, and Met-838), rendering two conformational populations: model 1 (*E*) and model 2 (*F*). *G–I*, Tg docking simulation was performed on the SPCA1a homology model (side-chain torsion rotations were assigned to Leu-264, Leu-265, Leu-269, Tyr-272, Leu-707, Ile-711, Ile-770, Leu-771, Ile-776, and Ile-779), rendering three conformational populations (*G–I*), which are corresponding to two major models according to the orientation of the Tg O-2 and O-8 side chains: model 1 (*G*) and model 2 (*H* and *I*). The O-2 and O-8 chains are indicated in *red text boxes*. Top (*J*) and side (*K*) view of the superimposed 10 Tg scaffolds from the docking result of *G–I*. The residue Leu-265 is highlighted. *TM*, transmembrane helix. One-way ANOVA was performed followed by a post hoc Fisher test. *, $p < 0.05$; **, $p < 0.01$.

tains two lipid-binding sites and can be stimulated by PS, PA, phosphatidylinositol bisphosphate, and cardiolipin (47). SERCA pumps are inhibited by sphingosine (48) and CL (49), whereas SPCA1a associates with CL-rich microdomains of human colon adenocarcinoma cells (30). Also, SPCA2 is inhibited by two endogenous signaling lipids oleamide and linoleamide (34). Here, we demonstrate that SPCA1a is inactive in a lipid-free detergent-solubilized state, but the activity restores upon reconstitution into a PC-rich lipid environment. In proteoliposomes, SPCA1a displays a higher apparent Ca^{2+} affinity and lower maximal ATPase activity than SERCA1a. The K_m value of the purified and reconstituted SPCA1a falls within the

Inhibition of SPCA1a by thapsigargin

Table 5
Scores of the best Tg dockings in SPCA1a and SERCA1a
Poses obtained by *in silico* docking of Tg in SERCA1a or SPCA1a are divided into different models (1, 2′, and 2″) that show a closely resembling docking position.

SPCA1a		SERCA1a	
Docking score by Gold.Chemscore. Fitness	Population	Docking score by Gold.Chemscore. Fitness	Population
30.22	1	31.68	1
27.92	2′	30.25	1
27.80	2″	30.21	1
27.57	2′	29.81	1
26.96	1	29.68	1
26.06	1	28.61	2
25.55	2″	28.58	2
24.99	2″	28.30	2
24.95	2″	28.19	1
24.87	2″	28.06	2

reported range for SPCA1 in cell membrane fractions (0.04–0.26 μM (8, 21, 50)). The variation in the reported K_m values presumably relates to slight differences in the free Ca^{2+} concentrations, the choice of the SPCA1 splice variant, and the selected cellular expression system, which may affect the regulation of SPCA1.

Moreover, SPCA1a is sensitive to the SERCA inhibitors Tg, CPA, and BHQ but also to bisphenol and CHEMS. SPCA1a was previously considered as Tg-insensitive, whereas a few studies reported a Tg sensitivity in the range between 0.1 and 30 μM (13, 24, 36). Here, we report that purified SPCA1a in reconstituted proteoliposomes displays an IC_{50} for Tg of 7.7 μM, which is four times lower than the reported IC_{50} value of 28 μM in microsomal fractions (24). The variations in the reported Tg sensitivities of SPCA1 may be due to differences in the experimental systems (membrane lipid composition and presence of other proteins or detergent). Thus, overall, the properties of the purified protein correspond well with SPCA1a in a cellular membrane context.

The inclusion of specific lipids in the proteoliposomes impacts on the activity of SPCA1a, with PA and SM leading to stimulation, whereas PE is inhibitory. PA is typically added during the reconstitution of SERCA1a to prevent aggregation (51). Because the stimulatory effect of PA was not observed with other charged lipids, it is also possible that PA serves as a regulatory lipid of SPCA1a. Although PA is a low-abundant lipid in the Golgi/secretory pathway, it can be locally formed by phospholipase D as a signaling lipid that may regulate SPCA1a activity (52, 53). Moreover, we showed that SPCA1a preferentially accumulates in lipid rafts (30), which is in line with the stimulatory effect of SM on the ATPase activity of SPCA1a. The cholesteric compound CHEMS only moderately inhibits SPCA1a, while exhibiting a more potent inhibitory effect on SERCA1a, in line with a different impact of CL on SPCA1a and SERCA1a as suggested previously (30). Although our reconstitution conditions were selected to promote the proper orientation of the protein in the membrane (*i.e.* the large hydrophilic cytosolic domain facing the outside of the vesicles) (51), we cannot fully rule out the possibility that the functional effects of the lipids may relate to an impact on the distribution between inward-facing and outward-facing enzymes in the proteoliposomes.

Of interest, the potency and efficacy of the CHEMS inhibition is higher in SPCA1a mutants with a more SERCA1a-like Tg pocket. The changes between the Tg-binding site of SERCA1a and SPCA1a might also explain the different sensitivity of SPCA1a and SERCA1a to cholesteric compounds. Although we cannot rule out that these mutations might exert an allosteric effect via an unrelated binding site for cholesteric compounds, it is reasonable to propose that the cholesteric compound binds and overlaps the Tg pocket. Indeed, it was already previously proposed that the SERCA1a Tg pocket might be a CL regulation site (39, 54). In the SERCA1a crystal structure 2EAU, the Tg-binding site was occupied by a lipid (55). Moreover, a fluorescence quenching study suggested the existence of hydrophobic non-annular binding sites for CL in SERCA1a (56), whereas a computational docking analysis modeled the steroid compound Alisol B, which targets SERCA pumps and enhances autophagy, in the Tg site (57). However, a more recent molecular dynamics simulation rather indicates that little CL may occupy the Tg-binding site (58), suggesting that the CL effect on SERCA1a may also be indirect via the impact on the membrane properties.

Inhibition of SPCA1a and SERCA1a by Tg is largely determined by the Tg scaffold

Of all tested pharmacological compounds, we observed the most potent inhibition of SPCA1a with Tg, a plant-derived sesquiterpene lactone that is generally accepted as a highly selective SERCA1a inhibitor. Over the years, structures of the Tg-SERCA1a complex (59–62), supported by extensive functional studies (38–40, 42, 43, 63–66), rendered a comprehensive pharmacophore model that explains the sub-nanomolar affinity of SERCA1a for Tg. The availability of purified SPCA1a and a library of Tg analogues now offered an opportunity to determine the SAR of Tg on SPCA1a, which might be helpful for the design of more specific SERCA1a or SPCA1a inhibitors.

In accordance with the view that Tg targets the same binding pocket in SPCA1a as in SERCA1a, amino acid substitutions in the predicted M3/M5 pocket of SPCA1a impact the affinity for Tg. According to our *in silico* docking, the Tg scaffold is aligned on the same plane irrespective of the side chain orientations. It was previously demonstrated that an F256L mutation in SERCA1a led to a 4-fold reduction in the Tg sensitivity (67), whereas our complementary experiment shows that the L265F substitution in SPCA1a significantly enhanced SPCA1a's affinity for Tg. Thus, the Phe-256/Leu-265 substitution at least in part explains the lower Tg affinity for SPCA1a than SERCA1a. The Tg scaffold might possibly undergo π-stacking with the L265F residue in the SPCA1a mutant. The importance of the Tg scaffold for inhibition is supported by findings with the 7,11-epoxide, which show a major reduction in the binding energy for both SPCA1a (Table 2) and SERCA1a (38, 39), pointing to possible similarities in the mechanism of inhibition in SPCA1a and SERCA1a.

Tg side groups differently contribute to the inhibition of SPCA1a versus SERCA1a

We further approached the SAR of Tg for SPCA1a by analyzing the IC_{50} values of a series of Tg analogues with modified side chains. Strikingly, removal of the O-3, O-8, and O-10 acyl groups have little effect on the binding energy of Tg in SPCA1a,

which is different for SERCA1a (Table 2) (40, 43). Moreover, substitution by slightly bulkier groups at these sites on SPCA1a is well tolerated, indicating that the Tg pocket in SPCA1a is spacious near O-3, O-8, and O-10 and that only few functional contacts exist between the side chains of Tg and residues of the protein. The removal of O-2, the longest side chain of Tg, leads to a higher IC_{50} value in SPCA1a, suggesting that besides the relevance of the Tg scaffold, O-2 also contributes to the inhibition of SPCA1a. The analysis of Tg analogues with various O-2 substitutions further indicates that the O-2 chain is accommodated in a narrow hydrophobic cleft, which is restricted in volume. Noteworthy, the change in binding energy of the ΔO-2 compound is remarkably similar for SPCA1a and SERCA1a possibly pointing to a comparable binding mechanism.

By *in silico* docking analysis, two major docking solutions of Tg O-2 in SPCA1a were predicted. Of interest, the docking model 1 predicts a similar Tg orientation in SPCA1a as observed in the solved SERCA1a-Tg complex, which also might point to a similar inhibitory mechanism in SPCA1a and SERCA1a. This model may explain why a prolonged incubation of Leu-8ADT shows a more potent inhibition in SPCA1a (Table 3), because a similar effect of Leu-8ADT was observed on SERCA1a (44). Alternatively, in line with O-2 being accommodated into a tight hydrophobic cleft, the Tg O-2 chain in the SPCA1a model 2 protrudes into the M3/M5 region. Such a flipped orientation of Tg is also predicted for SERCA1a, although this is not experimentally observed in the solved SERCA1a-Tg complex, which may question the validity of such an orientation.

Toward the design of more specific SPCA1a inhibitors

We demonstrate that the SAR of Tg differs for SPCA1a and SERCA1a, which is mainly attributed to amino acid changes in the Tg pocket that prevent most interactions of the Tg side chains in SPCA1a, but it still allows the Tg scaffold to be accommodated in the pocket. The different SAR of Tg for SERCA1a and SPCA1a provides a strong rationale to consider the Tg scaffold as a lead compound for the development of more specific SPCA1a inhibitors. Solving the crystal structure of SPCA1a in the presence of Tg will greatly facilitate a rational design approach for a Tg-based SPCA1a inhibitor with higher potency and specificity, but so far, crystallization of SPCA1a turns out to be difficult in our hands.

In the absence of detailed structural information, we need to test additional Tg analogues with substitutions of the O-2, O-3, O-8, and O-10 chains to develop Tg analogues with a higher SPCA1a/SERCA1a specificity. Tg analogues with O-2 acyl chains that are slightly shorter would be interesting for establishing the optimal fit of O-2 within the SPCA1a Tg pocket. Moreover, our results indicate that single or combined bulky substitutions at O-3, O-8, and O-10 might lower the potency in SERCA1a, while having little impact on SPCA1a inhibition, favoring a higher SPCA1a/SERCA1a specificity. The more spacious environment near O-3 and O-10 indicates that bulkier side groups on both positions might lead to a tighter fit of Tg within the pocket.

A specific SPCA1a inhibitor might not only be a powerful tool to dissect the cellular and pathological role of SPCA1a in the Ca^{2+} (dys)homeostasis of various diseases, it might also be of therapeutic interest. Gain of SPCA1a and SPCA2 function is observed in breast cancer, because SPCA1a and/or SPCA2 proteins are up-regulated in various breast cancer sub-types contributing to a pathological Ca^{2+} dyshomeostasis (17, 18). Knockdown of endogenous SPCA2 prevents Orai1 activation, which reduces the transforming phenotype of MCF-7 cells in soft agar and impairs tumor generation upon injection in nude mice (18). Although this mainly depends on the direct interaction of SPCA2 with Orai1 leading to constitutive cytosolic Ca^{2+} influx (18), SPCA2 and Orai1 are likely mechanistically coupled, suggesting that also a higher Golgi Ca^{2+} uptake is contributing to the pathological Ca^{2+} dyshomeostasis (19). In line with this view, knockdown of SPCA1a in the basal-type breast cancer cell line MDA-MB-231 reduces, independent of Orai1, the processing of insulin-like growth factor receptor IGF1R (17), which might counteract its mitogenic and anti-apoptotic actions. Of further interest, the absence of PMR1, the SPCA1a orthologue in lower eukaryotes such as yeast, flies, and *Caenorhabditis elegans*, prevents the elevation of cytosolic Ca^{2+} and cell death caused by α-synuclein overexpression, a major toxic effector in Parkinson disease (68). Finally, SPCA1a mutations lead to a dominant skin disorder, Hailey-Hailey disease, which is generally considered to be caused by loss-of-function mutations that cause haploinsufficiency (15, 16). However, it was recently proposed that dominant disease mutations in ion pumps might introduce a gating defect resulting in ion leakage, which would represent a gain-of-function effect (69). In mice, heterozygous loss of SPCA1a does not trigger a similar skin disease, but it increases the risk of developing squamous cell tumors (70), further highlighting the importance of a balanced SPCA1a activity.

In conclusion, we demonstrate that Tg and cholesteric compounds in SPCA target an overlapping binding site on SPCA1a, and the differences in the SAR of Tg for SPCA1a and SERCA1a might allow the development of more specific inhibitors of SPCA1a.

Experimental procedures

Human SPCA1a expression in yeast

The recombinant human SPCA1a was cloned in the vector pTV001E with a C-terminal His_8 tag (CATCATCACCATCACCATCACCAT) via Gateway cloning. Mutations were introduced via Q5 site-directed mutagenesis (New England Biolabs). pTV001-SPCA1a wild-type (WT) or mutant vectors were transformed into the *S. cerevisiae* strain BY4741a (his3Δ1; leu2Δ0;met15Δ0;ura3Δ0;MATa) as described previously (71). The yeast clone was inoculated in 10 ml of minimal medium (MM) deprived of Leu for overnight growth at 30 °C and gradually expanded into 2 liters MM-Leu culture over 3 days. On day 4, the yeast pellet was transferred into 25 liters of yeast peptone dextrose medium in a 50-liter Cell Bag (GE Healthcare), for 30 h of growth on a shaking system supplied with 30% O_2, 70% N_2 air mixture. Yeast cells were harvested by centrifugation (5,000 × *g*, 5 min, 4 °C) and washed with milli-Q water, and the pellets were weighted, flash-frozen, and stored at −20 °C.

Inhibition of SPCA1a by thapsigargin

Yeast membrane isolation

The yeast membrane was isolated based on the protocol described in Ref. 72. Briefly, the yeast pellet was suspended in lysis buffer (50 mM Tris-HCl, pH 7.5, 1 mM EDTA, 0.6 M sorbitol, 250 μM PMSF, 1 mM DTT, SIGMA*FAST*™ protease inhibitor mixture) and subjected twice to high pressure homogenization at 140,000 kPa (High Pressure Homogenizer, Avestin). The membrane fractions were collected by differential centrifugation at 1,000 and 16,000 × *g*, and they were suspended in solubilization buffer (10 mM imidazole, pH 7.5, 50 mM NaH_2PO_4, pH 7.5, 500 mM NaCl, 20% glycerol, 250 μM PMSF, 1 mM DTT, SIGMA*FAST*™). Protein concentration was determined by the Bradford assay. The yeast membrane fraction was aliquoted, flash-frozen in liquid N_2, and stored at −80 °C.

Purification of SPCA1a and SERCA1a by affinity chromatography

SERCA1a was purified from rabbit fast twitch skeletal muscle as described before (29), whereas a purification protocol for SPCA1a was optimized as detailed below. The His_8-labeled SPCA1a was purified via nickel-affinity chromatography using nickel-charged agarose beads coupled to Ni-NTA. One column volume (CV) of nickel-Sepharose high performance beads (GE Healthcare) was pre-equilibrated with 6 CV of equilibration buffer (50 mM NaH_2PO_4, pH 7.5, 75 mM imidazole, pH 7.5, 500 mM NaCl, 20% glycerol, 5 mM 2-mercaptoethanol (2-ME), 250 μM PMSF, SIGMA*FAST*™, 20 mg/ml DDM (Isogen Life Science, SOL-grade)). The yeast membrane proteins were solubilized in a triple weight amount of DDM detergent solution (200 mg/ml DDM, 250 μM PMSF, SIGMA*FAST*™ protease inhibitor mixture, 5 mM 2-ME), and non-soluble material was removed by ultracentrifugation (160,000 × *g*, 45 min, 4 °C). After binding of the supernatant to the column for 1 h at 4 °C, the liquid was drained off. The beads were washed with 6 CV of three consecutive washing buffers composed of binding buffer with a stepwise reduction in the NaCl and DDM concentrations: from 500 to 50 and 50 mM NaCl combined with 5, 1, and 0.25 mg/ml DDM, respectively. SPCA1a became eluted in the final equilibration buffer with 50 mM NaCl and 0.25 mg/ml DDM. The washing and elution buffers were supplemented with PC (Avanti Polar Lipids) at the ratio 1:0.67 (DDM/PC). Afterward, the buffer component of purified SPCA1a was exchanged into 20 mM imidazole, pH 7.5, 100 mM KCl, 20% glycerol, 0.25 mg/ml DDM, 0.167 mg/ml PC, 5 mM 2-ME, SIGMA*FAST*™ via PD Mantrap G-25 (GE Healthcare) column. Aggregates were removed by centrifugation at 20,000 × *g* for 20 min at 4 °C. The supernatant was collected and flash-frozen in liquid N_2 and stored at −80 °C. The purified SPCA1a was analyzed by MALDI-TOF mass spectrometry (4800 Proteomics Analyzer, AB Sciex) in the linear ion mode in the presence of α-cyano-4-hydroxycinnamic acid (5 mg/ml).

Reconstitution of the SPCA1a and SERCA1a Ca^{2+}-ATPases

The 550-μg lipid mixture dissolved with chloroform in a glass tube was dried in a vacuum desiccator under a N_2 stream and overnight in a vacuum desiccator. Liposome buffer (150 μl of 20 mM imidazole, pH 7, 100 mM NaCl, 10 mM $MgCl_2$, and 1 mM DTT) was added and incubated at 37 °C water bath for 1 h with short vortex periods in between. To this (unless otherwise specified) 30 μg of Triton X-100 was added at room temperature, and the mixture was vortexed for 3 min followed by addition of purified SPCA1a (200 μg of protein at a concentration 0.667 mg/ml). Detergent was extracted to form proteoliposomes by treatment with excess Bio-Beads SM-2 (Bio-Rad) for 2.5 h.

The proteoliposomes were purified by sucrose gradient centrifugation (20 and 50% sucrose in 20 mM imidazole, pH 7, 0.2% azide, 100 mM NaCl) at 150,000 × *g*, 75 min, and 4 °C from which a 450-μl proteoliposome fraction was collected from the turbid layer present between the two sucrose fractions. This sample was flash-frozen in liquid N_2 and stored at −80 °C. The reconstitution of SERCA1a was performed according to Ref. 29. PC, PA, and PE from chicken egg, PS and SM from porcine brain, and phosphatidylinositol from bovine liver were purchased from Avanti Polar Lipids, whereas CL was purchased from Sigma.

Protein electrophoresis and immunoblotting

Purified or reconstituted SPCA1a or SERCA1a was separated on NuPAGE 4–12% BisTris polyacrylamide gel (200 V, 35 min, MES buffer) (Thermo Fisher Scientific) and visualized with Imperial Protein Stain (Thermo Fisher Scientific). SeeBlue Plus2 pre-stained protein standard (Thermo Fisher Scientific) was used as a molecular weight marker. The concentration of purified protein was determined on a denaturing gel by comparison with 0.125 to 2 μg/μl bovine serum albumin (BSA) standards (BSA Standard Ampules, Pierce). For immunoblotting, primary antibodies against the His tag (1:2,000 dilution, penta-His, Qiagen) or SPCA1a (1:50,000 dilution, Frodo, homemade) were used. Horseradish peroxidase-linked secondary antibodies (Cell Signaling Technology) were used for enhanced chemiluminescent detection (Bio-Rad ChemiDoc). MagicMark (Thermo Fisher Scientific) was used as the molecular weight marker.

ATPase assay

The Ca^{2+}-dependent ATPase activity assay was performed on reconstituted SPCA1a or SERCA1a samples according to the Baginsky protocol as described previously (73). The reactions were performed for 15 min (SERCA1a, 150 ng in 50 μl) or 30 min SPCA1a (300 ng in 50 μl). The results were fitted with a Hill function.

The dose response of the ATPase to various compounds was performed by measuring the ATPase activity at 1 μM free Ca^{2+} concentration with increasing concentrations of compounds to be tested in the reaction mix. Reactions with Tg (200 nM for SERCA1a and 500 μM for SPCA1a) samples were used as blanks to correct for irrelevant color development. The data were normalized as the percentage of inhibition compared with that obtained in the absence of inhibitor and fitted with a logistic curve. The CHEMS, CPA, BHQ, BP, and oleamide were purchased from Sigma. Linoleamide was purchased from Enzo Life Sciences, Tg was purchased from Alomone Labs. All compounds were dissolved in dimethyl sulfoxide (DMSO, Sigma).

In silico modeling

The SPCA1a homology model was generated with the homology model module in MOE 2014.09 (74) based on the

SERCA1a E2 crystal structure with Tg bound (PDB code 1IWO (41)). Subsequently, the structure of the homology model was energy-minimized using Amber99 (75) force field in the energy minimization module of MOE. Tg was docked in the SPCA1a homology model or SERCA1a crystal structure via GOLD version 5.2 (Genetic Optimization for Ligand Docking (76, 77)). Tg was docked in the SERCA1a E2 crystal structure without any inhibitors (PDB code 3W5C (46)) and compared with the crystal structure 1IWO with Tg bound. We specified the center of the Tg-binding site (*x*, 33.422; *y*, −18.503; and *z*, 82.4683) and selected all atoms in a radius of 11 Å. 10 residues in the Tg-binding site (Glu-255, Phe-256, Gln-259, Leu-260, Val-263, Ile-765, Val-769, Ile-829, Phe-834, and Met-838) were selected to allow for receptor flexibility through side-chain torsion rotations. For each of these residues, flexibility was limited to a library of selected side chain conformers extracted from published crystal structures. Docking conformations for Tg were generated by performing 20 runs using standard Genetic Algorithm parameters. The docking results were scored and sorted using the Chemscore scoring function of GOLD.

The docking poses for Tg or the analogues were generated in the SPCA1a E2 homology model using the GOLD version 5.2 docking software. Here, we specified the center of the binding site (*x*, −2.8375; *y*, −22.0812; and *z*, 12.2) and selected all atoms in a radius of 10 Å. 10 residues in the binding site (Leu-264, Leu-265, Leu-269, Tyr-272, Leu-707, Ile-711, Ile-770, Leu-771, Ile-776, and Ile-779) were selected to allow for receptor flexibility through side-chain torsion rotations. To generate docking conformations, 100 runs were performed for each ligand using Genetic Algorithm parameters. The docking results were scored and sorted using the Chemscore scoring function of GOLD.

Synthesis of Tg analogues

The synthesis of the Tg analogues is described in supplemental Materials and methods.

Statistical analysis

Values are provided as mean ± S.E. Hill or logistic fitting was performed via OriginPro 9 software. Statistical significance was calculated by one-way *t* test and indicated by *asterisks*: *, $p < 0.05$; **, $p < 0.01$; and ***, $p < 0.001$.

Author contributions—P. V. conceived the idea for the project and coordinated the study. J. C. conducted most of the experiments and analyzed the data. J. D. R., M. D. M., J. B. H., S. S., and I. V. conducted experiments on *in silico* modeling, Tg analogue synthesis, and SPCA1a purification. J. V. M., J. E., S. B. C., P. V., and F. W. analyzed the data and critically reviewed the manuscript. P. V. and J. C., wrote the manuscript. All authors reviewed the results and approved the final version of the manuscript.

References

1. Berridge, M. J., Bootman, M. D., and Roderick, H. L. (2003) Calcium signalling: dynamics, homeostasis and remodelling. *Nat. Rev. Mol. Cell Biol.* **4,** 517–529
2. Monteith, G. R., McAndrew, D., Faddy, H. M., and Roberts-Thomson, S. J. (2007) Calcium and cancer: targeting Ca^{2+} transport. *Nat. Rev. Cancer* **7,** 519–530
3. Palmgren, M. G., and Nissen, P. (2011) P-type ATPases. *Annu. Rev. Biophys.* **40,** 243–266
4. Vangheluwe, P., Sepúlveda, M. R., Missiaen, L., Raeymaekers, L., Wuytack, F., and Vanoevelen, J. (2009) Intracellular Ca^{2+}- and Mn^{2+}-transport ATPases. *Chem. Rev.* **109,** 4733–4759
5. Behne, M. J., Tu, C. L., Aronchik, I., Epstein, E., Bench, G., Bikle, D. D., Pozzan, T., and Mauro, T. M. (2003) Human keratinocyte ATP2C1 localizes to the Golgi and controls Golgi Ca^{2+} stores. *J. Invest. Dermatol.* **121,** 688–694
6. Xiang, M., Mohamalawari, D., and Rao, R. (2005) A novel isoform of the secretory pathway Ca^{2+},Mn^{2+}-ATPase, hSPCA2, has unusual properties and is expressed in the brain. *J. Biol. Chem.* **280,** 11608–11614
7. Wuytack, F., Raeymaekers, L., and Missiaen, L. (2002) Molecular physiology of the SERCA and SPCA pumps. *Cell Calcium* **32,** 279–305
8. Ton, V. K., Mandal, D., Vahadji, C., and Rao, R. (2002) Functional expression in yeast of the human secretory pathway Ca^{2+}, Mn^{2+}-ATPase defective in Hailey-Hailey disease. *J. Biol. Chem.* **277,** 6422–6427
9. Mitchell, K. J., Tsuboi, T., and Rutter, G. A. (2004) Role for plasma membrane-related Ca^{2+}-ATPase-1 (ATP2C1) in pancreatic beta-cell $^{2+}$ homeostasis revealed by RNA silencing. *Diabetes* **53,** 393–400
10. Van Baelen, K., Vanoevelen, J., Callewaert, G., Parys, J. B., De Smedt, H., Raeymaekers, L., Rizzuto, R., Missiaen, L., and Wuytack, F. (2003) The contribution of the SPCA1 Ca^{2+} pump to the Ca^{2+} accumulation in the Golgi apparatus of HeLa cells assessed via RNA-mediated interference. *Biochem. Biophys. Res. Commun.* **306,** 430–436
11. Micaroni, M., Giacchetti, G., Plebani, R., Xiao, G. G., and Federici, L. (2016) ATP2C1 gene mutations in Hailey-Hailey disease and possible roles of SPCA1 isoforms in membrane trafficking. *Cell Death Dis.* **7,** e2259
12. Vanoevelen, J., Dode, L., Van Baelen, K., Fairclough, R. J., Missiaen, L., Raeymaekers, L., and Wuytack, F. (2005) The secretory pathway Ca^{2+}/Mn^{2+}-ATPase 2 is a Golgi-localized pump with high affinity for Ca^{2+} ions. *J. Biol. Chem.* **280,** 22800–22808
13. Baron, S., Struyf, S., Wuytack, F., Van Damme, J., Missiaen, L., Raeymaekers, L., and Vanoevelen, J. (2009) Contribution of intracellular Ca^{2+} stores to Ca^{2+} signaling during chemokinesis of human neutrophil granulocytes. *Biochim. Biophys. Acta* **1793,** 1041–1049
14. Faddy, H. M., Smart, C. E., Xu, R., Lee, G. Y., Kenny, P. A., Feng, M., Rao, R., Brown, M. A., Bissell, M. J., Roberts-Thomson, S. J., and Monteith, G. R. (2008) Localization of plasma membrane and secretory calcium pumps in the mammary gland. *Biochem. Biophys. Res. Commun.* **369,** 977–981
15. Missiaen, L., Raeymaekers, L., Dode, L., Vanoevelen, J., Van Baelen, K., Parys, J. B., Callewaert, G., De Smedt, H., Segaert, S., and Wuytack, F. (2004) SPCA1 pumps and Hailey-Hailey disease. *Biochem. Biophys. Res. Commun.* **322,** 1204–1213
16. Burge, S. M. (1992) Hailey-Hailey disease: the clinical features, response to treatment and prognosis. *Br. J. Dermatol.* **126,** 275–282
17. Grice, D. M., Vetter, I., Faddy, H. M., Kenny, P. A., Roberts-Thomson, S. J., and Monteith, G. R. (2010) Golgi calcium pump secretory pathway calcium ATPase 1 (SPCA1) is a key regulator of insulin-like growth factor receptor (IGF1R) processing in the basal-like breast cancer cell line MDA-MB-231. *J. Biol. Chem.* **285,** 37458–37466
18. Feng, M., Grice, D. M., Faddy, H. M., Nguyen, N., Leitch, S., Wang, Y., Muend, S., Kenny, P. A., Sukumar, S., Roberts-Thomson, S. J., Monteith, G. R., and Rao, R. (2010) Store-independent activation of Orai1 by SPCA2 in mammary tumors. *Cell* **143,** 84–98
19. Smaardijk, S., Chen, J., Wuytack, F., and Vangheluwe, P. (2016) SPCA2 couples Ca^{2+} influx via Orai1 to Ca^{2+} uptake into the Golgi/secretory pathway. *Tissue Cell* 2016, S0040
20. Cross, B. M., Hack, A., Reinhardt, T. A., and Rao, R. (2013) SPCA2 regulates Orai1 trafficking and store independent Ca^{2+} entry in a model of lactation. *PLoS ONE* **8,** e67348
21. Dode, L., Andersen, J. P., Raeymaekers, L., Missiaen, L., Vilsen, B., and Wuytack, F. (2005) Functional comparison between secretory pathway Ca^{2+}/Mn^{2+}-ATPase (SPCA) 1 and sarcoplasmic reticulum Ca^{2+}-ATPase (SERCA) 1 isoforms by steady-state and transient kinetic analyses. *J. Biol. Chem.* **280,** 39124–39134
22. Michelangeli, F., and East, J. M. (2011) A diversity of SERCA Ca^{2+} pump inhibitors. *Biochem. Soc. Trans.* **39,** 789–797

Inhibition of SPCA1a by thapsigargin

23. Sorin, A., Rosas, G., and Rao, R. (1997) PMR1, a Ca^{2+}-ATPase in yeast Golgi, has properties distinct from sarco/endoplasmic reticulum and plasma membrane calcium pumps. *J. Biol. Chem.* **272,** 9895–9901
24. Dode, L., Andersen, J. P., Vanoevelen, J., Raeymaekers, L., Missiaen, L., Vilsen, B., and Wuytack, F. (2006) Dissection of the functional differences between human secretory pathway Ca^{2+}/Mn^{2+}-ATPase (SPCA) 1 and 2 isoenzymes by steady-state and transient kinetic analyses. *J. Biol. Chem.* **281,** 3182–3189
25. Missiaen, L., Vanoevelen, J., Parys, J. B., Raeymaekers, L., De Smedt, H., Callewaert, G., Erneux, C., and Wuytack, F. (2002) Ca^{2+} uptake and release properties of a thapsigargin-insensitive nonmitochondrial Ca^{2+} store in A7r5 and 16HBE14o− cells. *J. Biol. Chem.* **277,** 6898–6902
26. Denmeade, S. R., Mhaka, A. M., Rosen, D. M., Brennen, W. N., Dalrymple, S., Dach, I., Olesen, C., Gurel, B., Demarzo, A. M., Wilding, G., Carducci, M. A., Dionne, C. A., Møller, J. V., Nissen, P., Christensen, S. B., and Isaacs, J. T. (2012) Engineering a prostate-specific membrane antigen-activated tumor endothelial cell prodrug for cancer therapy. *Sci. Transl. Med.* **4,** 140ra186
27. Doan, N. T., Paulsen, E. S., Sehgal, P., Møller, J. V., Nissen, P., Denmeade, S. R., Isaacs, J. T., Dionne, C. A., and Christensen, S. B. (2015) Targeting thapsigargin toward tumors. *Steroids* **97,** 2–7
28. Rigaud, J. L. (2002) Membrane proteins: functional and structural studies using reconstituted proteoliposomes and 2-D crystals. *Braz. J. Med. Biol. Res.* **35,** 753–766
29. Young, H. S., Rigaud, J. L., Lacapère, J. J., Reddy, L. G., and Stokes, D. L. (1997) How to make tubular crystals by reconstitution of detergent-solubilized Ca^{2+}-ATPase. *Biophys. J.* **72,** 2545–2558
30. Baron, S., Vangheluwe, P., Sepúlveda, M. R., Wuytack, F., Raeymaekers, L., and Vanoevelen, J. (2010) The secretory pathway Ca^{2+}-ATPase 1 is associated with cholesterol-rich microdomains of human colon adenocarcinoma cells. *Biochim. Biophys. Acta* **1798,** 1512–1521
31. Kadowaki, H., Grant, M. A., and Seyfried, T. N. (1994) Effect of Golgi membrane phospholipid composition on the molecular species of GM3 gangliosides synthesized by rat liver sialyltransferase. *J. Lipid Res.* **35,** 1956–1964
32. van Meer, G., Voelker, D. R., and Feigenson, G. W. (2008) Membrane lipids: where they are and how they behave. *Nat. Rev. Mol. Cell Biol.* **9,** 112–124
33. Lambert, O., Levy, D., Ranck, J. L., Leblanc, G., and Rigaud, J. L. (1998) A new "gel-like" phase in dodecyl maltoside-lipid mixtures: implications in solubilization and reconstitution studies. *Biophys. J.* **74,** 918–930
34. Yamamoto, S., Takehara, M., Kabashima, Y., Fukutomi, T., and Ushimaru, M. (2016) Identification of novel inhibitors of human SPCA2. *Biochem. Biophys. Res. Commun.* **477,** 266–270
35. Lai, P., and Michelangeli, F. (2012) Bis(2-hydroxy-3-tert-butyl-5-methylphenyl)-methane (bis-phenol) is a potent and selective inhibitor of the secretory pathway Ca^{2+}-ATPase (SPCA1). *Biochem. Biophys. Res. Commun.* **424,** 616–619
36. Harper, C., Wootton, L., Michelangeli, F., Lefièvre, L., Barratt, C., and Publicover, S. (2005) Secretory pathway Ca^{2+}-ATPase (SPCA1) Ca^{2+} pumps, not SERCAs, regulate complex $[Ca^{2+}]$, signals in human spermatozoa. *J. Cell Sci.* **118,** 1673–1685
37. Plenge-Tellechea, F., Soler, F., and Fernandez-Belda, F. (1997) On the inhibition mechanism of sarcoplasmic or endoplasmic reticulum Ca^{2+}-ATPases by cyclopiazonic acid. *J. Biol. Chem.* **272,** 2794–2800
38. Quynh Doan, N. T., and Christensen, S. B. (2015) Thapsigargin, origin, chemistry, structure-activity relationships and prodrug development. *Curr. Pharm. Des.* **21,** 5501–5517
39. Winther, A. M., Liu, H., Sonntag, Y., Olesen, C., le Maire, M., Soehoel, H., Olsen, C. E., Christensen, S. B., Nissen, P., and Møller, J. V. (2010) Critical roles of hydrophobicity and orientation of side chains for inactivation of sarcoplasmic reticulum Ca^{2+}-ATPase with thapsigargin and thapsigargin analogs. *J. Biol. Chem.* **285,** 28883–28892
40. Skytte, D. M., Møller, J. V., Liu, H., Nielsen, H. Ø., Svenningsen, L. E., Jensen, C. M., Olsen, C. E., and Christensen, S. B. (2010) Elucidation of the topography of the thapsigargin binding site in the sarco-endoplasmic calcium ATPase. *Bioorg. Med. Chem.* **18,** 5634–5646
41. Toyoshima, C., and Nomura, H. (2002) Structural changes in the calcium pump accompanying the dissociation of calcium. *Nature* **418,** 605–611
42. Søhoel, H., Liljefors, T., Ley, S. V., Oliver, S. F., Antonello, A., Smith, M. D., Olsen, C. E., Isaacs, J. T., and Christensen, S. B. (2005) Total synthesis of two novel subpicomolar sarco/endoplasmatic reticulum Ca^{2+}-ATPase inhibitors designed by an analysis of the binding site of thapsigargin. *J. Med. Chem.* **48,** 7005–7011
43. Christensen, S. B., Andersen, A., Poulsen, J. C., and Treiman, M. (1993) Derivatives of thapsigargin as probes of its binding site on endoplasmic reticulum Ca^{2+}-ATPase. Stereoselectivity and important functional groups. *FEBS Lett.* **335,** 345–348
44. Dubois, C., Vanden Abeele, F., Sehgal, P., Olesen, C., Junker, S., Christensen, S. B., Prevarskaya, N., and Møller, J. V. (2013) Differential effects of thapsigargin analogues on apoptosis of prostate cancer cells: complex regulation by intracellular calcium. *FEBS J.* **280,** 5430–5440
45. Wootton, L. L., and Michelangeli, F. (2006) The effects of the phenylalanine 256 to valine mutation on the sensitivity of sarcoplasmic/endoplasmic reticulum Ca^{2+}-ATPase (SERCA) Ca^{2+} pump isoforms 1, 2, and 3 to thapsigargin and other inhibitors. *J. Biol. Chem.* **281,** 6970–6976
46. Toyoshima, C., Iwasawa, S., Ogawa, H., Hirata, A., Tsueda, J., and Inesi, G. (2013) Crystal structures of the calcium pump and sarcolipin in the Mg^{2+}-bound E1 state. *Nature* **495,** 260–264
47. Strehler, E. E., and Zacharias, D. A. (2001) Role of alternative splicing in generating isoform diversity among plasma membrane calcium pumps. *Physiol. Rev.* **81,** 21–50
48. Benaim, G., Pimentel, A. A., Felibertt, P., Mayora, A., Colman, L., Sojo, F., Rojas, H., and De Sanctis, J. B. (2016) Sphingosine inhibits the sarco(endo)plasmic reticulum Ca^{2+}-ATPase (SERCA) activity. *Biochem. Biophys. Res. Commun.* **473,** 572–577
49. Li, Y., Ge, M., Ciani, L., Kuriakose, G., Westover, E. J., Dura, M., Covey, D. F., Freed, J. H., Maxfield, F. R., Lytton, J., and Tabas, I. (2004) Enrichment of endoplasmic reticulum with cholesterol inhibits sarcoplasmic-endoplasmic reticulum calcium ATPase-2b activity in parallel with increased order of membrane lipids: implications for depletion of endoplasmic reticulum calcium stores and apoptosis in cholesterol-loaded macrophages. *J. Biol. Chem.* **279,** 37030–37039
50. Fairclough, R. J., Dode, L., Vanoevelen, J., Andersen, J. P., Missiaen, L., Raeymaekers, L., Wuytack, F., and Hovnanian, A. (2003) Effect of Hailey-Hailey disease mutations on the function of a new variant of human secretory pathway Ca^{2+}/Mn^{2+}-ATPase (hSPCA1). *J. Biol. Chem.* **278,** 24721–24730
51. Rigaud, J. L., and Lévy, D. (2003) Reconstitution of membrane proteins into liposomes. *Methods Enzymol.* **372,** 65–86
52. Selvy, P. E., Lavieri, R. R., Lindsley, C. W., and Brown, H. A. (2011) Phospholipase D: enzymology, functionality, and chemical modulation. *Chem. Rev.* **111,** 6064–6119
53. Holemans, T., Sørensen, D. M., van Veen, S., Martin, S., Hermans, D., Kemmer, G. C., Van den Haute, C., Baekelandt, V., Günther Pomorski, T., Agostinis, P., Wuytack, F., Palmgren, M., Eggermont, J., and Vangheluwe, P. (2015) A lipid switch unlocks Parkinson's disease-associated ATP13A2. *Proc. Natl. Acad. Sci. U.S.A.* **112,** 9040–9045
54. Lee, A. G. (2003) Lipid-protein interactions in biological membranes: a structural perspective. *Biochim. Biophys. Acta* **1612,** 1–40
55. Takahashi, M., Kondou, Y., and Toyoshima, C. (2007) Interdomain communication in calcium pump as revealed in the crystal structures with transmembrane inhibitors. *Proc. Natl. Acad. Sci. U.S.A.* **104,** 5800–5805
56. Simmonds, A. C., East, J. M., Jones, O. T., Rooney, E. K., McWhirter, J., and Lee, A. G. (1982) Annular and non-annular binding sites on the $(Ca^{2+} + Mg^{2+})$-ATPase. *Biochim. Biophys. Acta* **693,** 398–406
57. Law, B. Y., Wang, M., Ma, D. L., Al-Mousa, F., Michelangeli, F., Cheng, S. H., Ng, M. H., To, K. F., Mok, A. Y., Ko, R. Y., Lam, S. K., Chen, F., Che, C. M., Chiu, P., and Ko, B. C. (2010) Alisol B, a novel inhibitor of the sarcoplasmic/endoplasmic reticulum Ca^{2+} ATPase pump, induces autophagy, endoplasmic reticulum stress, and apoptosis. *Mol. Cancer Ther.* **9,** 718–730
58. Autzen, H. E., Siuda, I., Sonntag, Y., Nissen, P., Møller, J. V., and Thøgersen, L. (2015) Regulation of the Ca^{2+}-ATPase by cholesterol: a specific or non-specific effect? *Mol. Membr. Biol.* **32,** 75–87

59. Jensen, A. M., Sørensen, T. L., Olesen, C., Møller, J. V., and Nissen, P. (2006) Modulatory and catalytic modes of ATP binding by the calcium pump. *EMBO J.* **25,** 2305–2314
60. Obara, K., Miyashita, N., Xu, C., Toyoshima, I., Sugita, Y., Inesi, G., and Toyoshima, C. (2005) Structural role of countertransport revealed in Ca^{2+} pump crystal structure in the absence of Ca^{2+}. *Proc. Natl. Acad. Sci. U.S.A.* **102,** 14489–14496
61. Toyoshima, C., Norimatsu, Y., Iwasawa, S., Tsuda, T., and Ogawa, H. (2007) How processing of aspartylphosphate is coupled to lumenal gating of the ion pathway in the calcium pump. *Proc. Natl. Acad. Sci. U.S.A.* **104,** 19831–19836
62. Toyoshima, C., Yonekura, S., Tsueda, J., and Iwasawa, S. (2011) Trinitrophenyl derivatives bind differently from parent adenine nucleotides to Ca^{2+}-ATPase in the absence of Ca^{2+}. *Proc. Natl. Acad. Sci. U.S.A.* **108,** 1833–1838
63. Andersen, A., Cornett, C., Lauridsen, A., Olsen, C. E., and Christensen, S. B. (1994) Selective transformations of the Ca^{2+} pump inhibitor thapsigargin. *Acta Chem. Scand.* **48,** 340–346
64. Smitt, U. W., and Christensen, S. B. (1991) Nortrilobolide, a new potent guaianolide secretagogue from *Thapsia garganica*. *Planta Med.* **57,** 196–197
65. Xu, C., Ma, H., Inesi, G., Al-Shawi, M. K., and Toyoshima, C. (2004) Specific structural requirements for the inhibitory effect of thapsigargin on the Ca^{2+} ATPase SERCA. *J. Biol. Chem.* **279,** 17973–17979
66. Yu, M., Lin, J., Khadeer, M., Yeh, Y., Inesi, G., and Hussain, A. (1999) Effects of various amino acid 256 mutations on sarcoplasmic/endoplasmic reticulum Ca^{2+} ATPase function and their role in the cellular adaptive response to thapsigargin. *Arch. Biochem. Biophys.* **362,** 225–232
67. Yu, M., Zhong, L., Rishi, A. K., Khadeer, M., Inesi, G., Hussain, A., and Zhang, L. (1998) Specific substitutions at amino acid 256 of the sarcoplasmic/endoplasmic reticulum Ca^{2+} transport ATPase mediate resistance to thapsigargin in thapsigargin-resistant hamster cells. *J. Biol. Chem.* **273,** 3542–3546
68. Büttner, S., Faes, L., Reichelt, W. N., Broeskamp, F., Habernig, L., Benke, S., Kourtis, N., Ruli, D., Carmona-Gutierrez, D., Eisenberg, T., D'hooge, P., Ghillebert, R., Franssens, V., Harger, A., Pieber, T. R., *et al.* (2013) The Ca^{2+}/Mn^{2+} ion-pump PMR1 links elevation of cytosolic Ca^{2+} levels to α-synuclein toxicity in Parkinson's disease models. *Cell Death Differ.* **20,** 465–477
69. Kaneko, M., Desai, B. S., and Cook, B. (2014) Ionic leakage underlies a gain-of-function effect of dominant disease mutations affecting diverse P-type ATPases. *Nat. Genet.* **46,** 144–151
70. Okunade, G. W., Miller, M. L., Azhar, M., Andringa, A., Sanford, L. P., Doetschman, T., Prasad, V., and Shull, G. E. (2007) Loss of the Atp2c1 secretory pathway Ca^{2+}-ATPase (SPCA1) in mice causes Golgi stress, apoptosis, and midgestational death in homozygous embryos and squamous cell tumors in adult heterozygotes. *J. Biol. Chem.* **282,** 26517–26527
71. Vandecaetsbeek, I., Christensen, S. B., Liu, H., Van Veldhoven, P. P., Waelkens, E., Eggermont, J., Raeymaekers, L., Møller, J. V., Nissen, P., Wuytack, F., and Vangheluwe, P. (2011) Thapsigargin affinity purification of intracellular P(2A)-type Ca^{2+} ATPases. *Biochim. Biophys. Acta* **1813,** 1118–1127
72. Jidenko, M., Lenoir, G., Fuentes, J. M., le Maire, M., and Jaxel, C. (2006) Expression in yeast and purification of a membrane protein, SERCA1a, using a biotinylated acceptor domain. *Protein Expr. Purif.* **48,** 32–42
73. Holemans, T., Vandecaetsbeek, I., Wuytack, F., and Vangheluwe, P. (2014) Measuring Ca^{2+} pump activity in overexpression systems and cardiac muscle preparations. *Cold Spring Harb Protoc* **2014,** 876–886
74. Chemical Computing Group Inc. (2014) *Molecular Operating Environment (MOE)*, version 2014.09, Chemical Computing Group Inc., Montreal, Quebec, Canada
75. Wang, J. M., Cieplak, P., and Kollman, P. A. (2000) How well does a restrained electrostatic potential (RESP) model perform in calculating conformational energies of organic and biological molecules? *J. Comput. Chem.* **21,** 1049–1074
76. Jones, G., Willett, P., and Glen, R. C. (1995) Molecular recognition of receptor-sites using a genetic algorithm with a description of desolvation. *J. Mol. Biol.* **245,** 43–53
77. Jones, G., Willett, P., Glen, R. C., Leach, A. R., and Taylor, R. (1997) Development and validation of a genetic algorithm for flexible docking. *J. Mol. Biol.* **267,** 727–748

Supplementary Material and Methods

Title: Structure/activity Relationship of Thapsigargin Inhibition on the Purified Golgi/secretory Pathway Ca^{2+}/Mn^{2+} Transport ATPase (SPCA1a)

Authors: Jialin Chen, Joren De Raeymaecker, Jannik Hougaard, Susanne Smaardijk, Ilse Vandecaetsbeek, Frank Wuytack, Jesper Vuust Møller, Jan Eggermont, Marc De Maeyer, Søren Brøgger Christensen, Peter Vangheluwe

Supplementary Material and Methods

The substitution of the acyl group at O-2 was performed using the previous described protocol (1) starting with compound **I** as illustrated in Scheme S1:

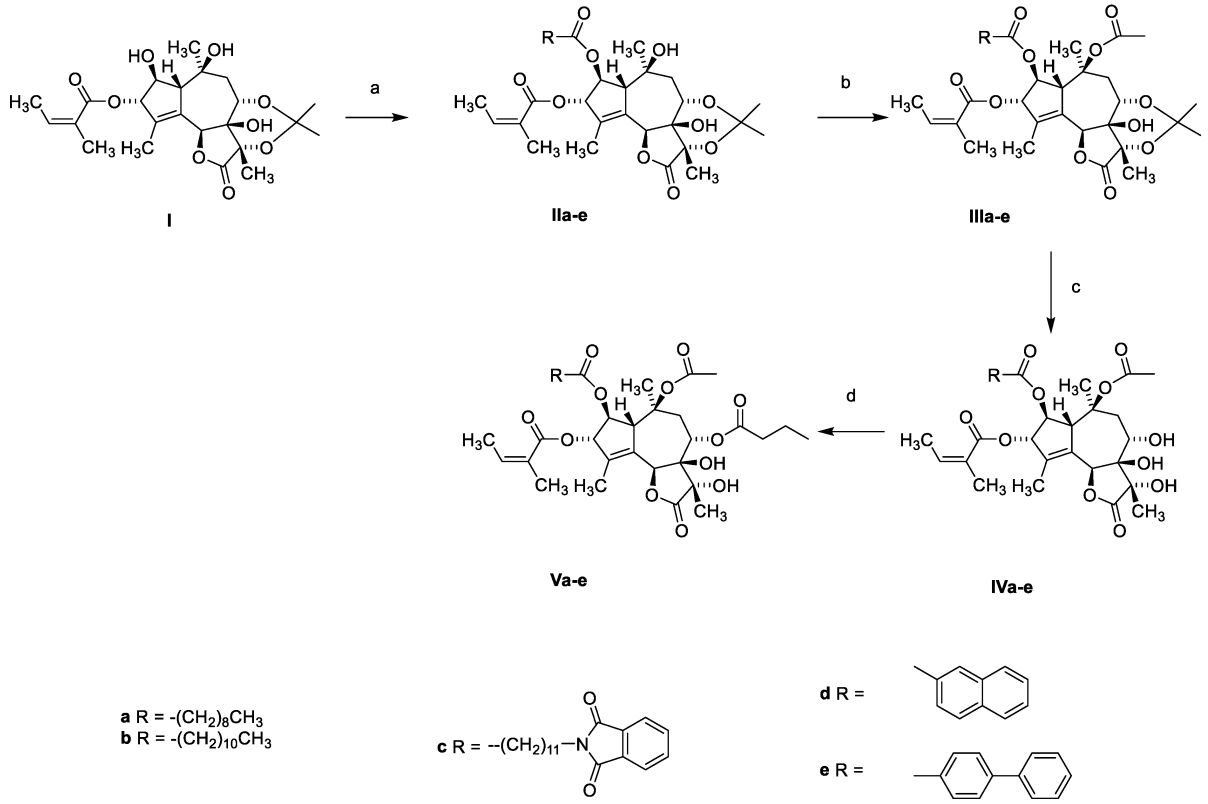

Scheme S1. RCOOH, N,N'-dicyclohexylcarbodiimide (DCC), 4-dimethylaminopyridine (DMAP), dicholoromethane (DCM), b Acetic anhydride, toluenesufonic acid, DCM, c Methanol added hydrochloric acid, d Butanoic anhydride, DCC, DMAP, DCC.

Nortrilobolide (ΔO-2) was isolated as previously described (2). ΔO-3 (1), HzL09012012 (1), HzL170809 (1), ΔO-8 (3), Leu8ADT (4), ΔO-10 (5), HzL12012012 (1), HzL271009 (1), HzL20072015 (1) and Tg-epoxide (6) were synthesized as described previously.

Compound **IIa.** Compound **I** (100 mg, 0.22 mmol), decanoic acid (45.68 mg, 0.27 mmol), 4–dimethylaminopyridine (DMAP, 20 mg, 0.16 mmol) and N,N'–dicyclohexylcarbodiimide (DCC, 54.68 mg, 0.27 mmol) was dissolved in dichloromethane DCM (3 ml). The mixture was stirred at room temperature overnight. The mixture was filtrated and concentrated in vacuo. The residue was purified by column

chromatography using petroleum ether-EtOAc (2:1) as an eluent to give compound **IIa** (112 mg, 83.5%). ^{1}H NMR ($CDCl_3$) δ (ppm): 6.11 (q, J = 7.3 Hz, 1H, angeloyl H-3); 5.79 (s, 2H, H-3 and H-6); 5.36 (t, J = 4.6 Hz, 1H, H-2); 4.22 (s, 1H, H-8); 3.39 (s, 1H, H-1); 2.34 (m, 2H, decanoyl H-2); 2.24 (dd, J = 4.1 and 15.6 Hz, 1H, H-9); 2.04 (d, J = 15.6 Hz, 1H, H-9'); 1.97 (d, J = 7.3 Hz, 3H, angeloyl H-4); 1.89 (m, 6H, H-15 and angeloyl C-2 CH_3); 1.59 (m, 2H, decanoyl H-3); 1.53 (s, 6H, H-13 and Isopropylidene CH_3); 1.41 (s, 3H, isopropylidene CH_3'); 1.26 (m, 15H, H-14 and decanoyl H-4 to H-9); 0.87 (t, J = 6.7 Hz, 3H, decanoyl H-10). ^{13}C NMR ($CDCl_3$) δ (ppm): 174.7 (C=O, C-12); 172.8 (C=O, decanoyl C-1); 167.5 (C=O, angeloyl C-1); 139.1 (C=C, C-5); 137.5 (C=C, angeloyl C-3); 129.5 (C=C, C-4); 127.4 (C=C, angeloyl C-2); 100.9 ($C(CH_3)_2$); 83.5 (C-10); 79.2 (C-3); 78.8 (C-11); 77.9 (C-7); 76.0 (C-2); 72.9 (C-6); 65.8 (C-8); 59.8 (C-1); 44.3 (C-9); 34.5 (decanoyl C-2); 33.7 (decanoyl C-4); 31.9 (isopropylidene CH_3); 30.5 (decanoyl C-5); 29.4 (decanoyl C-6); 29.3 (decanoyl C-7); 29.3 (decanoyl C-8); 29.1 (decanoyl C-9); 24.7 (decanoyl C-3); 24.0 (isopropylidene CH_3'); 23.7 (C-14); 20.6 (angeloyl C-2 CH_3); 15.9 (angeloyl C-4); 15.9 (C-13); 14.1 (decanoyl C-10); 12.6 (C-15).

Compound **IIIa**. To a solution of **IIa** (91 mg, 0.15 mmol) in DCM (11 ml) was added acetic anhydride (0.35 ml, 3.75 mmol) and *p*–TsOH (77.49 mg, 0.41 mmol). The mixture was stirred at room temperature for 2 h and 15 min added saturated aqueous $NaHCO_3$ (50 ml) and the mixture extracted three times with EtOAc (50 ml). The organic layers were combined and washed with brine (50 ml), dried over Na_2SO_4, filtered and concentrated in vacuo. The residue was purified by column chromatography using heptane-EtOAc (2:1) as an eluent to give compound **IIIa** (83 mg, 85.3%). ^{1}H NMR ($CDCl_3$) δ (ppm): 6.09 (qq, J = 1.5 and 7.2 Hz, 1H, angeloyl H-3); 5.94 (br s, 1H, H-6); 5.80 (br s, 1H, H-3); 5.41 (t, J = 4.6 Hz, 1H, H-2); 5.13 (br s, 1H, H-8); 3.76 (br s, 1H, H-1); 2.74 (dd, J = 4.7 and 15.1 Hz, 1H, H-9); 2.58 (dd, J = 3.0 and 15.1 Hz, 1H, H-9'); 2.28 (m, 2H, decanoyl H-2); 2.16 (s, 3H, acetyl H-2); 1.99 (dq, J = 1.6 and 7.2 Hz, 3H, angeloyl H-4); 1.91 (m, 6H, H-15 and angeloyl C-2 CH_3); 1.57 (m, 8H, decanoyl H-3 and isopropylidene CH_3 and CH_3'); 1.46 (s, 3H, H-13); 1.43 (s, 3H, H-14); 1.26 (m, 12H, decanoyl H-4 to H-9); 0.88 (t, J = 6.8 Hz, 3H, decanoyl H-10). ^{13}C NMR ($CDCl_3$) δ (ppm): 173.1 (C=O, C-12); 172.6 (C=O, decanoyl C-1); 170.5 (C=O, acetyl C-1); 167.5 (C=O, angeloyl C-1); 138.7 (C=C, C-5); 138.5 (C=C, angeloyl C-3); 128.7 (C=C, C-4); 127.5 (C=C, angeloyl C-2); 101.1 ($C(CH_3)_2$); 84.9 (C-10); 84.1 (C-3); 79.4 (C-11); 78.0 (C-7); 77.8 (C-2); 75.9 (C-6); 65.8 (C-8); 57.2 (C-1); 38.1 (C-9); 38.0 (decanoyl C-2); 34.3 (decanoyl C-4); 31.9 (isopropylidene CH_3); 30. 5 (decanoyl C-5); 29.5 (decanoyl C-6); 29.3 (decanoyl C-7); 29.3 (decanoyl C-8); 29.2 (decanoyl C-9); 24.7 (decanoyl C-3); 23.6 (isopropylidene CH_3'); 22.6 (decanoyl C-11); 22.5 (C-14); 21.3 (acetyl C-2); 20.5 (angeloyl C-2 CH_3); 15.8 (angeloyl C-4); 15.8 (C-13); 14.1 (decanoyl C-10); 12.6 (C-15).

Compound **IVa**: To a solution of **IIIa** (103 mg, 0.16 mmol) in methanol (10 ml) was added 4N hydrochloric acid (0.14 ml). The mixture was stirred at room temperature for 3 h and 15 min. The reaction mixture was concentrated in vacuo and the residue dissolved in toluene (10 ml) and concentrated. The residue was concentrated in vacuo to give compound **IVa** (101 mg, 100%). ^{1}H NMR ($CDCl_3$) δ (ppm): 6.10 (qq, J = 1.6 and 7.2 Hz, 1H, angeloyl H-3); 5.80 (s, 1H, H-6); 5.69 (s, 1H, H-3); 5.46 (t, J = 3.5 Hz, 1H, H-2); 4.36 (s, 1H, H-8); 4.20 (s, 1H, H-1); 2.84 (dd, J = 1.9 and 14.1 Hz, 1H, H-9); 2.48 (dd, J = 3.3 and 14.5 Hz, 1H, H-9'); 2.29 (m, 2H, decanoyl H-2); 1.98 (dq, J = 1.6 and 7.3 Hz, 3H, angeloyl H-4); 1.91 (m, 6H, acetyl H-2 and H-15); 1.85 (s, 3H, angeloyl C-2 CH_3); 1.60 (m, 2H, decanoyl H-3); 1.50 (s, 3H, H-13); 1.44 (s, 3H, H-14); 1.30 (m, 12H, decanoyl H-4 to H-9); 0.87 (t, J = 6.7 Hz, 3H, decanoyl H-10). ^{13}C NMR ($CDCl_3$) δ (ppm): 175.9 (C=O, C-12); 172.7 (C=O, decanoyl C-1); 171.4 (C=O, acetyl C-1); 167.4 (C=O, angeloyl C-1); 140.7 (C=C, C-5); 138.9 (C=C, angeloyl C-3); 130.2 (C=C, C-4); 127.4 (C=C, angeloyl C-2); 85.6 (C-10); 84.2 (C-3); 79.6 (C-11); 79.3 (C-7); 78.0 (C-2); 77.2 (C-6); 68.6 (C-8); 57.4 (C-1); 39.1 (C-9); 34.3 (decanoyl C-2); 31.9 (decanoyl C-4); 29.4 (decanoyl C-5); 29. 3 (decanoyl C-6); 29.3 (decanoyl C-7); 29.1 (decanoyl C-8); 24.8 (decanoyl C-

9); 22.8 (decanoyl C-3); 22.7 (C-14); 22.6 (acetyl C-2); 20.5 (angeloyl C-2 CH_3); 16.1 (angeloyl C-4); 15.8 (C-13); 14.1 (decanoyl C-12); 12.8 (C-15).

Compound **Va (JBH04012016).** A solution of **IVa** (107 mg, 0.18 mmol), butyric anhydride (30.61 mg, 0.19 mmol) and DMAP (10 mg, 0.08 mmol) in dichloromethane (5 ml) was stirred at room temperature for 2 h and added saturated aqueous $NaHCO_3$ (10 ml). The reaction mixture was extracted three times with dichloromethane (10 ml). The organic layers was combined and dried over Na_2SO_4, filtered and concentrated in vacuo. The residue was purified by column chromatography using heptane-EtOAc (2:1) as an eluent to give compound **Va** (83 mg, 69.6%). ^{1}H NMR ($CDCl_3$) δ (ppm): 6.08 (qq, J = 1.5 and 7.2 Hz, 1H, angeloyl H-3); 5.65 (s, 1H, H-6); 5.64 (s, 1H, H-3); 5.62 (t, J = 3.8 Hz, 1H, H-2); 5.45 (t, J = 3.2 Hz, 1H, H-8); 4.32 (br s, 1H, H-1); 3.07 (dd, J = 3.6 and 14.8 Hz, 1H, H-9); 2.27 (m, 5H, decanoyl H-2 and butanoyl H-2 and H-9'); 1.97 (dq, J = 1.6 and 7.3 Hz, 3H, angeloyl H-4); 1.89 (br s, 3H, H-15); 1.87 (s, 3H, acetyl H-2); 1.84 (br s, 3H, angeloyl C-2 CH_3); 1.59 (m, 4H, decanoyl H-3 and butanoyl H-3); 1.44 (s, 3H, H-13); 1.37 (s, 3H, H-14); 1.25 (m, 12H, decanoyl H-4 to H-9); 0.92 (t, J = 7.4 Hz, 3H, butanoyl H-4); 0.85 (t, J = 7.0 Hz, 3H, decanoyl H-10). ^{13}C NMR ($CDCl_3$) δ (ppm): 175.9 (C=O, C-12); 172.9 (C=O, decanoyl C-1); 172.7 (C=O, butanoyl C-1); 171.1 (C=O, acetyl C-1); 167.1 (C=O, angeloyl C-1); 141.3 (C=C, C-5); 138.7 (C=C, angeloyl C-3); 130.5 (C=C, C-4); 127.5 (C=C, angeloyl C-2); 84.9 (C-10); 84.2 (C-3); 78.6 (C-11); 78.5 (C-7); 77.8 (C-2); 77.0 (C-6); 66.2 (C-8); 57.3 (C-1); 38.2 (C-9); 36.6 (butanoyl C-2); 34.2 (decanoyl C-2); 31.9 (decanoyl C-4); 29.4 (decanoyl C-5); 29.4 (decanoyl C-6); 29.3 (decanoyl C-7); 29.1 (decanoyl C-8); 24.8 (decanoyl C-9); 23.0 (decanoyl C-3); 22.6 (C-14); 22.6 (acetyl C-2); 20.6 (butanoyl C-3); 18.0 (angeloyl C-2 CH_3); 16.0 (angeloyl C-4); 15.8 (C-13); 14.0 (butanoyl C-4); 13.7 (decanoyl C-10); 12.9 (C-15). HRMS 701.35090, Calc. $(C_{36}H_{54}NaO_{12})^+$: 701.35075.

Compound **IIb.** Compound **IIb** was prepared in the same way as **IIa** using **I** (100 mg, 0.22 mmol) and dodecanoic acid (53.08 mg, 0.27 mmol) as starting materials. The crude reaction product was purified by column chromatography using petroleum ether:EtOAc (3:1) as an eluent to give compound **IIb** (133 mg, 94.8%). ^{1}H NMR ($CDCl_3$) δ (ppm): 6.11 (qq, J = 1.6 and 7.3 Hz, 1H, angeloyl H-3); 5.81 (s, 1H, H-6); 5.80 (s, 1H, H-3); 5.37 (t, J = 4.6 Hz, 1H, H-2); 4.24 (t, J = 3.7 Hz, 1H, H-8); 3.36 (br s, 1H, H-1); 2.33 (m, 2H, dodecanoyl H-2); 2.25 (dd, J = 4.4 and 15.4 Hz, 1H, H-9); 2.05 (dd, J = 2.9 and 15.0 Hz, 1H, H-9'); 1.98 (d, J = 7.5 Hz, 3H, angeloyl H-4); 1. 90 (m, 6H, H-15 and angeloyl C-2 CH_3); 1.56 (m, 8H, dodecanoyl H-3 and H-13 and isopropylidene CH_3); 1.42 (s, 3H, isopropylidene CH_3'); 1.25 (m, 19H, H-14 and dodecanoyl H-4 to H-11); 0.88 (t, J = 6.7 Hz, 3H, dodecanoyl H-12). ^{13}C NMR ($CDCl_3$) δ (ppm): 174.6 (C=O, C-12); 172.7 (C=O, dodecanoyl C-1); 167.4 (C=O, angeloyl C-1); 139.0 (C=C, C-5); 137.7 (C=C, angeloyl C-3); 129.3 (C=C, C-4); 127.4 (C=C, angeloyl C-2); 100.9 ($C(CH_3)_2$); 83.4 (C-10); 79.2 (C-3); 78.7 (C-11); 77.8 (C-7); 76.1 (C-2); 72.8 (C-6); 65.8 (C-8); 60.0 (C-1); 44.3 (C-9); 34.5 (dodecanoyl C-2); 33.8 (dodecanoyl C-4); 31.9 (isopropylidene CH_3); 30.5 (dodecanoyl C-5); 29.6 (dodecanoyl C-6); 29.5 (dodecanoyl C-7); 29.3 (dodecanoyl C-8); 29.3 (dodecanoyl C-9); 29.1 (dodecanoyl C-10); 24.8 (dodecanoyl C-3); 23.7 (isopropylidene CH_3'); 22.7 (dodecanoyl C-11); 22.7 (C-14); 20.6 (angeloyl C-2 CH_3); 15.9 (angeloyl C-4); 15.9 (C-13); 14.1 (dodecanoyl C-12); 12.6 (C-15).

Compound **IIIb**. Compound **IIIb** was prepared in the same way as compound **IiIa** using **IIb** (133 mg, 20.95 mmol) and acetic anhydride (0.49 ml, 5.24 mmol) as starting materials. The crude reaction product was purified by column chromatography using petroleum ether:EtOAc (3:1) as an eluent to give compound **IIIb** (71.3 mg, 50.3%). ^{1}H NMR ($CDCl_3$) δ (ppm): 6.10 (qq, J = 1.5 and 7.3 Hz, 1H, angeloyl H-3); 5.78 (br s, 1H, H-6); 5.73 (br s, 1H, H-3); 5.49 (t, J = 4.6 Hz, 1H, H-2); 4.26 (t, J = 3.5 Hz, 1H, H-8); 3.96 (br s, 1H, H-1); 2.79 (dd, J = 4.7 and 14.8 Hz, 1H, H-9); 2.64 (dd, J = 3.0 and 14.7 Hz, 1H, H-9'); 2.30 (m, 2H, dodecanoyl H-2); 1.98 (dq,

J = 1.5 and 7.2 Hz, 3H, angeloyl H-4); 1.91 (dq, J = 1.6 and 7.2 Hz, 3H, angeloyl C-2 CH_3); 1.87 (m, 6H, H-15 and acetyl H-2); 1.56 (m, 8H, dodecanoyl H-3 and isopropylidene CH_3 and CH_3'); 1.46 (s, 3H, H-13); 1.42 (s, 3H, H-14); 1.25 (m, 16H, dodecanoyl H-4 to H-11); 0.88 (t, J = 7.2 Hz, 3H, dodecanoyl H-12). ^{13}C NMR ($CDCl_3$) δ (ppm): 172.9 (C=O, C-12); 172.6 (C=O, dodecanoyl C-1); 170.4 (C=O, acetyl C-1); 167.4 (C=O, angeloyl C-1); 138.8 (C=C, C-5); 138.7 (C=C, angeloyl C-3); 128.5 (C=C, C-4); 127.5 (C=C, angeloyl C-2); 101.1 ($C(CH_3)_2$); 84.7 (C-10); 84.0 (C-3); 79.4 (C-11); 78.0 (C-7); 77.7 (C-2); 76.0 (C-6); 65.8 (C-8); 57.3 (C-1); 38.1 (C-9); 34.3 (dodecanoyl C-2); 31.9 (dodecanoyl C-4); 30.5 (isopropylidene CH_3); 29. 6(dodecanoyl C-5); 29.6 (dodecanoyl C-6); 29.5 (dodecanoyl C-7); 29.3 (dodecanoyl C-8); 29.3 (dodecanoyl C-9); 29.2 (dodecanoyl C-10); 24.8 (dodecanoyl C-3); 23.6 (isopropylidene CH_3'); 22.7 (dodecanoyl C-11); 22.5 (C-14); 21.2 (acetyl C-2); 20.5 (angeloyl C-2 CH_3); 15.8 (angeloyl C-4); 15.8 (C-13); 14.1 (dodecanoyl C-12); 12.6 (C-15).

Compound **IVb.** Compound **IVb** was prepared in the same way as compound **IVa** using **IIIb** (71.3 mg, 0.11 mmol) as starting material. The reaction mixture was concentrated in vacuo to give compound **IVb** (64 mg, 95.4%). ^{1}H NMR ($CDCl_3$) δ (ppm): 6.10 (qq, J = 1.3 and 7.3 Hz, 1H, angeloyl H-3); 5.79 (s, 1H, H-6); 5.68 (s, 1H, H-3); 5.44 (t, J = 3.6 Hz, 1H, H-2); 4.35 (s, 1H, H-8); 4.21 (s, 1H, H-1); 2.83 (d, J = 13.9 Hz, 1H, H-9); 2.45 (d, J = 13.9 Hz, 1H, H-9'); 2.27 (m, 2H, dodecanoyl H-2); 1.97 (m, 3H, angeloyl H-4); 1.89 (m, 6H, acetyl H-2 and H-15); 1.83 (br s, 3H, angeloyl C-2 CH_3); 1.58 (m, 2H, dodecanoyl H-3); 1.48 (s, 3H, H-13); 1.43 (s, 3H, H-14); 1.25 (m, 16H, dodecanoyl H-4 to H-1); 0.87 (t, J = 7.0 Hz, 3H, dodecanoyl H-12). ^{13}C NMR ($CDCl_3$) δ (ppm): 175.9 (C=O, C-12); 172.7 (C=O, dodecanoyl C-1); 171.4 (C=O, acetyl C-1); 167.4 (C=O, angeloyl C-1); 140.7 (C=C, C-5); 138.8 (C=C, angeloyl C-3); 130.2 (C=C, C-4); 127.4 (C=C, angeloyl C-2); 85.6 (C-10); 84.2 (C-3); 79.6 (C-11); 79.3 (C-7); 78.0 (C-2); 77.2 (C-6); 68.6 (C-8); 57.4 (C-1); 39.1 (C-9); 34.3 (dodecanoyl C-2); 31.9 (dodecanoyl C-4); 29.6 (dodecanoyl C-5); 29. 6(dodecanoyl C-6); 29.5 (dodecanoyl C-7); 29.3 (dodecanoyl C-8); 29.3 (dodecanoyl C-9); 29.2 (dodecanoyl C-10); 24.8 (dodecanoyl C-3); 22.8 (dodecanoyl C-11); 22.7 (C-14); 22.7 (acetyl C-2); 20.5 (angeloyl C-2 CH_3); 16.2 (angeloyl C-4); 15.8 (C-13); 14.1 (dodecanoyl C-12); 12.8 (C-15).

Compound **Vb (JBH09022016)**. Compound **Vb** was prepared the same way as compound **Va** using **IVb** (64 mg, 0.10 mmol) and butyric anhydride (25.46 mg, 0.16 mmol) as starting materials. The crude reation product was purified by column chromatography using heptane-EtOAc (3:1) as an eluent to give compound **Vb** (53 mg, 74.6%). ^{1}H NMR ($CDCl_3$) δ: 6.10 (qq, J = 1.5 and 7.2 Hz, 1H, angeloyl H-3); 5.68 (s, 1H, H-6); 5.65 (s, 1H, H-3); 5.62 (t, J = 3.7 Hz, 1H, H-2); 5.48 (t, J = 3.4 Hz, 1H, H-8); 4.27 (s, 1H, H-1); 3.03 (dd, J = 3.6 and 14.8 Hz, 1H, H-9); 2.29 (m, 5H, dodecanoyl H-2 and butanoyl H-2 and H-9'); 1.99 (dq, J = 1.5 and 7.1 Hz, 3H, angeloyl H-4); 1.91 (p, J = 1.6 Hz, 3H, H-15); 1.89 (s, 3H, acetyl H-2); 1.86 (br s, 3H, angeloyl C-2 CH_3); 1.61 (m, 4H, dodecanoyl H-3 and butanoyl H-3); 1.48 (s, 3H, H-13); 1.40 (s, 3H, H-14); 1.25 (m, 16H, dodecanoyl H-4 to H-11); 0.94 (t, J = 7.4 Hz, 3H, butanoyl H-4); 0.86 (t, J = 6.7 Hz, 3H, dodecanoyl H-12). ^{13}C NMR ($CDCl_3$) δ: 175.4 (C=O, C-12); 172.6 (C=O, dodecanoyl C-1); 172.6 (C=O, butanoyl C-1); 170.8 (C=O, acetyl C-1); 167.1 (C=O, angeloyl C-1); 141.8 (C=C, C-5); 138.7 (C=C, angeloyl C-3); 130.2 (C=C, C-4); 127.5 (C=C, angeloyl C-2); 84.6 (C-10); 84.1 (C-3); 78.6 (C-11); 78.6 (C-7); 77.8 (C-2); 76.9 (C-6); 66.2 (C-8); 57.5 (C-1); 38.3 (C-9); 36.7 (butanoyl C-2); 34.2 (dodecanoyl C-2); 31.9 (dodecanoyl C-4); 29.6 (dodecanoyl C-5); 29.6 (dodecanoyl C-6); 29.5 (dodecanoyl C-7); 29.4 (dodecanoyl C-8); 29.3 (dodecanoyl C-9); 29.1 (dodecanoyl C-10); 24.8 (dodecanoyl C-3); 22.9 (dodecanoyl C-11); 22.7 (C-14); 22.6 (acetyl C-2); 20.6 (butanoyl C-3); 18.0 (angeloyl C-2 CH_3); 16.2 (angeloyl C-4); 15.8 (C-13); 14.1 (butanoyl C-4); 13.7 (dodecanoyl C-12); 13.0 (C-15). HRMS 729.382250, Calc. $(C_{38}H_{58}NaO_{12})^+$: 729.38205.

Compound **IIc**. Compound **IIc** was prepared in the same way as **IIa** using **I** (70 mg, 0.15 mmol), phtalimid-dodecanoic acid (97 mg, 0.18 mmol), DCC (40 mg, 0.18 mmol), and 20 mg of DMAP as starting materials. After stirring for 18 h the crude reaction product was purified by column chromatography using toluene-EtOAc (3:1) as an eluent to give compound **IIc** (86 mg, 57%). ^{1}H NMR (600 MHz, $CDCl_3$) δ: 1.27 (s, 3 H, H-14), 1.21 - 1.37 (m, 14 H, dodecanoyl H-4 – H-10), 1.43 (s, 3 H, isopropylidene H-1), 1.55 (s, 3 H, H-13) 1.57 (s, 3 H, isopropylidene H-3), 1.58 - 1.64 (m, 2 H, dodecanoyl, H-3) 1.64 - 1.72 (m, 2 H, dodecanoyl, H-10) 1.89 (s, 3 H, H-15) 1.92 (s, 3 H, angeloyl H-5) 1.99 (d, *J*=6.97 Hz, 3 H, angeloyl H-4) 2.06 (dd, *J*=15.04, 2.57 Hz, 1 H, H-9b), 2.28 (dd, *J*=17.24, 4.77 Hz, 1 H, H-9a), 2.31 - 2.40 (m, 2 H, dodecanoyl H-2), 2.81 (s, 1 H, OH), 3.37 (s, 1 H, OH), 3.42 (br. s., 1 H, H-1) 3.68 (t, *J*=7.34 Hz, 2 H, dodecanoyl H-12), 4.27 (t, *J*=3.48 Hz, 1 H, H-8) 5.39 (t, *J*=4.59 Hz, 1 H, H-2) 5.81 (br. s, 1 H, H-6) 5.81 (br. s, 1 H, H-3), 6.12 (qq, *J*=7.10, 1.00 Hz, 1 H, angeloyl H-3) 7.68 - 7.76 (m, 2 H, phtalimid H-4 and 7) 7.81 - 7.88 (m, 2 H, phatalimid H-5 and 6). ^{13}C NMR (150 MHz, $CDCl_3$) δ: 12.56 (C-15), 15.90 (angeloyl C-5), 20.58 (angeloyl C-4), 23.68 (C-14), 24.05 (isopropylidene C-1), 24.72, 26.81, 28.54, 28.93, 29.09, 29.14, 29.29, 29.36, 29.37 (dodecanoyl C-3 – C-11), 30.50 (isopropylidene C-3), 34.43 (dodecanoyl C-2), 38.10 (C-9), 44.37 (dodecanoyl C-12), 59.85 (C-1), 65.83 (C-8), 72.89 (C-6), 76.02 (C-6), 77.95, 78.77 (C-7 and 10), 79.22 (C-10), 83.45 (C-3), 100.88 (isopropylidene C-2), 123.19 (phtalimide C-5, C-6), 127.40 (angeloyl C-2), 129.54 (C-4), 132.11 (phtalimide C-3, C-8), 133.91 (phtalimide C-4, C-7), 137.33 (angeloyl C-3), 138.96 (C-5), 167.42 (phtalimide C-2, C-9), 168.56 (angelolyl C-1), 172.88 (dodecanoyl C-1), 174.59 (C-12).

Compound **IIIc**: To a solution of compound **IIc** (86 mg, 0.11 mmol) in 5 mL of isopropenyl acetate was added 10 mg of p-TsOH and the mixture was stirred at room temperature for 2 h. The mixture was added 10 mL of aqueous $NaCO_3$ (saturated) and extracted three times with EtOAc (10 mL). The organic phases were combined and concentrated in vacuo. The residue was purified by reversed phase chromatography (Rp-18) chromatography using CH_3OH-H_2O (5:1) added 0.1 % acetic acid to give compound **IIIc** (56 mg, 62%). ^{1}H NMR (600 MHz, $CDCl_3$) δ 1.20 - 1.35 (m, 14 H, Dodecanoyl H-4 – Dodecanoyl H-10), 1.41 (s, 3 H, H-14), 1.47 (s, 3 H, Ket-3), 1.53 (br. s., 3 H, H-13), 1.56 (s, 3 H, Ket-1), 1.58 - 1.62 (m, 2 H, Dodecanoyl H-3) 1.62 – 1.68 (m, 2 H, Dodecanoyl H-10), 1.86 (br. s., 3 H, H-15) 1.87 (br. s., 3 H, Ac-2) 1.93 (m, 3 H, Angeloyl H-5), 1.97 (dq, *J*=5.20, 3.40 Hz, 3 H, Angeloyl H-4), 2.22 - 2.30 (m, 1 H, Dodecanoyl H-2b), 2.30 - 2.37 (m, 1 H, Dodecanoyl H-2a), 2.64 (dd, *J*=15.40, 2.00 Hz, 1 H, H-9b), 2.76 (dd, *J*=14.31, 3.67 Hz, 1 H, H-9a) 3.66 (m, 2 H, Dodecanoyl H-12), 4.00 (br. s., 1 H, H-1), 4.29 (br. s., 1 H, H-8), 5.49 (dd, *J*=7.40, 3.70 Hz, 1 H, H-2), 5.70 (br. s., 1 H, H-6), 5.78 (br. d, *J*=1.50 Hz, 1 H, H-3) 6.09 (br. q, *J*=7.10, 7.10, 7.10 Hz, 1 H, Angeloyl H-3), 7.69 - 7.73 (m, 2 H, Phtalimid-5 and 6), 7.83 (td, *J*=5.41, 3.12 Hz, 2 H, Phtalimid-4 and 7). ^{13}C NMR (150 MHz, $CDCl_3$) d ppm 12.59 (C-15), 15.80 (C-13), 20.53 (Angeloyl C-5), 21.20 (Angeloyl C-4), 22.54 (Ac-2), 23.61 (C-14), 24.71, 26.83, 28.56, 29.11, 29.14, 29.25, 29.39, 29.42, 29.47, (Dodecanoyl C-3 – 11), 34.27 (Dodecanoyl C-2), 38.06 (Dodecanoyl C-12), 57.24 (C-1), 65.84 (C-8), 75.89 (C-6), 77.83, 78.02 (C-7 and C-11), 79.44 (C-2), 84.07 (C-10), 84.86 (C-3), 101.06 (Ket-2), 123.16 (Phtalimid-4 and 7), 127.46 (Angeloyl C-2), 128.78 (C-4), 132.11 (Angeloyl C-3), 133.89 (Phtalimid-5 and 6), 138.21 (C-5), 138.64 (Phtalimid-3 and 8), 167.42 (Angeloyl C-1), 168.52 (Phtalimid-2 and 9), 170.45 (Ac-1), 172.60 (Dodecanoyl C-1), 172.12 (C-12).

Compound **IVc**: Compound **IVc** was prepared the same way as compound **IVa** using **IIIc** (56 mg, 0.06 mmol) as starting material. After workup the residue was purified by RP-18 chromatography using CH_3OH-H_2O (5:1, 0.1% AcOH) as eluent to give compound **IVc** (50 mg, 94%). ^{1}H NMR (600 MHz, $CDCl_3$) δ: 1.19 - 1.35 (m, 14 H, Dodecanoyl H-4 – Dodecanoyl H -10), 1.45 (s, 3 H, H-14), 1.50 (s, 3 H, H-13), 1.58 (sxt, *J*=8.10 Hz, 2 H, Dodecanoyl -3), 1.65 (quin, *J*=7.15 Hz, 2 H, Dodecanoyl H-10), 1.84 (s, 3 H, H-15), 1.91 (m, 3 H, Acetyl-2), 1.92 (m, 3 H, Angeloyl H-5), 1.98 (m, 3 H, Angeloyl H-5), 2.24 (dt, *J*=16.50, 6.60 Hz, 1 H, Dodecanoyl

H-2b), 2.31 (dt, *J*=16.50, 6.60 Hz, 1 H, Dodecanoyl H-2a), 2.49 (br. dd, *J*=11.40, 2.00 Hz, 1 H, H-9b), 2.83 (dd, *J*=12.50, 2.00 Hz, 1 H, H-9a) 3.66 (t, *J*=7.34 Hz, 2, Dodecanoyl H-12 H), 3.92 (s, 1 H, OH), 4.24 (br. s., 1 H, H-1) 4.32 (s, 1 H, OH) 4.38 (br. t, *J*=3.00, 3.00 Hz, 1 H, H-8) 5.40 (s, 1 H, OH) 5.46 (t, *J*=3.48 Hz, 1 H, H-3) 5.68 (br. s., 1 H, H-6) 5.81 (br. s., 1 H, H-3) 6.10 (qq, *J*=7.30, 1.30 Hz, 1 H, Angeloyl H-4) 7.69 - 7.73 (m, 2 H, Phtalimid-5 and 6) 7.81 - 7.85 (m, 2 H, Phtalimid-4 and 7). ^{13}C NMR (150 MHz, $CDCl_3$) δ: 12.83 (C-15), 15.83 (C-13), 16.16 (Angeloyl H-5), 20.56 (Angeloyl C-4), 22.69 (Ac-2), 22.73 (C-14), 42 24.77, 26.82, 28.53, 29.08, 29.22, 29.37, 29.39, 29.44 (Dodecanoyl C-3 -11), 34.26 (Dodecanoyl C-2), 38.10 (Dodecanoyl C-12), 39.15 (C-9), 57.51 (C-1), 68.67 (C-8), 77.04 (C-6), 78.01, C-2), 79.31, 79.54 (C-7 and 11), 84.20 (C-10), 85.55 (C-3), 123.21 (Phtalimid-7 and 4), 127.43 (Angeloyl C-2), 130.40 (C-4), 132.05 (Phtalimid-3 and 8), 133.95 (Phtalimid-5 and 6), 138.77 (Angeloyl C-3), 140.51 (C-5), 167.32 (Angeloyl C-1), 168.64 (Phtalimid-2 and 9), 171.26 (Acetyl-1), 172.66 (Dodecanoyl C-1), 175.73 (C-12).

Compound **Vc (HzL24042015)**: Compound **Vc** was prepared the same way as compound **Va** using **IVc** (50 mg, 0.06 mmol), 11mg of butyric anhydride and 10 mg of DMAP as starting materials. The mixture was stirred at RT for 2h. After workup the residue was purifed by chromatograpy using toluene-ethyl acetate (4:1) added 0.1 % acetic acid to give **Vc** (45mg, 84%). ^{1}H NMR (600 MHz, $CDCl_3$) δ ppm 0.94 (t, *J*=7.40 Hz, 3 H, Bu-4) 1.21 - 1.35 (m, 14 H, Dodecanoyl H-4 – Dodecanoyl H-9) 1.40 (s, 3 H, H-14) 1.48 (s, 3 H, H-13) 1.56 - 1.69 (m, 6 H, Bu-3, Dodecanoyl H-3, Dodecanoyl H-10) 1.86 (s, 3 H, H-15) 1.89 (s, 3 H, Angeloyl H-5) 1.92 (d, *J*=1.10 Hz, 3 H, Angeloyl H-5) 1.99 (dd, *J*=7.34, 1.47 Hz, 3 H, Angeloyl H-4) 2.23 - 2.37 (m, 5 H, Bu-2, Dodecanoyl H-2, H-9b), 3.05 (dd, *J*=14.49, 3.12 Hz, 1 H, H-9a) 3.30 - 3.41 (m, 1 H, OH) 3.67 (t, *J*=7.34 Hz, 2 H, Dodecanoyl H-12), 3.94 - 4.03 (m, 1 H, OH), 4.32 (br. s., 1 H, H-1) 5.49 (t, *J*=2.90 Hz, 1 H, H-2) 5.66 (t, *J*=4.00 Hz, 3 H, H-8), 5.64 - 5.70 (m, 2 H, H-3 and H-6) 6.10 (qq, *J*=7.00, 1.00 Hz, 1 H, Angeloyl H-3), 7.69 - 7.73 (m, 2 H, Pht-5 and 6), 7.81 - 7.86 (m, 2 H, Pht-4 and 7). ^{13}C NMR (150 MHz, $CDCl_3$) δ ppm 12.93 (C-15), 13.71 (Bu-4), 15.81 (C-13), 16.08 (Angeloyl C-5), 17.97 (Bu-3), 20.56 (Angeloyl C-4), 22.58 (Ac-2), 22.86 (C-14), 24.78, 26.83, 28.55, 29.05, 29.12, 29.23, 29.36, 29.39, 29.44 (Dodecanoyl C-3 to 11), 34.18 (Bu-2), 36.58 (Dodecanoyl C-2), 38.10 (Dodecanoyl C-12), 38.25 (C-9), 57.48 (C-1), 66.20 (C-8), 76.92 (C-6, 77.79 (C-2), 78.51, 78.60 (C-7 and 11), 84.20 (C-10), 84.74 (C-3), 123.18 (Pht-4 and 7), 127.46 (Angeloyl C-2), 130.47 (C-4), 132.11 (Pht-3 and 8), 133.89 (Pht-5 and 6), 138.61 (Angeloyl C-3), 141.40 (C-5), 167.11. (Angeloyl C-1), 168.56 (Pht-2 and 9), 170.85 (Ac-1), 172.60 (Bu-1), 172.66 (Dodecanoyl C-1), 175.70 (C-12). HRMS 874,39712, Calc. $(C_{48}H_{61}NaO_{14})^{+}$: 874,3984.

Compound **IId**: Compound **IId** was prepared in the same way as **IIa** using **I** (100 mg, 0.2 mmol), 2-naphtoic acid (42 mg, 0.24 mmol), DCC (50 mg, 0.24 mmol), and 20 mg of DMAP as starting materials. After stirring for 18 h the crude reaction product was purified by column chromatography using toluene-EtOAc (3:1) as an eluent to give compound **IId** (99 mg, 74%). ^{1}H NMR (600 MHz, $CDCl_3$) δ: 1.29 (s, 3 H, H-14) 1.40 (s, 3 H, isopropylidene H-3), 1.45 (br. s., 3 H, H-13) 1.51 (s, 3 H, isopropylidene H-1) 1.91 (s, 3 H, H-15) 1.94 (br. s., 3 H, angeloyl H-5) 1.96 (d, *J*=6.97 Hz, 3 H, angeloyl H-4), 2.00 (d, *J*=15.41 Hz, 1 H, H-9b), 2.17 (dd, *J*=15.41, 3.67 Hz, 1 H, H-9a) 3.67 (s, 1 H, H-1), 4.13 (br. s., 1 H, H-8), 5.64 (t, *J*=2.90 Hz, 1 H, H-2), 5.84 (br. s., 1 H, H-6), 6.04 (br. s., 1 H, H-3), 6.10 (qq, *J*=8.10, 1.10 Hz, 1 H, angeloyl H-3), 7.51 (t, *J*=6.60 Hz, 1 H, naphtoyl H-7), 7.58 (t, *J*=6.60 Hz, 1 H, naphtoyl H-6), 7.82 (d, *J*=7.50 Hz, 1 H, H-5), 7.83 (d, *J*=6.24 Hz, 1 H, H-8), 7.88 (d, *J*=7.70 Hz, 1 H, naphtoyl H-10), 8.03 (d, *J*=8.80 Hz, 1 H, naphtoyl H-11), 8.60 (s, 1 H, naphtoyl H-3). ^{13}C NMR (150 MHz, $CDCl_3$) δ: 12.64 (C-15), 15.80 (isopropylidene C-3), 15.89 (C-13), 20.58 (angeloyl C-4), 23.57 (isopropylidene C-3), 24.07 (C-14), 30.48 (isopropylidene C-1), 44.42 (C-9), 60.50 (C-1), 65.81 (C-8), 73.10 (C-6), 75.96 (C-2), 77.85, 79.27 (C-7/C-11), 79.95 (C-10), 83.61 (C-3), 100.90 (isopropylidene C-2), 125.30 (naphtoyl C-11), 126.73 (naphtoyl-C-2), 126.82 (naphtoyl C-6), 127.33 (naphtoyl C-3), 127.73 (naphtotyl C-10), 128.14 (naphtoyl C-7), 128.47 (naphtoyl C-8), 129.38 (naphtoyl C-5), 130.21 (angeloyl C-

2), 131.64 (naphtoyl C-4), 132.34 (C-4), 135.68 (naphtoyl C-9), 137.47 (angeloyl C-3), 139.18 (C-5), 167.44 (angeloyl C-1), 167.48 (naphtoyl C-1), 173.14 C-12).

Compound **IIId.** To a solution of compoud **IId** (99 mg, 0.16 mmol) in 10 mL of Isopropenyl acetate was added 5 mg of p-TsOH and the mixture was stirred at room temperature for 18h. The mixture was added 10 mL of aqueous $NaCO_3$ (saturated) and extracted three times with EtOAc (10 mL). The organic phases were combined and concentrated in vacuo. The residue was purified by reversed phase chromatography (Rp-18) chromatography using CH_3OH/H_2O (5:1) added 0.1 % acetic acid to give compound **IIId** (60 mg, 58%). ^{1}H NMR (600 MHz, $CDCl_3$) δ: 1.42 (s, 3 H, H-14), 1.51 (s, 3 H, isopropylidene H-3), 1.54 (s, 3 H, H-13), 1.55 (s, 3 H, isopropylidene H-1), 1.63 (s, 3 H, H-15), 1.92 (br. s., 1 H, angeloyl H-5), 1.95 (s, 3 H, acetyl H-2), 1.98 (d, *J*=7.34 Hz, 3 H, angeloyl H-4), 2.56 (d, *J*=14.67 Hz, 1 H, H-9b), 2.73 (dd, *J*=14.67, 4.03 Hz, 1 H, H-9a), 4.19 (br. s., 2 H, H-1 and H-8), 5.80 (t, *J*=3.50 Hz, 1 H, H-2), 5.82 (br. s, 1 H, H-6), 5.95 (br. s., 1 H, H-3), 6.11 (qq, *J*=7.30, 1.10 Hz, 1 H, angeloyl H-3), 7.50 (t, *J*=7.00 Hz, 1 H, naphtoyl H-7), 7.56 (t, *J*=7.34 Hz, 1 H, napthoyl H-6), 7.84 (d, *J*=8.07 Hz, 2 H, H-5 and 8), 7.90 (d, *J*=8.44 Hz, 1 H, naphtoyl H-10), 8.03 (d, *J*=8.44 Hz, 1 H, naphtoyl H-11), 8.59 (s, 1 H, H-3). ^{13}C NMR (150 MHz, $CDCl_3$) δ: 12.67 (C-15), 15.77 (angeloyl C-5), 15.84 (C-13), 20.59 (acetyl C-2), 21.33 (isopropylidene C-3), 22.49 (angeloyl C-4), 23.61 (C-14), 30.49 (isopropylidene C-1), 37.87 (C-9), 56.56 (C-1), 65.81 (C-8), 75.96 (C-6), 78.05 (C-2), 79.05, 79.41 (C-7/C-11), 83.63 (C-10), 84.92 (C-3), 101.11 (isopropylidene C-2), 125.33 (naphtoyl C-11), 126.62 (naphtoyl C-2), 127.26 (naphtoyl C-6), 127.55 (naphtoyl C-3), 127.77 (naphtoyl C-10), 128.20 (naphtoyl C-7), 128.26 (angeloyl C-2), 128.32 (naphtoyl C-8), 129.39 (naphtoyl C-5), 131.29 (naphtoyl C-4), 132.48 (C-4), 135.62 (naphtoyl C-9), 138.46 (angeloyl C-3), 138.67 (C-5), 165.73 (naphtoyl C-1), 167.50 (angeloyl C-1), 170.67 (acetyl C-1), 173.14 (C-12).

Compound **IVd.** To a solution compound **IIId** (61 mg, 0.09 mmol) in 5 mL of CH_3OH was added 0.1 mL of 6N HCl and the mixture was stirred at room temperature for 4h. The mixture was concentrated and the residue was purified by rversed phase chromatography (Rp-18) using CH_3OH-H_2O (5:1) added 0.1 % of acetic acid to give the compound **IVd** (57 mg, 99%). ^{1}H NMR (400 MHz, $CDCl_3$) δ: 1.35 (s, 3 H, H-14), 1.4s (m, 3 H, H-13) 1.61 (s, 3 H, acetyl H-2) 1.79 (s, 3 H, H-15) 1.87 (quin, *J*=1.50 Hz, 3 H, angeloyl H-5) 1.91 (dq, *J*=7.30, 1.50 Hz, 3 H, angeloyl H-4) 2.35 (dd, *J*=14.18, 2.93 Hz, 1 H, H-9b) 2.76 (br. dd, *J*=12.00, 2.90 Hz, 1 H, H-9a) 3.58 (br. s., 1 H, OH) 4.21 (br. t, *J*=4.20, 4.20 Hz, 1 H, H-8) 4.36 (br. s., 1 H, H-1) 5.69 (t, *J*=4.16 Hz, 1 H, H-2), 5.73 (br. s., 1 H, H-6), 5.85 (br. s., 1 H, H-3), 6.04 (qq, *J*=7.20, 1.30 Hz, 1 H, angeloyl H-3), 7.42 (t, *J*=7.10 Hz, 1 H, naphtoyl H-7), 7.47 (t, *J*=7.10 Hz, 1 H, naphtoyl H-6), 7.75 (d, *J*=8.56 Hz, 2 H, naphtoyl H-5, H-8) 7.83 (d, *J*=8.07 Hz, 1 H, naphtoyl H-10), 7.92 (dd, *J*=8.68, 1.59 Hz, 1 H, naphtoyl H-11) 8.48 (s, 1 H, naphtoyl H-3). ^{13}C NMR (100 MHz, $CDCl_3$) δ: 12.93 (C-15), 15.87 (angeloyl C-4), 16.14 (C-13), 20.61 (acetyl C-2), 22.61 (angeloyl C-5), 22.84 (C-14), 39.06 (C-9), 56.83 (C-1), 68.59 (C-8), 77.24 (C-6), 79.11 (C-2), 79.41, 79.55 (C-7/C-11), 83.89 (C-3), 85.69 (C-10), 125.22 (naphtoyl C-11), 126.70 (naphtoyl C-2), 127.06 (naphtoyl C-3), 127.50 (naphtoyl C-10), 127.75 (naphtoyl C-6), 128.21 (naphtoyl C-7), 128.37 (naphtoyl C-8), 129.39 (angeloyl C-2), 129.80 (naphtoyl C-5), 131.33 (naphtoyl C-4), 132.47 (C-4), 135.62 (naphtoyl C-9), 138.81 (angeloyl C-3), 140.65 (C-5), 165.68 (naphtoyl C-1), 167.47 (angeloyl C-1), 171.62 (acetyl C-1), 175.82 (C-12).

Compound **Vd (HzL18072015).** To solution compound **IVd** (57mg, 0.01mmol) in 2 mL of CH_2Cl_2 was added butyric anhydride (18 mg, 0.11 mmol) and 10 mg of DMAP (10 mg, 0.03 mmol). The reaction mixture was stirred at room temperature for 18 h. The mixture was concentrated in vacuo and residue was purified by reversed phase chromatography (Rp-18) to give compound **Vd** (50 mg, 78%). ^{1}H NMR (600 MHz, $CDCl_3$) δ: ^{1}H NMR (600 MHz, $CDCl_3$) δ ppm 0.92 (t, *J*=7.52 Hz, 3 H, butanoly H-4) 1.48 (s, 3 H, H-13) 1.49 (br. s., 3

H, H-14) 1.62 (dq, *J*=14.31, 7.21 Hz, 2 H, butanoly H-3) 1.69 (s, 3 H, acetyl H-2) 1.92 (s, 3 H, H-15) 1.95 - 1.99 (m, 3 H, angeloyl H-4) 2.01 (dd, *J*=7.15, 1.28 Hz, 3 H, angeloyl H-5) 2.26 (td, *J*=7.61, 1.65 Hz, 2 H, butanoyl H-2) 2.29 (dd, *J*=15.00, 3.70 Hz, 1 H, H-9b) 2.95 (br. s., 1 H, OH) 3.08 (dd, *J*=14.86, 3.12 Hz, 1 H, H-9a) 3.64 (br. s., 1 H, OH) 4.54 (br. s., 1 H, H-1) 5.64 (t, *J*=3.67 Hz, 1 H, H-2) 5.72 (br. s., 1 H, H-6) 5.81 (t, *J*=4.03 Hz, 1 H, H-8) 5.95 (d, *J*=0.73 Hz, 1 H, H-3) 6.13 (qd, *J*=7.21, 1.47 Hz, 1 H, angeloyl H-3) 7.51 (t, *J*=7.3 Hz, 1 H, naphtoyl H-7) 7.556 (t, J=7.3 Hz, 1 H, naphtoyl H-6) 7.83 (d, *J*=8.07 Hz, 1 H, naphtoyl H-8) 7.86 (d, *J*=8.44 Hz, 1 H, naphtoyl H-5) 7.92 (d, *J*=8.07 Hz, 1 H, naphtoyl H-10) 8.02 (dd, *J*=8.62, 1.65 Hz, 1 H, naphtoyl H-11) 8.59 (s, 1 H, naphtoyl H-3). ^{13}C NMR (150 MHz, $CDCl_3$) δ:13.06 (C-15), 13.69 (butanoyl C-4), 15.85 (angeloyl C-4), 16.18 (C-13), 17.98 (butanoly C-3), 20.62 (acetyl C-2), 22.46 C-5), 22.97 (C-14), 36.57 (butanoyl C-2), 38.21 (C-9), 56.57 (C-1), 66.23 (C-8), 77.30 (C-6), 78.63, 78.66 (C-7/C-11), 79.02 (C-2), 83.79 (C-3), 84.84 (C-10), 125.25 (naphtoyl C-11), 126.63 (napthtoyl C-8), 127.02 (naphtoyl C-10), 127.57 (naphtoyl C-3), 127.74 (naphtoyl C-2), 128.26 (naphtoyl C-7), 128.32 (naphtoyl C-6), 129.42 (naphtoyl C-5), 129.75 (angeloyl C-2), 131.37 (naphtoyl C-4), 132.48 (C-4), 135.64 (napthoyl C-9), 138.58 (angeloyl C-3), 141.60 (C-5), 165.73 (naphtoyl C-1), 167.22 (angeloyl C-1), 171.07 (acetyl C-1), 172.69 (butanoly C-1), 175.64 (C-1). HRMS 701,25683, Calc. $(C_{37}H_{42}NaO_{12})^+$: 701,25685.

Compound IIe: To solution of **I** (100 mg, 0.2 mmol) in 3 mL of dichloromethane was added 4-phenylbenzoic acid (50 mg, 0.24 mmol), DCC (50 mg, 0.24 mmol), and DMAP (20 mg, 0.16 mmol) and the reaction mixture was stirred at room temperaturet for 18 h. The mixture was filtered and the filtrate was concentrated in vacuo. The residue was purified by column chromatography using toluene ethyl acetate (3:1) as an eluent to give the compound **IIe** (101 mg, 73%). ^{1}H NMR (600 MHz, $CDCl_3$) δ: 1.31 (s, 3 H, H-14) 1.43 (s, 3 H, isoropylidene H-3) 1.52 (s, 3 H, H-13) 1.54 (s, 3 H, isoipropylidene H-1) 1.93 (d, *J*=1.10 Hz, 3 H, angeloyl H-4) 1.95 (br. s., 3 H, H-15) 1.98 (d, *J*=7.34 Hz, 3 H, angeloyl H-4) 2.06 (br. d, *J*=14.70 Hz, 1 H, H-9b)) 2.25 (dd, *J*=14.31, 4.40 Hz, 1 H, H-9a) 3.63 (br. s, 1 H, H-8) 4.21 (br. s, 1 H, H-1) 5.63 (t, *J*=4.40 Hz, 1 H, H-2) 5.86 (br. s, 1 H, H-6) 6.02 (br. s, 1 H, H-3) 6.12 (q, *J*=6.20 Hz, 1 H, angeloyl H-3) 7.41 (t, *J*=7.00 Hz, 1 H, biphenyl H-9) 7.47 (t, *J*=6.20 Hz, 2 H, biphenyl H-8 and 10) 7.63 (d, *J*=7.70 Hz, 2 H, biphenyl H-4 and 12) 7.60 (d, *J*=7.70 Hz, 2 H, biphenyl H-7 and 11) 8.10 (d, *J*=8.44 Hz, 2 H, biphenyl H-3 and 13). ^{13}C NMR (150 MHz, $CDCl_3$) δ: 12.64 (C-15), 15.83 (angeloyl C-5), 15.90 (C-13) 20.60 (angeloyl C-4), 23.65 (isopropylidene C-3), 24.10 (C-13), 30.50 (isopropylidene C-1), 44.41 (C-9), 60.35 (C-1), 65.85 (C-8), 76.03 (C-6), 77.72 (C-2), 77.88, 79.26 (C-7/C-11), 79.76 (C-10), 83.52 (C-3), 100.93 (isopropylidene C-2), 127.04 (bibenzoyll C-13 and 3), 127.25 (bibenzoyl C-7 and 11), 127.27 (bibenzoyl C-7), 127.35 (angeloyl C-2), 128.31 (C-5) 128.94 (bibenzoyl C-4 and 12), 130.47 (bibenzoyl C-10), 130.47 (angeloyl C-3), 130.47 (bibezoyl C-8) 137.53 (bibenzoyl C-5), 139.85 (C-5), 146.10 (bibenzoyl C-5), 167.17 (bibenzoyl C-1), 167.49 (angeloyl C-1), 173.03 (C-12).

Compound IIIe: To a solution of compoud **IIe** (101 mg, 0.16 mmol) in Isopropenyl acetate (5 mL) was added p-toluenesulfonic acid (10 mg, 0.34 mmol) and the mixture was stirred at rt for 18 h. Ten mL of aqueous $NaHCO_3$ (saturated) was added and the mixture was extracted with EtOAc (3x10 mL). The organic phases were combined and then concentrated in vacuo. The residue was purified by Rp-18 chromatography using CH_3OH/H_2O (5:1) added 0.1% glacial acetic acid as an eluent to give **IIIe** (55 mg, 51%).^{1}H NMR (600 MHz, $CDCl_3$) δ: 1.43 (s, 3 H, H-14), 1.53 (s, 3 H, isopropylidene H-3), 1.54 (s, 3 H, H-13), 1.57 (s, 3 H, isopropylidene H-1), 1.64 (s, 3 H, H-15), 1.91 (br. s., 1 H, angeloyl H-5), 1.95 (s, 3 H, acetyl H-2), 1.99 (dq, *J*=7.11 and 1.42 Hz, 3 H, angeloyl H-4), 2.60 (d, *J*=14.67 Hz, 1 H, H-9b), 2.83 (dd, *J*=14.67 and 4.58 Hz, 1 H, H-9a), 3.32 (br.s, 1 H, OH), 4.17 (br. s., 1 H, H-1 and H-8), 4.26 (dd, J=4.6 and 3.1 Hz, H-8), 5.77 (dd, *J*=5.87 and 4.77 Hz, 1 H, H-2), 5.83 (br. q, J=2.9 Hz, 1 H, H-2), 5.93 (br. s, 1 H, H-3), 6.11 (qq, *J*=5.90 and 1.50 Hz, 1 H, angeloyl H-3), 7.37 (tt, *J*=7.30 and 1.10 Hz, 1 H, bibenzoyl H-9), 7.44 (br. t, *J*=7.70 Hz, 2 H, bibenzoyl H-8 and 10), 7.58 (br.d, *J*=7.70 Hz, 2 H, bibenzoyl H-7 and 11), 7.62 (br.d, *J*=7.80 Hz, 2 H, bibenzoyl H-4

and 12), 8.08 (d, *J*=7.80 Hz, 2 H, bibenzoyl H-3 and 13). ^{13}C NMR (150 MHz, $CDCl_3$) δ: 12.66 (C-15), 15.77 (angeloyl C-5), 15.83 (C-13) 20.58 (angeloyl C-4), 22.48 (isopropylidene C-3), 21.36 (acetyl C-2), 22.49 (angeloyl C-4), 23.64 (C-14), 30.49 (isopropylidene C-1), 37.92 (C-9), 56.44 (C-1), 65.86 (C-8), 76.03 (C-6), 78.02 (C-2), 78.96, 79.40 (C-7/C-11), 83.58 (C-10), 84.86 (C-3), 101.15 (isopropylidene C-2), 127.08 (bibenzoyll C-11 snd 7), 127.25 (bibenzoyl C-4 and 12), 128.16 (bibenzoyl C-9), 128.73 (angeloyl C-3), 12.93 (bibenzoyl C-3 and 13), 130.29 (bibenzoyl C-10), 130.29 (angeloyl C-2), 138.59 (bibenzoyl C-6), 138.69 (angeloyl C-3), 139.65 (C-5), 145.79 (bibenzoyl C-5), 165.47 (bibenzoyl C-1), 167.48 (angeloyl C-1), 170.67 (acetyl C-1), 173.04 (C-12).

Compound IVe: A solution of **IIIe** (23mg, 0.03 mmol) in methanol (2 mL) was added 6N HCl (0.1 mL) and stirred at rt for 4h. The mixture was concentrated and the residue was purified by Rp-18 using CH_3OH-H_2O (5:1) added 0.1% glacial acetic acid as an eluent to give **Vf** (20 mg, 91%). ^{1}H NMR (600 MHz, $CDCl_3$) δ: 1.39 (s, 3H, H-13), 1.43 (s, 3H, H-14), 1.63 (s, 3 H, H-15) 1.79 (br.s, 3 H, angeloyl H-5), 1.83 (br.d, *J*=4.44, 3 H, angeloyl H-4), 2.37 (br.d, *J*=12.10, 1 H, H-9b), 2.83 (br.d, *J*=13.20, 1 H, H-9a), 4.27 (br. s., 1 H, H-8), 4.35 (br.s, 1H, H-1) 5.48 (t, *J*=3.85 Hz, 1 H, H-2) 5.65 (t, *J*=4.03 Hz, 1 H, H-2), 5.76 (br.s, 1 H, H-6), 5.81 (br.s, 1H, H-3), 6.03 (br.q, *J*=7.30 Hz, 1 H, angeloyl H-3) 7.27 (t, *J*=7.29, 1 H, bibenzoyl H-9) 7.36 (br. t, *J*=7.70, Hz, 2 H, bibenzoyl H-8 and H-10) 7.51 (br.d, *J*=7.34, 2 H, bibenzoyl H-7 and H-11) 7.55 (br. d, *J*=8.10 Hz, 2 H, bibenzoyl H-4 and 12) 7.97 (br. d, *J*=8.07 Hz, 2 H, binbenzoyl H-3 and H-13). ^{13}C NMR (150 MHz, $CDCl_3$) δ: 12.84 (C-15), 14.07 (angeloyl C-5), 15.84 (C-13), 20.56 (acetyl C-2), 22.73 (angeloyl C-4), 24.80 (C-14), 39.10 (C-9), 56.68 (C-1), 68.65 (C-8), 77.35 (C-6), 79.03, 79.41 (C-7/C-11), 79.57 (C-2), 83.85 (C-10), 85.69 (C-3), 127.09 (bibenzoyl C-15), 127.27 (bibenzoyl C-12 and 14), 127.51 (bibenzoyl C-11 and 17), 128.57 (angelooyl C-2), 128.94 (bibenzoyl C-8 and 10) 129.77 (C-4), 130.26 (bibenzoyl C-3 and 13), 138.72 (bibenzoyl C-6) 139.86 (angeloyl C-3), 140.58 (C-5), 145.87 (bibenzoyl C-2) 165.47 (bibenzoyl C-1), 167.48 (angeloyl C-1), 171.58 (acetyl C-1), 175.88 (C-1).

Compound Ve (HzL17072015): A solution of **IVe** (20mg, 0.03mmol) dichloromethane (2 mL) was added butyric anhydride (6 mg, 0.04 mmol) and 10 mg of DMAP (10 mg, 0.16 mmol). The reaction mixture was stirred at room temperature for 18 h and concentrated in vacco. The residue was purified by Rp-18 chromatography using using CH_3OH-H_2O (5:1) added 0.1% glacial acetic acid as an eluent to give **Ve** (19 mg, 86%). ^{1}H NMR (600 MHz, $CDCl_3$) δ: 0.76 (t, *J*=7.34 Hz, 3 H, butanoyl H-4) 1.31 (s, 10 6H, H-13 and H-14) 1.46 (sxtd, *J*=7.60, Hz, 2 H, butanoyl H-3) 1.53 (s, 3 H, acetyl H-2) 1.73 (s, 3 H, H-15) 1.79 (quin, *J*=1.50 Hz, 3 H, angeloyl H-4) 1.83 (dq, *J*=7.70, 1.50 Hz, 3 H, angeloyl H-5) 2.10 (t, *J*=8.40 Hz, 2 H, butanoly H-2) 2.12 (dd, *J*=14.00, 4.00 Hz, 1 H, H-9b) 2.64 (s, 1 H, OH) 2.96 (dd, *J*=14.86, 3.48 Hz, 1 H, H-9a) 3.28 (s, 1 H, OH) 4.34 (br. s., 1 H, H-1) 5.48 (t, *J*=3.85 Hz, 1 H, H-2) 5.54 (br. d, *J*=1.10 Hz, 1 H, H-6) 5.60 (t, *J*=3.30 Hz, 1 H, H-8) 5.74 (br. d, *J*=1.10 Hz, 1 H, H-3) 5.94 (qq, *J*=7.70, 1.80 Hz, 1 H, angeloyl H-3) 7.21 (tt, *J*=7.30, 1.50 Hz, 1 H, bibenzoyl H-9) 7.28 (br. t, *J*=7.30, 7.30 Hz, 2 H, bibenzoyl H-8 and H-10) 7.43 (br. dd, *J*=7.00, 1.50 Hz, 2 H, bibenzoyl H-7 and H-11) 7.47 (br. d, *J*=8.10 Hz, 2 H, bibenzoyl H-4 and 12) 7.90 (br. d, *J*=8.40 Hz, 2 H, binbenzoyl H-3 and H-13). ^{13}C NMR (150 MHz, $CDCl_3$) δ: 13.06 (C-15), 13.71 (butanoyl C-4), 15.84 (angeloyl C-5), 16.25 (C-13), 18.01 (butanoly C-3), 20.61 (acetyl C-2), 22.46 (angeloyl C-4), 22.99 (C-14), 36.58 (butanoyl C-2), 38.27 (C-9), 56.53 (C-1), 66.22 (C-8), 77.20 (C-6), 78.65, 78.68 (C-7/C-11), 78.91 (C-2), 83.72 (C-10), 84.65 (C-3), 127.30 (bibenzoyl C-12 and 4), 127.57 (bibenzoyl C-11 and 7))128.15 (bibenzoyl C-9), 128.52 (angelooyl C-2), 128.91 (bibenzoyl C-10) 129.51 (C-4), 130.28 (bibenzoyl C-13 and 3), 138.55 (bibenzoyl C-3 and 6) 139.98 (angeloyl C-3), 141.72 (C-5), 145.48 (bibenzoyl C-2) 165.47 (bibenzoyl C-1), 167.19 (angeloyl C-1), 170.95 (acetyl C-1), 172.61 (butanoly C-1), 175.42 (C-1). HRMS 727,27234, Calc. $(C_{39}H_{44}NaO_{12})^+$: 727,2725.

References

1. Skytte, D. M., Moller, J. V., Liu, H., Nielsen, H. O., Svenningsen, L. E., Jensen, C. M., Olsen, C. E., and Christensen, S. B. (2010) Elucidation of the topography of the thapsigargin binding site in the sarco-endoplasmic calcium ATPase. *Bioorg. Med. Chem.* **18**, 5634-5646
2. Smitt, U. W., and Christensen, S. B. (1991) Nortrilobolide, a new potent guaianolide secretagogue from Thapsia garganica. *Planta Med.* **57**, 196-197
3. Christensen, S. B. (1985) Radiolabeling of the Histamine Liberating Sesquiterpene Lactone, Thapsigargin. *Journal of Labelled Compounds & Radiopharmaceuticals* **22**, 71-77
4. Jakobsen, C. M., Denmeade, S. R., Isaacs, J. T., Gady, A., Olsen, C. E., and Christensen, S. B. (2001) Design, synthesis, and pharmacological evaluation of thapsigargin analogues for targeting apoptosis to prostatic cancer cells. *J. Med. Chem.* **44**, 4696-4703
5. Andersen, A., Cornett, C., Lauridsen, A., Olsen, C. E., and Christensen, S. B. (1994) Selective Transformations of the Ca-2+ Pump Inhibitor Thapsigargin. *Acta Chem. Scand.* **48**, 340-346
6. Christensen, S. B., Larsen, I. K., Rasmussen, U., and Christophersen, C. (1982) Thapsigargin and Thapsigargicin, 2 Histamine Liberating Sesquiterpene Lactones from Thapsia-Garganica - X-Ray-Analysis of the 7,11-Epoxide of Thapsigargin. *J. Org. Chem.* **47**, 649-652

2. An N-terminal Ca^{2+} binding motif regulates the secretory pathway Ca^{2+}/Mn^{2+}-transport ATPase SPCA1

Jialin Chen, Susanne Smaardijk, Charles-Alexandre Mattelaer, Filip Pamula, Ilse Vandecaetsbeek, Jo Vanoevelen, Frank Wuytack, Eveline Lescrinier, Jan Eggermont, Peter Vangheluwe

Abstract:

The Ca^{2+}/Mn^{2+} transport ATPases 1a and 2 (SPCA1a/2) are closely related to the sarco(endo)plasmic reticulum Ca^{2+}-ATPase (SERCA) and are implicated in breast cancer and Hailey–Hailey skin disease. Here, we purified the human SPCA1a/2 isoforms from a yeast recombinant expression system and compared their biochemical properties after reconstitution. We observed that the purified SPCA1a displays a lower Ca^{2+} affinity and slightly lower Mn^{2+} affinity than SPCA2. Remarkably, the turnover rates of SPCA1a in the presence of Mn^{2+} and of SPCA2 incubated with Ca^{2+} and Mn^{2+} were comparable, whereas the turnover rate of SPCA1a in Ca^{2+} was two-fold higher. Moreover, we noted an unusual biphasic activation curve for the SPCA1a ATPase and autophosphorylation activity, not observed with SPCA2. We also found that the biphasic pattern and low apparent ion affinity of SPCA1a critically depends on ATP concentration. We further show that the specific properties of SPCA1a at least partially depend on an N-terminal EF-hand-like motif, which is present only in the SPCA1a isoform and absent in SPCA2. This motif binds Ca^{2+}, and its mutation lowered the Ca^{2+} turnover rate relative to that of Mn^{2+}, increased substrate affinity, and reduced the level of biphasic activation of SPCA1a. A biochemical analysis indicated that Ca^{2+} binding to the N-terminal EF-hand-like motif promotes the activity of SPCA1a by facilitating autophosphorylation. We propose that this regulation may be physiologically relevant in cells with a high Ca^{2+} load, such as mammary gland cells during lactation, or in cells with a low ATP content, such as keratinocytes.

Author contributions:

Author contributions: JC, FW, and PV conceptualization; JC, SS, and CAM formal analysis; JC validation; JC, SS, CAM, FP, IV, JV, EL, and PV investigation; JC visualization; JC, CAM, IV, JV, EL, and PV methodology; JC and PV writing-original draft; JC, JE, and PV writing-review and editing; EL and PV resources; EL, JE, and PV supervision; PV funding acquisition; PV project administration.

JBC ARTICLE

An N-terminal Ca^{2+}-binding motif regulates the secretory pathway Ca^{2+}/Mn^{2+}-transport ATPase SPCA1

Received for publication, October 12, 2018, and in revised form, March 23, 2019 Published, Papers in Press, March 28, 2019, DOI 10.1074/jbc.RA118.006250

Jialin Chen[‡], Susanne Smaardijk[‡], Charles-Alexandre Mattelaer[§1], Filip Pamula[‡], Ilse Vandecaetsbeek[‡], Jo Vanoevelen[‡], Frank Wuytack[‡], Eveline Lescrinier[§], Jan Eggermont[‡], and Peter Vangheluwe[‡2]

From the [‡]Laboratory of Cellular Transport Systems, Department of Cellular and Molecular Medicine and [§]Medicinal Chemistry, Department of Pharmaceutical and Pharmacological Sciences, Rega Institute, KU Leuven, Belgium

Edited by Phyllis I. Hanson

The Ca^{2+}/Mn^{2+} transport ATPases 1a and 2 (SPCA1a/2) are closely related to the sarco(endo)plasmic reticulum Ca^{2+}-ATPase (SERCA) and are implicated in breast cancer and Hailey–Hailey skin disease. Here, we purified the human SPCA1a/2 isoforms from a yeast recombinant expression system and compared their biochemical properties after reconstitution. We observed that the purified SPCA1a displays a lower Ca^{2+} affinity and slightly lower Mn^{2+} affinity than SPCA2. Remarkably, the turnover rates of SPCA1a in the presence of Mn^{2+} and SPCA2 incubated with Ca^{2+} and Mn^{2+} were comparable, whereas the turnover rate of SPCA1a in Ca^{2+} was 2-fold higher. Moreover, we noted an unusual biphasic activation curve for the SPCA1a ATPase and autophosphorylation activity, not observed with SPCA2. We also found that the biphasic pattern and low apparent ion affinity of SPCA1a critically depends on ATP concentration. We further show that the specific properties of SPCA1a at least partially depend on an N-terminal EF-hand–like motif, which is present only in the SPCA1a isoform and absent in SPCA2. This motif binds Ca^{2+}, and its mutation lowered the Ca^{2+} turnover rate relative to that of Mn^{2+}, increased substrate affinity, and reduced the level of biphasic activation of SPCA1a. A biochemical analysis indicated that Ca^{2+} binding to the N-terminal EF-hand–like motif promotes the activity of SPCA1a by facilitating autophosphorylation. We propose that this regulation may be physiologically relevant in cells with a high Ca^{2+} load, such as mammary gland cells during lactation, or in cells with a low ATP content, such as keratinocytes.

Transient alterations in subcellular Ca^{2+} concentrations drive numerous physiological processes. The local Ca^{2+} levels in cells are tightly regulated by membrane transport proteins such as ion channels, exchangers, and active transport ATPases (1, 2). Among them, the Ca^{2+} transport ATPases utilize the energy released from ATP hydrolysis to pump Ca^{2+} ions against the concentration gradient, *i.e.* from the cytosol to the exoplasmic compartments. In humans, three types of Ca^{2+}-ATPases were identified that are localized in distinct membrane compartments: the closely related P2A-type ATPases sarco(endo-)plasmic reticulum Ca^{2+}-ATPase (SERCA)[3] and secretory pathway Ca^{2+}-ATPase (SPCA), sharing 29% sequence identity and over 40% sequence similarities, and the P2B-type ATPase plasma membrane Ca^{2+}-ATPase (PMCA), which is more distantly related (3). All Ca^{2+}-ATPases undergo transient autophosphorylation during the transport cycle.

The SPCA pumps are located in later compartments of the Golgi/secretory pathway and transport both Ca^{2+} and Mn^{2+} ions with high affinities, which represents a unique feature among the Ca^{2+} transport ATPases. SPCA isoforms ensure a constant filling of the Golgi and secretory pathway with Ca^{2+} and also Mn^{2+}. Both ions are cofactors of many Golgi enzymes that support protein trafficking and post-translational modifications (reviewed in Ref. 3). Excess Mn^{2+} intake leads to manganism, a Parkinson-like disease that affects miners, welders, steel, and battery workers due to Mn^{2+} intoxication (4), and SPCA1 may play a role in Mn^{2+} detoxification in the liver (5).

Most eukaryotes express a single SPCA orthologue, which is called plasma membrane-related Ca^{2+}-ATPase 1 (PMR1). In tetrapods, two isoforms are found, SPCA1 and SPCA2, which share 63% sequence identity and 73% similarity. The human isoform SPCA1 is ubiquitously expressed from the *ATP2C1* gene. Haplo-insufficiency of SPCA1 leads to Hailey–Hailey disease, an autosomal dominant skin disorder characterized by loss of cell–cell adhesion (6). The second human isoform, SPCA2, is encoded by the *ATP2C2* gene and SPCA2 protein expression is constrained to brain, testis, and actively secreting cells, such as mammary gland epithelial cells, suggesting a more specialized function (7–10).

The two human SPCA isoforms activate the plasma membrane Ca^{2+} channel Orai1, which is referred to as store-independent Ca^{2+} entry (SICE) (11, 12). Although store-operated Ca^{2+} entry (SOCE) relies on the depletion of the endoplasmic reticulum Ca^{2+} store that triggers STIM1-mediated Orai1 acti-

This work was supported by Flanders Research Foundation FWO Grants G044212N and G0B1115N (to P. V.) and Inter-University Attraction Poles program P7/13. The authors declare that they have no conflicts of interest with the contents of this article.

This article contains Figs. S1–S6.

[1] Strategic Basic Research Ph.D. fellow at FWO supported by Grant 1S23217N.

[2] To whom correspondence should be addressed: ON1 Campus Gasthuisberg, KU Leuven Herestraat 49/box 802, B3000 Leuven, Belgium. Tel: 32-16-330720; E-mail: peter.vangheluwe@kuleuven.be.

[3] The abbreviations used are: SERCA, sarco(endo)plasmic reticulum Ca^{2+}-ATPase; SPCA, secretory pathway Ca^{2+}-ATPase; PMCA, plasma membrane Ca^{2+}-ATPase; PMR1, plasma membrane-related Ca^{2+}-ATPase 1; SICE, store-independent Ca^{2+} entry; SOCE, store-operated Ca^{2+} entry; HA, hydroxylamine; GST, glutathione *S*-transferase; HSQC, heteronuclear single quantum coherence; BisTris, 2-[bis(2-hydroxyethyl)amino]-2-(hydroxymethyl)propane-1,3-diol; TES, 2-{[2-hydroxy-1,1-bis(hydroxymethyl)ethyl]amino}ethanesulfonic acid; ANOVA, analysis of variance; AA, double alanine mutant.

© 2019 Chen et al. Published under exclusive license by The American Society for Biochemistry and Molecular Biology, Inc.

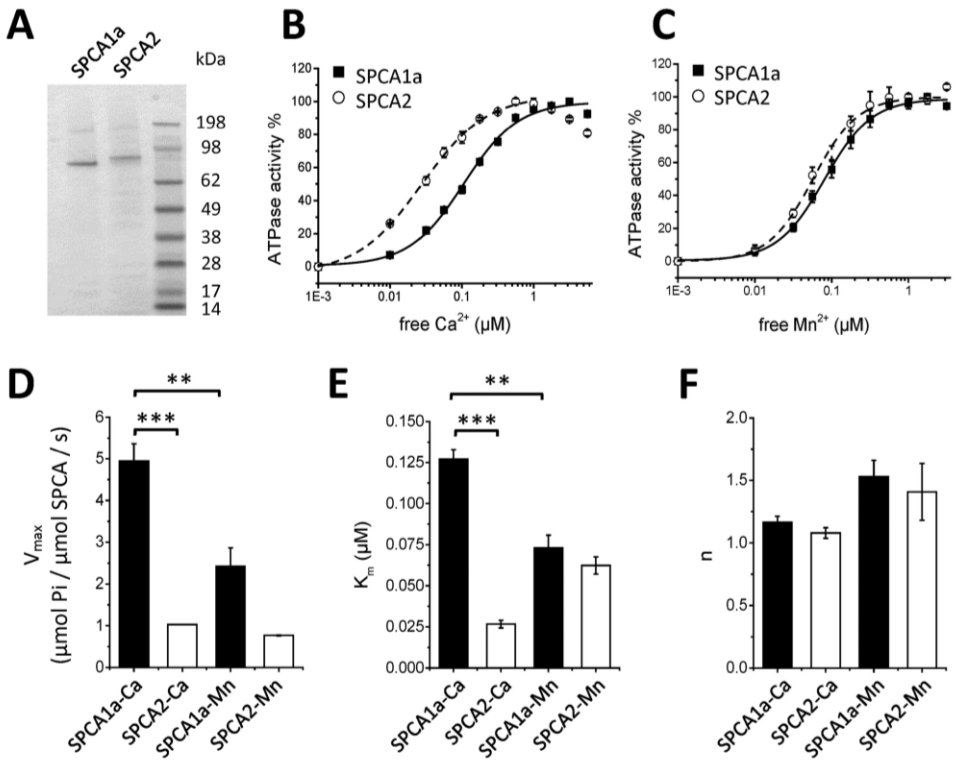

Figure 1. ATPase activity of reconstituted SPCA1a and SPCA2. *A*, a Coomassie-stained SDS-PAGE gel displays purified and reconstituted SPCA1a and SPCA2 proteins. The SeeBlue Plus2 was used as molecular weight marker. Ca^{2+} (*B*) and Mn^{2+} (*C*)- dependent ATPase activities measured on reconstituted SPCA1a (*filled squares*) and SPCA2 (*empty circles*) were normalized to their maximal activities, and fitted with logistic functions. *D–F*, bar graphs depicting the parameters of the maximal ATPase activity (V_{max}, *D*), apparent affinities (K_m, *E*) and cooperativities (*n*, *F*) for Ca^{2+} and Mn^{2+} were derived from *B* and *C* ($n = 3–5$).

vation, SICE leads to Ca^{2+} entry through the Orai1 channel independently of STIM1 (11, 12). The incoming Ca^{2+} in cells is subsequently transferred to the secretory pathway (12, 13). Because both SPCA1 and SPCA2 are up-regulated in the mammary gland during lactation, SICE may promote cellular Ca^{2+} uptake for subsequent secretion in the milk via the secretory pathway (14, 15). In addition, SICE is chronically activated by SPCA2 in luminal-type breast cancer cells, which causes Ca^{2+} dyshomeostasis and aberrant cell proliferation (11). SPCA1 is implicated in the basal-type breast cancer (16, 17), whereas up-regulation of both SPCA genes is associated with microcalcifications during breast cancer (16).

Structures of the SERCA1a Ca^{2+} pump were solved in the main catalytic states providing detailed insights into its Ca^{2+} transport mechanism and domain architecture, which seems to be highly conserved between Ca^{2+}-ATPases (18, 19). But compared with SERCA1a, the PMCA and SPCA pumps contain longer N- and C-terminal extensions, which presumably act as regulatory elements. The C terminus of PMCA clearly serves as an autoinhibitory domain that is regulated by calmodulin, protein kinases, and lipids (20). The functional role of the N or C termini of SPCA isoforms is also gradually emerging. Truncations of the SPCA2 N and C termini functionally impair SPCA2 (12). Moreover, a motif in the N terminus of SPCA2 controls the binding to Orai1 (11), whereas at the corresponding position of the *Saccharomyces cerevisiae* orthologue PMR1, a Ca^{2+}-binding EF-hand–like motif is found, which is important for ion selectivity (21). Of interest, the ion selectivity of the yeast PMR1 protein to Ca^{2+} and Mn^{2+} depends on this N-terminal element (21), although other residues in the TM region are also important (22).

In this study, we directly compared the functional properties of the purified SPCA1a and SPCA2 protein in reconstituted proteoliposomes and discovered unexpected isoform-specific differences in Ca^{2+} *versus* Mn^{2+} affinities and turnover rates. These differences depend at least in part on a Ca^{2+}-binding EF-hand–like motif in the SPCA1a N terminus that is absent in SPCA2.

Results

Purified SPCA1a and SPCA2 present different Ca^{2+}-, but not Mn^{2+}-dependent activities

To functionally compare the SPCA1a and SPCA2 isoforms, we purified both isoforms and reconstituted them in proteoliposomes following the same procedure as we described before for SPCA1a (23). In short, the human His-tagged SPCA1a or SPCA2 isoforms were expressed in *S. cerevisiae*, affinity purified from solubilized membrane fractions, and then incorporated into lipid vesicles (Fig. 1*A*). The His_{10}-tagged SPCA2 monomer (105.9 kDa) ran at a slightly higher position on SDS-PAGE than the His_8-tagged SPCA1a (101.8 kDa), matching their predicted molecular masses. To compare the functional properties of the reconstituted SPCA1a and SPCA2 isoforms, we evaluated the Ca^{2+}- (Fig. 1*B*) or Mn^{2+}-dependent (Fig. 1*C*) ATPase activities with a colorimetric method to detect P_i levels (24), and observed remarkable isoform-specific differences. SPCA1a displays a 2-fold higher Ca^{2+}-dependent maximal ATPase activity

Regulation of SPCA1 by the N terminus

Table 1
Summary of parameters obtained from the ATPase assay

	K_m	n	V_{max}
	μM		μmol P_i/μmol SPCA/s
SPCA1a-Ca	0.13 ± 0.01	1.17 ± 0.05	4.94 ± 0.42
SPCA2-Ca	0.03 ± 0.00	1.08 ± 0.04	1.03 ± 0.01
SPCA1a-Mn	0.07 ± 0.01	1.53 ± 0.13	2.43 ± 0.44
SPCA2-Mn	0.06 ± 0.01	1.41 ± 0.23	0.77 ± 0.01

(V_{max}) as compared with Mn^{2+}, whereas SPCA2 presents a similar V_{max} for both substrates (Fig. 1*D*). SPCA1a also exhibits a lower affinity for Ca^{2+} than for Mn^{2+}, whereas this is opposite for SPCA2 (Fig. 1*E*). The cooperativity (n) of both enzymes for Ca^{2+} approximates 1, confirming that one Ca^{2+} is transported per ATP. The cooperativity of both isoforms toward Mn^{2+} is slightly, but not significantly higher (Fig. 1*F*). In conclusion, SPCA1a presents similar properties as SPCA2 in Mn^{2+} conditions, but a higher V_{max} and lower apparent affinity in Ca^{2+} conditions (Table 1, Fig. 1, *B–E*).

SPCA1a, but not SPCA2, autophosphorylation presents a biphasic activation pattern

Like other P-type ATPases, SPCA isoforms catalyze a substrate-dependent autophosphorylation reaction on a conserved Asp residue in the phosphorylation domain (3, 25). We here confirm that the reconstituted SPCA isoforms form Ca^{2+}- or Mn^{2+}-dependent phospho-enzyme (EP) intermediates when incubated with radiolabeled ATP (Fig. 2, *A* and *B*). Note that a batch-dependent background phosphorylation was sometimes detected in the EGTA conditions, which most likely represents another low abundant phosphorylated protein that runs higher than SPCA1a. Because SPCA2 is slightly larger than SPCA1, this background signal runs at the same height as SPCA2, making it impossible to separate both phosphorylation signals. Because this additional signal is Ca^{2+}- and Mn^{2+}-independent, we subtracted it as background from the Ca^{2+}- or Mn^{2+}-dependent EP levels that represent the SPCA activity.

Interestingly, we observed a remarkable difference between the Ca^{2+}-dependent autophosphorylation behavior of both isoforms (Fig. 2, *A* and *C*). SPCA2 reached maximal autophosphorylation already at low micromolar free Ca^{2+}, whereas the SPCA1a EP level raised further above 3 μM and reached a maximum at 3 mM free Ca^{2+}, *i.e.* well above the physiological Ca^{2+} concentrations in the cytosol. Thus, the difference between the apparent Ca^{2+} affinities of SPCA1a and SPCA2 is much more pronounced in the EP assay (Table 2) than in the ATPase assay (Fig. 1 and Table 1). This most likely relates to the difference in ATP concentration between both assays (5 mM ATP in ATPase assay, *versus* 5 μM cold and radiolabeled ATP in the autophosphorylation assay). Indeed, increasing the ATP concentration from 5 to 50 μM shifts the SPCA1a EP curve to higher affinity, whereas reducing the ATP to 0.5 μM lowers the Ca^{2+} affinity (Fig. S1*A*). Conversely, decreasing the ATP concentration from 5 mM to 500 μM in an enzyme-coupled ATPase assay (which ensures that ATP is not depleted) also lowers the Ca^{2+} affinity of SPCA1a (Fig. S1*B*). This highlights that the Ca^{2+} affinity of SPCA1a is highly sensitive to the available ATP concentration. Moreover, the apparent Ca^{2+} affinity of SPCA1a autophosphorylation would be considerably higher at physiological ATP concentrations, *i.e.* more in line with the ATPase assay.

A similar EP pattern is observed in Mn^{2+} conditions (Fig. 2, *B* and *D*). SPCA2 already reached a maximal EP level in the presence of 0.3 μM free Mn^{2+}, in line with a very high apparent Mn^{2+} affinity of SPCA2, whereas SPCA1a displayed a biphasic stimulation by Mn^{2+}. The first part of the curve plateaus at ~3 μM Mn^{2+}, when ~60% of the maximal EP level is reached (Fig. 2*D*). The second part of the curve rises from ~30 μM Mn^{2+} onwards, and the maximal EP level is obtained around 1 mM. Like for the ATPase activities, both SPCA1a and SPCA2 present n values higher than 1 in Mn^{2+}-induced phosphorylation, indicating positive cooperativities (Table 2). However, SPCA1a's cooperativity toward Ca^{2+} is lower than one.

Inspired by the biphasic profile of the Mn^{2+}-dependent EP formation results, we carefully re-analyzed the results of the Ca^{2+}-dependent EP assays and fitted a biphasic instead of a mono-sigmoidal curve in the data presented in Fig. 2*C*. Fitting with two logistic curves that are separated at 30 μM Ca^{2+} rendered an SPCA1a cooperativity for both the first and second phases of $n = 1$ (Fig. 2*E*, Table 2), suggesting that this may represent a better fit of the data. However, the biphasic pattern is not observed in ATPase measurements at 5 mM ATP, because at high Ca^{2+} or Mn^{2+} concentrations (*i.e.* above 10 μM) the ATPase activity of both isoforms decreases, which is known as back-inhibition of the pump (Fig. S2, *A* and *B*). However, once the ATP concentration in the ATPase assay is lowered to 0.5 mM, we found that SPCA1a also displayed a biphasic activation profile in the physiological Ca^{2+} concentration range (above 1 μM Ca^{2+}) (Fig. S3). We therefore conclude that at low ATP concentration SPCA1a presents an unusual biphasic activation behavior, which may point to an autoregulatory mechanism that controls SPCA1a's activity and substrate affinity and is sensitive to the ATP concentration.

The efficacy of SPCA1a's autophosphorylation is higher with Ca^{2+} than Mn^{2+}

SPCA proteins transport Ca^{2+} and Mn^{2+} via the same ion-binding pocket in the transmembrane domain (26). Because binding of Mn^{2+} or Ca^{2+} at this binding pocket causes EP formation, we anticipated that saturating Ca^{2+}/Mn^{2+} concentrations (3 μM for SPCA2 or 3 mM for SPCA1a) should yield similar EP levels for each isoform. To verify this, we directly compared the EP levels of both isoforms at 3 μM and 3 mM Ca^{2+} or Mn^{2+}. As predicted, we observed that the SPCA2 EP levels were comparable at saturating concentrations of Ca^{2+} or Mn^{2+} (3 μM). No stimulation of EP levels was observed at higher Ca^{2+} or Mn^{2+} concentrations (Fig. 3, *A* and *B*). Although the EP level at 3 μM Ca^{2+} or Mn^{2+} was also similar for SPCA1a, the maximal EP level at 3 mM Ca^{2+} was 4.2-fold higher than at 3 mM Mn^{2+} (Fig. 3, *A* and *B*), which indicates that the autophosphorylation reaction of SPCA1a is more stimulated by Ca^{2+} than Mn^{2+}. To further test the ion specificity of this EP stimulation, we compared normal (5 mM) *versus* higher (8 mM) Mg^{2+} concentrations. Mg^{2+} is an essential divalent ion that is included in the assay at 5 mM to support the ATP coordination and autophosphorylation reaction. However, Mg^{2+} ions, in the absence of Ca^{2+} or Mn^{2+}, did not induce any EP formation of the SPCA

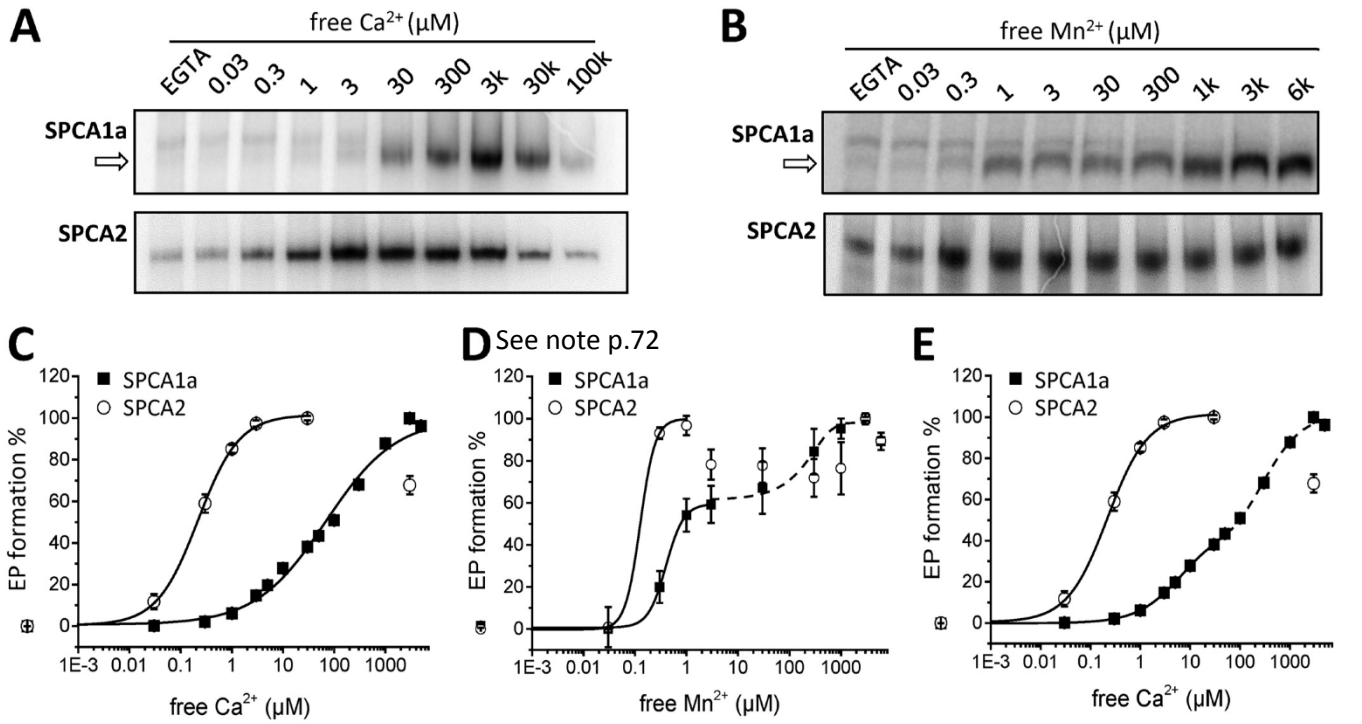

Figure 2. Autophosphorylation of reconstituted SPCA1a and SPCA2. *A* and *B*, phosphorimages depict the radiolabeled SPCA1a (*upper*) and SPCA2 (*lower*) phospho-intermediates (EP) at various Ca^{2+} (*A*) or Mn^{2+} (*B*) concentrations, separated by gel electrophoresis. The *arrows* indicate the Ca^{2+}- or Mn^{2+}-sensitive phosphorylated SPCA1a bands. The radioactivity was quantified with ImageJ software and the EGTA signal was subtracted as background. *C* and *D*, radioactivity was used as a measure of EP formation, which was plotted in a Ca^{2+} (*C*)- or Mn^{2+} (*D*)-dependent manner and was fitted with logistic functions. The SPCA1a Mn^{2+}-dependent autophosphorylation curve was fitted with two consecutive logistic functions, revealing a biphasic activation curve. *E*, re-fitting of the SPCA1a Ca^{2+}-dependent autophosphorylation data in *C* with two consecutive logistic functions, revealing a biphasic activation pattern (n = 3–7).

Table 2
Summary of parameters obtained from the autophosphorylation assay of SPCA1 and SPCA2

	K_m	n	Fitting
	μM		
SPCA1a-Ca	68.5 ± 10.4	0.63 ± 0.05	Monophasic
	7.9 ± 0.1	0.95 ± 0.03	Biphasic part I
	294.0 ± 51.0	1.14 ± 0.27	Biphasic part II
SPCA2-Ca	0.22 ± 0.01	1.08 ± 0.07	Monophasic
SPCA1a-Mn	0.43 ± 0.03	1.89 ± 0.32	Biphasic part I
	103.2 ± 52.4	0.004 ± 0.001	Biphasic part II
SPCA2-Mn	0.13 ± 0.05	2.99 ± 1.38	Monophasic

isoforms (Fig. 3, *A* and *B*), indicating that only Ca^{2+} is able to maximally activate SPCA1a autophosphorylation.

The maximal EP levels observed at 3 μM Ca^{2+} for SPCA2 and 3 mM Ca^{2+} for SPCA1a reflect the active protein fractions, which can be used to determine the maximal turnover rates. The ratio between the maximal ATPase activity (nmol of P_i released/μg of protein/s) and the maximal level of autophosphorylated protein (nmol of protein phosphorylated/μg of protein) is typically used to calculate the maximal turnover rates of Ca^{2+} transport ATPases (s^{-1}), as described before (27–29). The maximal turnover rate of SPCA1a is almost twice as high with Ca^{2+} than with Mn^{2+}, or as compared with SPCA2 (Fig. 3*C*). For SPCA2, the maximal turnover rates are similar with Mn^{2+} or Ca^{2+} (Fig. 3*C*).

Next, we verified that the second activation step of the SPCA1a autophosphorylation represents the catalytic autophosphorylation of the conserved Asp residue. It is possible that the second activation step may be caused by a low abundant kinase that promotes phosphorylation of SPCA1a on a Ser/Thr/Tyr acceptor site. To discriminate between both possibilities, we administered hydroxylamine (HA) to the phosphoenzymes, which specifically quenches acyl phosphates on the Asp, but is not reactive to phospho-Ser/Thr/Tyr residues (30). HA treatment completely abolished the Ca^{2+}-dependent phosphorylation signal of SPCA1a and SPCA2, confirming that the EP levels represent aspartyl phosphorylation at the catalytic autophosphorylation site (Fig. 3, *D* and *E*). In contrast, HA treatment did not quench the Ca^{2+}-insensitive background phosphorylation signal, confirming that it occurs independently of the autophosphorylation reaction, most likely on an unrelated trace protein (Fig. 3, *D* and *E*). Together, only Ca^{2+} is able to maximally activate catalytic SPCA1a autophosphorylation, which may point to a Ca^{2+}-dependent regulation mechanism of SPCA1a.

Only in SPCA1a, Ca^{2+} is able to replace Mg^{2+} to induce autophosphorylation

We hypothesized that the strongest stimulation of SPCA1a autophosphorylation by Ca^{2+} and the two-step activation pattern may be explained by a regulatory Ca^{2+}-binding site that is only present in SPCA1a and not in SPCA2. The presence of such an ion-binding element is supported by the observation that high concentrations of Ca^{2+} result in a mobility shift of the SPCA1a monomer on native PAGE (Fig. 4*A*). The sharp SPCA1a monomer band that is observed in the EGTA condition becomes more diffuse and migrates at a higher part of the gel when 3 mM Ca^{2+} is supplied (*box* in Fig. 4*A*). This behavior is less pronounced with 3 μM Ca^{2+} or 3 μM/3 mM Mn^{2+} (Fig.

Regulation of SPCA1 by the N terminus

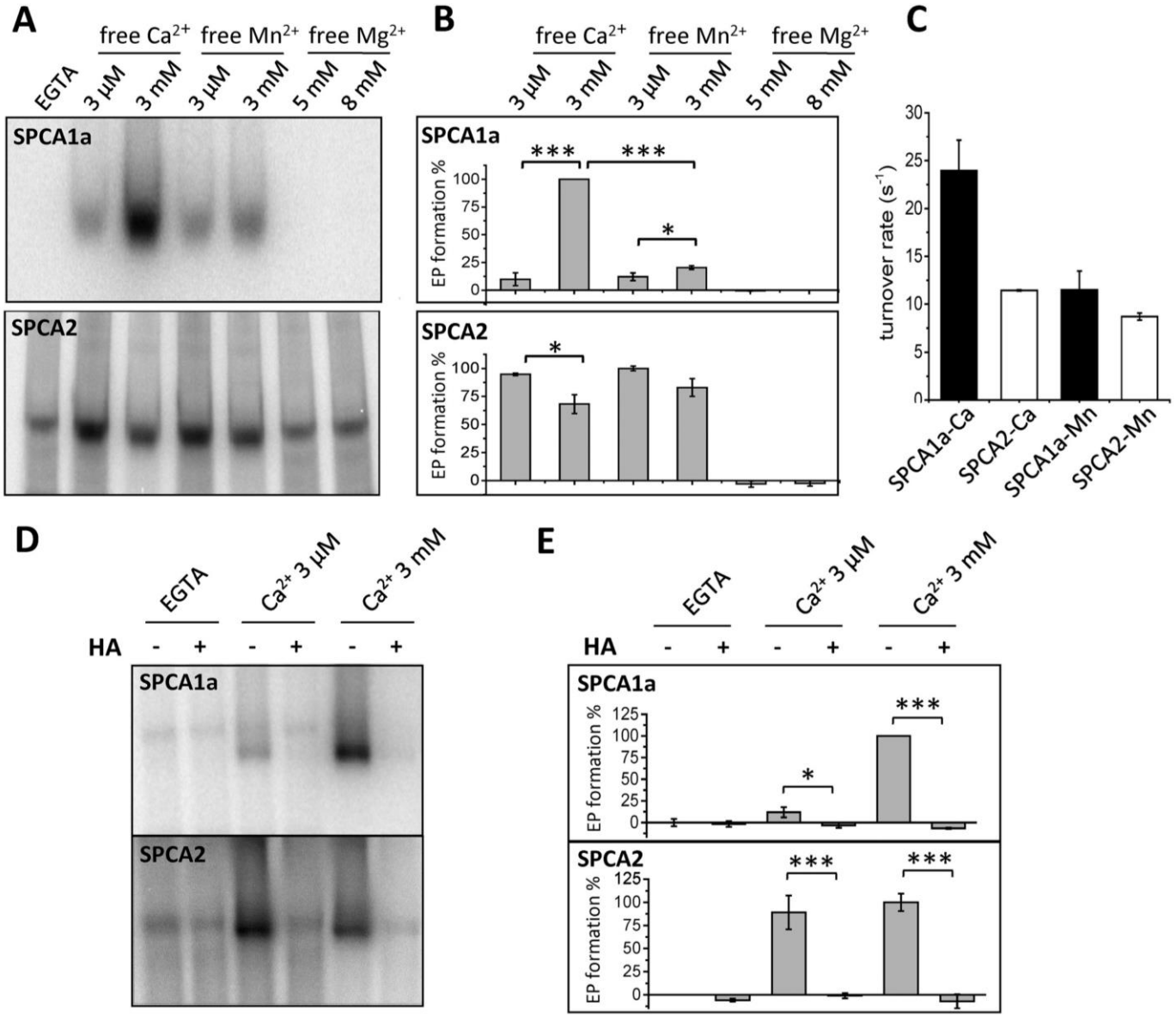

Figure 3. Comparison of the Ca^{2+}-, Mn^{2+}-, or Mg^{2+}-induced autophosphorylation in SPCA1a and SPCA2. *A,* phosphorimages of the radiolabeled SPCA1a (*upper*) and SPCA2 (*lower*) phospho-intermediates (EP) separated by gel electrophoresis. Indicated concentrations of Mn^{2+} or Ca^{2+} were supplied in the presence of 5 mM $MgCl_2$. In the Mg^{2+} conditions, only 5 or 8 mM $MgCl_2$ was administered. *B,* bar graphs depicting the EP levels in various conditions. The radioactivity was quantified with ImageJ software and the EGTA signal was subtracted as background. *C,* bar graph depicting the turnover rates of both isoforms. Turnover rates were calculated by dividing the maximal ATPase activities over the maximal phosphorylation activities ($n = 3$). *D,* representative phosphorimages of SPCA1a or SPCA2 treated with radiolabeled ATP followed by administration of HA, a quencher of aspartyl-phosphate intermediates. Experiments were conducted in the presence of EGTA, 3 μM or 3 mM Ca^{2+} ($n = 3$). *E,* quantification of radioactivity in *D* was performed using ImageJ software. One-way ANOVA was performed followed by post hoc Bonferroni test. *, $p < 0.05$; **, $p < 0.01$; ***, $p < 0.001$.

4*A*). Note that we also observed SPCA1a dimers on native PAGE, which were less influenced by Ca^{2+} binding (presumably due to the low resolution of the separation of larger protein complexes in gradient gels). The addition of Ca^{2+} had no effect on the SPCA1a monomer/dimer ratio (Fig. 4*B*). Furthermore, no mobility shift of the monomer band was observed for SPCA2 and SERCA1a at 3 μM or 3 mM Ca^{2+}, although the monomer/dimer ratio was altered (Fig. S4). Together this indicates that the Ca^{2+}-induced mobility shift of the monomer is an SPCA1a-specific behavior, which may be due to changes in charge, mass, and/or conformation of SPCA1a caused by the binding of Ca^{2+}. Because the mobility shift was less pronounced with Mn^{2+}, this indicates that the regulatory binding site of Ca^{2+} may differ from the Ca^{2+}/Mn^{2+}-binding site for transport in the transmembrane region.

As a first possibility for a regulatory divalent cation-binding site, we considered the conserved Mg^{2+}-binding site near the ATP-binding site that is present in all P-type ATPases. It is known that high Mn^{2+} levels interfere with Mg^{2+} binding in proteins (31, 32). We therefore reasoned that by competing with Mg^{2+} at this site, the millimolar concentrations of Ca^{2+} or Mn^{2+} may affect the ATP coordination and autophosphorylation reaction of SPCA1a in a different way than SPCA2. We therefore tested if the elevated EP level in SPCA1a may be

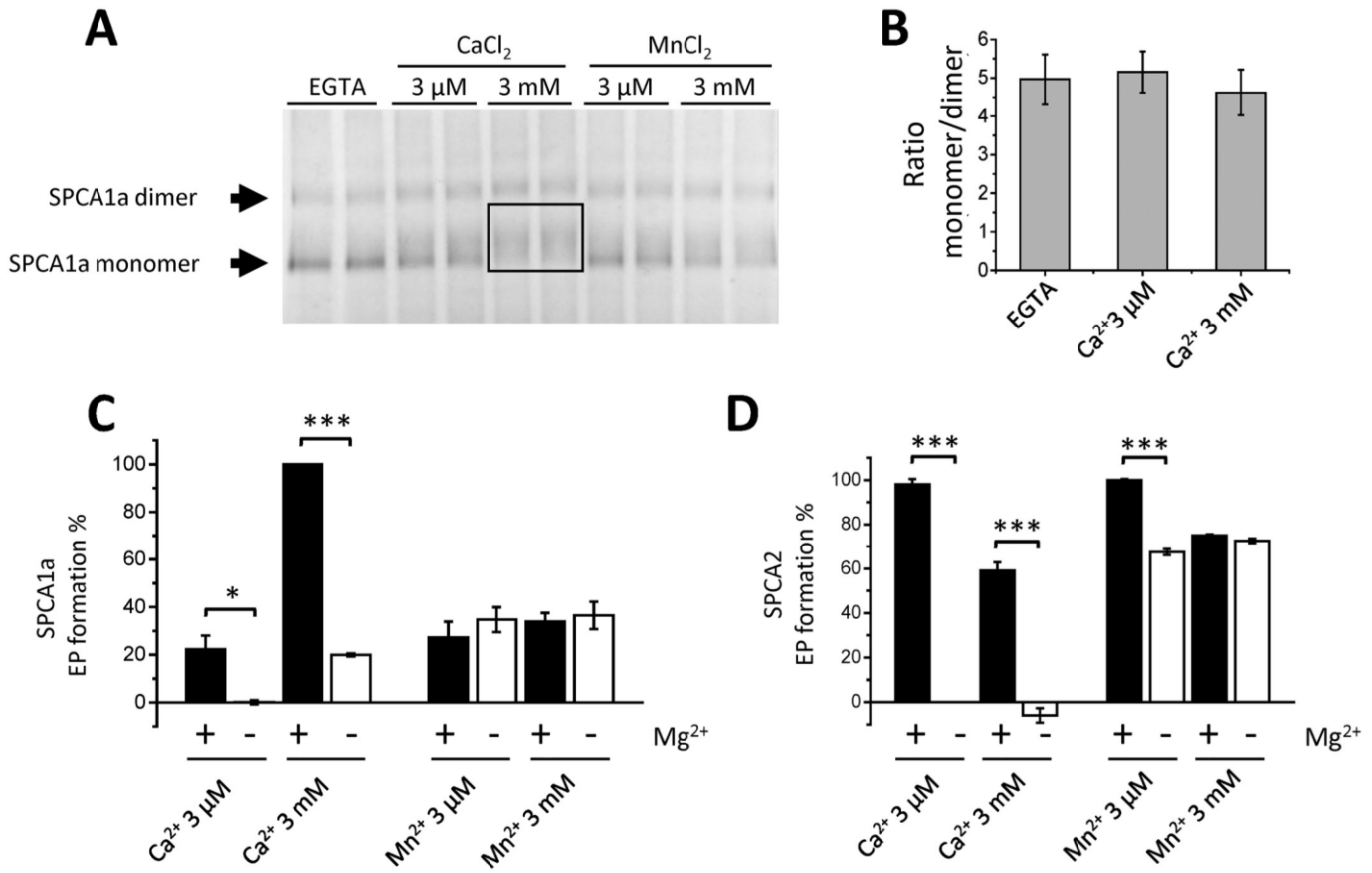

Figure 4. Binding of Ca^{2+} and Mn^{2+} to SPCA proteins. *A,* native PAGE of purified SPCA1a protein following incubation with varying concentrations of Ca^{2+} or Mn^{2+}. Bands were visualized by Coomassie staining. The *arrows* point to the SPCA1a monomer and dimer bands in the EGTA condition. The monomer protein band appears less focused in the presence of 3 μM Ca^{2+} and migrates higher as a smear in the 3 mM Ca^{2+} condition (*boxed region*). *B,* quantified monomer/dimer band ratio of the SPCA1a in Native PAGE ($n = 7$). *C* and *D,* bar graphs depicting the quantified EP levels of SPCA1a (*C*) and SPCA2 (*D*). Indicated concentrations of Mn^{2+} or Ca^{2+} were supplied in the presence (5 mM) or absence (0 mM) of $MgCl_2$ ($n = 2$). The EP levels were normalized to the maximal level of each isoform. *, $p < 0.05$; **, $p < 0.01$; ***, $p < 0.001$.

explained by the competition between Mg^{2+} and Ca^{2+} or Mn^{2+} (Fig. 4, *C* and *D*). Both SPCA1a and SPCA2 largely retained high EP levels when 5 mM Mg^{2+} was replaced by 3 μM or 3 mM Mn^{2+} (Fig. 4, *C* and *D*), indicating that Mn^{2+} is able to substitute for Mg^{2+} in both isoforms. In contrast, in the absence of Mg^{2+}, 3 μM or 3 mM Ca^{2+} is unable to induce EP formation in SPCA2 (Fig. 4*D*). Remarkably, EP formation is observed for SPCA1a when 3 mM Ca^{2+} is used, albeit significantly lower (19.3%) than when Mg^{2+} is present (100.0%) (Fig. 4*C*).

Thus, SPCA2 can be autophosphorylated with Mg^{2+} or Mn^{2+} as ATP coordinating ions, whereas SPCA1a is also able to use Ca^{2+} for ATP coordination and autophosphorylation. However, Ca^{2+} is 4-fold less efficient to induce autophosphorylation in the absence of Mg^{2+}. Because the strong stimulatory effect of millimolar Ca^{2+} on the SPCA1a autophosphorylation depends on the presence of Mg^{2+} (Fig. 4*C*), we hypothesized that another SPCA1a-specific region than the Mg^{2+}-binding site may be responsible.

The N terminus of SPCA1a, but not SPCA2, contains a Ca^{2+}-binding site

Yeast PMR1 possesses a Ca^{2+}-binding EF-hand–like motif in its N terminus, which determines substrate selectivity and pumping activity (21). This motif is partially conserved in SPCA1a sequences of higher vertebrates (Fig. 5*A*), but the loop of the EF-hand–like motif of PMR1 comprises one extra amino acid. The critical acidic residues at positions Asp-51, Asp-53, and Glu-63 of the motif in PMR1 are reasonably conserved in SPCA1a (Gln-39, Asp-41, and Glu-50), but less conserved in SPCA2 (Cys-70, Asp-72, and Ser-81) or in invertebrate PMR1 sequences. Based on this alignment, we hypothesized that the N-terminal region of SPCA1a may hold a Ca^{2+}-binding motif that may explain the Ca^{2+}-dependent stimulation of SPCA1a's autophosphorylation activity.

We turned to an NMR analysis of the human SPCA1a N terminus to pinpoint residues that may contribute to Ca^{2+} binding. We first purified a GST-labeled N-terminal SPCA1 fragment and removed the GST tag via thrombin cleavage. This rendered a >95% pure protein fragment corresponding to Val-20 to Glu-67 of SPCA1a (Fig. 5*B*), which was suitable for NMR analysis. This purified peptide was analyzed in the absence and presence of Ca^{2+} using NMR spectroscopy (Fig. 5*C*). Based on the chemical shift changes of backbone amide signals in ^{15}N-HSQC spectra at different titration steps, we were able to unambiguously identify a stretch of residues that are significantly affected at their backbone by Ca^{2+} binding:

Regulation of SPCA1 by the N terminus

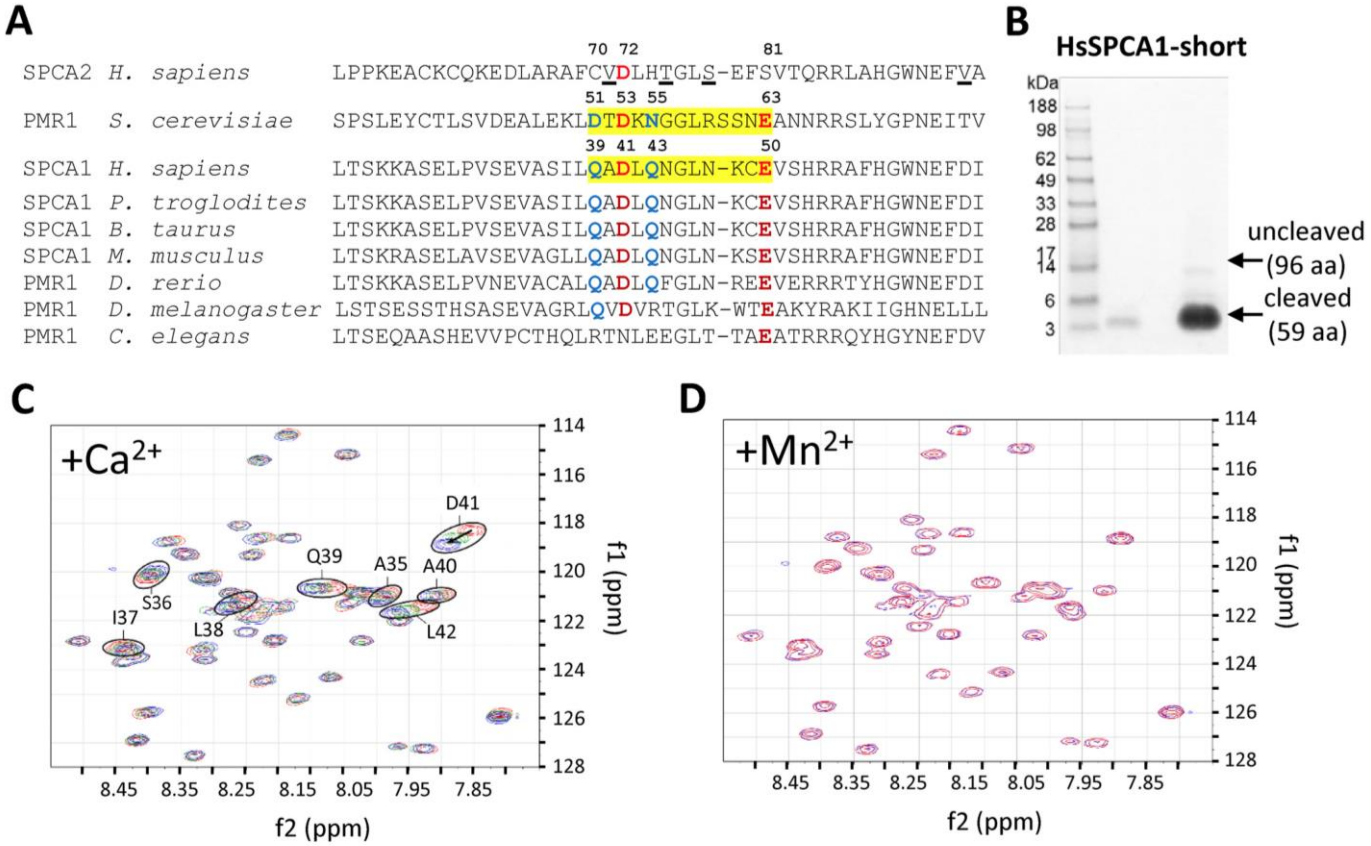

Figure 5. Binding of Ca^{2+} to the N-terminal EF-hand–like motif in SPCA1a. *A,* MUSCLE alignment of part of the N-terminal sequences of yeast PMR1 (NP_011348.1), human SPCA1 (NP_001186110.1), and SPCA2 (B4E2Q0), with various animal SPCA1/PMR1 orthologues (XP_001146246.2; NP_786979.1; NP_001240760.1; XP_003200287.2; NP_730742.1; NP_001021862.1). The regions highlighted in *yellow* in yeast PMR1 and human SPCA1 correspond to the loop of the EF-hand–like motif. The critical residues that are identical (*red*) or conserved (*blue*) between yeast PMR1 and human SPCA1 are indicated with numbering. In SPCA2, the *underlined* residues interact with Orai1 during store-independent Ca^{2+} entry (11). *B,* Coomassie staining of purified N-terminal fragment of SPCA1a (including an N-terminal linker SPMGYRGSM followed by the human SPCA1a sequence Val-20 to Glu-67). *C,* the heteronuclear single quantum coherence spectra overlay of the SPCA1a N-terminal peptide purified from *B* in the presence of 0 (*red*), 4.65 (*green*), and 9 mM (*blue*) Ca^{2+} ions. *Encircled* residues with the indicated numbers were identified in close vicinity of a Ca^{2+} ion. *D,* overlay of heteronuclear single quantum coherence spectra before (*blue*) and after (*red*) further addition of Mn^{2+} after the Ca^{2+} titration.

Ser-36 to Leu-42 (Fig. 5*C*). The observed chemical shift changes can be attributed to direct interaction with Ca^{2+} or local conformational changes upon Ca^{2+} binding (33). The identified region contains Gln-39 and Asp-41, which are conserved residues in the EF-hand–like motif of PMR1 and SPCA1a (Fig. 5*A*).

After titrating with $CaCl_2$, we also added $MnSO_4$ as a competition experiment. Strong impact on protein signals upon binding Mn^{2+} is expected because its unpaired electron induces paramagnetic relaxation effects on NMR active nuclei within a distance of about 15 Å. Therefore, binding of the peptide with Mn^{2+} would result in line broadening and potentially removing signals from the NMR spectra (34). To avoid this problem and to potentially allow a second titration, the amount of Mn^{2+} added was an order of magnitude smaller than the added amount of Ca^{2+} but should still suffice to establish any influence (binding) of Mn^{2+} to the peptide. The absence of any observable changes in NMR spectra after the addition of $MnSO_4$ indicates that this N-terminal peptide of SPCA1a does not bind Mn^{2+} (Fig. 5*D*). Together, our data show that SPCA1a harbors a Ca^{2+}-selective EF-hand–like motif in its N terminus.

The N-terminal EF-hand–like motif provides Ca^{2+} specific control of SPCA1a activity

Next, we explored whether the N-terminal EF-hand–like motif of SPCA1a is responsible for the Ca^{2+}-specific activation mechanism of autophosphorylation. We performed site-directed mutagenesis to disturb the motif, and generated two single mutants, Q39C and E50S, in which SPCA1a residues are substituted by the corresponding SPCA2 residues. Because SPCA2 may not bind Ca^{2+} at the N terminus (Fig. S4), we hypothesize that by introducing SPCA2 elements, we will affect the 3D configuration of the EF-hand–like motif and compromise Ca^{2+} coordination. Note also that Glu-50 is a highly conserved acidic residue in the canonical EF-hand sequences (35). Finally, we constructed a double mutant in which the two conserved acidic residues between SPCA1 and PMR1 are replaced by alanines (D41A/E50A). The three SPCA1a mutants were purified and reconstituted following the same procedure as for WT (Fig. 6*A*). Interestingly, the Ca^{2+}-dependent mobility shifts of the mutant proteins are less prominent as compared with the purified WT protein, indicating that Ca^{2+} binding is hampered by the EF-hand mutations (Fig. 6*B*).

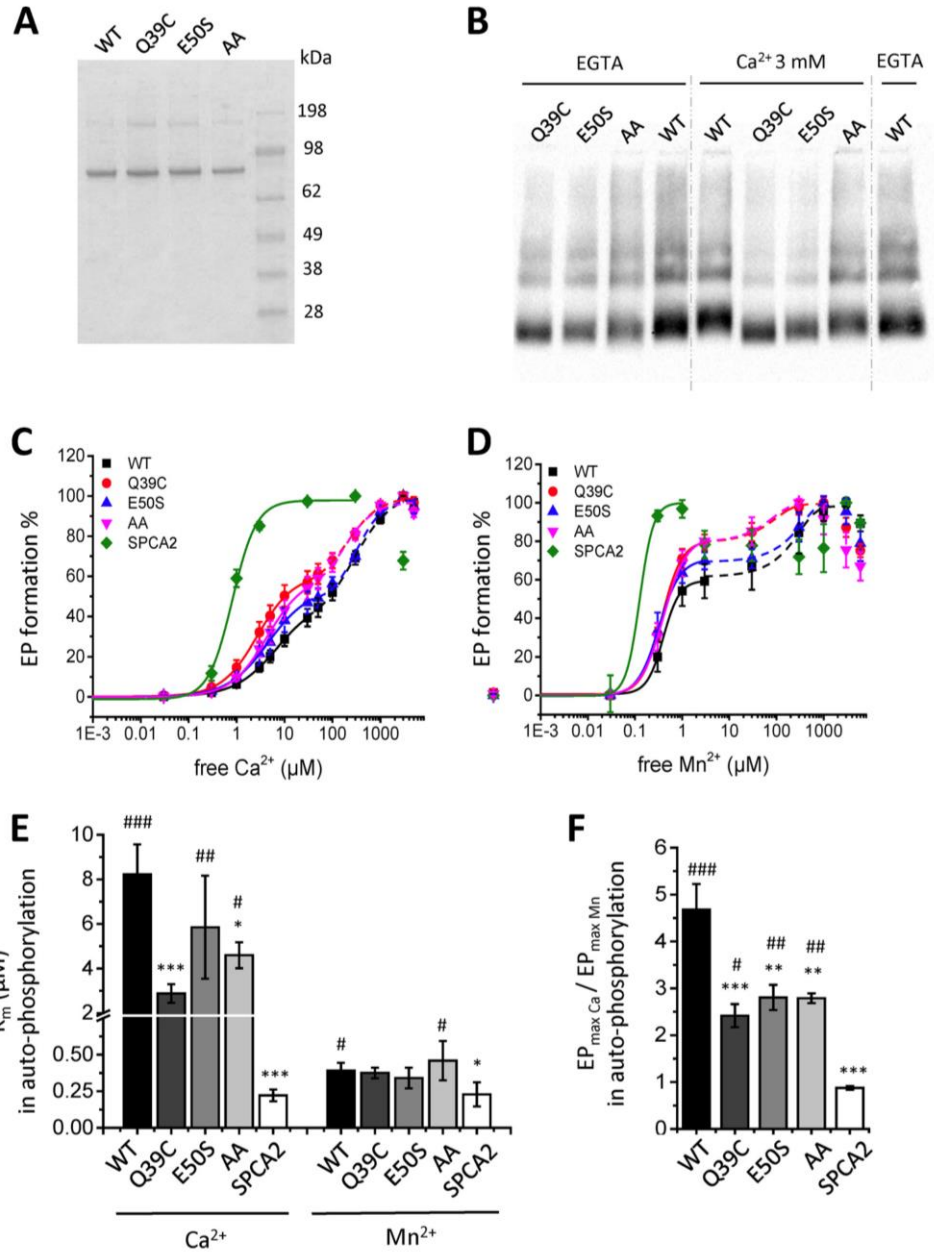

Figure 6. Autophosphorylation activities of SPCA1a WT and N-terminal EF-hand–like mutants. *A*, a Coomassie-stained SDS-PAGE gel of the reconstituted SPCA1a WT and mutants. *B*, native PAGE of the SPCA1a WT and mutants incubated with or without Ca^{2+}, followed by immunoblotting for detection with a SPCA1-specific antibody (1:50,000 dilution, Frodo, homemade). *C* and *D*, Ca^{2+}- and Mn^{2+}-dependent autophosphorylation activities were measured from radiograms for all constructs, and fitted with either one (for SPCA2) or two (for SPCA1a and the mutants) logistic curves (n = 3–7). Bar graphs depict the apparent ion affinities of the first phase (K_m, *E*) and the ratio of the maximal phosphorylation levels of Ca^{2+} over Mn^{2+} (*F*), which were derived from the measurements by fitting of each individual measurement, shown in *B* and *C*. One-way ANOVA was performed followed by post hoc Fisher (*E*) and Bonferroni (*F*) tests. *, significantly different compared with SPCA1a WT. #, significantly different compared with SPCA2. *, $p < 0.05$; **, $p < 0.01$; ***, $p < 0.001$. AA, double alanine mutant.

Remarkably, the biphasic pattern of the Ca^{2+}-dependent autophosphorylation at 5 μM ATP is more pronounced for the SPCA1a mutants than for WT (Fig. 6*B*), which further shows that our earlier formulated proposal for a biphasic fitting of the Ca^{2+}-dependent autophosphorylation of WT is justified (Fig. 2*E*). The mutants Q39C and AA displayed a significantly higher Ca^{2+} affinity in the first activation phase of Ca^{2+}-dependent autophosphorylation, whereas the affinity shift for E50S is more modest (Fig. 6, *C* and *E*, Table 3). In ATPase assays in the presence of 5 mM ATP, all mutants exhibited a significantly higher apparent affinity for Ca^{2+}, *i.e.* shifting the K_m value closer to SPCA2's K_m (Fig. 7, *A* and *C*). A more modest effect of the mutations was observed on the apparent Mn^{2+} affinity (Figs. 6, *D* and *E*, and 7, *A*–*C*, Table 3). Thus, we show that the EF-hand–like motif mainly regulates the apparent Ca^{2+} affinity of SPCA1a, but has a lower impact on Mn^{2+} affinity, which is in line with the selectivity of the EF-hand–like motif for Ca^{2+} over Mn^{2+} (Fig. 5, *C* and *D*).

Moreover, the EF-hand–like motif also plays a role in the biphasic activation pattern of SPCA1a (Fig. 6, *C* and *D*). Indeed, the relative magnitudes of the second phosphorylation phase were reduced in all three mutants (Fig. 6, *C* and *D*). The appar-

Regulation of SPCA1 by the N terminus

Table 3
The affinity of Ca^{2+} and Mn^{2+} obtained from autophosphorylation assay of SPCA1 mutants

	K_m, biphasic part I[a]	K_m, biphasic part II[b]
	μM	
WT-Ca	7.9 ± 0.1	285
Q39C-Ca	2.8 ± 0.1	204
E50S-Ca	4.6 ± 0.4	373
AA-Ca	4.4 ± 0.1	189
WT-Mn	0.43 ± 0.03	242
Q39C-Mn	0.37 ± 0.02	78
E50S-Mn	0.32 ± 0.01	259
AA-Mn	0.40 ± 0.02	73

[a] The K_m of biphasic part I is calculated from the overall fitting of $n = 3$–7 curves via logistic function in Origin Pro9.
[b] K_m of biphasic part II is calculated by enabling "finding x from y" function in Origin Pro 9. The y values are determined with formula, $100 - 0.5 \times (100 - A1)$, A1 is the starting y value of the biphasic part II.

ent Ca^{2+} and Mn^{2+} affinity of the second phase was higher for the Q39C and AA mutants as compared with E50S and WT (Fig. 6, *C* and *D*, Table 3). However, the ratio of the maximal EP levels obtained in Ca^{2+} over Mn^{2+} ($EP_{max(Ca)}/EP_{max(Mn)}$) shows that the three mutants became less responsive to Ca^{2+} relative to Mn^{2+} (Fig. 6*F*). In addition, we confirmed in ATPase measurements that the single mutants displayed a lower $V_{max(Ca)}/V_{max(Mn)}$ ratio, more closely resembling SPCA2 (Fig. 7*D*). Thus, these results reveal that the EF-hand–like motif contributes to the Ca^{2+}-specific activation of autophosphorylation in SPCA1a, which regulates the maximal Ca^{2+}-dependent ATPase activity.

Also the maximal ATPase activity of the double mutant is severely impaired (Fig. S5). However, the V_{max} for Mn^{2+} reduced more than the V_{max} for Ca^{2+}, resulting in a remarkably high $V_{max(Ca)}/V_{max(Mn)}$ ratio (Fig. 7*D*). Furthermore, the back-inhibition of the double mutant already takes place at lower Ca^{2+} or Mn^{2+} concentrations than WT (Fig. S2, *C* and *D*). Thus, disrupting the N-terminal motif by two alanine mutations dramatically impairs the overall activity of SPCA1a. However, the difference between the ATPase and EP results of the double mutant suggests a more complex regulatory mechanism that most likely also involves downstream steps in EP turnover. In conclusion, Ca^{2+} binding at the EF-hand–like motif in the N terminus of SPCA1a is at least partially responsible for the biphasic stimulation pattern of SPCA1a autophosphorylation, and contributes to the lower Ca^{2+} affinity and higher maximal activity of SPCA1a *versus* SPCA2.

Discussion

In the present study, we compared the properties of the Golgi/secretory pathway Ca^{2+}/Mn^{2+}-ATPases SPCA1a and SPCA2 in a purified, reconstituted system. We report isoform-specific differences between the Ca^{2+}- and Mn^{2+}-dependent properties of SPCA1a and SPCA2 that can at least in part be attributed to a Ca^{2+}-binding regulatory motif in the N terminus of SPCA1a, which is absent in SPCA2.

An N-terminal EF-hand–like motif regulates the ion affinity and maximal activity of SPCA1a

Via a diverse set of approaches on purified SPCA1a and N-terminal fragments, we revealed a previously unrecognized Ca^{2+}-dependent regulatory element that is present in SPCA1a, but absent in SPCA2. First, we observed a biphasic curve for SPCA1a autophosphorylation, which points to a regulatory mechanism that controls the activation state in a substrate-dependent manner. Second, we found that Ca^{2+} stimulates SPCA1a's EP formation more than Mn^{2+}, in line with a Ca^{2+}-specific regulatory site. Third, through NMR experiments, we confined the Ca^{2+} binding to specific Ca^{2+}-coordinating residues belonging to the EF-hand–like motif in the SPCA1a N terminus. No Mn^{2+} binding was observed to this site. Fourth, Ca^{2+} alters the mobility of purified SPCA1a on native PAGE, which is less clear with Mn^{2+} or with mutations in the EF-hand–like motif. Fifth, via mutagenesis we demonstrated that the EF-hand–like motif contributes to the stronger Ca^{2+}-dependent activation of autophosphorylation, the higher turnover rate and lower apparent Ca^{2+} affinity of SPCA1a as compared with SPCA2. In contrast, the mutations minimally affect the Mn^{2+} properties of SPCA1a. Taken together, the N-terminal EF-hand–like motif specifically binds Ca^{2+} and contributes to the isoform-specific properties of SPCA1a.

Besides the EF-hand–like motif, also the ATP concentration critically influences (i) the apparent Ca^{2+} affinity, and (ii) biphasic activation behavior of SPCA1a. Indeed, we first observed that the Ca^{2+} affinity of SPCA1a in the autophosphorylation assay at 5 μM ATP is unusually low, whereas SPCA1a's Ca^{2+} affinity increases at higher ATP concentrations. Conversely, reducing the ATP concentration in the ATPase assay lowers the apparent Ca^{2+} affinity of SPCA1a. Second, the biphasic activation pattern of SPCA1a is most clear at low ATP concentrations in both the autophosphorylation (Fig. 2*E*) and ATPase assay (Fig. S3). Moreover, the ATP concentration determines the Ca^{2+} sensitivity of the SPCA1a activation. At 0.5 mM ATP, the second activation step takes place between 1 and 10 μM Ca^{2+} (Fig. S3), *i.e.* at physiological Ca^{2+} concentrations. However, at 5 μM ATP, Ca^{2+} concentrations between 30 μM and 3 mM are required to trigger maximal autophosphorylation, *i.e.* well above physiological Ca^{2+} concentrations.

We therefore conclude that at high Ca^{2+} concentrations, Ca^{2+} binds to the N-terminal EF-hand–like motif of SPCA1a, and activates it. In contrast, at low Ca^{2+} concentrations SPCA1a is in a less active state due to the lack of Ca^{2+} binding to the EF-hand–like motif, which hinders autophosphorylation. Overall, this explains the low apparent Ca^{2+} affinity of SPCA1a and its higher Ca^{2+}-dependent ATPase activity. We showed that this system is sensitive to the ATP concentration. When the ATP concentration is low, a Ca^{2+} concentration above 10 μM is required to maximally activate SPCA1a, whereas at more physiological ATP concentrations a Ca^{2+} level between 1 and 10 μM is sufficient to maximally activate SPCA1a. These observations suggest that ATP binding and N-terminal regulation are mechanistically linked.

It is not entirely clear how the N terminus may regulate the relative substrate affinities or how ATP may control this system. Because the distal N-terminal region is not directly involved in Ca^{2+} coordination in the membrane domain, it most likely modulates the substrate affinity indirectly. The N terminus may influence the packing of the Ca^{2+}- and or Mn^{2+}-coordinating residues in the ion entry/exit channels in the membrane domain or at the substrate-binding site. The ionic

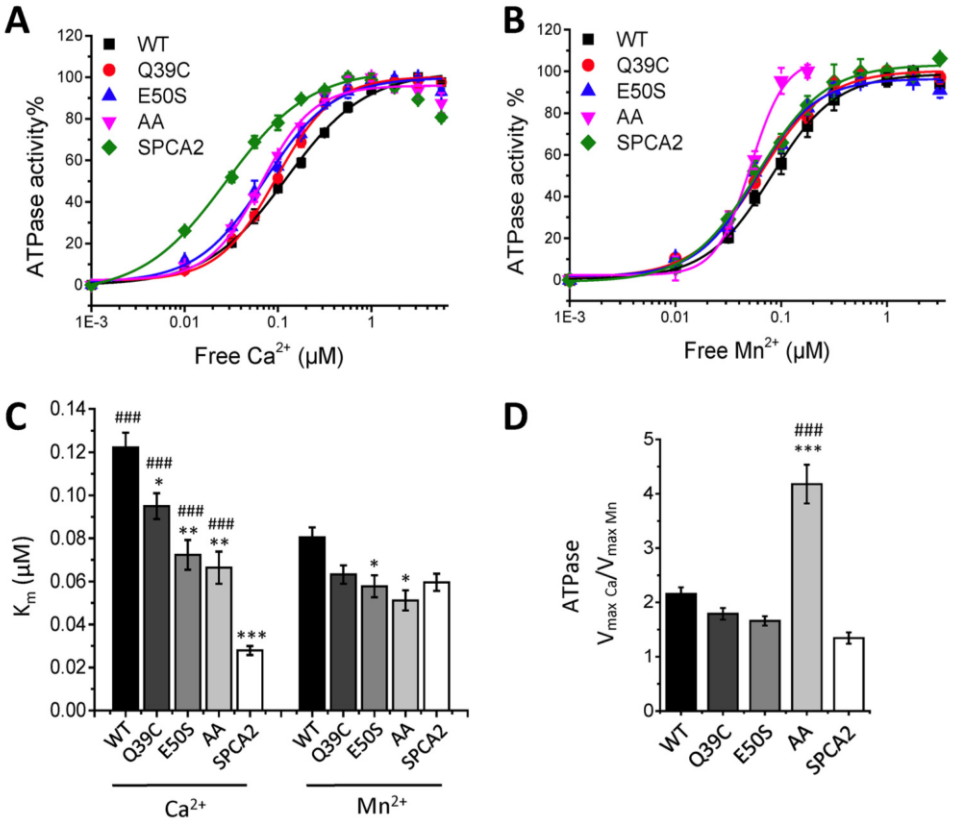

Figure 7. ATPase activities of SPCA1a WT and N-terminal EF-hand–like mutants. *A* and *B*, Ca^{2+}- and Mn^{2+}-dependent ATPase activities were measured on all constructs and fitted with logistic curves. Bar graphs depict the apparent ion affinities (K_m, *C*) and the ratio of maximal ATPase activities with Ca^{2+} over Mn^{2+} (*D*) ($n = 3$). Statistical analysis was performed using one-way ANOVA followed by a post hoc Bonferroni test. *, significantly different from SPCA1a WT. #, significantly different from SPCA2. *, $p < 0.05$; **, $p < 0.01$; ***, $p < 0.001$.

radius of Mn^{2+} (0.8 Å) is smaller than that of Ca^{2+} (0.99 Å) (36) and the N terminus may induce a local change at the ion-binding sites that differently affects the ion affinity. Alternatively, the N terminus of SPCA1a may modulate the conformational transitions in the catalytic cycle. A reduced apparent Ca^{2+} affinity may, for instance, be explained by stabilizing the SPCA1a protein more in the E2 than E1 state.

Both models depend on the interaction of the N terminus with downstream elements of the pump. Such a mode of action was already proposed for the yeast PMR1 protein. PMR1 also contains a Ca^{2+} binding N-terminal EF-hand–like motif that regulates the substrate affinities and Ca^{2+}/Mn^{2+} selectivity, and a partial proteolytic digestion analysis indicated that the N-terminal region may interact with the catalytic ATP-binding domain of PMR1 (21). An interaction between the N terminus and the ATP-binding domain may offer a mechanistic explanation of how ATP may modulate the regulation by the N terminus. Future work will focus on identifying the interacting site of the N terminus in SPCA1a, which will further reveal the mechanism of SPCA1a activation.

Post-translational modifications may influence SPCA1a activity in a cellular context

In a previous report from our lab we compared the biochemical properties of SPCA1d and SPCA2 in membrane fractions of HEK-293 overexpressing cells (27). In that study, SPCA1d and SPCA2 displayed a similar apparent affinity in the ATPase assay (K_m of 0.041 and 0.037 μM, respectively), whereas the catalytic turnover rate of SPCA1a was lower (27). This is clearly different from the measurements on purified SPCA1a and SPCA2 in this study. Also the biphasic activation pattern of SPCA1a was not observed before. Because the SPCA1a and SPCA1d splice variants only differ in the C terminus and contain the same N terminus, the discrepancies between both studies may not merely reflect differences between splice variants. Instead, several factors may influence the N-terminal activation mechanism in a cellular context, such as post-translational modifications, lipid interactions, or regulatory proteins that are absent in the purified systems. In that respect, we observed remarkable differences in the mobility of SPCA1a in HEK-293 microsomes *versus* proteoliposomes. The purified SPCA1a from yeast runs as a single monomer and single dimer band (Fig. 1*A*), whereas we, and others (14, 37, 38), observe that monomers of the SPCA1 splice variants in mammalian membrane fractions migrate as a double band (Fig. S6*A*). Remarkably, the lower band of SPCA1a in microsomes diminishes after treatment with reducing agent in combination with heating, and the higher band becomes stronger, which is not observed for SPCA1a in proteoliposomes (Fig. S6*B*). This may point to post-translational modifications of SPCA1a, such as disulfide bridges, which are only present in microsomes. These modifications may influence the biochemical properties, possibly explaining the difference between SPCA1a in proteoliposomes and in microsomes. These intrigu-

ing observations may point to an unknown regulatory system of SPCA1a in the cell, but future studies are needed to clarify this point. Analyzing the purified proteins, *i.e.* in the absence of confounding cellular elements, revealed an N-terminal regulatory element in SPCA1a, which otherwise would have been missed in the microsome context.

Physiological implications of the Ca^{2+}-dependent regulation of SPCA1a

We compared the biochemical properties of purified SPCA1a and SPCA2 proteins in a fixed membrane environment, which eliminated cell-based confounding factors. The two human SPCA isoforms present different affinities and turnover rates toward Ca^{2+} and Mn^{2+} ions, their preferred substrates. SPCA1a displayed a 2-fold higher maximal turnover rate with Ca^{2+} than with Mn^{2+}, whereas SPCA2 presented similar turnover rates for both substrates. In addition, the two isoforms exhibited similar Mn^{2+} affinities, whereas the apparent Ca^{2+} affinity of SPCA1a is significantly lower as compared with SPCA2.

These isoform-specific properties may have important physiological implications. Due to its extremely high Ca^{2+} affinity, but 2-fold lower Mn^{2+} affinity, SPCA2 may mainly transport Ca^{2+} ions. The dominant Ca^{2+} transport function of SPCA2 may be relevant for secretory cells where SPCA2 is predominantly expressed (7, 8). In secretory cell types like mammary gland, SPCA2 is functionally coupled to the Orai1 Ca^{2+} channel where it transports Ca^{2+} that comes in from the extracellular environment via Orai1 into the secretory pathway (11, 13). In contrast, SPCA1a is ubiquitously expressed and fulfills a housekeeping function by delivering both Ca^{2+} and Mn^{2+} into the Golgi/secretory compartment to support protein folding and maturation (3). The slightly higher affinity of SPCA1a for Mn^{2+} than Ca^{2+} suggests that at low ion availability the relative Ca^{2+} and Mn^{2+} concentrations will determine which ion will be transported by SPCA1a.

Our biochemical analysis further suggests that depending on the Ca^{2+} and ATP concentration, the EF-hand–like motif may switch SPCA1a between a high affinity/low capacity Ca^{2+}/Mn^{2+} pump to a lower affinity, but higher capacity Ca^{2+} pump. Consequently, SPCA1a presents a higher Ca^{2+} transport capacity when the cytosolic Ca^{2+} load increases, which may occur in cell types undergoing Ca^{2+} signaling or fulfilling secretory functions. Like SPCA2, SPCA1a expression is elevated in mammary gland during lactation (14, 38), and both isoforms may operate together to transfer Ca^{2+} into the milk (11, 13). Although SPCA2 may be the major activator of Orai1 (11), SPCA1a may present a higher Ca^{2+} transport capacity than SPCA2. SPCA1a is detected in the subplasma membrane region close to the plasma membrane Ca^{2+} channel Orai1, where it may participate in SICE (13) and may become fully activated by the local Ca^{2+} increase (up to 300 μM in microdomains near Ca^{2+} channels (39)). Our data suggest that SPCA2 may not be further activated by Ca^{2+}, but this does not exclude that the SPCA2 activity may respond to other stimuli such as the direct interaction with Orai1.

Mutations in SPCA1a lead to the skin disease Hailey–Hailey, which is manifested in the keratinocytes. Keratinocytes undergo substantial changes in their intracellular ATP and Ca^{2+} concentrations, and in this context, SPCA1a regulation by the EF-hand–like motif may take place. Keratinocytes contain merely one-third to one-fourth of the ATP concentration of artery smooth muscle cells (40). These low ATP levels further decrease when extracellular Ca^{2+} levels are increased (40), which may resemble the situation in the outer layers of the skin epidermis where extracellular Ca^{2+} progressively increases (41). The local environment with low ATP and high Ca^{2+} concentrations may affect the activity of SPCA1 via the N-terminal EF-hand–like motif. Moreover, in isolated keratinocytes of Hailey–Hailey disease patients with dysfunctional SPCA1, the ATP concentration is reduced, whereas the ATP levels fail to increase when extracellular Ca^{2+} is supplied (40). The altered ATP and Ca^{2+} concentrations in Hailey–Hailey disease may contribute to the dysregulation of SPCA1a activity.

In conclusion, our work on purified SPCA1a and SPCA2 proteins provides a comprehensive analysis of the isoform-specific Ca^{2+}- and Mn^{2+}-dependent activities. We discovered a Ca^{2+}-binding EF-hand–like motif in the N terminus of SPCA1a that is absent in SPCA2. This motif is at least partially responsible for the SPCA1a-specific biochemical properties. Depending on the ATP concentration, the N terminus switches SPCA1a between a high affinity/low capacity state at low Ca^{2+} concentrations, and a low affinity/high capacity state at high Ca^{2+} loads. This mechanism may play a role in secreting cells like mammary gland during lactation, or in keratinocytes in the outer layers of the skin epidermis.

Experimental procedures

Plasmids and mutagenesis

The C-terminal His_8-tagged human SPCA1a WT or mutants were introduced via Q5 site-directed mutagenesis (New England Biolabs) as previously described (23). The C-terminal His_{10}-tagged human SPCA2 in the pADANS vector was a kind gift from Dr. S. Yamamoto, Kyorin University School of Medicine (42).

Purification and reconstitution of SPCA1a/2

Vectors containing SPCA1a and SPCA2 WT or mutants were transformed into *S. cerevisiae* strain BY4741a (his3Δ1; leu2Δ0;met15Δ0;ura3Δ0;MATa) as previously described (23). Each yeast clone was inoculated in minimal medium deprived of Leu for selection, then grown in yeast peptone dextrose medium for 30 h before harvesting. Yeast cells were pelleted at 5,000 × *g* for 5 min, 4 °C, washed with Milli-Q water, flash-frozen, and stored at −20 °C. The membrane fractions of yeast were isolated via differential centrifugations as previously described (23). The purification of His-tagged SPCA1a and SPCA2 proteins was performed by nickel-nitrilotriacetic acid affinity chromatography (23). Reconstitution of SPCA1a and SPCA2 in proteolipsomes composed of 80% phosphatidylcholine and 20% phosphatidic acid (Avanti Polar Lipids) was performed following the protocol in Ref. 23.

SDS protein electrophoresis and protein quantification

Purified or reconstituted SPCA1a or SPCA2 was separated on a NuPAGE 4–12% BisTris polyacrylamide gel (200 V, 35

min, MES buffer) (Thermo Fisher Scientific) and visualized with Imperial Protein Stain (Thermo Fisher Scientific). SeeBlue Plus2 Pre-stained Protein Standard (Thermo Fisher Scientific) was used as a molecular weight marker. The concentration of purified protein was determined by direct comparison to a bovine serum albumin (BSA) standard on the same gel (BSA Standard Ampules, Pierce).

Native PAGE

Purified proteins were incubated for 15 min at room temperature in buffer containing 100 mM MOPS, pH 7.0, 1 mM EGTA, 160 mM KCl, 0.2 mg/ml of dodecyl maltoside and $CaCl_2$ or $MnCl_2$ to reach the final Ca^{2+} or Mn^{2+} concentration indicated in the experimental conditions. The samples were then mixed with 4× native PAGE sample buffer supplemented with NativePAGE™ 5% G-250 Sample Additive according to the instructions from the manufacturer. The electrophoresis was performed at 150 V for 100 min at room temperature using native PAGE running buffer as the anode buffer, and the cathode buffer was supplemented with 0.02% Coomassie Blue G-250. The native PAGE gel, sample buffer, sample additive and Coomassie Blue G-250 were purchased from Thermo Fisher Scientific. The protein bands were visualized by destaining or immunoblotting.

ATPase assay

The ATPase activity of reconstituted samples was assayed by a colorimetric assay via the detection of P_i in the presence of 5 mM ATP, as previously described (43). The reactions were performed for 30 min using 300 ng of purified SPCA1a or SPCA2 in a reaction volume of 50 μl. The ATPase measurements with lower ATP concentrations were performed using the NADH-coupled assay in a 96-well plate. A total reaction mix of 250 μl contained 100 ng of purified SPCA1a, 50 mM TES/Tris, pH 7, 100 mM KCl, 7 mM $MgCl_2$, 1 mM EGTA, 0.36 mM NADH, 1 mM phosphoenolpyruvate, 2.4 units of pyruvate kinase, 2.4 units of lactate dehydrogenase and the indicated free Ca^{2+} concentrations. The reaction was started by addition of the required amount of ATP. After 20 s mixing, the absorbance was read at 340 nm over 10 min in 30-s intervals with a SPECTRAmax PLUS^{384} Microplate Spectrophotometer (Molecular Devices). The slope of the decreased absorbance over time was used as a measure of the ATPase rate. All products were purchased from Merck.

Autophosphorylation assay

The autophosphorylation reaction was performed as described in Ref. 44 with slight modifications. Briefly, the reaction mixture contains 0.5 μg of purified SPCA1a or SPCA2 and 40 μg of BSA in a buffer containing 160 mM KCl, 17 mM Hepes, pH 7.0, 1 mM DTT, 5 mM $MgCl_2$, 1 mM EGTA and various concentration of $CaCl_2$, $MnCl_2$, or $MgCl_2$ as indicated in the experimental conditions. Unless specified otherwise, all autophosphorylation experiments were performed with 5 mM Mg^{2+}. The reaction was initiated by addition of 0.074 MBq of radioactively labeled [γ-^{32}P]ATP (PerkinElmer Life Sciences) in a final concentration of 5 μM. After a 20-s reaction on ice, 500 μl of stop solution containing 6% TCA, 10 mM phosphoric acid, and 1 mM ATP was added to the reaction mixture for precipitation. The pellet was washed three times with stop solution before detection in a scintillation counter (Packard, 2900TR) or by running on an acidic gel as previously described (44) and then detected with a phosphorimager (Typhoon, FLA9500). For HA treatment an additional washing step with 0.25 M HA was performed.

NMR analysis

A GST-labeled N-terminal fragment of the human SPCA1a (Val-20 to Glu-67) was cloned in the pET41a(+) vector and expressed in BL21 *Escherichia coli* with ^{15}N-enriched growth medium. After affinity purification and thrombin cleavage to remove GST, a 59-amino acid long peptide (HsSPCA1-short) was obtained that consists of a 9-residue long linker (SPMGYRGSM) and the N-terminal SPCA1a sequence (^{20}VLTSKKASELPVSEVASILQADLQNGLNKCVSHRRAFHGWNEFDISEDE^{69}). NMR experiments were conducted with a Bruker Avance 600 MHz (^{1}H) Ultrashield™ Plus with a CP TCI 600 S3 H-C/N-D-05 Z probe (Bruker, Fällanden, Switzerland). All data were processed using the TopSpin software (version 3.2) provided by Bruker and the resulting spectra were analyzed using the computer-aided resonance assignment software. ^{1}H,^{15}N-HSQC spectra (45, 46) were recorded at 5 °C using 12 scans with 4096 data points in the t_2 dimension and 200 data points in the t_1 dimension. The spectral width for the t_1 dimension was 2311 Hz (38 ppm) and for the t_2 dimension 9615 Hz (16 ppm). During each titration step, 0.5 μl of a $CaCl_2$ solution (0.5 M) was added. After the Ca^{2+} titration, 5 μl of a $MnSO_4$ solution (0.1 mM) was added to verify interactions between the SPCA1 N terminus and Mn^{2+}.

Statistical analysis

Values are provided as mean ± S.E. from a n number of independent measurements. Radiograms and gel images are representative for a minimum of $n = 3$ experiments. Logistic fitting was performed via OriginPro 9 software. Statistical significance was calculated by one-way ANOVA followed by a Bonferroni post hoc test and indicated by asterisks: *, $p < 0.05$; **, $p < 0.01$; ***, $p < 0.001$.

Author contributions—J. C., F. W., and P. V. conceptualization; J. C., S. S., and C.-A. M. formal analysis; J. C. validation; J. C., S. S., C.-A. M., F. P., I. V., J. V., E. L., and P. V. investigation; J. C. visualization; J. C., C.-A. M., I. V., J. V., E. L., and P. V. methodology; J. C. and P. V. writing-original draft; J. C., J. E., and P. V. writing-review and editing; E. L. and P. V. resources; E. L., J. E., and P. V. supervision; P. V. funding acquisition; P. V. project administration.

References

1. Berridge, M. J., Bootman, M. D., and Roderick, H. L. (2003) Calcium signalling: dynamics, homeostasis and remodelling. *Nat. Rev. Mol. Cell Biol.* **4,** 517–529 CrossRef Medline
2. Monteith, G. R., McAndrew, D., Faddy, H. M., and Roberts-Thomson, S. J. (2007) Calcium and cancer: targeting Ca^{2+} transport. *Nat. Rev. Cancer* **7,** 519–530 CrossRef Medline
3. Vangheluwe, P., Sepúlveda, M. R., Missiaen, L., Raeymaekers, L., Wuytack, F., and Vanoevelen, J. (2009) Intracellular Ca^{2+}- and Mn^{2+}-transport ATPases. *Chem. Rev.* **109,** 4733–4759 CrossRef Medline

4. Sepulveda, M. R., Dresselaers, T., Vangheluwe, P., Everaerts, W., Himmelreich, U., Mata, A. M., and Wuytack, F. (2012) Evaluation of manganese uptake and toxicity in mouse brain during continuous $MnCl_2$ administration using osmotic pumps. *Contrast Media Mol. Imaging* **7,** 426–434 CrossRef Medline
5. Leitch, S., Feng, M., Muend, S., Braiterman, L. T., Hubbard, A. L., and Rao, R. (2011) Vesicular distribution of secretory pathway Ca^{2+}-ATPase isoform 1 and a role in manganese detoxification in liver-derived polarized cells. *Biometals* **24,** 159–170 CrossRef Medline
6. Hu, Z., Bonifas, J. M., Beech, J., Bench, G., Shigihara, T., Ogawa, H., Ikeda, S., Mauro, T., and Epstein, E. H., Jr. (2000) Mutations in ATP2C1, encoding a calcium pump, cause Hailey-Hailey disease. *Nat. Genet.* **24,** 61–65 CrossRef Medline
7. Xiang, M., Mohamalawari, D., and Rao, R. (2005) A novel isoform of the secretory pathway Ca^{2+}, Mn^{2+}-ATPase, hSPCA2, has unusual properties and is expressed in the brain. *J. Biol. Chem.* **280,** 11608–11614 CrossRef Medline
8. Vanoevelen, J., Dode, L., Van Baelen, K., Fairclough, R. J., Missianen, L., Raeymaekers, L., and Wuytack, F. (2005) The secretory pathway Ca^{2+}/Mn^{2+}-ATPase 2 is a Golgi-localized pump with high affinity for Ca^{2+} ions. *J. Biol. Chem.* **280,** 22800–22808 CrossRef Medline
9. Baron, S., Struyf, S., Wuytack, F., Van Damme, J., Missiaen, L., Raeymaekers, L., and Vanoevelen, J. (2009) Contribution of intracellular Ca^{2+} stores to Ca^{2+} signaling during chemokinesis of human neutrophil granulocytes. *Biochim. Biophys. Acta* **1793,** 1041–1049 CrossRef Medline
10. Faddy, H. M., Smart, C. E., Xu, R., Lee, G. Y., Kenny, P. A., Feng, M., Rao, R., Brown, M. A., Bissell, M. J., Roberts-Thomson, S. J., and Monteith, G. R. (2008) Localization of plasma membrane and secretory calcium pumps in the mammary gland. *Biochem. Biophys. Res. Commun.* **369,** 977–981 CrossRef Medline
11. Feng, M., Grice, D. M., Faddy, H. M., Nguyen, N., Leitch, S., Wang, Y., Muend, S., Kenny, P. A., Sukumar, S., Roberts-Thomson, J. J., Monteith, G. R., and Rao, R. (2010) Store-independent activation of Orai1 by SPCA2 in mammary tumors. *Cell* **143,** 84–98 Medline
12. Smaardijk, S., Chen, J., Wuytack, F., and Vangheluwe, P. (2017) SPCA2 couples Ca^{2+} influx via Orai1 to Ca^{2+} uptake into the Golgi/secretory pathway. *Tissue Cell* **49,** 141–149 CrossRef Medline
13. Smaardijk, S., Chen, J., Kerselaers, S., Voets, T., Eggermont, J., and Vangheluwe, P. (2018) Store-independent coupling between the secretory pathway Ca^{2+} transport ATPase SPCA1 and Orai1 in Golgi stress and Hailey-Hailey disease. *Biochim. Biophys. Acta* **1865,** 855–862 CrossRef
14. Cross, B. M., Hack, A., Reinhardt, T. A., and Rao, R. (2013) SPCA2 regulates Orai1 trafficking and store independent Ca^{2+} entry in a model of lactation. *PLoS ONE* **8,** e67348 CrossRef Medline
15. Cross, B. M., Breitwieser, G. E., Reinhardt, T. A., and Rao, R. (2014) Cellular calcium dynamics in lactation and breast cancer: from physiology to pathology. *Am. J. Physiol. Cell Physiol.* **306,** C515–C526 CrossRef
16. Dang, D., Prasad, H., and Rao, R. (2017) Secretory pathway Ca^{2+}-ATPases promote *in vitro* microcalcifications in breast cancer cells. *Mol. Carcinogen.* **56,** 2474–2485 CrossRef
17. Grice, D. M., Vetter, I., Faddy, H. M., Kenny, P. A., Roberts-Thomson, S. J., and Monteith, G. R. (2010) Golgi calcium pump secretory pathway calcium ATPase 1 (SPCA1) is a key regulator of insulin-like growth factor receptor (IGF1R) processing in the basal-like breast cancer cell line MDA-MB-231. *J. Biol. Chem.* **285,** 37458–37466 CrossRef Medline
18. Sitsel, A., De Raeymaecker, J., Drachmann, N. D., Derua, R., Smaardijk, S., Andersen, J. L., Vandecaetsbeek, I., Chen, J., De Maeyer, M., Waelkens, E., Olesen, C., Vangheluwe, P., and Nissen, P. (2019) Structures of the heart specific SERCA2a Ca^{2+}-ATPase. *EMBO J.* **38,** e100020 CrossRef Medline
19. Gong, D., Chi, X., Ren, K., Huang, G., Zhou, G., Yan, N., Lei, J., and Zhou, Q. (2018) Structure of the human plasma membrane Ca^{2+}-ATPase 1 in complex with its obligatory subunit neuroplastin. *Nat. Commun.* **9,** 3623 CrossRef Medline
20. Lopreiato, R., Giacomello, M., and Carafoli, E. (2014) The plasma membrane calcium pump: new ways to look at an old enzyme. *J. Biol. Chem.* **289,** 10261–10268 CrossRef Medline
21. Wei, Y., Marchi, V., Wang, R., and Rao, R. (1999) An N-terminal EF hand-like motif modulates ion transport by Pmr1, the yeast Golgi Ca^{2+}/Mn^{2+}-ATPase. *Biochemistry* **38,** 14534–14541 CrossRef Medline
22. Mandal, D., Woolf, T. B., and Rao, R. (2000) Manganese selectivity of pmr1, the yeast secretory pathway ion pump, is defined by residue Gln-783 in transmembrane segment 6: residue Asp-778 is essential for cation transport. *J. Biol. Chem.* **275,** 23933–23938 CrossRef Medline
23. Chen, J., De Raeymaecker, J., Hovgaard, J. B., Sammrdijk, S., Vandecaetsbeek, I., Wuytack, F., Møller, J. V., Eggermont, J., De Maeyer, M., Christensen, S. B., and Vangheluwe, P. (2017) Structure/activity relationship of thapsigargin inhibition on the purified Golgi/secretory pathway Ca^{2+}/Mn^{2+}-transport ATPase (SPCA1a). *J. Biol. Chem.* **292,** 6938–6951 CrossRef Medline
24. Baginski, E. S., Foà, P. P., and Zak, B. (1967) Microdetermination of inorganic phosphate, phospholipids, and total phosphate in biologic materials. *Clin. Chem.* **13,** 326–332 Medline
25. Kühlbrandt, W. (2004) Biology, structure and mechanism of P-type ATPases. *Nat. Rev. Mol. Cell Biol.* **5,** 282–295 CrossRef Medline
26. Ton, V. K., Mandal, D., Vahadji, C., and Rao, R. (2002) Functional expression in yeast of the human secretory pathway Ca^{2+}, Mn^{2+}-ATPase defective in Hailey-Hailey disease. *J. Biol. Chem.* **277,** 6422–6427 CrossRef Medline
27. Dode, L., Andersen, J. P., Vanoevelen, J., Raeymaekers, L., Missiaen, L., Vilsen, B., and Wuytack, F. (2006) Dissection of the functional differences between human secretory pathway Ca^{2+}/Mn^{2+}-ATPase (SPCA) 1 and 2 isoenzymes by steady-state and transient kinetic analyses. *J. Biol. Chem.* **281,** 3182–3189 CrossRef Medline
28. Dode, L., Andersen, J. P., Raeymaekers, L., Missiaen, L., Vilsen, B., and Wuytack, F. (2005) Functional comparison between secretory pathway Ca^{2+}/Mn^{2+}-ATPase (SPCA) 1 and sarcoplasmic reticulum Ca^{2+}-ATPase (SERCA) 1 isoforms by steady-state and transient kinetic analyses. *J. Biol. Chem.* **280,** 39124–39134 CrossRef Medline
29. Lytton, J., Westlin, M., Burk, S. E., Shull, G. E., and MacLennan, D. H. (1992) Functional comparisons between isoforms of the sarcoplasmic or endoplasmic reticulum family of calcium pumps. *J. Biol. Chem.* **267,** 14483–14489 Medline
30. Post, R. L., and Kume, S. (1973) Evidence for an aspartyl phosphate residue at the active site of sodium and potassium ion transport adenosine triphosphatase. *J. Biol. Chem.* **248,** 6993–7000 Medline
31. Bolton, E. C., Mildvan, A. S., and Boeke, J. D. (2002) Inhibition of reverse transcription *in vivo* by elevated manganese ion concentration. *Mol. Cell* **9,** 879–889 CrossRef Medline
32. Beckman, R. A., Mildvan, A. S., and Loeb, L. A. (1985) On the fidelity of DNA replication: manganese mutagenesis *in vitro*. *Biochemistry* **24,** 5810–5817 CrossRef Medline
33. Drmota Prebil, S. D., Slapšak, U., Pavšič, M., Ilc, G., Puž, V., de Almeida Ribeiro, E., Anrather, D., Hartl, M., Backman, L., Plavec, J., Lenarčič, B., and Djinović-Carugo, K. (2016) Structure and calcium-binding studies of calmodulin-like domain of human non-muscle α-actinin-1. *Sci. Rep.* **6,** 27383 CrossRef Medline
34. Rule, G. S., and Hitchens, T. K. (2006) Fundamentals of protein NMR spectroscopy. in *Focus on Structural Biology* (Kaptein, R., ed) pp. 530, Springer, Dordrecht
35. Zhou, Y., Frey, T. K., and Yang, J. J. (2009) Viral calciomics: interplays between Ca^{2+} and virus. *Cell Calcium* **46,** 1–17 CrossRef Medline
36. Moody, B. J. (1991) *Comparative Inorganic Chemistry* (Bernard, M., ed) 3rd Ed, pp. xiii and 562, Academic Press, Washington, D. C
37. Sepúlveda, M. R., Marcos, D., Berrocal, M., Raeymaekers, L., Mata, A. M., and Wuytack, F. (2008) Activity and localization of the secretory pathway Ca^{2+}-ATPase isoform 1 (SPCA1) in different areas of the mouse brain during postnatal development. *Mol. Cell. Neurosci.* **38,** 461–473 CrossRef Medline
38. Reinhardt, T. A., Filoteo, A. G., Penniston, J. T., and Horst, R. L. (2000) Ca^{2+}-ATPase protein expression in mammary tissue. *Am. J. Physiol. Cell Physiol* **279,** C1595–1602 CrossRef Medline
39. Llinás, R., Sugimori, M., and Silver, R. B. (1992) Microdomains of high calcium concentration in a presynaptic terminal. *Science* **256,** 677–679 CrossRef Medline

40. Aronchik, I., Behne, M. J., Leypoldt, L., Crumrine, D., Epstein, E., Ikeda, S., Mizoguchi, M., Bench, G., Pozzan, T., and Mauro, T. (2003) Actin reorganization is abnormal and cellular ATP is decreased in Hailey-Hailey keratinocytes. *J. Investig. Dermatol.* **121,** 681–687 CrossRef Medline
41. Elias, P., Ahn, S., Brown, B., Crumrine, D., and Feingold, K. R. (2002) Origin of the epidermal calcium gradient: regulation by barrier status and role of active *vs* passive mechanisms. *J. Investig. Dermatol.* **119,** 1269–1274 CrossRef Medline
42. Yamamoto, S., Takehara, M., Kabashima, Y., Fukutomi, T., and Ushimaru, M. (2016) Identification of novel inhibitors of human SPCA2. *Biochem. Biophys. Res. Commun.* **477,** 266–270 CrossRef Medline
43. Vandecaetsbeek, I., Holemans, T, Wuytack, F., and Vangheluwe, P. (2014) High-throughput measurement of the Ca^{2+}-dependent ATPase activity in COS microsomes. *Cold Spring Harb. Protoc.* **2014,** 865–875 Medline
44. Holemans, T., Sørensen, D. M., van Veen, S., Martin, S., Hermans, D., Kemmer, G. C., Van den Haute, C., Baekelandt, V., Günther Pomorski, T., Agostinis, P., Wuytack, F., Palmgren, M., Eggermont, J., and Vangheluwe, P. (2015) A lipid switch unlocks Parkinson's disease-associated ATP13A2. *Proc. Natl. Acad. Sci. U.S.A.* **112,** 9040–9045 CrossRef Medline
45. Davis, A. L., Keeler, J., Laue, E. D., and Moskau, D. (1992) Experiments for recording pure-absorption heteronuclear correlation spectra using pulsed field gradients. *J. Magn. Res.* **98,** 207–216 CrossRef
46. Grzesiek, S., and Bax, A. (1993) The importance of not saturating H_2O in protein NMR: application to sensitivity enhancement and NOE measurements. *J. Am. Chem. Soc.* **115,** 12593–12594 CrossRef

Note: The biphasic trend of SPCA1a curves in figure 2D, 2E, 6C and 6D were fitted with two separate logistic functions in order to obtain K_m values of each phase. The Ca^{2+}-dependent curves were fitted for the first phase from 0.0001 to 30 µM free Ca^{2+}, and for the second phase from 30 µM free Ca^{2+} to when the plateau is reached. The Mn^{2+}-dependent curves were fitted for the first phase from 0.0001 to 3 µM free Mn^{2+}, and for the second phase from 3 to when the plateau is reached.

Suppl. Fig. 1

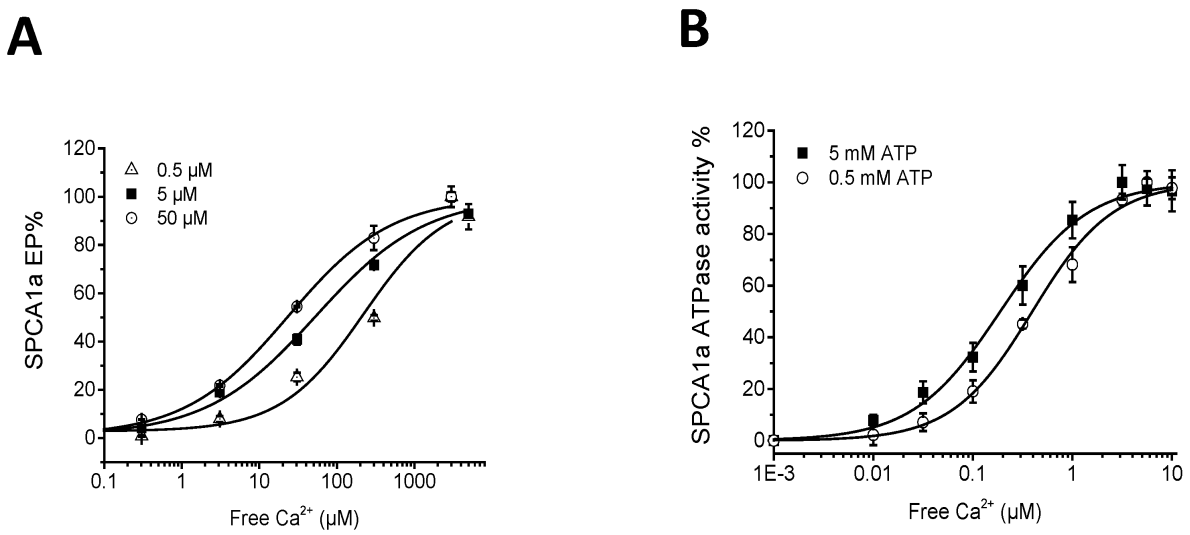

Suppl. Fig. 2

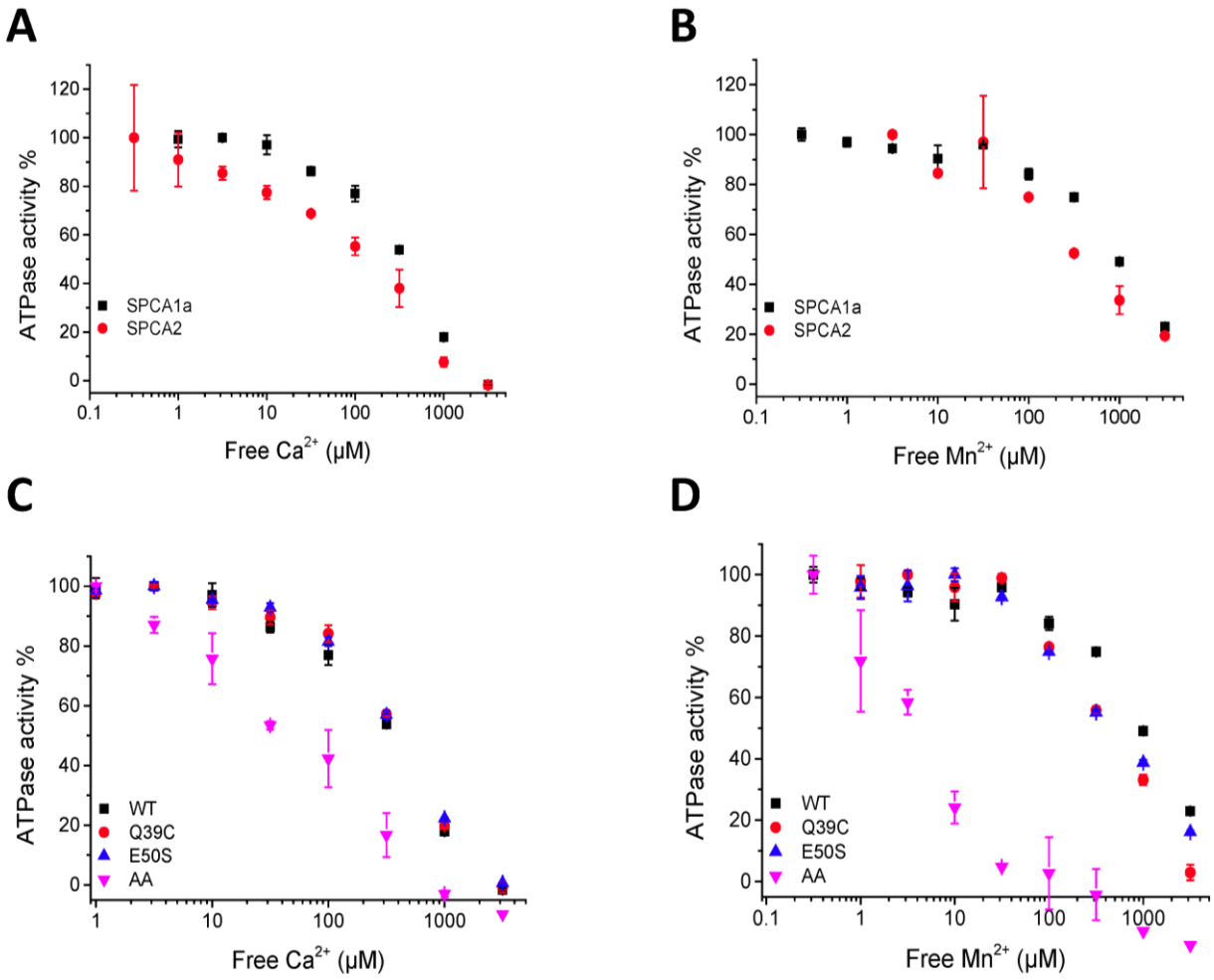

Suppl. Fig. 3

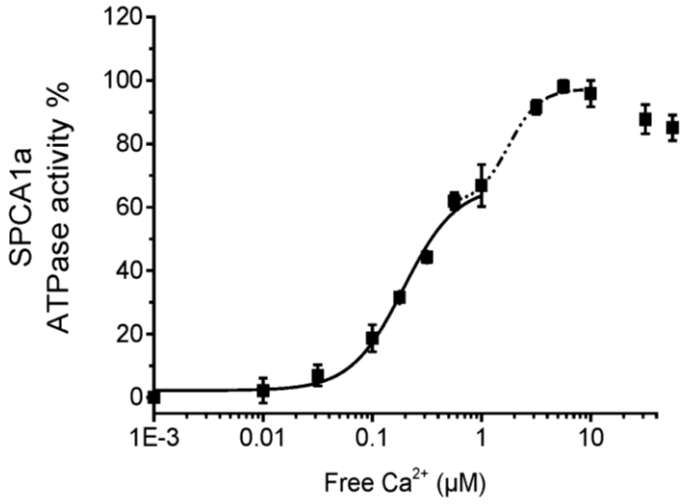

Suppl. Fig. 4

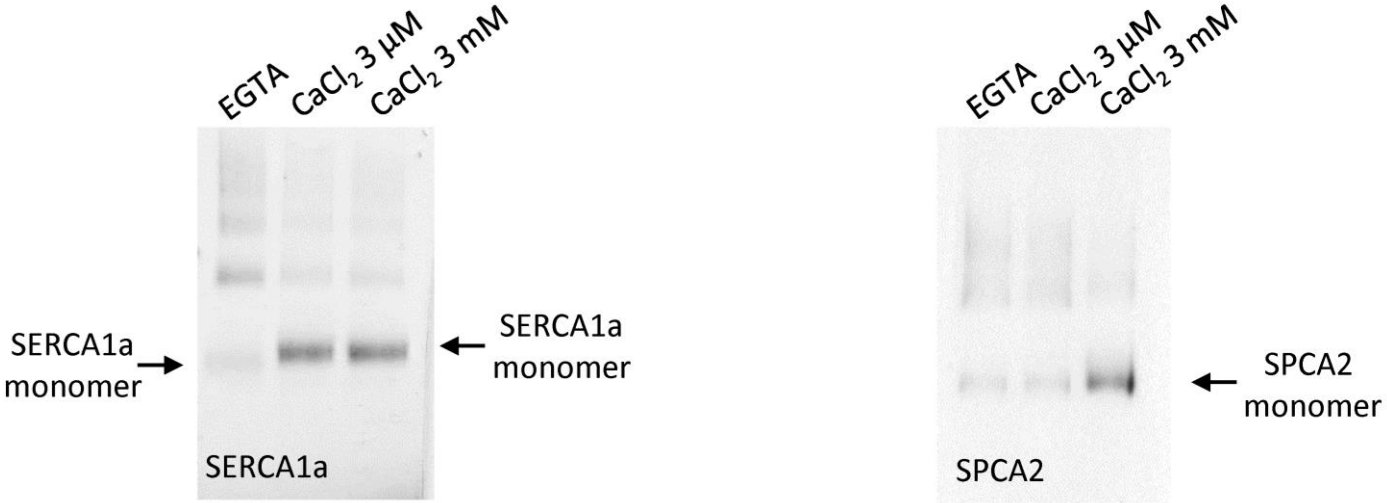

Suppl. Fig. 5

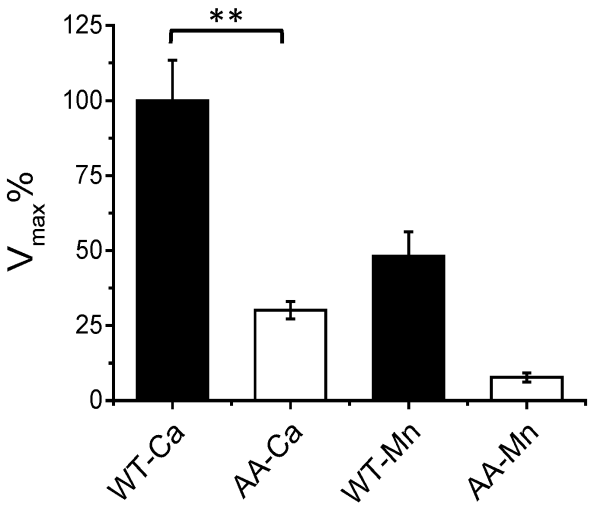

Suppl. Fig. 6

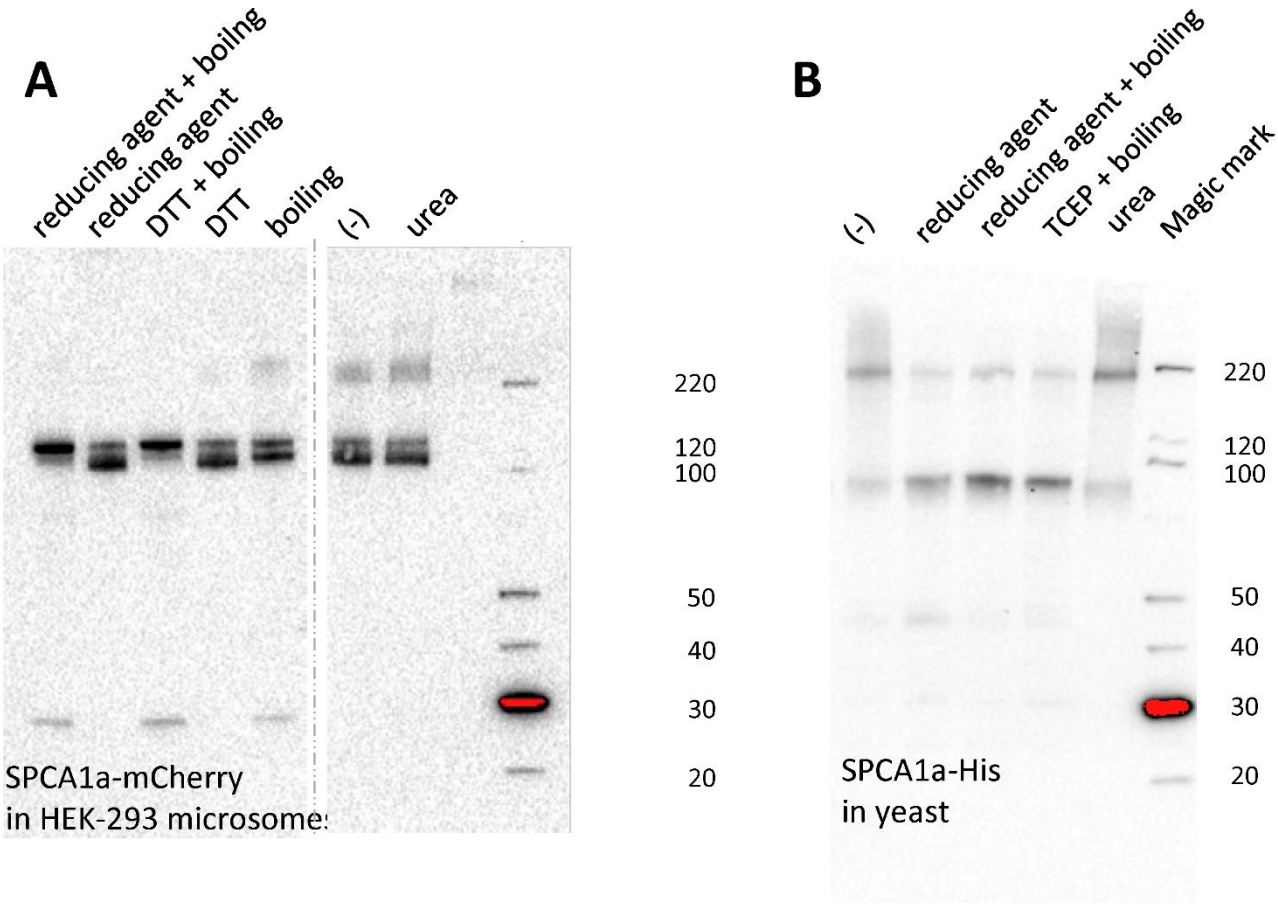

Title: An N-terminal Ca^{2+} binding motif regulates the secretory pathway Ca^{2+}/Mn^{2+}-ATPase SPCA1

Authors: Jialin Chen, Susanne Smaardijk, Charles-Alexandre Mattelaer, Filip Pamuła, Ilse Vandecaetsbeek, Jo Vanoevelen, Frank Wuytack, Eveline Lescrinier, Jan Eggermont, Peter Vangheluwe

Supplementary figure legends

Suppl. Fig. 1. Changes in ATP concentration affect the apparent Ca^{2+} affinity of SPCA1a
A. Ca^{2+} dependent phospho-intermediate levels at varying total ATP concentrations were quantified by radio-activity measurements. B. Ca^{2+} dependency of the ATPase activity at varying ATP concentrations (N = 4). The ATP concentrations was kept constant by a regenerating enzyme system. In both the auto-phosphorylation assay (A) and the enzyme-coupled ATPase assay (B), the apparent Ca^{2+} affinity of SPCA1a decreases when the ATP concentration is reduced. Increase of ATP concentration in the auto-phosphorylation assay increases the apparent Ca^{2+} affinity.

Suppl. Fig. 2. Back-inhibition of the ATPase activities at high Ca^{2+} or Mn^{2+} concentrations
ATPase activities were measured for wild-type SPCA1a and SPCA2 at Ca^{2+} (A) or Mn^{2+} (B) concentrations above 10 µM. This resulted in downward curves of ATPase activity, which reflect the back-inhibition of the pump. ATPase activities for SPCA1a wild-type and mutants at high Ca^{2+} (C) or Mn^{2+} (D) concentrations also displayed downward ATPase activity curves. One representative result is shown for each isoform or mutant. The standard deviation for each point is shown as error bar.

Suppl. Fig. 3. At 0.5 mM ATP, SPCA1a presents a biphasic activation pattern in ATPase assays
Via an enzyme-coupled assay, we determined the Ca^{2+} dependent ATPase activity of SPCA1a in the presence of 0.5 mM ATP. SPCA1a presents a two-step activation pattern (N = 4).

Suppl. Fig. 4. Native Page of purified SERCA1a and SPCA2 incubated with various amount of Ca^{2+}
SERCA1a (left) purified from skeletal muscle of rabbit or SPCA2 (right) overexpressed and purified from yeast were incubated with EGTA, 3 µM or 3 mM of $CaCl_2$, and separated by Native PAGE. The protein bands were visualized via de-staining for SERCA1a, or via immunoblotting for SPCA2 (SC376917, 1:2000, Santa Cruz). The monomer bands were indicated by arrows.

Suppl. Fig. 5. Maximal activities of the SPCA1a WT and the D41A/E50A mutant
ATPase activities (A) and auto-phosphorylation activity (B) of the D41A/E50A (AA) mutant normalized to the maximal activity of the WT in presence of Ca^{2+} (N = 3-6). One-way ANOVA was performed followed by *post-hoc* Bonferroni test. ** $P < 0.01$.

Suppl. Fig. 6. The effect of reducing agent and urea on SPCA1a obtained from microsomes
A. N-terminal mCherry tagged SPCA1a was overexpressed in HEK-293 cells. The microsome fraction was either not treated, or treated with reducing agent purchased from ThermoFisher Scientific Novex kit, with 40 mM reducing agent DTT, or with 8 M urea, with or without boiling, as indicated on top of each lane. Samples are then subjected to SDS-PAGE followed by immunoblotting using an SPCA1 antibody (Frodo, homemade, 1:50,000). B. Immunoblotting of the C-terminal His-tagged SPCA1a purified from yeast and reconstituted in proteoliposomes. The SPCA1a proteoliposomes are either not treated or treated with reducing agent purchased from ThermoFisher Scientific Novex kit, with 20 mM reducing agent TCEP and boiling, or with 8 M urea. These samples are then subjected to SDS-PAGE followed by immunoblotting with an SPCA1a antibody (Frodo, homemade, 1:50,000).

IV. General discussion and future perspectives

The understanding of Ca^{2+}-transporting ATPases has greatly advanced over the past decades, due to the availability of novel techniques, such as crystallography, cryo-EM and computational modelling. However, the amount of knowledge on each individual members of the Ca^{2+}-ATPase family is extremely imbalanced. For example, as compared to SERCA and PMCA isoforms, SPCAs remain relatively poorly characterized despite that they are implicated in many physiological and pathological processes, such as lactation/breast cancer, HHD, and manganese detoxification.

1. The proteoliposome system as an improved method to study SPCA1/2

To overcome the difficulties in studying the lowly abundant membrane protein SPCA1, we focused in the first part of this thesis on constructing proteoliposomal systems with purified SPCA1 or SPCA2. These systems eliminate the noise signals in biochemical assays as compared to isolated membrane fractions of cells expressing SPCAs, and prevent the denaturing effect from detergent micelles as compared to the detergent solubilized samples. Here, this system has proven to be a powerful tool for the functional characterization, and may be used for future drug discovery efforts. Proteoliposomes also allow further optimization and modification for other purposes. For example, giant unimicellar vesicles with a diameter above 20 µm are suitable for optical tweezers, micropipettes microelectrodes, or atomic force microscopy (190). Via total internal reflection microscopy, the transport activity could even be resolved at the single molecular level for the reconstituted proton pumps from *Arabidopsis thaliana*, which were tethered to a solid support (191). Therefore, the experience we gained in this work from SPCA overexpression, purification and reconstitution is a valuable exploration of the proteoliposome system that will allow detailed characterization of SPCA isoforms using more advanced techniques in the future and that may be transferred for studying other related membrane transporters.

In addition to the rational design of small molecule inhibitors, which we set up in this thesis, such a proteoliposome system can also be used in high throughput screening for small compounds that modulate SPCA activity. Compared to the detergent-solubilized membrane proteins, proteoliposomes not only offer better stability for the membrane proteins, but also provide a membrane barrier when membrane permeability/or luminal accessibility needs to be explored.

2. Stimulation of SPCA1 activity by lipids

This study has shown that the SPCA1 activity is influenced by lipids. To ensure the activity of SPCA after reconstitution, lipid extracts from native sources with mixed alkyl chain length (to avoid hydrophobic mismatch (192)) were chosen for each type of phospholipids. After supplementing 20% of another type of lipid to phosphatidylcholine, we observed differences in the specific SPCA1 ATPase activities. We cannot completely rule out the possibility that the lipid composition of the vesicles influenced the orientation of the inserted SPCA1 proteins, but we used minimal amount of detergent to destabilize the detergent, so that the insertion of SPCA proteins via the smaller luminal loops would be favored compared to the insertion via the huge cytoplasmic domains. Therefore, the changes of SPCA1 specific ATPase activity are most likely due to the lipid interaction with SPCA1.

Two lipids were identified to have a stimulatory effect on SPCA1 ATPase activity. Phosphatidic acid is a negatively charged lipid that protects the vesicles from aggregation and contributes to the stability of vesicles. It might also have a specific activation role on SPCA1, since other negatively charged lipids (phosphatidylserine and phosphatidylinositol) did not show any stimulation. Sphingomyelin, alone or in combination with cholesterol, also stimulated the SPCA1 activity. Cholesterol (or its derivative) by itself, however, showed a moderate and non-significant stimulation of SPCA1 at low doses, suggesting that sphingomyelin might be more important for SPCA1 stimulation than cholesterol. Sphingomyelin synthesis takes place in the Golgi compartment, whereas like the plasma membrane, the Golgi also contains lipid rafts that are enriched in sphingomyelin and cholesterol and with which SPCA1 preferably associates (193). These membrane microdomains have been suggested to play a role in protein sorting in polarized cells (194). It was also found that the actin severing protein cofilin-1 activates SPCA1, which is critical for Cab45 mediated secretory protein sorting (99,195). Together, the association and activation of SPCA1 with lipid rafts and cofilin-1 suggest a critical role of SPCA1 in protein sorting via Golgi/TGN. In contrast, the related SERCA1 is more sensitive to cholesterol inhibition (196). This is in accordance with its ER localization which is low in cholesterol content.

3. A deep narrow groove for Tg in SPCA1

Due to the hydrophobic nature, it has been suggested that the Tg binding pocket in SERCA may be a regulatory site for cholesterol (136). Via our mutagenesis study, we proved that a conserved Tg binding pocket formed by M3, M5 and M7 is present in SPCA. Recently, an *in silico* study on the plant P4-type ATPase ALA10 suggested that this region shapes a cavity that determines the lipid head group selectivity and that overlaps with the Tg binding pocket in SERCA (197). Therefore, the hydrophobic pocket is likely to be evolutionary conserved among P-type ATPases.

Among the Tg analogues tested, Leu8ADT showed improved SPCA1 binding affinity after overnight equilibration, similar to what has been reported for Boc8ADT on SERCA1, whereas the analogue in which the end Boc group is replaced with Leu, only takes minutes to equilibrate with SERCA1 (147). The crystal structure of Boc8ADT-SERCA1 showed that the compound binds to the same Tg cavity, but the long flexible linker pierced through the TM region and pointed to the Ca^{2+} gating residue E309 **(Figure 1)** (198). Considering the similar equilibration behavior for Boc8ADT and SERCA1 and for Leu8ADT and SPCA1, it is likely that the Leu8ADT is positioned similarly in SPCA1 as is Boc8ADT in SERCA1. In fact, this could also apply to other ligands. Linoleamide, which in this study was confirmed as an SPCA1 inhibitor, is very thin, long and flexible in structure. It possibly functions as a wedge to hinder the relative movements of the SPCA1 transmembrane domain, or may even reach the ion binding site and disrupt the Ca^{2+}/Mn^{2+} binding. Furthermore, reconstitution with the thin, linear detergent C12E8 renders SPCA1 inactive (our unpublished data), which might also reflect the inhibition of SPCA1 by a similar structural mechanism. This might be a useful feature to be integrated in the future design of SPCA inhibitors.

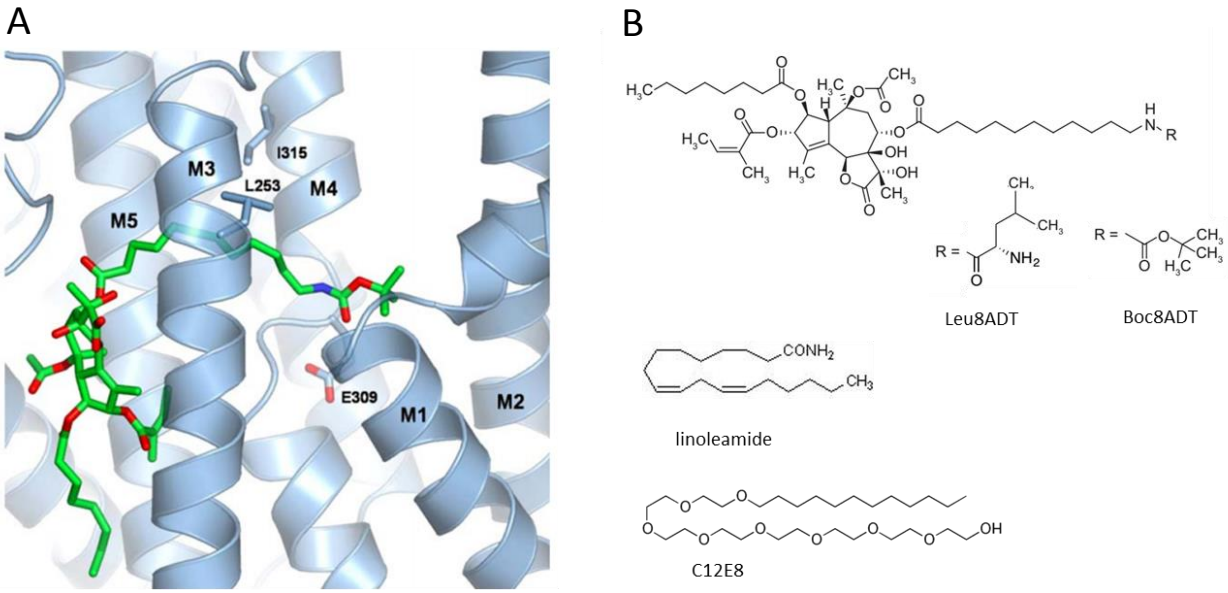

Figure 1. Structure of Boc8ADT binding to SERCA1a and the structures of compounds. A. Crystal structure of Boc8ADT in SERCA1a (PDB: 2BY4). The transmembrane helices are numbered. The sidechains of L253 and I315 have different conformations compared to SERCA-Tg structure (1IWO). The Boc group of Boc8ADT is located in a solvent exposed cavity between transmembrane helices 1, 2, 3 and 4, and close to the gating residue E309. Figure is taken from (198) in which the ligand is referred to as Boc12ADT whereas it is named Boc8ADT in (147) and in this figure. B. Structures of the mentioned Tg analogues, linoleamide and detergent C12E8.

4. Future design of SPCA1 specific inhibitors based on Tg analogues

The SAR comparisons of Tg inhibition in SPCA1 and SERCA1 suggested a similarly important role of the Tg scaffold in SERCA1/SPCA1 inhibition. However the Tg sidechains showed clear differences in their

contribution to SERCA1/SPCA1 inhibition. The Tg O3, O8 and O10 chains that critically contribute to the sub-nM affinity to SERCA1, played a negligible role in SPCA1. Whereas the Tg O2 chain minimally interacts with SERCA1 and hardly contributes to its inhibition, O2 contributed the most to the SPCA1-Tg binding energy among all the sidechains we measured. Therefore, this difference can be used to guide the design of a Tg analogue with increased specificity for SPCA1. For example, Tg analogues with modification on one of the O3, O8 and O10 groups in combination with deletion of two other chains could be tested on SPCA1, to explore the preferred interaction within the SPCA1 pocket at the surrounding of these sidechains. Any substitutions at these sidechains that result in a better SPCA1 inhibition could be combined and modified for the second round to obtain an improved SPCA1 inhibitor. Since Tg binds to SERCA1 with almost perfect complementarity, we suppose most of the changes made on Tg would lead to the reduction in SERCA1 binding affinity. Nevertheless, new analogues should be tested on SERCA1 for confirmation of improved specificity toward SPCA1.

5. The discrepancy between the phosphorylation and the ATPase assay in relation to the active state distribution

Experimental assays to measure kinetic parameters of P-type ATPases may yield quantitatively different outcomes for the same parameter due to differences in the read out of the assay or the experimental conditions. In the ATPase assay, the K_m values represent the concentration of Ca^{2+}/Mn^{2+} to reach the half maximal ATP hydrolysis rate, which is normally coupled to the Ca^{2+}/Mn^{2+} transport. In the phosphorylation assay of P2-type ATPases, the signal arises from the partial reaction of the pump from a non-phosphorylated state to a phosphorylated state (either E1P or E2P), without turning over to the next cycle. In this case the K_m represents the concentration of Ca^{2+}/Mn^{2+} to reach half of the maximal EP accumulation.

A single molecule study on the reconstituted proton pump from *Arabidopsis thaliana* AHA2 suggested that the activity of an individual pump molecule is not constant over time, and that it switches instead between active and inactive states (even leaky states) (191). According to this theory and for the sake of this discussion, we assume the SPCA1 pump to be distributed in three states (not considering the leaky states for simplification): 1) The inactive state, in which SPCA1 always remains inactive. This can be due to degradation, or defects in folding after extensive preparations. 2) The less active state, in which the pump is active for a short period of time. 3) The more active state, in which the pump is in the active state for a longer period of time. The sum of the three states accounts for the total amount of SPCA1 in our experiments, but each state contributes differently to the overall SPCA1 activity **(Figure 2)**.

In macroscopic assays such as the ATPase and phosphorylation assays, the results represent the combined effects of the intrinsic pump activity and the active-state probability distribution (191). Therefore, besides the experimental conditions (such as differences in ATP concentration and assay temperature), there are intrinsic differences between the two assays. The phosphorylation assay emphasizes the equality of each single active pump: once a pump is switched to the active state and becomes phosphorylated, the assay takes into account its signal. Therefore, both active fractions (active+ and active+++) of SPCA1 contribute equally to the outcome of the autophosphorylation assay. In contrast, the results of the ATPase assay are dominated by the SPCA1 pumps in the highly active state (fraction active +++), because overtime these pumps split more ATP than those that spend less time in the active state (fraction active +). Hence, the phosphorylation assay is better suited for interpreting the mechanistic aspects of the pump, since each active molecule can only give one signal at equal level (one phosphorylation per molecule at the catalytic Asp). The ATPase assay is better suited to look at the population level, since the more active pumps are contributing more strongly than the less active pumps.

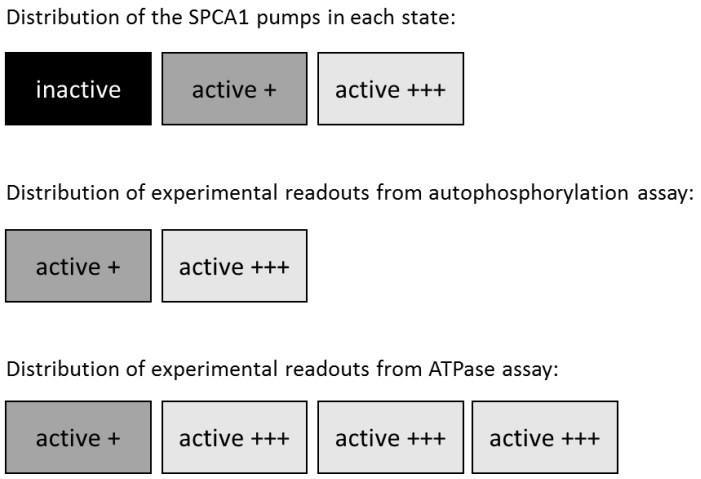

Figure 2. Distributions of SPCA1 in different states. SPCA1 can reside in either of three (in)activity states (top). However, these activity states contribute differently to the outcome of the autophosphorylation assay (middle) versus the ATPase assay (bottom).

6. Possible mechanisms of N-terminal regulation of SPCA1

In the phosphorylation assay, a unique bi-phasic profile in the SPCA1 EP formation was observed. SPCA1 phosphoenzyme formation could be stimulated by both substrates at higher concentration. However, the effect in the presence of Ca^{2+} was much more pronounced than for Mn^{2+}, suggesting a Ca^{2+} specific concentration dependent activation mechanism. This Ca^{2+} specific stimulation effect on phosphorylation became less prominent when SPCA1 was mutated at the N-terminal EF-hand-like

motif, indicating this Ca^{2+}-binding motif was involved in the stimulation. Furthermore, we noticed that SPCA1 was sensitive to the ATP concentration: higher ATP concentrations shifted the Ca^{2+}-dependent activation curve to the left, allowing SPCA1 to operate already at lower Ca^{2+} concentrations.

Based on these findings, we propose that the activation of SPCA1 might involve interaction between two structural elements: 1) The N-terminal EF-hand-like motif that upon binding of Ca^{2+} leads to further activation of SPCA1a (second EP phase); and 2) a region at or near the ATP binding pocket that is sensitive to the ATP concentration in the environment. Taking the two elements into consideration, we propose a model in which the N-terminal region works as an auto-inhibitory domain that folds back onto the N-/P-domain. In doing so the N-terminus of SPCA1 might not only restrict the access of ATP for auto-phosphorylation to occur, but may also hinder the movement of the A-domain and reduce the turnover rate. When the Ca^{2+} level in the local environment increases, Ca^{2+} binds to the N-terminus, which may prevent the interaction of the N-terminus to the N-/P-domain, allowing easier access of ATP for phosphorylation. In addition and still according to this model, we assume that high ATP concentrations will activate the pump by competing with and displacing the N-terminus **(Figure 3)**.

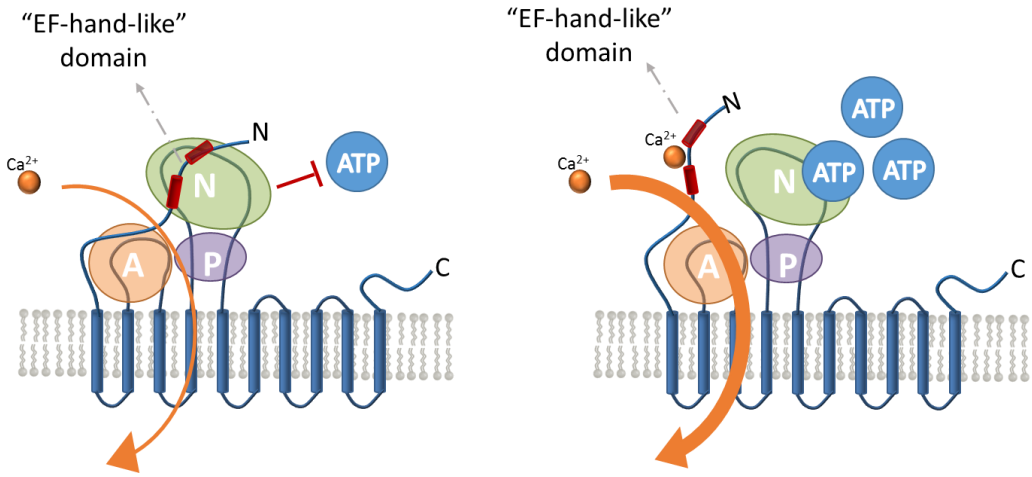

Figure 3. A possible model of SPCA1 activation mechanism. In the ground states (left) the N-terminal EF-hand-like domain does not bind Ca^{2+} and is folded onto the loop where N-/P-domain is. This hinders the accessibility of ATP to catalyze the auto-phosphorylation step. When cytosolic Ca^{2+} level rises (right), the N-terminal EF-hand-like domain binds Ca^{2+} and the accompanied conformational change makes the ATP-binding pocket on the N-domain available. This activation can also be achieved by having more ATP in the solution.

Although this hypothesis needs further experimental validation, such as looking into the interaction sites between the N-terminus and the N-/P-domain, it is supported by some prior knowledge of the yeast orthologue PMR1 and other Ca^{2+}-transport ATPases. Wei *et al.* found that the N-terminal EF-hand-like domain of PMR1 protects the partial trypsinolysis of the region including the ATP-binding site, suggesting the possible interaction between the two regions (69). In the human PMCA pump, it is

well-studied that the C-terminal auto-inhibitory domain binds to two regions in the main body, including a cytosolic region in the N-domain (199). The auto-inhibition is relieved when Ca^{2+}-loaded calmodulin binds to the C-terminus (199). Moreover, interfering with ATP binding is a mechanism shared by some inhibitors of the Ca^{2+}-transport ATPases. For example, binding of curcumin and flavonoids to SERCA induces a conformational change and prevents ATP from binding (141). Furthermore, cofilin-1 activates SPCA1 by binding to the P-domain (99), indicating that the large cytosolic loop is a site for regulation. Therefore, it will be interesting to further verify the molecular mechanisms of the Ca^{2+}-specific activation of SPCA1a. Insights in the auto-inhibition mechanism can be useful in designing peptides or its mimetics for inhibition-activation regulation.

7. Different physiological roles of SPCA1 and SPCA2

SPCA2 evolved from a gene duplication of SPCA1 after the split between fish and amphibia (27), and it shows a restricted expression pattern mainly in secreting cells, suggesting a specialized function in these cells. It was found that the coupling between the SPCA2 C-terminus and Orai1 activates the Ca^{2+} influx through the Orai1 channel (10). This mechanism is important during lactation when SPCA2 expression is highly elevated. Notably, a C-terminal SPCA2 splice variant of ~20 kDa is expressed under the regulation of the transcription factor MIST1 in cells specialized with active regulated exocytosis, which may be a modulator of the SPCA2-Orai1 mediated Ca^{2+} import (200).

SPCA1 is evolutionary older and serves a housekeeping function in mammals, like PMR1 in lower eukaryotes such as fungi, worm and fly (27). SPCA1 is responsible for a high affinity basal Ca^{2+} uptake into Golgi compartments and TGN at resting conditions, thereby ensuring the proper functioning of Golgi-resident enzymes. The expression of SPCA1 is also significantly upregulated during lactation, suggesting that besides a housekeeping role, SPCA1 may also play a more specialized role when needed (13,201). Upon overexpression, SPCA1 can be found in sub-plasma membrane areas activating Orai1 for increased cellular Ca^{2+} uptake (11). The SPCA1 proteins that are in close vicinity to Orai1 might sense the higher Ca^{2+} level with their N-terminal EF-hand-like motifs and shift to the more active state. This could result in more Ca^{2+} being transported into the secretory pathway while the cytosolic Ca^{2+} concentration will not rise above a toxic level.

Defects in SPCA1 are also implicated in HHD skin disease that only affects keratinocytes (OMIM 169600). The symptoms are exacerbated during mechanical stress such as friction, which could cause Ca^{2+} waves with increased $[Ca^{2+}]_{cyt}$ in these cells (202). Due to the lower ATP concentration in keratinocytes compared to other cell types (203), the Ca^{2+} activated SPCA1 activity might be more

important than in other cell types. Hence it might partially explain why the phenotypic consequences of heterozygous mutations in SPCA1 only affect the skin.

8. Extending the functional characterization to Ca^{2+} transport assays

As was mentioned in the introduction, substrate transport activity of P-type ATPases is powered by ATP hydrolysis. In normal conditions, movements at the TM region during substrate binding and release are transmitted to the cytoplasmic domain for ATP binding and hydrolysis, ADP release and finally dephosphorylation, and vice versa (26). Hence substrate transport and ATP hydrolysis are tightly coupled. In this study, we limited the functional characterization to the ATPase and phosphorylation assays, which indirectly reflect the Ca^{2+}/Mn^{2+} transport activity of SPCA. More recently, it has been reported for SERCA and PMCA that uncoupling of transport and ATPase activity occurs in certain conditions, for example under the regulation of SLN (155) or when the pumps are mutated (51). In the absence of substrate one can easily detect uncoupling via the ATPase assay. However, in the presence of transported substrate it is not possible to differentiate in the ATPase assay whether ATP hydrolysis is used for pumping or is expended as heat in our ATPase setup.

The transport activity can be determined via a transport assay, which is in theory feasible in vesicular systems such as proteoliposomes. In case of SPCA, the Ca^{2+} transported into the vesicles can be either read out as radioactivity (by using $^{45}Ca^{2+}$), or converted into a fluorescence signal (by trapping fluorescent dye in the vesicles) (204). Since SPCA transport is electrogenic (there is no countertransport of protons) (27), one might adsorb proteoliposomes onto electrodes and follow the change of electric signals from the imported ions, which can be either Ca^{2+} or Mn^{2+} (205).

However, to be able to measure the ion transport activity, further optimization and characterization of the proteoliposome system will be required. Firstly, the lipid bilayer of vesicles needs to be tightly sealed and impermeable to the transported ions. Secondly, it would be preferable to have large unimicellar vesicles with low protein density. In this case ion transport can occur for a longer time without causing back inhibition even when oxalate is not present.

V. Summary

The organnellar P2-type Ca^{2+}-transport ATPases, namely sarco/endoplasmic reticulum Ca^{2+}-ATPase (SERCA) and secretory pathway Ca^{2+}-ATPase (SPCA), are essential to maintain a low resting cytosolic Ca^{2+} level. At the same time they load respectively the intracellular endoplasmic reticulum (ER) and Golgi stores with Ca^{2+}. This allows Ca^{2+} signaling to occur and it supports several organellar processes such as protein folding and maturation. Besides Ca^{2+}, SPCA also transports Mn^{2+}. The structure of SERCA1a has been solved by crystallography in different conformational states of the transport cycle. It serves as an excellent template for exploring and understanding the structural features of SPCA that share 40% sequence similarity with SERCA. The study of SPCA pumps in cells is hampered because its enzymatic readouts are overshadowed by the stronger signals of the more active SERCA and PMCA Ca^{2+}-ATPases. We therefore set up a purified, native-like proteoliposome system for the two SPCA isoforms SPCA1 and SPCA2, which was used throughout the two projects in this thesis.

In the first chapter, we showed that the SPCA1 ATPase activity was activated by various lipids, especially sphingomyelin and phosphatidic acid. Next, we explored the possibility to develop an SPCA1 specific inhibitor based on the SERCA1 specific inhibitor thapsigargin (Tg). To this end, we proved with the mutagenesis study that Tg bound to SPCA1 at a conserved pocket similar to SERCA1. Next, by comparing the variable inhibition potencies of Tg analogues on SPCA1, we characterized the structure-activity relationship on SPCA1. Our results showed that the Tg sidechains O3, O8 and O10, that critically contribute to SERCA1 inhibition, were only weakly involved in SPCA1 inhibition. It is therefore possible to alter the specificity of Tg towards SPCA by modifying these SERCA-critical sidechains into more SPCA1 compatible groups.

In the second chapter, we compared side by side the Ca^{2+}- and Mn^{2+}-dependent SPCA1 and SPCA2 activities. Based on the ATPase and auto-phosphorylation assays, we determined the Ca^{2+} and Mn^{2+} affinities and turnover rates for both SPCA1 and SPCA2. We found that SPCA1 had a higher affinity for Mn^{2+} than for Ca^{2+}, which was opposite for SPCA2. SPCA1 displayed a higher Ca^{2+} turnover rate compared to Mn^{2+}, while SPCA2 showed similar turnover rates for both substrates.

Unlike SPCA2, the Ca^{2+}- and Mn^{2+}-dependent autophosphorylation of SPCA1 presented a biphasic behavior. Micromolar concentration of Ca^{2+} dramatically stimulated SPCA1 phospho-enzyme formation at low ATP concentration, while the stimulation by micromolar Mn^{2+} was moderate. Since the N-terminus of the yeast orthologue PMR1 contains a Ca^{2+} binding regulatory EF-hand-like motif, we investigated the role of this conserved region in SPCA1 by mutagenesis. The SPCA1 N-terminal mutants displayed reduced Ca^{2+} binding and a stronger increase in the affinity for Ca^{2+} than for Mn^{2+}

in both the ATPase assay and the first phase of the phosphorylation assay. The latter suggests that a larger fraction of SPCA1 mutants compared to WT were active at a physiological Ca^{2+} concentration. At the same time, the relative magnitude of activation by the second phase was lowered. Taken together, these results suggest that the N-terminal region indeed plays a role in SPCA1 activation, in particular by Ca^{2+}, and may at least partially be responsible for the different enzymatic activities between SPCA1 and SPCA2.

We also showed that the Ca^{2+} affinity of SPCA1 was sensitive to the ATP concentrations in the reaction medium, and that higher amounts of ATP promoted the phospho-enzyme formation at lower Ca^{2+} concentrations. Therefore, in a cellular context in the presence of millimolar ATP, SPCA1 activation can be achieved at physiologically relevant Ca^{2+} concentrations in a microdomain close to a Ca^{2+} channel. On the other hand, the combinatorial effect of ATP and Ca^{2+} on SPCA activity may come into action in keratinocytes, in which the cytosolic ATP level is lower compared to other cell types, whereas the cytosolic Ca^{2+} concentration is higher, *e.g.* after mechanical stimulation.

In conclusion, we showed that a purified and reconstituted system is a useful tool for the functional and pharmacological exploration of SPCA. More specifically, this thesis contributes to a better understanding of Tg inhibition of SPCA1 as well as the biochemical properties and differences in the regulation of SPCA1/2.

VI. Samenvatting

De intracellulaire P2-type Ca^{2+}-transport ATPasen zijn gelokaliseerd in het endoplasmatisch reticulum (SERCA) en het Golgi complex (SPCA). Zij verwijderen Ca^{2+} uit het cytosol en zorgen zo voor een lage cytosolaire Ca^{2+}-concentratie. Tegelijkertijd stapelen SERCA en SPCA Ca^{2+} op in het lumen van respectievelijk het endoplasmatisch reticulum en het Golgi complex. SPCA transporteert ook Mn^{2+}. Door hun transportactiviteit creëren deze Ca^{2+} pompen de gepaste condities voor intracellulaire signaaltransductie via Ca^{2+} en ondersteunen zij ook Ca^{2+} afhankelijke processen in het endoplasmatisch reticulum en het Golgi complex zoals eiwitvouwing en -maturatie.

De studie van SPCA-pompen in de cel wordt bemoeilijkt, enerzijds door de sterkere enzymatische activiteit van de andere P2-type Ca^{2+}-ATPasen, SERCA en PMCA, en anderzijds door de afwezigheid van een experimenteel geverifieerd structuurmodel van SPCA. We ontwikkelden daarom een testsysteem op basis van proteoliposomen waarin gezuiverde SPCA eiwitten in een dubbellaag van lipiden gereconstitueerd werden. Deze reconstitutie bleek van cruciaal belang in de gedetailleerde karakterisering van de SPCA activiteit en vormde de basis van de twee projecten in dit proefschrift. Naast de constructie van het proteoliposoomsysteem toonden we aan dat verschillende lipiden, voornamelijk sfingomyeline en fosfatidinezuur, de SPCA1-ATPase-activiteit stimuleerden. Vervolgens hebben we de mogelijkheid onderzocht om een SPCA1-specifieke remmer te ontwikkelen op basis van de SERCA-specifieke inhibitor thapsigargin (Tg). Hiervoor hebben we ons gebaseerd op de gekende kristalstructuur voor verschillende conformaties van het Ca^{2+}-ATPase SERCA1a. Door de 40% gelijkenis in aminozuursequentie tussen SERCA en SPCA1, fungeert de kristalstructuur van SERCA als een uitstekend sjabloon voor het onderzoeken van de structurele kenmerken van SPCA. Via een mutagenesestudie hebben we aangetoond dat Tg bond in een regio die geconserveerd is in zowel SPCA1 als SERCA. Door de vergelijking van het inhibitorische effect van verschillende Tg-analogen op SPCA1 karakteriseerden we vervolgens de structuur-activiteitsrelatie op SPCA1. Onze resultaten tonen aan dat de Tg-zijketens O3, O8 en O10 die kritisch bijdragen aan SERCA1-inhibitie, slechts minimaal betrokken waren bij SPCA1-inhibitie. Het is dus mogelijk om de specificiteit van Tg voor SPCA te wijzigen door deze SERCA-kritische zijketens aan te passen naar meer SPCA1-specifieke groepen.

In het tweede hoofdstuk hebben we verschillende biochemische parameters van SPCA1 en SPCA2 activiteit vergeleken en de mogelijkheid onderzocht of het N-terminale gedeelte van SPCA belangrijk is voor de regeling van de enzymatische activiteit. Verder hebben we de Ca^{2+}- en Mn^{2+}-afhankelijke SPCA1- en SPCA2-activiteiten met elkaar vergeleken. Op basis van de ATPase en autofosforylering assays hebben we voor zowel SPCA1 als SPCA2 de Ca^{2+} en Mn^{2+} affiniteiten en de maximale enzymatische activiteit bepaald. In tegenstelling tot SPCA2 had SPCA1 een hogere affiniteit voor Mn^{2+}

dan voor Ca^{2+}. Verder ontwikkelde SPCA1 een hogere maximale enzymatische activiteit in aanwezigheid van Ca^{2+} dan in aanwezigheid van Mn^{2+}, terwijl voor SPCA2 de maximale snelheden voor beide substraten vergelijkbaar waren. Daarenboven vertoonde de grafiek van de SPCA1 activiteit een bifasisch verloop voor zowel de Ca^{2+}- als de Mn^{2+}-afhankelijke autofosforylering, terwijl een sigmoïdaal verloop geobserveerd werd voor de SPCA2 autofosforylering. Tot slot hadden micromolaire concentraties van Ca^{2+} bij lage ATP-concentratie een sterker effect op de autofosforylering van SPCA1 dan micromolaire concentraties van Mn^{2+}.

Vermits de N-terminus van het gistortholoog PMR1 een Ca^{2+}-bindend "EF-hand-like" motief bevat, hebben we de rol van deze geconserveerde regio in SPCA1 onderzocht door middel van mutagenese. SPCA1 N-terminale mutanten met verminderde Ca^{2+}-binding vertoonden een sterkere toename in de affiniteit voor Ca^{2+} dan voor Mn^{2+}, in zowel de ATPase assay als in de eerste fase van de autofosforylering. Bovendien bleek uit de autofosforyleringsexperimenten dat bij fysiologische Ca^{2+}-concentratie een grotere fractie van SPCA1-mutanten actief was in vergelijking met wild type SPCA1. Terzelfdertijd vertoonden de N-terminale mutanten van SPCA1 een lagere relatieve activering in het tweede deel van de bifasische autofosforylering. Samengevat suggereren deze resultaten dat de N-terminale regio inderdaad een rol speelt bij de activering van SPCA1, vooral dan in aanwezigheid van Ca^{2+}, en dat deze regio bijdraagt aan de verschillende enzymatische activiteiten van SPCA1 en SPCA2.
Tot slot toonden we ook aan dat de Ca^{2+}-affiniteit van SPCA1 beïnvloed werd door de concentratie van ATP in het reactiemedium. Autofosforylering van SPCA1 kon optreden bij lagere Ca^{2+}-concentraties indien de ATP-concentratie voldoende hoog was. Bij een lagere cytosolische concentratie van ATP was een hogere concentratie Ca^{2+} nodig voor activatie. De regeling van SPCA1 door een combinatie van ATP en Ca^{2+} kan een rol spelen in keratinocyten, waar de cytosolische concentratie van ATP lager is in vergelijking met andere celtypes, maar tegelijk de cytosolische Ca^{2+}-concentratie hoger is na bijvoorbeeld mechanische stimulatie.

Samengevat toonden we aan dat een gezuiverd en gereconstitueerd systeem niet alleen een robuust testsysteem is, maar ook een onmisbaar hulpmiddel voor de functionele en farmacologische karakterisering van SPCA. Meer specifiek draagt dit proefschrift bij aan een beter begrip van de inhibitie van SPCA1 door Tg en werpt het een licht op de biochemische eigenschappen en verschillen in de regeling van SPCA1 en SPCA2.

References

1. Monteith, G. R., McAndrew, D., Faddy, H. M., and Roberts-Thomson, S. J. (2007) Calcium and cancer: targeting Ca^{2+} transport. *Nat Rev Cancer* **7**, 519-530
2. Berridge, M. J., Bootman, M. D., and Roderick, H. L. (2003) Calcium signalling: dynamics, homeostasis and remodelling. *Nat Rev Mol Cell Biol* **4**, 517-529
3. Carafoli, E. (1987) Intracellular calcium homeostasis. *Annu Rev Biochem* **56**, 395-433
4. Pizzo, P., Lissandron, V., and Pozzan, T. (2010) The trans-golgi compartment: A new distinct intracellular Ca^{2+} store. *Commun Integr Biol* **3**, 462-464
5. Van Baelen, K., Vanoevelen, J., Callewaert, G., Parys, J. B., De Smedt, H., Raeymaekers, L., Rizzuto, R., Missiaen, L., and Wuytack, F. (2003) The contribution of the SPCA1 Ca^{2+} pump to the Ca^{2+} accumulation in the Golgi apparatus of HeLa cells assessed via RNA-mediated interference. *Biochem Biophys Res Commun* **306**, 430-436
6. Vanoevelen, J., Raeymaekers, L., Dode, L., Parys, J. B., De Smedt, H., Callewaert, G., Wuytack, F., and Missiaen, L. (2005) Cytosolic Ca^{2+} signals depending on the functional state of the Golgi in HeLa cells. *Cell Calcium* **38**, 489-495
7. Hoffmann, H. H., Schneider, W. M., Blomen, V. A., Scull, M. A., Hovnanian, A., Brummelkamp, T. R., and Rice, C. M. (2017) Diverse viruses require the calcium transporter SPCA1 for maturation and spread. *Cell Host Microbe* **22**, 460-470 e465
8. Liou, J., Kim, M. L., Heo, W. D., Jones, J. T., Myers, J. W., Ferrell, J. E., and Meyer, T. (2005) STIM is a Ca^{2+} sensor essential for Ca^{2+}-store-depletion-triggered Ca^{2+} influx. *Curr Biol* **15**, 1235-1241
9. Prakriya, M., and Lewis, R. S. (2015) Store-operated calcium channels. *Physiol Rev* **95**, 1383-1436
10. Feng, M., Grice, D. M., Faddy, H. M., Nguyen, N., Leitch, S., Wang, Y., Muend, S., Kenny, P. A., Sukumar, S., Roberts-Thomson, S. J., Monteith, G. R., and Rao, R. (2010) Store-independent activation of Orai1 by SPCA2 in mammary tumors. *Cell* **143**, 84-98
11. Smaardijk, S., Chen, J., Kerselaers, S., Voets, T., Eggermont, J., and Vangheluwe, P. (2018) Store-independent coupling between the Secretory Pathway Ca^{2+} transport ATPase SPCA1 and Orai1 in Golgi stress and Hailey-Hailey disease. *Biochim Biophys Acta* **1865**, 855-862
12. Smaardijk, S., Chen, J., Wuytack, F., and Vangheluwe, P. (2017) SPCA2 couples Ca^{2+} influx via Orai1 to Ca^{2+} uptake into the Golgi/secretory pathway. *Tissue Cell* **49**, 141-149
13. Cross, B. M., Hack, A., Reinhardt, T. A., and Rao, R. (2013) SPCA2 regulates Orai1 trafficking and store independent Ca2+ entry in a model of lactation. *PLoS One* **8**, e67348
14. Carafoli, E., and Krebs, J. (2016) Why Calcium? How Calcium Became the Best Communicator. *J Biol Chem* **291**, 20849-20857
15. Zhou, Y., Frey, T. K., and Yang, J. J. (2009) Viral calciomics: interplays between Ca2+ and virus. *Cell Calcium* **46**, 1-17
16. Kretsinger, R. H., and Nockolds, C. E. (1973) Carp muscle calcium-binding protein. II. Structure determination and general description. *J Biol Chem* **248**, 3313-3326
17. Lapinskas, P. J., Cunningham, K. W., Liu, X. F., Fink, G. R., and Culotta, V. C. (1995) Mutations in PMR1 suppress oxidative damage in yeast cells lacking superoxide dismutase. *Mol Cell Biol* **15**, 1382-1388
18. Powell, J. T., and Brew, K. (1976) Metal ion activation of galactosyltransferase. *J Biol Chem* **251**, 3645-3652
19. Missiaen, L., Raeymaekers, L., Dode, L., Vanoevelen, J., Van Baelen, K., Parys, J. B., Callewaert, G., De Smedt, H., Segaert, S., and Wuytack, F. (2004) SPCA1 pumps and Hailey-Hailey disease. *Biochem Biophys Res Commun* **322**, 1204-1213
20. Takeda, A. (2003) Manganese action in brain function. *Brain Res Brain Res Rev* **41**, 79-87
21. Lucchini, R. G., Martin, C. J., and Doney, B. C. (2009) From manganism to manganese-induced parkinsonism: a conceptual model based on the evolution of exposure. *Neuromolecular Med* **11**, 311-321

22. Sepulveda, M. R., Wuytack, F., and Mata, A. M. (2012) High levels of Mn^{2+} inhibit secretory pathway Ca^{2+}/Mn^{2+}-ATPase (SPCA) activity and cause Golgi fragmentation in neurons and glia. *J Neurochem* **123**, 824-836
23. Ton, V. K., Mandal, D., Vahadji, C., and Rao, R. (2002) Functional expression in yeast of the human secretory pathway Ca^{2+}, Mn^{2+}-ATPase defective in Hailey-Hailey disease. *J Biol Chem* **277**, 6422-6427
24. Leitch, S., Feng, M., Muend, S., Braiterman, L. T., Hubbard, A. L., and Rao, R. (2011) Vesicular distribution of Secretory Pathway Ca^{2+}-ATPase isoform 1 and a role in manganese detoxification in liver-derived polarized cells. *Biometals* **24**, 159-170
25. Sepulveda, M. R., Dresselaers, T., Vangheluwe, P., Everaerts, W., Himmelreich, U., Mata, A. M., and Wuytack, F. (2012) Evaluation of manganese uptake and toxicity in mouse brain during continuous $MnCl_2$ administration using osmotic pumps. *Contrast Media Mol Imaging* **7**, 426-434
26. Palmgren, M. G., and Nissen, P. (2011) P-type ATPases. *Annu Rev Biophys* **40**, 243-266
27. Vangheluwe, P., Sepulveda, M. R., Missiaen, L., Raeymaekers, L., Wuytack, F., and Vanoevelen, J. (2009) Intracellular Ca2+- and Mn2+-transport ATPases. *Chem Rev* **109**, 4733-4759
28. Sitsel, A., De Raeymaecker, J., Drachmann, N. D., Derua, R., Smaardijk, S., Andersen, J. L., Vandecaetsbeek, I., Chen, J., De Maeyer, M., Waelkens, E., Olesen, C., Vangheluwe, P., and Nissen, P. (2019) Structures of the heart specific SERCA2a Ca^{2+}-ATPase. *EMBO J* **38**
29. Gong, D., Chi, X., Ren, K., Huang, G., Zhou, G., Yan, N., Lei, J., and Zhou, Q. (2018) Structure of the human plasma membrane Ca^{2+}-ATPase 1 in complex with its obligatory subunit neuroplastin. *Nat Commun* **9**, 3623
30. Toyoshima, C., Nakasako, M., Nomura, H., and Ogawa, H. (2000) Crystal structure of the calcium pump of sarcoplasmic reticulum at 2.6 A resolution. *Nature* **405**, 647-655
31. Clausen, J. D., McIntosh, D. B., Anthonisen, A. N., Woolley, D. G., Vilsen, B., and Andersen, J. P. (2007) ATP-binding modes and functionally important interdomain bonds of sarcoplasmic reticulum Ca2+-ATPase revealed by mutation of glycine 438, glutamate 439, and arginine 678. *J Biol Chem* **282**, 20686-20697
32. Hovnanian, A. (2007) SERCA pumps and human diseases. *Subcell Biochem* **45**, 337-363
33. Dally, S., Monceau, V., Corvazier, E., Bredoux, R., Raies, A., Bobe, R., del Monte, F., and Enouf, J. (2009) Compartmentalized expression of three novel sarco/endoplasmic reticulum Ca2+ATPase 3 isoforms including the switch to ER stress, SERCA3f, in non-failing and failing human heart. *Cell Calcium* **45**, 144-154
34. Brandl, C. J., deLeon, S., Martin, D. R., and MacLennan, D. H. (1987) Adult forms of the Ca^{2+}-ATPase of sarcoplasmic reticulum. Expression in developing skeletal muscle. *J Biol Chem* **262**, 3768-3774
35. Zador, E., Vangheluwe, P., and Wuytack, F. (2007) The expression of the neonatal sarcoplasmic reticulum Ca^{2+} pump (SERCA1b) hints to a role in muscle growth and development. *Cell Calcium* **41**, 379-388
36. Brandl, C. J., Green, N. M., Korczak, B., and MacLennan, D. H. (1986) Two Ca^{2+}-ATPase genes: homologies and mechanistic implications of deduced amino acid sequences. *Cell* **44**, 597-607
37. Brody, I. A. (1969) Muscle contracture induced by exercise. A syndrome attributable to decreased relaxing factor. *N Engl J Med* **281**, 187-192
38. Odermatt, A., Taschner, P. E., Khanna, V. K., Busch, H. F., Karpati, G., Jablecki, C. K., Breuning, M. H., and MacLennan, D. H. (1996) Mutations in the gene-encoding SERCA1, the fast-twitch skeletal muscle sarcoplasmic reticulum Ca^{2+}-ATPase, are associated with Brody disease. *Nature Genet* **14**, 191-194
39. Wuytack, F., Raeymaekers, L., and Missiaen, L. (2002) Molecular physiology of the SERCA and SPCA pumps. *Cell Calcium* **32**, 279-305
40. Vangheluwe, P., Raeymaekers, L., Dode, L., and Wuytack, F. (2005) Modulating sarco(endo)plasmic reticulum Ca^{2+}-ATPase 2 (SERCA2) activity: cell biological implications. *Cell Calcium* **38**, 291-302

41. Campbell, A. M., Kessler, P. D., and Fambrough, D. M. (1992) The alternative carboxyl termini of avian cardiac and brain sarcoplasmic reticulum/endoplasmic reticulum Ca^{2+}-ATPases are on opposite sides of the membrane. *J Biol Chem* **267**, 9321-9325
42. Lytton, J., and MacLennan, D. H. (1988) Molecular cloning of cDNAs from human kidney coding for two alternatively spliced products of the cardiac Ca^{2+}-ATPase gene. *J Biol Chem* **263**, 15024-15031
43. Vandecaetsbeek, I., Trekels, M., De Maeyer, M., Ceulemans, H., Lescrinier, E., Raeymaekers, L., Wuytack, F., and Vangheluwe, P. (2009) Structural basis for the high Ca^{2+} affinity of the ubiquitous SERCA2b Ca^{2+} pump. *Proc Natl Acad Sci U S A* **106**, 18533-18538
44. Lytton, J., Zarain-Herzberg, A., Periasamy, M., and MacLennan, D. H. (1989) Molecular cloning of the mammalian smooth muscle sarco(endo)plasmic reticulum Ca^{2+}-ATPase. *J Biol Chem* **264**, 7059-7065
45. Zarain-Herzberg, A., MacLennan, D. H., and Periasamy, M. (1990) Characterization of rabbit cardiac sarco(endo)plasmic reticulum Ca^{2+}-ATPase gene. *J Biol Chem* **265**, 4670-4677
46. Gelebart, P., Martin, V., Enouf, J., and Papp, B. (2003) Identification of a new SERCA2 splice variant regulated during monocytic differentiation. *Biochem Biophys Res Commun* **303**, 676-684
47. Dally, S., Bredoux, R., Corvazier, E., Andersen, J. P., Clausen, J. D., Dode, L., Fanchaouy, M., Gelebart, P., Monceau, V., Del Monte, F., Gwathmey, J. K., Hajjar, R., Chaabane, C., Bobe, R., Raies, A., and Enouf, J. (2006) Ca^{2+}-ATPases in non-failing and failing heart: evidence for a novel cardiac sarco/endoplasmic reticulum Ca^{2+}-ATPase 2 isoform (SERCA2c). *Biochem J* **395**, 249-258
48. Sakuntabhai, A., Ruiz-Perez, V., Carter, S., Jacobsen, N., Burge, S., Monk, S., Smith, M., Munro, C. S., O'Donovan, M., Craddock, N., Kucherlapati, R., Rees, J. L., Owen, M., Lathrop, G. M., Monaco, A. P., Strachan, T., and Hovnanian, A. (1999) Mutations in ATP2A2, encoding a Ca^{2+} pump, cause Darier disease. *Nat Genet* **21**, 271-277
49. Savignac, M., Edir, A., Simon, M., and Hovnanian, A. (2011) Darier disease : a disease model of impaired calcium homeostasis in the skin. *Biochim Biophys Acta* **1813**, 1111-1117
50. Nellen, R. G., Steijlen, P. M., van Steensel, M. A., Vreeburg, M., Frank, J., and van Geel, M. (2017) Mendelian Disorders of Cornification Caused by Defects in Intracellular Calcium Pumps: Mutation Update and Database for Variants in ATP2A2 and ATP2C1 Associated with Darier Disease and Hailey-Hailey Disease. *Hum Mutat* **38**, 343-356
51. Kaneko, M., Desai, B. S., and Cook, B. (2014) Ionic leakage underlies a gain-of-function effect of dominant disease mutations affecting diverse P-type ATPases. *Nat Genet* **46**, 144-151
52. Vangheluwe, P., Louch, W. E., Ver Heyen, M., Sipido, K., Raeymaekers, L., and Wuytack, F. (2003) Ca^{2+} transport ATPase isoforms SERCA2a and SERCA2b are targeted to the same sites in the murine heart. *Cell Calcium* **34**, 457-464
53. MacLennan, D. H., and Kranias, E. G. (2003) Phospholamban: a crucial regulator of cardiac contractility. *Nat Rev Mol Cell Biol* **4**, 566-577
54. Bers, D. M. (2002) Cardiac excitation-contraction coupling. *Nature* **415**, 198-205
55. MacLennan, D. H., Abu-Abed, M., and Kang, C. (2002) Structure-function relationships in Ca^{2+} cycling proteins. *J Mol Cell Cardiol* **34**, 897-918
56. Vangheluwe, P., Sipido, K. R., Raeymaekers, L., and Wuytack, F. (2006) New perspectives on the role of SERCA2's Ca^{2+} affinity in cardiac function. *Biochim Biophys Acta* **1763**, 1216-1228
57. Mountian, I., Manolopoulos, V. G., De Smedt, H., Parys, J. B., Missiaen, L., and Wuytack, F. (1999) Expression patterns of sarco/endoplasmic reticulum Ca^{2+}-ATPase and inositol 1,4,5-trisphosphate receptor isoforms in vascular endothelial cells. *Cell Calcium* **25**, 371-380
58. Brouland, J. P., Gelebart, P., Kovacs, T., Enouf, J., Grossmann, J., and Papp, B. (2005) The loss of sarco/endoplasmic reticulum calcium transport ATPase 3 expression is an early event during the multistep process of colon carcinogenesis. *Am J Pathol* **167**, 233-242
59. Dode, L., Vilsen, B., Van Baelen, K., Wuytack, F., Clausen, J. D., and Andersen, J. P. (2002) Dissection of the functional differences between sarco(endo)plasmic reticulum Ca^{2+}-ATPase

(SERCA) 1 and 3 isoforms by steady-state and transient kinetic analyses. *J Biol Chem* **277**, 45579-45591

60. Periasamy, M., and Kalyanasundaram, A. (2007) SERCA pump isoforms: their role in calcium transport and disease. *Muscle Nerve* **35**, 430-442
61. MacLennan, D. H., Toyofuku, T., and Lytton, J. (1992) Structure-function relationships in sarcoplasmic or endoplasmic reticulum type Ca^{2+} pumps. *Ann N Y Acad Sci* **671**, 1-10
62. Grover, A. K., Kwan, C. Y., and Samson, S. E. (2003) Effects of peroxynitrite on sarco/endoplasmic reticulum Ca^{2+} pump isoforms SERCA2b and SERCA3a. *Am J Physiol Cell Physiol* **285**, C1537-1543
63. Rudolph, H. K., Antebi, A., Fink, G. R., Buckley, C. M., Dorman, T. E., LeVitre, J., Davidow, L. S., Mao, J. I., and Moir, D. T. (1989) The yeast secretory pathway is perturbed by mutations in PMR1, a member of a Ca^{2+}-ATPase family. *Cell* **58**, 133-145
64. Gunteski-Hamblin, A. M., Clarke, D. M., and Shull, G. E. (1992) Molecular cloning and tissue distribution of alternatively spliced mRNAs encoding possible mammalian homologues of the yeast secretory pathway calcium pump. *Biochemistry (Mosc)* **31**, 7600-7608
65. Wootton, L. L., Argent, C. C., Wheatley, M., and Michelangeli, F. (2004) The expression, activity and localisation of the secretory pathway Ca^{2+}-ATPase (SPCA1) in different mammalian tissues. *Biochim Biophys Acta* **1664**, 189-197
66. Vanoevelen, J., Dode, L., Van Baelen, K., Fairclough, R. J., Missiaen, L., Raeymaekers, L., and F, W. (2005) The secretory pathway Ca^{2+}/Mn^{2+}-ATPase 2 is a Golgi-localized pump with high affinity for Ca^{2+} ions. *J Biol Chem* **280**, 22800-22808
67. Xiang, M., Mohamalawari, D., and Rao, R. (2005) A novel isoform of the secretory pathway Ca^{2+},Mn^{2+}-ATPase, hSPCA2, has unusual properties and is expressed in the brain. *J Biol Chem* **280**, 11608-11614
68. Wei, Y., Chen, J., Rosas, G., Tompkins, D. A., Holt, P. A., and Rao, R. (2000) Phenotypic screening of mutations in Pmr1, the yeast secretory pathway Ca^{2+}/Mn^{2+}-ATPase, reveals residues critical for ion selectivity and transport. *J Biol Chem* **275**, 23927-23932
69. Wei, Y., Marchi, V., Wang, R., and Rao, R. (1999) An N-terminal EF hand-like motif modulates ion transport by Pmr1, the yeast Golgi Ca^{2+}/Mn^{2+}-ATPase. *Biochemistry (Mosc)* **38**, 14534-14541
70. Van Baelen, K., Vanoevelen, J., Missiaen, L., Raeymaekers, L., and Wuytack, F. (2001) The Golgi PMR1 P-type ATPase of Caenorhabditis elegans. Identification of the gene and demonstration of calcium and manganese transport. *J Biol Chem* **276**, 10683-10691
71. Dode, L., Andersen, J. P., Raeymaekers, L., Missiaen, L., Vilsen, B., and Wuytack, F. (2005) Functional comparison between secretory pathway Ca^{2+}/Mn^{2+}-ATPase (SPCA) 1 and sarcoplasmic reticulum Ca^{2+}-ATPase (SERCA) 1 isoforms by steady-state and transient kinetic analyses. *J Biol Chem* **280**, 39124-39134
72. Kho, C., Lee, A., Jeong, D., Oh, J. G., Chaanine, A. H., Kizana, E., Park, W. J., and Hajjar, R. J. (2011) SUMO1-dependent modulation of SERCA2a in heart failure. *Nature* **477**, 601-605
73. Vafiadaki, E., Arvanitis, D. A., Pagakis, S. N., Papalouka, V., Sanoudou, D., Kontrogianni-Konstantopoulos, A., and Kranias, E. G. (2009) The anti-apoptotic protein HAX-1 interacts with SERCA2 and regulates its protein levels to promote cell survival. *Mol Biol Cell* **20**, 306-318
74. Li, Y., and Camacho, P. (2004) Ca^{2+}-dependent redox modulation of SERCA 2b by ERp57. *J Cell Biol* **164**, 35-46
75. Periasamy, M., Reed, T. D., Liu, L. H., Ji, Y., Loukianov, E., Paul, R. J., Nieman, M. L., Riddle, T., Duffy, J. J., Doetschman, T., Lorenz, J. N., and Shull, G. E. (1999) Impaired cardiac performance in heterozygous mice with a null mutation in the sarco(endo)plasmic reticulum Ca^{2+}-ATPase isoform 2 (SERCA2) gene. *J Biol Chem* **274**, 2556-2562
76. Okunade, G. W., Miller, M. L., Azhar, M., Andringa, A., Sanford, L. P., Doetschman, T., Prasad, V., and Shull, G. E. (2007) Loss of the Atp2c1 secretory pathway Ca^{2+}-ATPase (SPCA1) in mice causes Golgi stress, apoptosis, and midgestational death in homozygous embryos and squamous cell tumors in adult heterozygotes. *J Biol Chem* **282**, 26517-26527

77. Hu, Z., Bonifas, J. M., Beech, J., Bench, G., Shigihara, T., Ogawa, H., Ikeda, S., Mauro, T., and Epstein, E. H., Jr. (2000) Mutations in ATP2C1, encoding a calcium pump, cause Hailey-Hailey disease. *Nat Genet* **24**, 61-65
78. Hanamura, T., Takeichi, T., Okuno, Y., Ichikawa, D., Kono, M., and Akiyama, M. (2018) Mild case of Hailey-Hailey disease caused by a novel ATP2C1 mutation. *J Dermatol* **45**, e207-e208
79. Prasad, V., Boivin, G. P., Miller, M. L., Liu, L. H., Erwin, C. R., Warner, B. W., and Shull, G. E. (2005) Haploinsufficiency of Atp2a2, encoding the sarco(endo)plasmic reticulum Ca^{2+}-ATPase isoform 2 Ca^{2+} pump, predisposes mice to squamous cell tumors via a novel mode of cancer susceptibility. *Cancer Res* **65**, 8655-8661
80. Neville, M. C. (2005) Calcium secretion into milk. *J Mammary Gland Biol Neoplasia* **10**, 119-128
81. McAndrew, D., Grice, D. M., Peters, A. A., Davis, F. M., Stewart, T., Rice, M., Smart, C. E., Brown, M. A., Kenny, P. A., Roberts-Thomson, S. J., and Monteith, G. R. (2011) ORAI1-mediated calcium influx in lactation and in breast cancer. *Mol Cancer Ther* **10**, 448-460
82. Reinhardt, T. A., Lippolis, J. D., Shull, G. E., and Horst, R. L. (2004) Null mutation in the gene encoding plasma membrane Ca^{2+}-ATPase isoform 2 impairs calcium transport into milk. *J Biol Chem* **279**, 42369-42373
83. Faddy, H. M., Smart, C. E., Xu, R., Lee, G. Y., Kenny, P. A., Feng, M., Rao, R., Brown, M. A., Bissell, M. J., Roberts-Thomson, S. J., and Monteith, G. R. (2008) Localization of plasma membrane and secretory calcium pumps in the mammary gland. *Biochem Biophys Res Commun* **369**, 977-981
84. Chen, J., Smaardijk, S., Vandecaetsbeek, I., and Vangheluwe, P. (2016) Regulation of Ca^{2+} transport ATPases by amino- and carboxy-terminal extensions: Mechanisms and (patho)physiological implications. *Regulation of Ca^{2+}-ATPases, V-ATPases and F-ATPases* **14**, 243-279
85. Verboomen, H., Wuytack, F., De Smedt, H., Himpens, B., and Casteels, R. (1992) Functional difference between SERCA2a and SERCA2b Ca^{2+} pumps and their modulation by phospholamban. *Biochem J* **286 (Pt 2)**, 591-595
86. Akin, B. L., Hurley, T. D., Chen, Z., and Jones, L. R. (2013) The structural basis for phospholamban inhibition of the calcium pump in sarcoplasmic reticulum. *J Biol Chem* **288**, 30181-30191
87. Toyoshima, C., Asahi, M., Sugita, Y., Khanna, R., Tsuda, T., and MacLennan, D. H. (2003) Modeling of the inhibitory interaction of phospholamban with the Ca^{2+} ATPase. *Proc Natl Acad Sci U S A* **100**, 467-472
88. Anderson, D. M., Makarewich, C. A., Anderson, K. M., Shelton, J. M., Bezprozvannaya, S., Bassel-Duby, R., and Olson, E. N. (2016) Widespread control of calcium signaling by a family of SERCA-inhibiting micropeptides. *Sci Signal* **9**, ra119
89. Nelson, B. R., Makarewich, C. A., Anderson, D. M., Winders, B. R., Troupes, C. D., Wu, F., Reese, A. L., McAnally, J. R., Chen, X., Kavalali, E. T., Cannon, S. C., Houser, S. R., Bassel-Duby, R., and Olson, E. N. (2016) A peptide encoded by a transcript annotated as long noncoding RNA enhances SERCA activity in muscle. *Science* **351**, 271-275
90. Gramolini, A. O., Kislinger, T., Asahi, M., Li, W., Emili, A., and MacLennan, D. H. (2004) Sarcolipin retention in the endoplasmic reticulum depends on its C-terminal RSYQY sequence and its interaction with sarco(endo)plasmic Ca^{2+}-ATPases. *Proc Natl Acad Sci U S A* **101**, 16807-16812
91. Tupling, A. R., Asahi, M., and MacLennan, D. H. (2002) Sarcolipin overexpression in rat slow twitch muscle inhibits sarcoplasmic reticulum Ca^{2+} uptake and impairs contractile function. *J Biol Chem* **277**, 44740-44746
92. Toyoshima, C., Iwasawa, S., Ogawa, H., Hirata, A., Tsueda, J., and Inesi, G. (2013) Crystal structures of the calcium pump and sarcolipin in the Mg^{2+}-bound E1 state. *Nature* **495**, 260-264
93. Winther, A. M., Bublitz, M., Karlsen, J. L., Moller, J. V., Hansen, J. B., Nissen, P., and Buch-Pedersen, M. J. (2013) The sarcolipin-bound calcium pump stabilizes calcium sites exposed to the cytoplasm. *Nature* **495**, 265-269

94. Gramolini, A. O., Trivieri, M. G., Oudit, G. Y., Kislinger, T., Li, W., Patel, M. M., Emili, A., Kranias, E. G., Backx, P. H., and Maclennan, D. H. (2006) Cardiac-specific overexpression of sarcolipin in phospholamban null mice impairs myocyte function that is restored by phosphorylation. *Proc Natl Acad Sci U S A* **103**, 2446-2451
95. Bhupathy, P., Babu, G. J., Ito, M., and Periasamy, M. (2009) Threonine-5 at the N-terminus can modulate sarcolipin function in cardiac myocytes. *J Mol Cell Cardiol* **47**, 723-729
96. Asahi, M., Kurzydlowski, K., Tada, M., and MacLennan, D. H. (2002) Sarcolipin inhibits polymerization of phospholamban to induce superinhibition of sarco(endo)plasmic reticulum Ca^{2+}-ATPases (SERCAs). *J Biol Chem* **277**, 26725-26728
97. Anderson, D. M., Anderson, K. M., Chang, C. L., Makarewich, C. A., Nelson, B. R., McAnally, J. R., Kasaragod, P., Shelton, J. M., Liou, J., Bassel-Duby, R., and Olson, E. N. (2015) A micropeptide encoded by a putative long noncoding RNA regulates muscle performance. *Cell* **160**, 595-606
98. Lissandron, V., Podini, P., Pizzo, P., and Pozzan, T. (2010) Unique characteristics of Ca^{2+} homeostasis of the trans-Golgi compartment. *Proc Natl Acad Sci U S A* **107**, 9198-9203
99. Kienzle, C., Basnet, N., Crevenna, A. H., Beck, G., Habermann, B., Mizuno, N., and von Blume, J. (2014) Cofilin recruits F-actin to SPCA1 and promotes Ca^{2+}-mediated secretory cargo sorting. *J Cell Biol* **206**, 635-654
100. Crevenna, A. H., Blank, B., Maiser, A., Emin, D., Prescher, J., Beck, G., Kienzle, C., Bartnik, K., Habermann, B., Pakdel, M., Leonhardt, H., Lamb, D. C., and von Blume, J. (2016) Secretory cargo sorting by Ca^{2+}-dependent Cab45 oligomerization at the trans-Golgi network. *J Cell Biol* **213**, 305-314
101. von Blume, J., Alleaume, A. M., Kienzle, C., Carreras-Sureda, A., Valverde, M., and Malhotra, V. (2012) Cab45 is required for Ca^{2+}-dependent secretory cargo sorting at the trans-Golgi network. *J Cell Biol* **199**, 1057-1066
102. Gourdon, P., Liu, X. Y., Skjorringe, T., Morth, J. P., Moller, L. B., Pedersen, B. P., and Nissen, P. (2011) Crystal structure of a copper-transporting PIB-type ATPase. *Nature* **475**, 59-64
103. Poulsen, H., Khandelia, H., Morth, J. P., Bublitz, M., Mouritsen, O. G., Egebjerg, J., and Nissen, P. (2010) Neurological disease mutations compromise a C-terminal ion pathway in the Na^+/K^+-ATPase. *Nature* **467**, 99-102
104. Toustrup-Jensen, M. S., Holm, R., Einholm, A. P., Schack, V. R., Morth, J. P., Nissen, P., Andersen, J. P., and Vilsen, B. (2009) The C terminus of Na^+,K^+-ATPase controls Na^+ affinity on both sides of the membrane through Arg935. *J Biol Chem* **284**, 18715-18725
105. Palmgren, M. G., Sommarin, M., Serrano, R., and Larsson, C. (1991) Identification of an autoinhibitory domain in the C-terminal region of the plant plasma membrane H^+-ATPase. *J Biol Chem* **266**, 20470-20475
106. Portillo, F., de Larrinoa, I. F., and Serrano, R. (1989) Deletion analysis of yeast plasma membrane H^+-ATPase and identification of a regulatory domain at the carboxyl-terminus. *FEBS Lett* **247**, 381-385
107. Zhou, X., Sebastian, T. T., and Graham, T. R. (2013) Auto-inhibition of Drs2p, a yeast phospholipid flippase, by its carboxyl-terminal tail. *J Biol Chem* **288**, 31807-31815
108. Natarajan, P., Liu, K., Patil, D. V., Sciorra, V. A., Jackson, C. L., and Graham, T. R. (2009) Regulation of a Golgi flippase by phosphoinositides and an ArfGEF. *Nat Cell Biol* **11**, 1421-1426
109. Sorensen, D. M., Buch-Pedersen, M. J., and Palmgren, M. G. (2010) Structural divergence between the two subgroups of P5 ATPases. *Biochim Biophys Acta* **1797**, 846-855
110. Holemans, T., Sorensen, D. M., van Veen, S., Martin, S., Hermans, D., Kemmer, G. C., Van den Haute, C., Baekelandt, V., Gunther Pomorski, T., Agostinis, P., Wuytack, F., Palmgren, M., Eggermont, J., and Vangheluwe, P. (2015) A lipid switch unlocks Parkinson's disease-associated ATP13A2. *Proc Natl Acad Sci U S A* **112**, 9040-9045
111. Maruyama, K., and MacLennan, D. H. (1988) Mutation of aspartic acid-351, lysine-352, and lysine-515 alters the Ca^{2+} transport activity of the Ca^{2+}-ATPase expressed in COS-1 cells. *Proc Natl Acad Sci U S A* **85**, 3314-3318

112. Zador, E., and Kosa, M. (2015) The neonatal sarcoplasmic/endoplasmic reticulum calcium ATPase (SERCA1b): a neglected pump in scope. *Pflugers Arch* **467**, 1395-1401
113. Gorski, P. A., Trieber, C. A., Lariviere, E., Schuermans, M., Wuytack, F., Young, H. S., and Vangheluwe, P. (2012) Transmembrane helix 11 is a genuine regulator of the endoplasmic reticulum Ca^{2+} pump and acts as a functional parallel of beta-subunit on alpha-Na^+,K^+-ATPase. *J Biol Chem* **287**, 19876-19885
114. Clausen, J. D., Vandecaetsbeek, I., Wuytack, F., Vangheluwe, P., and Andersen, J. P. (2012) Distinct roles of the C-terminal 11th transmembrane helix and luminal extension in the partial reactions determining the high Ca^{2+} affinity of sarco(endo)plasmic reticulum Ca^{2+}-ATPase isoform 2b (SERCA2b). *J Biol Chem* **287**, 39460-39469
115. Dode, L., Andersen, J. P., Vanoevelen, J., Raeymaekers, L., Missiaen, L., Vilsen, B., and Wuytack, F. (2006) Dissection of the functional differences between human secretory pathway Ca^{2+}/Mn^{2+}-ATPase (SPCA) 1 and 2 isoenzymes by steady-state and transient kinetic analyses. *J Biol Chem* **281**, 3182-3189
116. Micaroni, M., and Malquori, L. (2013) Overlapping ATP2C1 and ASTE1 genes in human genome: implications for SPCA1 expression? *Int J Mol Sci* **14**, 674-683
117. Hornbeck, P. V., Zhang, B., Murray, B., Kornhauser, J. M., Latham, V., and Skrzypek, E. (2015) PhosphoSitePlus, 2014: mutations, PTMs and recalibrations. *Nucleic Acids Res* **43**, D512-520
118. Sepulveda, M. R., Marcos, D., Berrocal, M., Raeymaekers, L., Mata, A. M., and Wuytack, F. (2008) Activity and localization of the secretory pathway Ca^{2+}-ATPase isoform 1 (SPCA1) in different areas of the mouse brain during postnatal development. *Mol Cell Neurosci* **38**, 461-473
119. Daiho, T., Yamasaki, K., Saino, T., Kamidochi, M., Satoh, K., Iizuka, H., and Suzuki, H. (2001) Mutations of either or both Cys(876) and Cys(888) residues of sarcoplasmic reticulum Ca^{2+}-ATPase result in a complete loss of Ca^{2+} transport activity without a loss of Ca^{2+}-dependent ATPase activity - Role of the Cys(876)-Cys(888) disulfide bond. *J Biol Chem* **276**, 32771-32778
120. Schoneich, C., Viner, R. I., Ferrington, D. A., and Bigelow, D. J. (1999) Age-related chemical modification of the skeletal muscle sarcoplasmic reticulum Ca^{2+}-ATPase of the rat. *Mech Ageing Dev* **107**, 221-231
121. Adachi, T., Weisbrod, R. M., Pimentel, D. R., Ying, J., Sharov, V. S., Schoneich, C., and Cohen, R. A. (2004) S-Glutathiolation by peroxynitrite activates SERCA during arterial relaxation by nitric oxide. *Nat Med* **10**, 1200-1207
122. Qin, F., Siwik, D. A., Lancel, S., Zhang, J., Kuster, G. M., Luptak, I., Wang, L., Tong, X., Kang, Y. J., Cohen, R. A., and Colucci, W. S. (2013) Hydrogen peroxide-mediated SERCA cysteine 674 oxidation contributes to impaired cardiac myocyte relaxation in senescent mouse heart. *J Am Heart Assoc* **2**, e000184
123. Viner, R. I., Ferrington, D. A., Williams, T. D., Bigelow, D. J., and Schoneich, C. (1999) Protein modification during biological aging: selective tyrosine nitration of the SERCA2a isoform of the sarcoplasmic reticulum Ca^{2+}-ATPase in skeletal muscle. *Biochem J* **340 (Pt 3)**, 657-669
124. Xu, S., Ying, J., Jiang, B., Guo, W., Adachi, T., Sharov, V., Lazar, H., Menzoian, J., Knyushko, T. V., Bigelow, D., Schoneich, C., and Cohen, R. A. (2006) Detection of sequence-specific tyrosine nitration of manganese SOD and SERCA in cardiovascular disease and aging. *Am J Physiol Heart Circ Physiol* **290**, H2220-2227
125. Tang, W. H., Cheng, W. T., Kravtsov, G. M., Tong, X. Y., Hou, X. Y., Chung, S. K., and Chung, S. S. M. (2010) Cardiac contractile dysfunction during acute hyperglycemia due to impairment of SERCA by polyol pathway-mediated oxidative stress. *Am J Physiol Cell Physiol* **299**, C643-C653
126. Tilemann, L., Lee, A., Ishikawa, K., Aguero, J., Rapti, K., Santos-Gallego, C., Kohlbrenner, E., Fish, K. M., Kho, C., and Hajjar, R. J. (2013) SUMO-1 gene transfer improves cardiac function in a large-animal model of heart failure. *Sci Transl Med* **5**, 211ra159
127. Foster, D. B., Liu, T., Rucker, J., O'Meally, R. N., Devine, L. R., Cole, R. N., and O'Rourke, B. (2013) The cardiac acetyl-lysine proteome. *PLoS One* **8**, e67513

128. Bidasee, K. R., Zhang, Y., Shao, C. H., Wang, M., Patel, K. P., Dincer, U. D., and Besch, H. R., Jr. (2004) Diabetes increases formation of advanced glycation end products on Sarco(endo)plasmic reticulum Ca^{2+}-ATPase. *Diabetes* **53**, 463-473
129. Gorski, P. A., Jang, S. P., Jeong, D., Lee, A., Lee, P., Oh, J. G., Chepurko, V., Yang, D. K., Kwak, T. H., Eom, S. H., Park, Z. Y., Yoo, Y. J., Kim, D. H., Kook, H., Sunagawa, Y., Morimoto, T., Hasegawa, K., Sadoshima, J., Hajjar, R. J., Park, W. J., and Kho, C. (2019) Role of SIRT1 in modulating acetylation of the sarco-endoplasmic reticulum Ca^{2+}-ATPase in heart failure. *Circ Res* **124**, e63-e80
130. Kusumoto, D., Yuasa, S., and Fukuda, K. (2019) SPEG, an Indispensable Kinase of SERCA2a for Calcium Homeostasis. *Circ Res* **124**, 668-670
131. Toyoshima, C., and Nomura, H. (2002) Structural changes in the calcium pump accompanying the dissociation of calcium. *Nature* **418**, 605-611
132. Olesen, C., Sorensen, T. L., Nielsen, R. C., Moller, J. V., and Nissen, P. (2004) Dephosphorylation of the calcium pump coupled to counterion occlusion. *Science* **306**, 2251-2255
133. Obara, K., Miyashita, N., Xu, C., Toyoshima, I., Sugita, Y., Inesi, G., and Toyoshima, C. (2005) Structural role of countertransport revealed in Ca^{2+} pump crystal structure in the absence of Ca^{2+}. *Proc Natl Acad Sci U S A* **102**, 14489-14496
134. Moncoq, K., Trieber, C. A., and Young, H. S. (2007) The molecular basis for cyclopiazonic acid inhibition of the sarcoplasmic reticulum calcium pump. *J Biol Chem* **282**, 9748-9757
135. Wootton, L. L., and Michelangeli, F. (2006) The effects of the phenylalanine 256 to valine mutation on the sensitivity of sarcoplasmic/endoplasmic reticulum Ca^{2+} ATPase (SERCA) Ca^{2+} pump isoforms 1, 2, and 3 to thapsigargin and other inhibitors. *J Biol Chem* **281**, 6970-6976
136. Winther, A. M., Liu, H., Sonntag, Y., Olesen, C., le Maire, M., Soehoel, H., Olsen, C. E., Christensen, S. B., Nissen, P., and Moller, J. V. (2010) Critical roles of hydrophobicity and orientation of side chains for inactivation of sarcoplasmic reticulum Ca^{2+}-ATPase with thapsigargin and thapsigargin analogs. *J Biol Chem* **285**, 28883-28892
137. Xu, C., Ma, H., Inesi, G., Al-Shawi, M. K., and Toyoshima, C. (2004) Specific structural requirements for the inhibitory effect of thapsigargin on the Ca^{2+} ATPase SERCA. *J Biol Chem* **279**, 17973-17979
138. Quynh Doan, N. T., and Christensen, S. B. (2015) Thapsigargin, Origin, Chemistry, Structure-Activity Relationships and Prodrug Development. *Curr Pharm Des* **21**, 5501-5517
139. Law, B. Y., Wang, M., Ma, D. L., Al-Mousa, F., Michelangeli, F., Cheng, S. H., Ng, M. H., To, K. F., Mok, A. Y., Ko, R. Y., Lam, S. K., Chen, F., Che, C. M., Chiu, P., and Ko, B. C. (2010) Alisol B, a novel inhibitor of the sarcoplasmic/endoplasmic reticulum Ca^{2+} ATPase pump, induces autophagy, endoplasmic reticulum stress, and apoptosis. *Mol Cancer Ther* **9**, 718-730
140. Yatime, L., Buch-Pedersen, M. J., Musgaard, M., Morth, J. P., Winther, A. M. L., Pedersen, B. P., Olesen, C., Andersen, J. P., Vilsen, B., Schiott, B., Palmgren, M. G., Moller, J. V., Nissen, P., and Fedosova, N. (2009) P-type ATPases as drug targets: Tools for medicine and science. *Biochim Biophys Acta Bioenerg* **1787**, 207-220
141. Michelangeli, F., and East, J. M. (2011) A diversity of SERCA Ca^{2+} pump inhibitors. *Biochem Soc Trans* **39**, 789-797
142. Bilmen, J. G., Khan, S. Z., Javed, M. H., and Michelangeli, F. (2001) Inhibition of the SERCA Ca^{2+} pumps by curcumin. Curcumin putatively stabilizes the interaction between the nucleotide-binding and phosphorylation domains in the absence of ATP. *Eur J Biochem* **268**, 6318-6327
143. Ogunbayo, O. A., and Michelangeli, F. (2014) Related flavonoids cause cooperative inhibition of the sarcoplasmic reticulum Ca^{2+}-ATPase by multimode mechanisms. *FEBS J* **281**, 766-777
144. Lai, P., and Michelangeli, F. (2012) Bis(2-hydroxy-3-tert-butyl-5-methyl-phenyl)-methane (bis-phenol) is a potent and selective inhibitor of the secretory pathway Ca^{2+}-ATPase (SPCA1). *Biochem Biophys Res Commun* **424**, 616-619
145. Yamamoto, S., Takehara, M., Kabashima, Y., Fukutomi, T., and Ushimaru, M. (2016) Identification of novel inhibitors of human SPCA2. *Biochem Biophys Res Commun* **477**, 266-270

146. Ambrosy, A. P., Butler, J., Ahmed, A., Vaduganathan, M., van Veldhuisen, D. J., Colucci, W. S., and Gheorghiade, M. (2014) The use of digoxin in patients with worsening chronic heart failure: reconsidering an old drug to reduce hospital admissions. *J Am Coll Cardiol* **63**, 1823-1832
147. Dubois, C., Vanden Abeele, F., Sehgal, P., Olesen, C., Junker, S., Christensen, S. B., Prevarskaya, N., and Moller, J. V. (2013) Differential effects of thapsigargin analogues on apoptosis of prostate cancer cells: complex regulation by intracellular calcium. *FEBS J* **280**, 5430-5440
148. Doan, N. T., Paulsen, E. S., Sehgal, P., Moller, J. V., Nissen, P., Denmeade, S. R., Isaacs, J. T., Dionne, C. A., and Christensen, S. B. (2015) Targeting thapsigargin towards tumors. *Steroids* **97**, 2-7
149. Denmeade, S. R., Mhaka, A. M., Rosen, D. M., Brennen, W. N., Dalrymple, S., Dach, I., Olesen, C., Gurel, B., Demarzo, A. M., Wilding, G., Carducci, M. A., Dionne, C. A., Moller, J. V., Nissen, P., Christensen, S. B., and Isaacs, J. T. (2012) Engineering a prostate-specific membrane antigen-activated tumor endothelial cell prodrug for cancer therapy. *Sci Transl Med* **4**, 140ra186
150. Mahalingam, D., Wilding, G., Denmeade, S., Sarantopoulas, J., Cosgrove, D., Cetnar, J., Azad, N., Bruce, J., Kurman, M., Allgood, V. E., and Carducci, M. (2016) Mipsagargin, a novel thapsigargin-based PSMA-activated prodrug: results of a first-in-man phase I clinical trial in patients with refractory, advanced or metastatic solid tumours. *Br J Cancer* **114**, 986-994
151. Harms, M., and Seale, P. (2013) Brown and beige fat: development, function and therapeutic potential. *Nat Med* **19**, 1252-1263
152. Block, B. A. (1994) Thermogenesis in muscle. *Annu Rev Physiol* **56**, 535-577
153. Smith, W. S., Broadbridge, R., East, J. M., and Lee, A. G. (2002) Sarcolipin uncouples hydrolysis of ATP from accumulation of Ca^{2+} by the Ca^{2+}-ATPase of skeletal-muscle sarcoplasmic reticulum. *Biochem J* **361**, 277-286
154. Mall, S., Broadbridge, R., Harrison, S. L., Gore, M. G., Lee, A. G., and East, J. M. (2006) The presence of sarcolipin results in increased heat production by Ca^{2+}-ATPase. *J Biol Chem* **281**, 36597-36602
155. Bal, N. C., Maurya, S. K., Sopariwala, D. H., Sahoo, S. K., Gupta, S. C., Shaikh, S. A., Pant, M., Rowland, L. A., Bombardier, E., Goonasekera, S. A., Tupling, A. R., Molkentin, J. D., and Periasamy, M. (2012) Sarcolipin is a newly identified regulator of muscle-based thermogenesis in mammals. *Nat Med* **18**, 1575-1579
156. Ikeda, K., Kang, Q., Yoneshiro, T., Camporez, J. P., Maki, H., Homma, M., Shinoda, K., Chen, Y., Lu, X., Maretich, P., Tajima, K., Ajuwon, K. M., Soga, T., and Kajimura, S. (2017) UCP1-independent signaling involving SERCA2b-mediated calcium cycling regulates beige fat thermogenesis and systemic glucose homeostasis. *Nat Med* **23**, 1454-1465
157. Park, S. W., Zhou, Y., Lee, J., and Ozcan, U. (2010) Sarco(endo)plasmic reticulum Ca^{2+}-ATPase 2b is a major regulator of endoplasmic reticulum stress and glucose homeostasis in obesity. *Proc Natl Acad Sci U S A* **107**, 19320-19325
158. Hasenfuss, G., Reinecke, H., Studer, R., Meyer, M., Pieske, B., Holtz, J., Holubarsch, C., Posival, H., Just, H., and Drexler, H. (1994) Relation between myocardial function and expression of sarcoplasmic reticulum Ca^{2+}-ATPase in failing and nonfailing human myocardium. *Circ Res* **75**, 434-442
159. Movsesian, M. A., Karimi, M., Green, K., and Jones, L. R. (1994) Ca^{2+}-transporting ATPase, phospholamban, and calsequestrin levels in nonfailing and failing human myocardium. *Circulation* **90**, 653-657
160. Meyer, M., Schillinger, W., Pieske, B., Holubarsch, C., Heilmann, C., Posival, H., Kuwajima, G., Mikoshiba, K., Just, H., Hasenfuss, G., and et al. (1995) Alterations of sarcoplasmic reticulum proteins in failing human dilated cardiomyopathy. *Circulation* **92**, 778-784
161. del Monte, F., Williams, E., Lebeche, D., Schmidt, U., Rosenzweig, A., Gwathmey, J. K., Lewandowski, E. D., and Hajjar, R. J. (2001) Improvement in survival and cardiac metabolism after gene transfer of sarcoplasmic reticulum Ca^{2+}-ATPase in a rat model of heart failure. *Circulation* **104**, 1424-1429

162. Kawase, Y., Ly, H. Q., Prunier, F., Lebeche, D., Shi, Y., Jin, H., Hadri, L., Yoneyama, R., Hoshino, K., Takewa, Y., Sakata, S., Peluso, R., Zsebo, K., Gwathmey, J. K., Tardif, J. C., Tanguay, J. F., and Hajjar, R. J. (2008) Reversal of cardiac dysfunction after long-term expression of SERCA2a by gene transfer in a pre-clinical model of heart failure. *J Am Coll Cardiol* **51**, 1112-1119
163. Miyamoto, M. I., del Monte, F., Schmidt, U., DiSalvo, T. S., Kang, Z. B., Matsui, T., Guerrero, J. L., Gwathmey, J. K., Rosenzweig, A., and Hajjar, R. J. (2000) Adenoviral gene transfer of SERCA2a improves left-ventricular function in aortic-banded rats in transition to heart failure. *Proc Natl Acad Sci U S A* **97**, 793-798
164. del Monte, F., Harding, S. E., Schmidt, U., Matsui, T., Kang, Z. B., Dec, G. W., Gwathmey, J. K., Rosenzweig, A., and Hajjar, R. J. (1999) Restoration of contractile function in isolated cardiomyocytes from failing human hearts by gene transfer of SERCA2a. *Circulation* **100**, 2308-2311
165. Greenberg, B., Butler, J., Felker, G. M., Ponikowski, P., Voors, A. A., Desai, A. S., Barnard, D., Bouchard, A., Jaski, B., Lyon, A. R., Pogoda, J. M., Rudy, J. J., and Zsebo, K. M. (2016) Calcium upregulation by percutaneous administration of gene therapy in patients with cardiac disease (CUPID 2): a randomised, multinational, double-blind, placebo-controlled, phase 2b trial. *Lancet* **387**, 1178-1186
166. Ziolo, M. T., Martin, J. L., Bossuyt, J., Bers, D. M., and Pogwizd, S. M. (2005) Adenoviral gene transfer of mutant phospholamban rescues contractile dysfunction in failing rabbit myocytes with relatively preserved SERCA function. *Circ Res* **96**, 815-817
167. Hoshijima, M., Ikeda, Y., Iwanaga, Y., Minamisawa, S., Date, M. O., Gu, Y., Iwatate, M., Li, M., Wang, L., Wilson, J. M., Wang, Y., Ross, J., Jr., and Chien, K. R. (2002) Chronic suppression of heart-failure progression by a pseudophosphorylated mutant of phospholamban via in vivo cardiac rAAV gene delivery. *Nat Med* **8**, 864-871
168. Nakayama, H., Otsu, K., Yamaguchi, O., Nishida, K., Date, M. O., Hongo, K., Kusakari, Y., Toyofuku, T., Hikoso, S., Kashiwase, K., Takeda, T., Matsumura, Y., Kurihara, S., Hori, M., and Tada, M. (2003) Cardiac-specific overexpression of a high Ca^{2+} affinity mutant of SERCA2a attenuates in vivo pressure overload cardiac hypertrophy. *FASEB J* **17**, 61-63
169. Dang, D., Prasad, H., and Rao, R. (2017) Secretory pathway Ca^{2+}-ATPases promote in vitro microcalcifications in breast cancer cells. *Mol Carcinog* **56**, 2474-2485
170. Grice, D. M., Vetter, I., Faddy, H. M., Kenny, P. A., Roberts-Thomson, S. J., and Monteith, G. R. (2010) Golgi calcium pump secretory pathway calcium ATPase 1 (SPCA1) is a key regulator of insulin-like growth factor receptor (IGF1R) processing in the basal-like breast cancer cell line MDA-MB-231. *J Biol Chem* **285**, 37458-37466
171. Cross, B. M., Breitwieser, G. E., Reinhardt, T. A., and Rao, R. (2014) Cellular calcium dynamics in lactation and breast cancer: from physiology to pathology. *Am J Physiol Cell Physiol* **306**, C515-526
172. Monteith, G. R., Davis, F. M., and Roberts-Thomson, S. J. (2012) Calcium channels and pumps in cancer: changes and consequences. *J Biol Chem* **287**, 31666-31673
173. Botstein, D., and Fink, G. R. (2011) Yeast: an experimental organism for 21st Century biology. *Genetics* **189**, 695-704
174. Ghiglieri, V., Calabrese, V., and Calabresi, P. (2018) Alpha-Synuclein: From Early Synaptic Dysfunction to Neurodegeneration. *Front Neurol* **9**, 295
175. Buttner, S., Faes, L., Reichelt, W. N., Broeskamp, F., Habernig, L., Benke, S., Kourtis, N., Ruli, D., Carmona-Gutierrez, D., Eisenberg, T., D'Hooge, P., Ghillebert, R., Franssens, V., Harger, A., Pieber, T. R., Freudenberger, P., Kroemer, G., Sigrist, S. J., Winderickx, J., Callewaert, G., Tavernarakis, N., and Madeo, F. (2013) The Ca^{2+}/Mn^{2+} ion-pump PMR1 links elevation of cytosolic Ca^{2+} levels to alpha-synuclein toxicity in Parkinson's disease models. *Cell Death Differ* **20**, 465-477
176. Seddon, A. M., Curnow, P., and Booth, P. J. (2004) Membrane proteins, lipids and detergents: not just a soap opera. *Biochim Biophys Acta* **1666**, 105-117

177. Gohon, Y., and Popot, J. L. (2003) Membrane protein-surfactant complexes. *Current Opinion in Colloid & Interface Science* **8**, 15-22
178. Pollock, N. L., Lee, S. C., Patel, J. H., Gulamhussein, A. A., and Rothnie, A. J. (2018) Structure and function of membrane proteins encapsulated in a polymer-bound lipid bilayer. *Biochim Biophys Acta* **1860**, 809-817
179. Rigaud, J. L., and Levy, D. (2003) Reconstitution of membrane proteins into liposomes. *Methods Enzymol* **372**, 65-86
180. Rigaud, J. L. (2002) Membrane proteins: functional and structural studies using reconstituted proteoliposomes and 2-D crystals. *Braz J Med Biol Res* **35**, 753-766
181. Lasic, D. D. (1988) The mechanism of vesicle formation. *Biochemical J* **256**, 1-11
182. Allen, T. M., Romans, A. Y., Kercret, H., and Segrest, J. P. (1980) Detergent removal during membrane reconstitution. *Biochim Biophys Acta* **601**, 328-342
183. Denisov, I. G., and Sligar, S. G. (2016) Nanodiscs for structural and functional studies of membrane proteins. *Nat Struct Mol Biol* **23**, 481-486
184. Skrzypek, R., Iqbal, S., and Callaghan, R. (2018) Methods of reconstitution to investigate membrane protein function. *Methods* **147**, 126-141
185. Bayburt, T. H., and Sligar, S. G. (2010) Membrane protein assembly into Nanodiscs. *FEBS Lett* **584**, 1721-1727
186. Gohon, Y., Giusti, F., Prata, C., Charvolin, D., Timmins, P., Ebel, C., Tribet, C., and Popot, J. L. (2006) Well-defined nanoparticles formed by hydrophobic assembly of a short and polydisperse random terpolymer, amphipol A8-35. *Langmuir* **22**, 1281-1290
187. Popot, J. L., Althoff, T., Bagnard, D., Baneres, J. L., Bazzacco, P., Billon-Denis, E., Catoire, L. J., Champeil, P., Charvolin, D., Cocco, M. J., Cremel, G., Dahmane, T., de la Maza, L. M., Ebel, C., Gabel, F., Giusti, F., Gohon, Y., Goormaghtigh, E., Guittet, E., Kleinschmidt, J. H., Kuhlbrandt, W., Le Bon, C., Martinez, K. L., Picard, M., Pucci, B., Sachs, J. N., Tribet, C., van Heijenoort, C., Wien, F., Zito, F., and Zoonens, M. (2011) Amphipols from A to Z. *Annu Rev Biophys* **40**, 379-408
188. Champeil, P., Menguy, T., Tribet, C., Popot, J. L., and le Maire, M. (2000) Interaction of amphipols with sarcoplasmic reticulum Ca^{2+}-ATPase. *J Biol Chem* **275**, 18623-18637
189. Dorr, J. M., Koorengevel, M. C., Schafer, M., Prokofyev, A. V., Scheidelaar, S., van der Cruijsen, E. A. W., Dafforn, T. R., Baldus, M., and Killian, J. A. (2014) Detergent-free isolation, characterization, and functional reconstitution of a tetrameric K^+ channel: The power of native nanodiscs. *Proc Natl Acad Sci U S A* **111**, 18607-18612
190. Girard, P., Pecreaux, J., Lenoir, G., Falson, P., Rigaud, J. L., and Bassereau, P. (2004) A new method for the reconstitution of membrane proteins into giant unilamellar vesicles. *Biophys J* **87**, 419-429
191. Veshaguri, S., Christensen, S. M., Kemmer, G. C., Ghale, G., Moller, M. P., Lohr, C., Christensen, A. L., Justesen, B. H., Jorgensen, I. L., Schiller, J., Hatzakis, N. S., Grabe, M., Pomorski, T. G., and Stamou, D. (2016) Direct observation of proton pumping by a eukaryotic P-type ATPase. *Science* **351**, 1469-1473
192. Killian, J. A. (1998) Hydrophobic mismatch between proteins and lipids in membranes. *Biochim Biophys Acta Rev Biomembr* **1376**, 401-416
193. Baron, S., Vangheluwe, P., Sepulveda, M. R., Wuytack, F., Raeymaekers, L., and Vanoevelen, J. (2010) The secretory pathway Ca^{2+}-ATPase 1 is associated with cholesterol-rich microdomains of human colon adenocarcinoma cells. *Biochim Biophys Acta* **1798**, 1512-1521
194. Simons, K., and Ikonen, E. (1997) Functional rafts in cell membranes. *Nature* **387**, 569-572
195. Blank, B., and von Blume, J. (2017) Cab45-Unraveling key features of a novel secretory cargo sorter at the trans-Golgi network. *Eur J Cell Biol* **96**, 383-390
196. Li, Y., Ge, M., Ciani, L., Kuriakose, G., Westover, E. J., Dura, M., Covey, D. F., Freed, J. H., Maxfield, F. R., Lytton, J., and Tabas, I. (2004) Enrichment of endoplasmic reticulum with cholesterol inhibits sarcoplasmic-endoplasmic reticulum calcium ATPase-2b activity in parallel with increased order of membrane lipids: implications for depletion of endoplasmic reticulum

calcium stores and apoptosis in cholesterol-loaded macrophages. *J Biol Chem* **279**, 37030-37039

197. Jensen, M. S., Costa, S. R., Duelli, A. S., Andersen, P. A., Poulsen, L. R., Stanchev, L. D., Gourdon, P., Palmgren, M., Gunther Pomorski, T., and Lopez-Marques, R. L. (2017) Phospholipid flipping involves a central cavity in P4 ATPases. *Sci Rep* **7**, 17621
198. Sohoel, H., Jensen, A. M., Moller, J. V., Nissen, P., Denmeade, S. R., Isaacs, J. T., Olsen, C. E., and Christensen, S. B. (2006) Natural products as starting materials for development of second-generation SERCA inhibitors targeted towards prostate cancer cells. *Bioorg Med Chem* **14**, 2810-2815
199. Lopreiato, R., Giacomello, M., and Carafoli, E. (2014) The plasma membrane calcium pump: new ways to look at an old enzyme. *J Biol Chem* **289**, 10261-10268
200. Garside, V. C., Kowalik, A. S., Johnson, C. L., DiRenzo, D., Konieczny, S. F., and Pin, C. L. (2010) MIST1 regulates the pancreatic acinar cell expression of Atp2c2, the gene encoding secretory pathway calcium ATPase 2. *Exp Cell Res* **316**, 2859-2870
201. Reinhardt, T. A., Filoteo, A. G., Penniston, J. T., and Horst, R. L. (2000) Ca^{2+}-ATPase protein expression in mammary tissue. *Am J Physiol Cell Physiol* **279**, C1595-1602
202. Tsutsumi, M., Inoue, K., Denda, S., Ikeyama, K., Goto, M., and Denda, M. (2009) Mechanical-stimulation-evoked calcium waves in proliferating and differentiated human keratinocytes. *Cell Tissue Res* **338**, 99-106
203. Aronchik, I., Behne, M. J., Leypoldt, L., Crumrine, D., Epstein, E., Ikeda, S., Mizoguchi, M., Bench, G., Pozzan, T., and Mauro, T. (2003) Actin reorganization is abnormal and cellular ATP is decreased in Hailey-Hailey keratinocytes. *J Invest Dermatol* **121**, 681-687
204. Bian, T., Autry, J. M., Casemore, D., Li, J., Thomas, D. D., He, G., and Xing, C. (2016) Direct detection of SERCA calcium transport and small-molecule inhibition in giant unilamellar vesicles. *Biochem Biophys Res Commun* **481**, 206-211
205. Barthmes, M., Liao, J., Jiang, Y., Bruggemann, A., and Wahl-Schott, C. (2016) Electrophysiological characterization of the archaeal transporter NCX_Mj using solid supported membrane technology. *J Gen Physiol* **147**, 485-496

Curriculum Vitae

Jialin Chen

Jialin.chen@kuleuven.be

shuyanchen0528@gmail.com

- **Education**

2012-2019	KU Leuven, Leuven, Belgium PhD in Biomedical Science "Purification of the Secretory Pathway Ca^{2+}/Mn^{2+} ATPases for Functional Analysis and Drug Discovery"
2010-2012	KU Leuven, Leuven, Belgium MSc in Molecular and Cellular Biophysics
2008-2010	GroupT Leuven Campus, Leuven, Belgium (exchange program)
2006-2008	Zhejiang University of Technology, Hangzhou, China Bachelor of Industrial Science Bachelor of Science in Pharmaceutical Sciences

- **Publications**

Research papers

Chen, J., Smaardijk, S., Mattelaer, C. A., Pamula, F., Vandecaetsbeek, I., Vanoevelen, J., Wuytack, F., Lescrinier, E., Eggermont, J., and Vangheluwe, P. (2019) An N-terminal Ca^{2+} binding motif regulates the secretory pathway Ca^{2+}/Mn^{2+}-transport ATPase SPCA1. *J Biol Chem doi 10.1074/jbc.RA118.006250*

Hamilton, N., Kieseier, B., Wüllner, V., **Chen, J.**, Kurschus, F., Herrmann, A.K., Vangheluwe, P., Moos, S., Albrecht, P., Graf, J., and Methner, A. (2019) Dimethyl fumarate alters intracellular Ca^{2+} handling in immune cells by redox-mediated pleiotropic effects. *Free Radic Biol Med* (in revision)

Sitsel, A., De Raeymaecker, J., Drachmann, N. D., Derua, R., Smaardijk, S., Andersen, J. L., Vandecaetsbeek, I., **Chen, J.**, De Maeyer, M., Waelkens, E., Olesen, C., Vangheluwe, P., and Nissen, P. (2019) Structures of the heart specific SERCA2a Ca^{2+}-ATPase. *EMBO J* 38: e100020

Pessina, F., Gamberucci, A., **Chen, J.**, Liu, B., Vangheluwe, P., Gorelli, B., Lorenzini, S., Spiga, O., Trezza, A., Sgaragli, G., and Saponara, S. (2018) Negative chronotropism, positive inotropism and lusitropism

of 3,5-di-t-butyl-4-hydroxyanisole (DTBHA) on rat heart preparations occur through reduction of RyR2 Ca^{2+} leak. *Biochem Pharmacol* 155, 434-443

Smaardijk, S., **Chen, J.**, Kerselaers, S., Voets, T., Eggermont, J., and Vangheluwe, P. (2018) Store-independent coupling between the secretory pathway Ca^{2+} transport ATPase SPCA1 and Orai1 in Golgi stress and Hailey-Hailey disease. *Biochim Biophys Acta* 1865, 855-862

Chen, J., De Raeymaecker, J., Hovgaard, J. B., Smaardijk, S., Vandecaetsbeek, I., Wuytack, F., Moller, J. V., Eggermont, J., De Maeyer, M., Christensen, S. B., and Vangheluwe, P. (2017) Structure/activity relationship of thapsigargin inhibition on the purified Golgi/secretory pathway Ca^{2+}/Mn^{2+}-transport ATPase (SPCA1a). *J Biol Chem* 292, 6938-6951

Smaardijk, S., **Chen, J.**, Wuytack, F., and Vangheluwe, P. (2017) SPCA2 couples Ca^{2+} influx via Orai1 to Ca^{2+} uptake into the Golgi/secretory pathway. *Tissue Cell* 49, 141-149

Reviews and book chapters

Chen J., Sitsel A., Benoy V., Rosario Sepúlveda M., Vangheluwe P. (2019). Primary active Ca^{2+} transport systems in health and disease. Cold Spring Harb Perspect Biol. doi: 10.1101/cshperspect.035113. (accepted)

Chen, J., Smaardijk, S., Vandecaetsbeek, I., and Vangheluwe, P. (2016) Regulation of Ca^{2+} transport ATPases by amino- and carboxy-terminal extensions: Mechanisms and (patho)physiological implications. *Regulation of Ca^{2+}-ATPases, V-ATPases and F-ATPases* 14, 243-279

Oral presentation

Regulation of the secretory pathway Ca^{2+} ATPases SPCA1a and SPCA2 by Ca^{2+} and Orai1. 24-30 Sep 2017, Otsu, Japan.

Posters and abstracts

Chen, J., De Raeymaecker, J., Hovgaard, J.B., Smaardijk, S., Vandecaetsbeek, I., Møller, J.V., Eggermont, J., De Maeyer, M., Christensen, S.B., Vangheluwe, P. (2017). Thapsigargin as a lead compound for developing other P-type ATPase inhibitors. P-ATPases meeting 2017, Otsu, Japan, 24 Sep 2017-30 Sep 2017.

Chen, J., Smaardijk, S., Arslan, T., Wuytack, F., Eggermont, J., Vangheluwe, P. (2017). Regulation of the secretory pathway Ca^{2+} ATPases SPCA1a and SPCA2 by Ca^{2+} and Orai1. P-ATPases meeting 2017, Otsu, Japan, 24 Sep 2017-30 Sep 2017.

Smaardijk, S., **Chen, J.**, Eggermont, J., Vangheluwe, P. (2017). Store-independent Orai1 activation and Golgi stress induction by secretory pathway Ca^{2+} ATPase 1. Gordon research conference calcium signaling, Barga, Italy, 18 Jun 2017-23 Jun 2017.

De Raemaecker, J., Smaardijk, S., **Chen, J.**, Vangheluwe, P., De Maeyer, M. (2016) Virtual screen for allosteric modulators of SERCA2A activity. 21st Europeam symposium on quantitative structure-activity relationship, 4 Sep 2016-8 Sep 2016.

Chen, J., Vandecaetsbeek, I., Schuermans, M., De Raeymaecker, J., Smaardijk, S., De Maeyer, M., Eggermont, J., Møller, J.V., Christensen, S.B., Klaassen, H., Chaltin, P., Vangheluwe, P. (2015). Purified Ca^{2+}-transport ATPases as targets for rational drug development and high throughput screening. BioMedical transporters conference, Lugano, Switzerland, 09 Aug 2015-13 Aug 2015.

Smaardijk, S., **Chen, J.**, Vandecaetsbeek, I., Eggermont, J., Vangheluwe, P. (2015). Store-independent Ca^{2+} entry mediated by SPCA1a and SPCA2. ECS Workshop, Onzain, France, 21 Jun 2015-25 Jun 2015.

Vandecaetsbeek, I.*, **Chen, J.***, Smaardijk, S., Paulsen, P.A., Nissen, P., Eggermont, J., Vangheluwe, P. (2014). Functional coupling of the secretory pathway Ca^{2+} pumps and the Orai1 Ca^{2+} channel. P-ATPases meeting, 30 Aug 2014-5 Sep 2014. (* shared first author)

Vandecaetsbeek, I., **Chen, J.**, Smaardijk, S., Eggermont, J., Vangheluwe, P. (2014). Structure/Function Analysis of the Ubiquitous Secretory Pathway Ca^{2+} Pump SPCA1a. In: *Biophysical Journal: vol. 106* (2) (586A-586A). Presented at the 58th annual meeting of the biophysical-society, San Francisco, CA, 15 Feb 2014-19 Feb 2014.

Smaardijk, S., Vandecaetsbeek, I., **Chen, J.**, Wuytack, F., Vangheluwe, P. (2013). The N- and C-terminal extensions of SPCA: effects on Ca^{2+} pump activity and store-independent Ca^{2+} entry through Orai1. Presented at the ECS Workshop, Leuven, Belgium, 11 Sep 2013-13 Sep 2013.

Acknowledgement, Personal Contribution and Conflict of Interest statement

Scientific acknowledgement

Chapter 1

This work has been funded by the Flanders Research Foundation FWO (G044212N and G0B1115N) and the inter-University Attraction Poles program (P7/13) and by the Danish Council for Strategic Research. We thank Marleen Schuermans and Els Lariviere for their excellent technical assistance.

Chapter 2

This work has been funded by the Flanders Research Foundation FWO (G044212N and G0B1115N) and the inter-University Attraction Poles program (P7/13). CM is an SB PhD fellow at FWO (1S23217N). We thank Diane Hermans, Marleen Schuermans and Tugce Arslan for their excellent technical assistance.

Personal contribution

Chapter 1

JC performed and analyzed the experiments on figure 1, 2, 3, 5A-C and table 1, 2, 3. JC analyzed data from *in silico* docking experiments, and co-wrote the manuscript.

Chapter 2

JC performed and analyzed the experiments except for the NMR study, and co-wrote the manuscript.

Conflict of interest statement

The author states no conflict of interest